Characterisation of Duramycin as an Anti-cancer Agent

Laura Broughton, BSc (Hons)

PhD in Medical Sciences

The University of Hull and the University of York

Hull York Medical School

December 2016

Abstract

Duramycin is a relatively small (~2kDa) tetracyclic peptide that has a defined three-dimensional (3D) structure, this structure forms a stable binding pocket which specifically recognises the plasma membrane phospholipid phosphatidylethanolamine (PE). PE usually resides on the inner membrane layer though can become exposed on the outer membrane during physiological processes such as apoptotic cell death, cytokinesis and coagulation. Expression of cell surface PE has been observed on cancer cell lines, tumour endothelium and tumour-derived microparticles and observed in higher abundance in a variety of tumour xenografts compared to their normal tissue counterparts. There is a need in medical oncology for the development of novel, effective therapies and anti-cancer agents. A form of therapy that has gained interest is targeted anti-cancer therapy (TAT) which aims to bring about selective damage to tumour cells while limiting effect on surrounding normal tissue by utilising agents that recognise structures specific to tumours. Therefore, as duramycin had the potential to bind to PE exposed on cancer cell surfaces, it was theorised that it could be a promising targeted anti-cancer agent. Thus the aim of this project was to characterise duramycin's anti-cancer properties and enhance its specificity to tumour cells. To achieve this a duramycin-porphyrin conjugate was developed as a novel photosensitiser and cancer cell lines were treated with photodynamic therapy (PDT). Duramycin was able to detect cell surface PE expression on cancer cell lines representing different cancer types including lymphoma, multiple myeloma and leukaemia and ovarian, pancreatic, breast and colon cancer. Duramycin was shown to have cytotoxic and anti-proliferative effects on cancer cell lines (ovarian and pancreatic), in both two-dimensional and 3D cell cultures, and a cytotoxic dose-dependent effect on a normal human endothelial cell line. Duramycin had been reported in the literature to have an effect on plasma membrane integrity and on a multitude of ion transport systems through the formation of membrane pores. Thus duramycin's effect on cancer cell membranes was investigated along with a focus on whether the cytotoxic effect observed in the cancer cell lines was due to a form of calcium ion (Ca^{2+}) overload. It was shown that duramycin treatment resulted in a concentration-dependent rise in intracellular Ca^{2+} concentration in cancer cell lines. The duramycin-porphyrin conjugate plus PDT light irradiation reduced cell proliferation of ovarian and pancreatic cancer cell lines in a dose-dependent manner and had a significantly enhanced effect over unconjugated duramycin and the free porphyrin. A preliminary investigation into the effect of duramycin-PDT treatment on tumour xenografts on the chorioallantoic membrane (CAM) of fertilised chicken eggs was undertaken with promising results. In summary, duramycin was shown to be an effective anti-cancer agent and was applicable to the PDT treatment of cancer *in vitro* and in a low level-*in vivo* tumour model and thus merits further studies.

Publications in support of this project

Research Publications

Broughton LJ, Giuntini F, Savoie H, Bryden F, Boyle RW, Maraveyas A, Madden LA. Duramycin-porphyrin conjugates for targeting of tumour cells using photodynamic therapy. *Journal of photochemistry and photobiology B, Biology*. 2016; 163:374-84.

Broughton LJ, Crow C, Maraveyas A, Madden LA. Duramycin-induced calcium release in cancer cells. *Anti-Cancer Drugs*. 2016; 27(3):173-82.

Poster Presentations

Broughton L, Maraveyas A, Madden L. Targeting phosphatidylethanolamine on tumour cells using duramycin. *Thrombosis Research*. 2014; 133(S2):S213.

Presented at International Conference on Thrombosis and Haemostasis Issues in Cancer, Bergamo, Italy, 2014.

List of Contents

List of Figures

List of Tables

List of Abbreviations

$[Ca^{2+}]_i$	Intracellular calcium ion concentration
$^1O_2$	Singlet oxygen
2D	Two-dimensional
3D	Three-dimensional
$^3O_2$	Molecular oxygen
5-FU	5-fluorouracil
ABAE	Adult bovine aortic endothelial cells
ABC	Adenosine triphosphate binding cassette
ALA	5-aminolevulanic acid
AlP_cS_n	Chloro-aluminium phthalocyanine
AM	Acetoxymethyl
ANO1	Anoctamin 1
APTL	Aminophospholipid translocase
ATP	Adenosine triphosphate
BPD-MA	Benzoporphyrin derivative monoacid A
Ca^{2+}	Calcium ion
CaCC	Calcium ion activated chloride ion channel
$CaCl_2$	Calcium chloride
Ca_{ext}	Extracellular calcium
CAM	Chorioallantoic membrane
cDNA	Complementary deoxyribonucleic acid
Ce-6	Chlorin-6
Cl^-	Chloride ion
CF	Cystic fibrosis
CFBE	Cystic fibrosis bronchial epithelial cells
CFTR	Cystic fibrosis transmembrane conductance regulator
CO_2	Carbon dioxide
CT	Computerised tomography
dH_2O	Distilled water

DLB	Biotinylated duramycin
DMSO	Dimethyl sulphoxide
DNA	Deoxyribonucleic acid
EDTA	Ethylenediaminetetraacetic acid
EOC	Epithelial ovarian cancer
ER	Endoplasmic reticulum
ESI-MS	Electrospray ionising mass spectrometry
EVA	Ethylene-vinyl acetate
FBS	Foetal bovine serum
FITC	Fluorescein isothiocynanate
FSC	Forward scatter
Gla	Gamma-carboxyglutamic acid
H&E	Haematoxylin and Eosin
HEPES	4-(2-hydroxyethyl)-1-piperazineethanesulfonic acid
HGSOC	High grade serous ovarian cancer
HIF-1	Hypoxia-inducible transcription factor-1
HPD	Haematoporphyrin derivative
HPLC	High performance liquid chromatography
HSP	Heat shock protein
HUVECs	Human umbilical vein endothelial cells
HYNIC	Hydrazinonicotinamide
IC	Internal conversion
IC_{50}	Half maximal inhibitory concentration
IKK	IκB kinase
ISC	Intersystem crossing
IP_3R	Inositol trisphosphate receptor
IPMN	Intraductal papillary mucinous neoplasms
K^+	Potassium ion
KCl	Potassium chloride
kDa	Kilo Dalton

LCMS	Liquid chromatography-mass spectrometry
LDL	Low density lipoprotein
Lyso-PE	Lysophosphatidylethanolamine
mAb	Monoclonal antibody
MCN	Mucinous cystic neoplasms
Mg^{2+}	Magnesium ion
MFIR	Median fluorescence intensity ratio
Min	Minute
MPs	Microparticles
MRI	Magnetic resonance imaging
mRNA	Messenger ribonucleic acid
miRNA	Micro ribonucleic acid
MS	Mass spectrometry
MTT	3-[4,5-dimethylthiazol-2-yl]-2,5- diphenyltetrazolium bromide
MTS	3-[4,5-dimethylthiazol-2-yl]-5-[3-carboxymethoxyphenyl]-2-[4-sulfophenyl]-2H-tetrazolium
MW	Molecular weight
Na^{+}	Sodium ion
NaCl	Sodium chloride
NADPH	Nicotinamide adenine dinucleotide phosphate
NCX	Sodium/calcium exchanger
NCKX	Sodium/calcium-potassium exchanger
NHS	*N*-hydroxysuccinimide
NMDA	N-methyl-D-aspartate
NMR	Nuclear magnetic resonance
NRF2	Nuclear factor erythroid 2-related factor 2
OD	Optical density
P/S	Penicillin/streptomycin
p130/Rb	p130 and retinoblastoma protein
PanIN	Pancreatic intraepithelial neoplasia
PBS	Phosphate buffer solution

PC	Phosphatidylcholine
PDAC	Pancreatic ductal adenocarcinoma
PDGF	Platelet-derived growth factor
PDMS	Polydimethylsiloxane
PDT	Photodynamic therapy
PE	Phosphatidylethanolamine
PET	Positron emission tomography
PhtS	Photosensitiser
PI	Propidium iodide
PLA	Poly(D,L-lactic acid)
PLSCR	Phospholipid scramblase
PMCA	Plasma membrane pumps calcium ion ATPase
PpIX	Protoporphyrin IX
PS	Phosphatidylserine
p-THPP	Meso-tetra(*p*-hydroxyphenyl)porphyrin
PVP	Polyvinylpyrrolidone
Q-TOF-MS	Quadrupole time-of-flight mass spectrometry
RBC	Red blood cell
RNA	Ribonucleic acid
ROS	Reactive oxygen species
RP-HPLC-PDA	Reversed phase HPLC photodiode array
R_t	Retention time
RyRs	Ryanodine receptors
ScFv	Short chain Fv fragment
SD	Standard deviation
Secs	Seconds
SERCA	Sarco/endoplasmic reticulum calcium ion ATPase
SOD	Superoxide dismutase
SPCA	Secretory pathway calcium ion ATPase
SPECT	Single-photon emission computed tomography

SR	Sarcoplasmic reticulum
SSC	Side scatter
TAT	Targeted anti-cancer therapy
TCPP	5,10,15,20-tetrakis(carboxyphenyl) porphyrin
TEA	Triethylamine
TFA	Trifluoroacetic acid
THNP	5,10,15,20-tetra-p-naphthyl-porphyrin
TRP	Transient receptor potential
TTP	5,10,15,20-tetra-p-tolyl porphyrin
UV-vis	Ultraviolet-visible
VEGF	Vascular endothelial growth factor
VGCC	Voltage-gated calcium ion channel
WHO	World Health Organisation
Xiap	X-linked inhibitors for apoptotic proteins

Acknowledgements

I would like to thank my supervisors Anthony Maraveyas and Leigh Madden for their continual support throughout this project, their contribution to the direction of the research and their invaluable intellectual and scientific insight. I would also like to thank my Thesis Advisory Panel chair Ross Boyle for his extremely valued help with the PDT part of my research and his contribution to the editing of the published PDT research paper. Following from this I would like to express gratitude to Francesca Giuntini without whom the synthesis of the duramycin-porphyrin conjugate would not have been possible. I have a great appreciation for Huguette Savoie for all of the work that she put into the PDT light experiments and her involvement with the CAM work. Thanks must also go to Francesca Bryden for the synthesis and analysis of the capped porphyrin control. I am very grateful to Yu-pei (Clover) Xiao for giving her last months at The University of Hull to the CAM work and for the early morning starts involved in the CAM plus PDT experiments. Chris Crow must be acknowledged for the method that he provided for the calcium assay, the time he gave for me to be able to use the laboratory facilities at Castle Hill Hospital and his valued contribution to the interpretation of the data. I would like to thank Justin Cooke who generously interpreted the histological stains from the CAM experiments. My sincere gratitude goes to He Liang and Jessica Hall for their contribution of cells to this project and again to Jessica for her support during the early stages of my research and for teaching me many laboratory techniques. I would also like to thank Andrew Gordon for his help with culturing HUVECs and Ann Lowry for her help with tissue sectioning. Lastly but by no means least I would like to extend thanks to Linsey Malcolm, the laboratory technician, who kept the laboratory running smoothly so that experiments were made much easier by her work and who kept me sane during any stressful moments throughout the project.

In addition, I would like to thank my parents (Angela Broughton and Julian Broughton) for their continual emotional and financial support, my best friend Samantha O'Callaghan Johnson for listening to any complaints I had throughout the project and my sister Bethany Broughton for the immeasurable support and encouragement she has given me over the past few years.

Author's Declaration

I confirm that this work is original and that if any passage(s) or diagram(s) have been modified from academic papers, books, the internet or any other sources these are clearly identified by the use of quotation marks and the reference(s) is fully cited. I certify that, other than where indicated, this is my own work and does not breach the regulations of HYMS, the University of Hull or the University of York regarding plagiarism or academic conduct in examinations. I have read the HYMS Code of Practice on Academic Misconduct, and state that this piece of work is my own and does not contain any unacknowledged work from any other sources.

Chapter 1 Introduction

1.1 Cancer

Over the past two decades cancer has persisted as one of the world's leading causes of death[1, 2]. In 2015 trachea, bronchus and lung cancers accounted for approximately 23 deaths per 100,000 of the world population, making it the 7th leading cause of death. In 2015, within the top twenty causes of death, cancer also took the 16th, 17th and 19th positions for liver, stomach and colon/ rectum cancers, respectively. The World Health Organisation (WHO) predicts that these cancers will remain as some of the world's top causes of death in 2030 along with breast cancer accounting for, in total, approximately 80 deaths per 100,000 of the population[2]. In England, in 2014, there were almost 297,000 new cancer registrations[3]. Of these the most common cancers diagnosed were breast cancer (31.6% of total female cancer registrations), prostate cancer (26.3% of total male cancer registrations), followed by lung cancer and colorectal cancers for both females and males. Advances in oncological medicine in screening and early diagnoses of malignant disease have, in part, lead to a higher cancer incidence rate over time. Despite the higher incidence of cancer the mortality rates have generally decreased[3], however in England and Wales in 2015 cancer remained the most common form of death (28% of registered deaths that year)[4].

According to the WHO International Classifications of Diseases (10th revision) there are almost 100 malignant cancer types and sub-types[5]. Yet, certain 'hallmark traits of cancer' have been identified that all cancer cells must acquire to become tumorigenic and subsequently malignant. Hanahan and Weinberg[6], in 2000, initially identified six of these hallmarks theorising them to be 'distinctive and complimentary capabilities that enable tumour growth and metastatic dissemination'. These included sustained proliferative signalling, the evasion of growth suppressors, the activation of invasion and metastasis, replicative immortality, angiogenesis inducement and resistance to cell death. A decade later, after advancements in oncological research, two more emerging cancer hallmarks were identified as; the ability to modify or reprogram cellular metabolism and the ability to evade immunological destruction, in particular by macrophages, T and B lymphocytes and natural killer cells[7]. Additionally, cancer cells require a level of genetic instability which ultimately leads to the acquisition of a mutant genotype that aids tumour progression. In particular, the mutation of genes that play a role in cell cycle arrest and programmed cell death can result in the evasion or removal of cancer cells from the tumour

microenvironment. Furthermore, immunological response from the innate immune system results in the infiltration of immune cells into the tumour microenvironment in a tumour-associated inflammatory response. This anti-tumour response has been seen to enhance tumour progression and the acquisition of the hallmark capabilities. For example, the inflammatory response can deliver biological molecules to the tumour microenvironment such as growth factors that aid sustained proliferation and enzymes that modify the extracellular matrix which can then lead to angiogenesis, invasion and metastasis[7]. Therefore, tumours exist as complex tissues, with interactions between tumorigenic cells and also normal cells such as tumour recruited stromal cells, and thus present a complicated target for anti-cancer therapies.

The application of conventional therapies for cancer treatment, surgery, radiotherapy and chemotherapy, can be challenged in some cancers through the development of chemotherapy resistant tumours[8-10] and a lack of applicability of treatments for recurrent disease[11]. Damage to surrounding non-tumour tissue can also occur during some treatments leading to the loss of function, for example in patients with head and neck cancers side-effects such as speech problems, tongue immobility and difficulty swallowing have been observed[11]. In addition, there is an increased risk of venous thromboembolic events associated with chemotherapy in a wide variety of malignancies[12, 13]. Therefore, there has been an increasing emphasis in oncological research on the development of targeted anti-cancer therapy (TAT). TAT aims to bring about selective destruction of cancer cells while minimising the effect on surrounding normal tissue. This can potentially be achieved through the delivery of anti-cancer agents (drugs, antibodies, proteins, peptides) that specifically recognise tumour structures, phenotypic properties or metabolisms that do not exist in normal cells[14]. Through activation or inactivation of these specific targets TAT can theoretically result in the destruction or regression of tumours. For example, peptides are an attractive delivery mechanism for anti-cancer agents as their relatively small size means that they have a rapid blood clearance and tissue penetration and usually renders them non-immunogenic[15]. A radiolabelled somatostatin (a peptide which inhibits the release of growth hormones, receptors for which are expressed in relatively high amounts in tumour cells) receptor analogue was used to treat 35 patients with neuroendocrine gastroenteropancreatic cancer (a cancer with a low chemotherapy success rate)[16]. Tumour response was significantly enhanced in tumours that showed higher levels of uptake of the radiolabelled peptide ($p < 0.05$). Imaging of the tumours by computerised tomography (CT) and magnetic resonance imaging (MRI) 3-6 months post-treatment (34

patients) showed that complete remission occurred in 1 patient, partial remission in 12 patients, stable disease in 14 patients and progressive disease in 7 patients. Side effects were few and transient. Thus the development of novel, effective TAT agents could offer promising application in the treatment of malignancy.

1.1.1 Ovarian cancer

Epithelial ovarian cancer (EOC) is the most lethal gynaecological cancer in the world[17] resulting in approximately 164,000 deaths in 2015[2]. Over 95% of ovarian malignancies are epithelial in origin[18]. The exact cellular origins of EOC are not fully understood, initial theories claimed that they were derived from ovarian surface epithelial cells. However, it is now widely proposed that EOC constitutes a diverse collection of tumours with specific morphologic and genetic characteristics and can arise from the malignant transformation of epithelium in the ovary, peritoneum or fallopian tube[19]. Histopathologically EOC can be divided into subtypes named for the tissue origin they most resemble and include serous, mucinous, endometrioid, clear cell and transitional cell tumours. The most common of these is the serous type, accounting for ~75% of cases. In a histological study of fallopian tubes of patients with early serous cancers almost 100% showed evidence of tubal lesions and this was associated with the genetic mutation of the BRCA genes (BRCA1 and BRCA2)[19]. The most common form of EOC, high grade serous ovarian cancer (HGSOC), is associated with these detrimental modifications to BRCA and also the TP53 gene. A study that analysed the mRNA, miRNA, DNA copy number and promoter methylation of 489 HGSOC found that 96% of the tumours had TP53 mutations and ~13% had BRCA mutations[20].

Metastatic progression can be lethal in ovarian cancer, the 5 year survival rate is less than 20%[18] compared with that of non-metastatic disease of approximately 45%[21]. Unlike the majority of cancers which take a haematological metastatic route ovarian cancer is unique in that it spreads locoregionally and is usually confined to the peritoneal cavity[17, 18]. Ovarian cancer cells become detached from the primary tumour and are carried by the intraperitoneal ascitic fluid to secondary sites within the abdomen. The formation of such peritoneal deposits is dependent on the cancer cells ability to attach and invade the submesothelial endothelial cell matrix and proliferate as metastases. The ascitic fluid of patients has been shown to contain the migrating ovarian cancer cells in both single cell and multicellular aggregate (spheroids) form. Successful establishment at a secondary site relies on the cells' or spheroids' ability to adhere to mesothelial cells (cells that line the surface of the peritoneum and provide a protective barrier). Ovarian cancer cell lines (SK-

OV-3, OV-90 and OVCAR3) were observed to invade into an *in vitro* model of mesothelium, to varying degrees, through destruction of the ectodermal layer and invasion and proliferation in the mesodermal layer[22]. Furthermore, the ascitic fluid contains many growth factors, cytokines, extracellular matrix components and active stromal and inflammatory cells which aid in the survival of the tumour cells[17].

The major therapy route for ovarian cancer is surgery, the extent (total/ hysterectomy, bilateral salpingo-oophorectomy or omentectomy) of which is based on the histopathological subtype and the stage at diagnosis. However in HGSOC or tumours in the later stages (stages III or IV) adjuvant chemotherapy is often employed to increase overall survival[19]. Eventual resistance to chemotherapy following recurrence of disease is a major limiting factor of EOC treatment and is the main factor in poor prognosis[8, 23]. Thus the identification of predictive markers for patients that will benefit from chemotherapy have been investigated, an example of a few identified include X-linked inhibitors for apoptotic proteins (Xiap) along with p53 status, BRCA alterations, cancerous ovarian stem cells and epithelial mesenchymal transition[23]. The lack of/ expression of certain proteins can also be targets for chemoresistance prediction. For example, the deregulation of survivin, a member of the inhibitor of apoptosis family, was found to be important in the paclitaxel-resistance of ovarian cancer cells[24]. A number of mechanisms have been identified in the resistance to platinum-based chemotherapy such as changes in cisplatin transport, resistance to cisplatin-DNA adducts and increased DNA repair in response to treatment[8]. Hence there is vital need for the development of new treatment options for ovarian cancer.

1.1.2 Pancreatic cancer

Pancreatic cancer is a relatively aggressive malignancy that is characterised by high therapy resistance and therefore is one of the most lethal cancers in the world. In a study of 24 of the most common cancers (91.1% of total cancers) in England, in patients diagnosed between 2010 and 2014 and followed up in 2015, pancreatic cancer had the lowest 1-year and 5-year survival rates for both females (22.9% and 6.2%, respectively) and males (21.1% and 5.2%, respectively)[21]. A reason for the high mortality rate in pancreatic cancer is that, due to a lack of symptoms, at diagnosis only 10-20% of patients have tumours localised to the pancreas and can be treated with surgery that has a curative intent. The majority of patients present with advanced cancers where approximately 40% have locally advanced tumours that extend into surrounding organs and ~40-50% of cases present with metastases[25, 26]. Another reason is that the pancreas is a difficult organ to visualise, often

limited to cross-sectional imaging and ultrasounds which makes early diagnosis/ screening challenging. Additionally, there is a high rate of recurrence in pancreatic cancer even after surgical resection and currently there are limited effective therapies.

Pancreatic cancers represent a heterogeneous group of tumours that can be divided into two types based on tumour origin, exocrine and endocrine. The majority (95%) of pancreatic tumours are exocrine in origin with pancreatic ductal adenocarcinoma (PDAC) by far the most common[26]. PDAC has been shown to develop from well-defined pre-malignant lesions. The most common of these lesions are the microscopic pancreatic intraepithelial neoplasias (PanIN)[27] found on small (<5 mm in diameter) pancreatic ducts[28]. These can be divided into subtypes (PanIN-1A/B, PanIN-2 and PanIN-3) dependent on the extent of change to architecture and cytological abnormalities e.g. nuclear enlargement, transition from cuboidal to tall columnar cells. The macroscopic cysts intraductal papillary mucinous neoplasms (IPMN) and mucinous cystic neoplasms (MCN) can also develop into invasive PDAC though these represent only 5% of primary pancreatic tumours[29]. Additionally, PDAC is characterised by having a dense stroma, made up of collagen and fibronectin, known as the desmoplasia. The main source of the excessive stromal desmoplasia comes from pancreatic stromal cells which can be activated by cellular damage and stress within the pancreas and from platelet cells, cytokines and growth factors released by inflammatory cells. Activation of the pancreatic stromal cells ultimately leads to the excessive production of extracellular matrix proteins[28]. The tumour microenvironment of PDAC has been well characterised and there exists a vast amount of knowledge of the involvement of immune, endocrine and epithelial cells and the effect of angiogenesis in the progression of the disease[27, 28]. For example, it has been observed that high expression of the angiogenic protein vascular endothelial growth factor (VEGF) in PDAC is associated with poor prognosis, local cancer growth and liver metastasis[28]. The presence of pro-inflammatory cytokines in the PDAC tumour microenvironment aids angiogenesis, progression, invasion and metastasis and anti-inflammatory cytokines have been shown to be involved in immune invasion[27]. Furthermore, there is a breadth of knowledge on the PDAC genome and mutations common to almost all pancreatic cancers have been identified as the oncogene KRAS and the tumour suppressor genes TP53, CDKN2A and SMAD4/DPC4[27].

The treatment of pancreatic cancer is highly dependent on the stage of disease which is classified as either resectable, unresectable locally advanced or metastatic. Surgical

resection is only possible in patients (~20%) that present with early tumours and is often associated with recurrence despite adjuvant treatment. The frontline anti-cancer agents in this setting are 5-fluorouracil (5-FU) or gemcitabine[9, 25]. There is no consensus for the treatment of unresectable locally advanced tumours due to ambiguous results from studies involving chemotherapy and radiotherapy alone or in combination. Metastatic pancreatic cancers are highly chemoresistant to a broad range of anti-cancer agents. Here gemcitabine, either alone or in combination with abraxane, is commonly used to prolong survival though this remains low at an average of approximately 6 months[9]. A small number of adequately fit patients are now being treated with the combination of FOLFIRINOX (combined 5-FU, oxaliplatin, leucovorin and irinotecan) that provides a survival advantage over gemcitabine but ultimately these patients relapse[30]. A factor for the poor prognosis may be the poor status that these patients have early in their disease due to many tumour related complications (e.g. obstruction of biliary tree and duodenum, early ascites due to portal vein thrombosis and intractable pain due to infiltration of the coeliac axis)[31]. However, particular biological factors may underpin the relatively high presentation of chemoresistance in pancreatic cancers. It is theorised that the genetic mutations involved in oncogene expression and the inactivation of tumour suppressor genes play a role[9, 25]. Pancreatic cancer cell lines (PANC-1, PancTuI and Colo357) were assessed for their sensitivity to gemcitabine treatment in which cell proliferation was inhibited in a dose dependent manner[10]. The resistance to gemcitabine correlated well with the level of expression of the anti-apoptotic protein Bcl-xL. The most gemcitabine-sensitive cell line (Colo357) was transduced with Bcl-xL cDNA and was subsequently found to be much more resistant to treatment both in cell culture and when implanted into mice. Alike ovarian cancer, there is a need for the development of new therapies and anti-cancer agents in the treatment of pancreatic cancer.

1.2 Phosphatidylethanolamine

1.2.1 Phospholipid membranes

In mammalian cells the membrane bilayer is composed of 60% glycoproteins and integral proteins and 40% lipids and glycolipids. The lipids are comprised of phospholipids, cholesterol and glycosphingolipids[32]. Mammalian cell membranes can contain over 100 different phospholipid species[33], which is due to the different fatty acyl chains that can be attached to the *sn*-1 and *sn*-2 positions of the glycerol backbone and the variety of polar headgroups that can attach at the *sn*-3 position (figure 1.1). Phosphatidylcholine (PC) is the

most abundant phospholipid in mammalian cell membranes constituting 40-50% of the total phospholipids[33]. Phosphatidylethanolamine (PE) is the second most abundant representing 20-50% of the total phospholipids, dependent on tissue and organ. For example, in the brain ~45% of the phospholipids are PE whereas in the liver PE only equates to ~20%[33]. Phosphatidylserine (PS) is present in less abundance, constituting 2-10% of the total phospholipid. In addition, other phospholipids such as phosphatidylinositol, phosphatidic acid, sphingomyelin and the mitochondrial phospholipid cardiolipin can be present in plasma cell membranes. As well as different compositions found in mammalian organs the phospholipids can be found in different abundances in the organelles of cells. For example, the organelle with the highest amount of PE is the mitochondria, particularly the inner membrane[33].

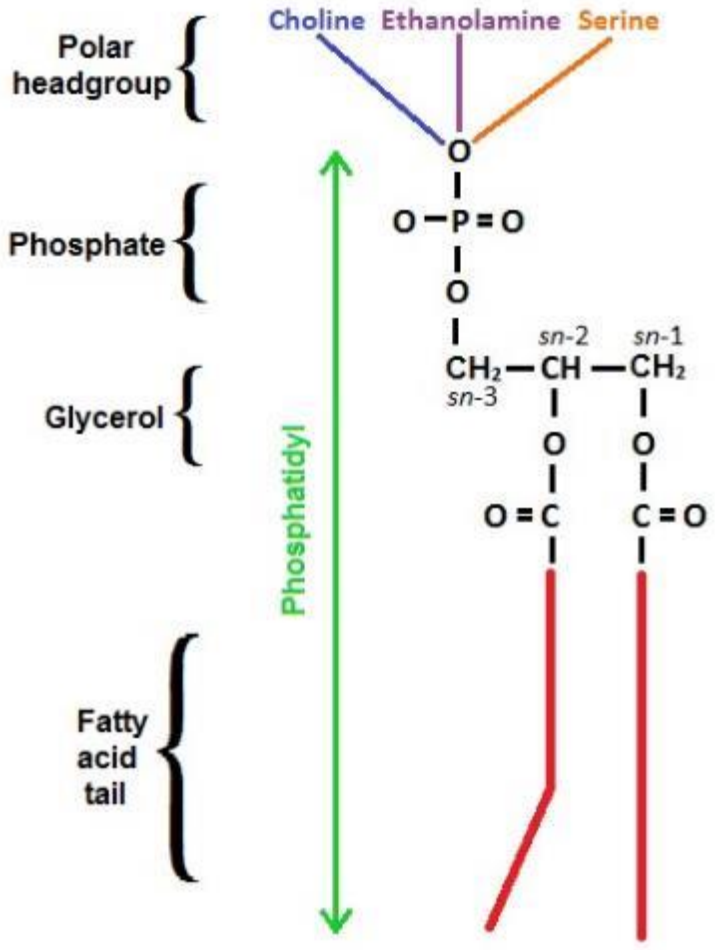

Figure 1.1: Structure of phospholipids.

The structure of membrane phospholipids is centred round the glycerol backbone which allows for the existence of a relatively large number of phospholipid types due to the different fatty acid chains that can exist at the *sn*-1 and *sn*-2 positions and the different headgroups at the *sn*-3 position.

It is well established that phospholipids are distributed asymmetrically in the majority of eukaryotic cell membranes[34, 35] including the plasma membrane and cell organelles e.g. golgi, endosomal membranes and secretory vesicles. In the plasma membrane of normal eukaryotic cells the choline-containing lipids, sphingomyelin and PC, predominately exist in the outer, non-cytosolic membrane layer whereas the majority (>80%)[33] of the aminophospholipids, PE and PS, primarily exist in the inner, cytosolic membrane layer[36].

The maintenance of, and commonly the loss of, asymmetrical phospholipid distribution is essential to the regulation of normal processes within the cell. For example, the transbilayer redistribution of PS so that it becomes exposed on the outer membrane layer can occur during apoptotic cell death and can serve as a cell surface signal for phagocytic degradation[37]. The passive transbilayer movement of phospholipids requires an input of energy in the form of adenosine triphosphate (ATP) and thus spontaneous loss of membrane asymmetry is prevented by a thermodynamic barrier[38]. Additionally, the passive outward translocation of phospholipids is slow with a half time of ~1.5 hours[39] though this is highly dependent on cell type and ranges from hours to days. A number of things have been observed to increase the speed of this process; i) introduction of different physical properties between the inner and outer membranes, ii) insertion of proteins which span the bilayer and iii) structural changes resulting in non-bilayer configuration of the lipid membrane[36]. The passive inward translocation of aminophospholipids is more efficient than the outward translocation[40]. Thus rapid movement of phospholipids in the maintenance and loss of membrane asymmetry needs to be controlled by energy-dependent processes. The unidirectional inward transportation of phospholipids is controlled by a group of enzymes from the P4-type ATPases, the aminophospholipid translocases (APTLs), commonly known as the flippases[41]. The P-type ATPases are a family of membrane embedded transporters that share a phosphorylated intermediate as part of their reaction cycle[42] and use energy from ATP hydrolysis to move ions and lipids across membranes[43]. They are divided into five sub-families, the first three of which transport a variety of metal ions across membranes in either prokaryotic (P1A-ATPases) or eukaryotic cells (P1B-, P2A/B/C/D- and P3A/B-ATPases). The ligands for the fifth class of P-type ATPases are yet to be elucidated but it is theorised that they play a role in the endosomal-lysosomal system[43]. The P4-ATPases exist only in eukaryotic cells, fourteen have been found to be encoded by the human genome and these are divided into five classes which have different lipids as their substrates (PE, PC, PS and currently unknown)[43]. The P4-type ATPases are both ATP and magnesium (Mg^{2+}) dependent[44]. The unidirectional outward

transport of phospholipids is controlled by a number of proteins from the ATP-binding cassette (ABC) transporter group and are commonly referred to as floppases. The ABC transporters constitute a wide variety of proteins that are generally involved in ATP-dependent movement of amphipathic compounds and so tend to be non-specific[38]. To enable interaction with a variety of amphipathic molecules bilayer lipid transporters are able to accommodate both polar headgroups and hydrophobic tails[45]. The most characterised floppases are ABCA1, ABCB1, ABCB4, and ABCC1[38] though only the latter was shown to be involved in the maintenance of membrane asymmetry, acting on choline-phospholipids. The others have been implicated in the efflux of lipids from cells rather than any specific activity in the maintenance of phospholipid membranes. The bidirectional movement of phospholipids is controlled by the phospholipid scramblases (PLSCRs or just scramblases)[33] which are ATP-independent due to the existence of a transbilayer lipid gradient[45], unlike the flippases and floppases which require the input of ATP to pump against a concentration gradient. It is widely theorised that scramblases function to remove membrane asymmetry upon activation, such as in apoptosis, rather than to assist in its maintenance[46, 47].

1.2.2 Cell surface expression of phosphatidylethanolamine

The loss of membrane asymmetry and the subsequent exposure of PE on the outer membrane layer plays an important role in the physiological process of apoptosis, cytokinesis and the initiation of coagulation. In the early stages of apoptosis PS is exposed on the outer cell membrane as a signal for macrophage recognition and removal[37]. The exposure of the aminophospholipids is proposed to occur by the downregulation of flippases and an enhanced scrambling of the phospholipids which results in bidirectional translocation. Emoto *et al.*[48] were the first to gain definitive evidence that PE is exposed during early apoptosis and that this exposure coincided with the loss of asymmetrical distribution of PS. Using a fluorescently labelled cinnamycin (a peptide closely related to duramycin) compound the expression of cell surface PE on apoptotic cells of a cytotoxic T cell line, CTLL-2, was imaged using microscopy. Significant staining of cytoplasmic organelles as well as the plasma membrane at incubation times >48 hours indicated that cinnamycin entered the cells in late stages of cell death once membrane integrity had been compromised[48]. Additionally, the level of cell surface PE expression (detected by duramycin) was increased on the pancreatic cancer cell lines AsPC-1 and CFPAC-1 when they were apoptotic (induced by camptothecin treatment) compared to untreated cells and was further increased when they were necrotic (induced by 30% H_2O_2 treatment)[49]. For

example, the mean fluorescence intensity ratio (the fluorescence of cells labelled for PE expression compared to the fluorescence of negative control cells) of PE expression for untreated AsPC-1 cells was 1.9 which increased to 3.1 for apoptotic cells and 7.4 for necrotic cells. Exposure of PE on the outer surface of the plasma membrane of dividing Chinese Hamster ovarian cells was observed during cytokinesis, specifically at the cleavage furrow during late telophase[50]. This was visualised using biotinylated cinnamycin in complex with fluorescently labelled streptavidin. The binding of the cinnamycin complex to PE resulted in cell division arrest in telophase due to inhibited actin filament disassembly at the cleavage furrow and membrane fusion. Inhibited cytokinesis occurred in ~80% of cells when treated with 7.2 µM cinnamycin. Thus it was shown that PE is likely an important regulator in the movement of the contractile ring (an arrangement of actin filaments attached to the plasma membrane at the site of cell division) and the plasma membrane in successful cell division. Exposure during cytokinesis was also observed as localised PE expression on the cytokinetic ends of *Saccharomyces cerevisiae*[51].

Exposure of PE and PS on the outer membrane can enhance the initiation of coagulation through a number of mechanisms. After cell damage or activation cell surface exposed PE and PS co-operate to create cell membrane binding sites for the N-terminal of gamma-carboxyglutamic acid (Gla) domains of clotting proteins. This occurs through phospho-L-serine specific and phosphate-specific interactions for PS and PE, respectively[52]. The anchoring of coagulation proteins (factors), through Gla domains, to the cell can initiate the coagulation process. PE, in the presence of PS, synergistically increases the rate of the coagulation cascade by playing a role in the activation and assembly of the factor (F) VIIIa-FIXa complex[53]. In the presence of PS alone the FVIIIa-FIXa complex requires an outer membrane content of ~20-25% PS for optimal activity[54]. This requirement is reduced to 1% in the presence of ~20-35% PE[53]. The expression of PE on the cell surface has also been shown to enhance the activation of prothrombin[55, 56], tissue factor-FVIIa activation of FX[57] and the binding of FVIII to membranes that contain low levels of PS[53]. It was shown that the blocking of PE with duramycin resulted in a lower pro-coagulant potential in the pancreatic cancer cell lines AsPC-1, CFPAC-1 and MIA PaCa-2[49, 58].

The exposure of cell surface PE has also been seen to occur on cancer cell lines, tumours, tumour vasculature and tumour-derived microparticles (MPs)[49, 59-61] and in the response to chemotherapy[62, 63]. The pancreatic cancer cell lines AsPC-1 and CFPAC-1 were shown to express cell surface PE via flow cytometric detection[49]. A duramycin compound was used

to assess if anti-cancer treatments or environmental factors commonly experienced by *in vivo* tumours had an effect on the level of cell surface PE exposure in the endothelium[59]. PE was seen to be increased on the surface of adult bovine aortic endothelial (ABAE) cells in response to irradiation, reactive oxygen species (ROS), low pH and hypoxia. Once it was shown that PE was exposed on endothelial cells the duramycin compound was used to assess PE presence in tumour endothelium. PE was seen to be exposed on the surface of the vascular endothelium of mice bearing subcutaneous RM-9 prostate tumours and this was most prominent in areas of hypoxia. Duramycin has also been used to detect cell surface PE on MPs from the human breast cancer cell line MDA-MB-231[60]. PE was detected on small membrane vesicles in microparticle-rich supernatant from the breast cancer cells via confocal microscopy. Flow cytometric analysis revealed that PE was detected in higher abundance than PS in the MDA-MB-231-derived MPs which correlated with the higher amount of PE content in mammalian cell membranes. Recently, the lipid composition of tumour xenografts, formed in nude mice, generated from a number of different cancer types (lung, colon, pancreatic and glioblastoma) was determined by imaging mass spectrometry (MS)[61]. The distribution of PE, PC and their ether derivatives was investigated and it was found that differences in the amount of phospholipid species present varied in the different xenograft types. This resembled closely the heterogeneity of their corresponding clinical tumours. Interestingly, both PC- and PE-ethers were found in much higher abundance in the tumour xenografts than in their normal tissue counterparts. It was theorised that this may have been because these phospholipid species are involved in the prevention of double bond oxidation, important in the oxidative stress conditions commonly found in tumours[61]. A duramycin radiotracer was used to assess the level of cell death induced in chemotherapy treated (5-FU, oxaliplatin, irinotecan) colon cancer cells and colon tumour bearing mice[62]. Chemotherapeutic treatment of the colon cancer cells increased cell death in a concentration dependent manner which corresponded to a significant increase in duramycin binding for cells treated with 5-FU (>310 μM) and oxaliplatin (>7 μM) compared to untreated cells. Tumour bearing mice were treated with intraperitoneal injections of oxaliplatin and/or irinotecan and assessed with the duramycin compound and single-photon emission computed tomography (SPECT) imaging 24 hours post-treatment. Specific uptake of duramycin occurred in the tumour tissue and histological analysis showed that this correlated well with apoptotic areas in the tumours[62]. No specific reference to an increase in PE exposure in the treated tumours was made in this study. However, as PE can become exposed during apoptotic cell death[48, 49, 64] it is likely

that an increased PE expression was the reason for the observed rise in duramycin binding. Indeed this was theorised to be the cause for the binding of radiolabelled duramycin in paclitaxel-treated breast cancer xenografts, as imaged by SPECT and supported by histological and flow cytometric analyses of cell death[63].

1.3 Duramycin

1.3.1 Structure and binding site

Duramycin is a tetracyclic peptide produced from the bacterium *Streptoverticillium cinnamoneus* and has been shown to exhibit weak anti-microbial activity against gram-positive organisms[65]. Being only 19 amino acids in length and having a molecular weight of ~2kDa duramycin is one of very few, relatively, small peptides to have a defined three-dimensional (3D) structure[59]. The initial analyses of duramycin's structure were performed by high performance liquid chromatography (HPLC) over 25 years ago[65]. It was revealed that duramycin's amino acid sequence constitutes 10 common amino acids, asparagine, glutamine, proline, glycine (2), valine, phenylalanine (3) and lysine, which are all present in the L-isomer form, and the uncommon amino acids β-methyllanthionine (2), meso-lanthionine, lysinoalanine and β-hydroxyaspartic. The presence of these unusual amino acids classifies duramycin as a type-B lantibiotic. The duramycin-type lantiobiotics duramycin, duramycin B, duramycin C and cinnamycin are structurally similar compounds and are characterised by 3 internal thioether bridges (2 β-methyllanthionine and 1 meso-lanthionine) and a lysinoalanine bridge between an L-alanine (Ala 6) and the C-terminal lysine (Lys 19)[66]. The bridging system within the duramycin-type peptides confers to them a rigid globular assembly which results in their stable and defined 3D structure. Duramycin is synthesised as a pro-peptide on ribosomes and subsequently undergoes an extensive amount of enzymatic post-translational modification (figure 1.2)[67]. The residues Ser 4, Ser 6, Thr 11 and Thr 18 are dehydrated and become didehydroalanine and didehydrobutyrine intermediates at the serine and threonine residues, respectively[68]. Nucleophilic addition from the Cys 14 side chain to didehydroalanine results in the formation of lanthionine. The formation of methyllanthionine occurs via nucleophilic addition from Cys 1 and Cys 5 to the didehydrobutyrines. Additionally the C-terminal Lys 19 reacts with the didehydroalanine at residue 6 to form the lysinoalanine. Thus the covalent bridges formed between these residues constitute the 3 thiother bridges and the lysinoalanine bridge that confers duramycin's structural stability. The uncommon amino acid, β-hydroxyaspartic acid, is located at residue Asp 15[68]. Duramycin is an amphipathic molecule with its hydrophobic

amino acid residues existing together on one side and its hydrophilic residues on the other[66] (figure 1.3a).

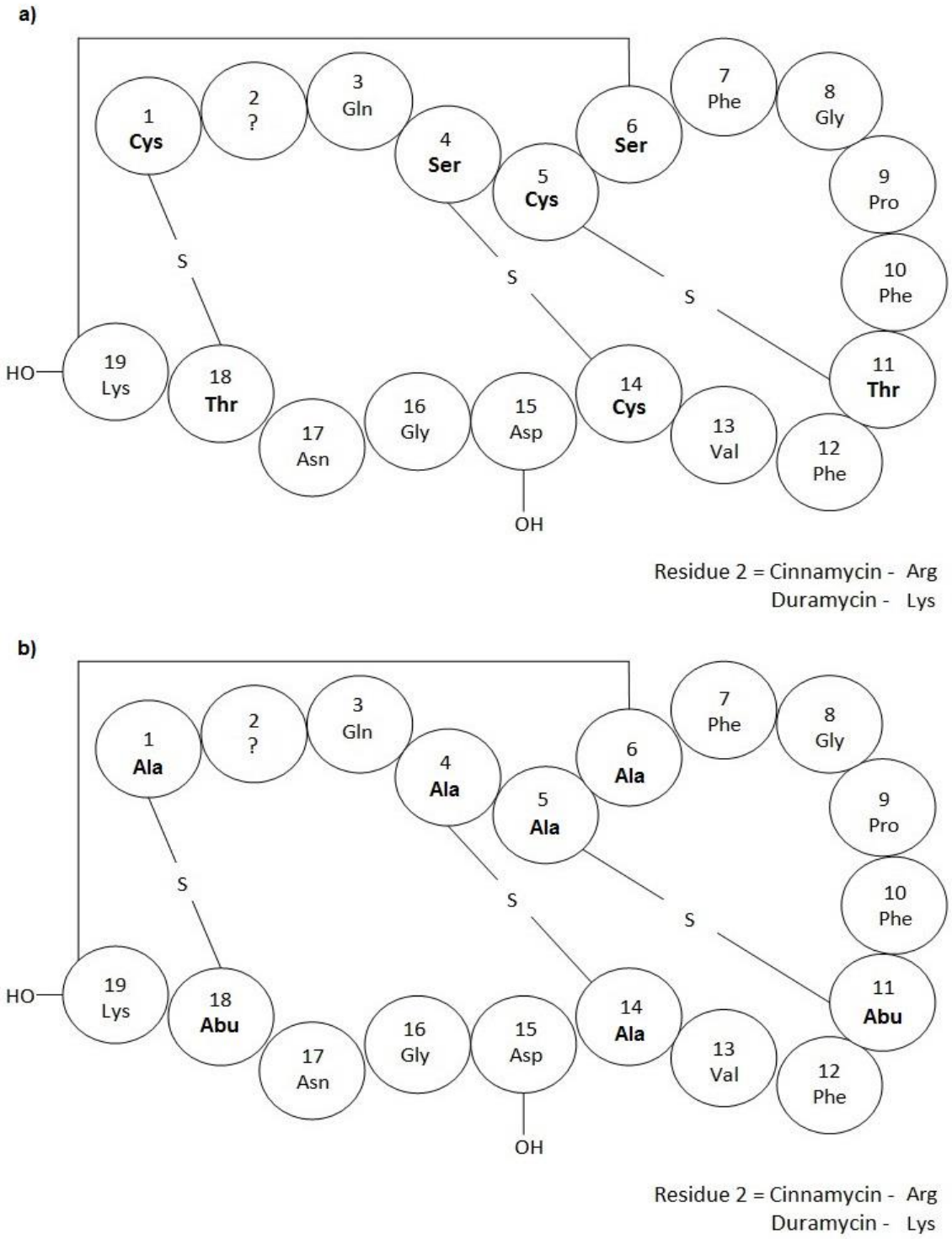

Figure 1.2: Structure of duramycin and cinnamycin before and after post-translational modification.

a) Amino acid sequence of duramycin's and cinnamycin's pro-peptide. b) The amino acid sequence of duramycin and cinnamycin after post-translational modification which is different to the pro-peptide at residue positions 1, 4, 5, 6, 11, 14 and 18.

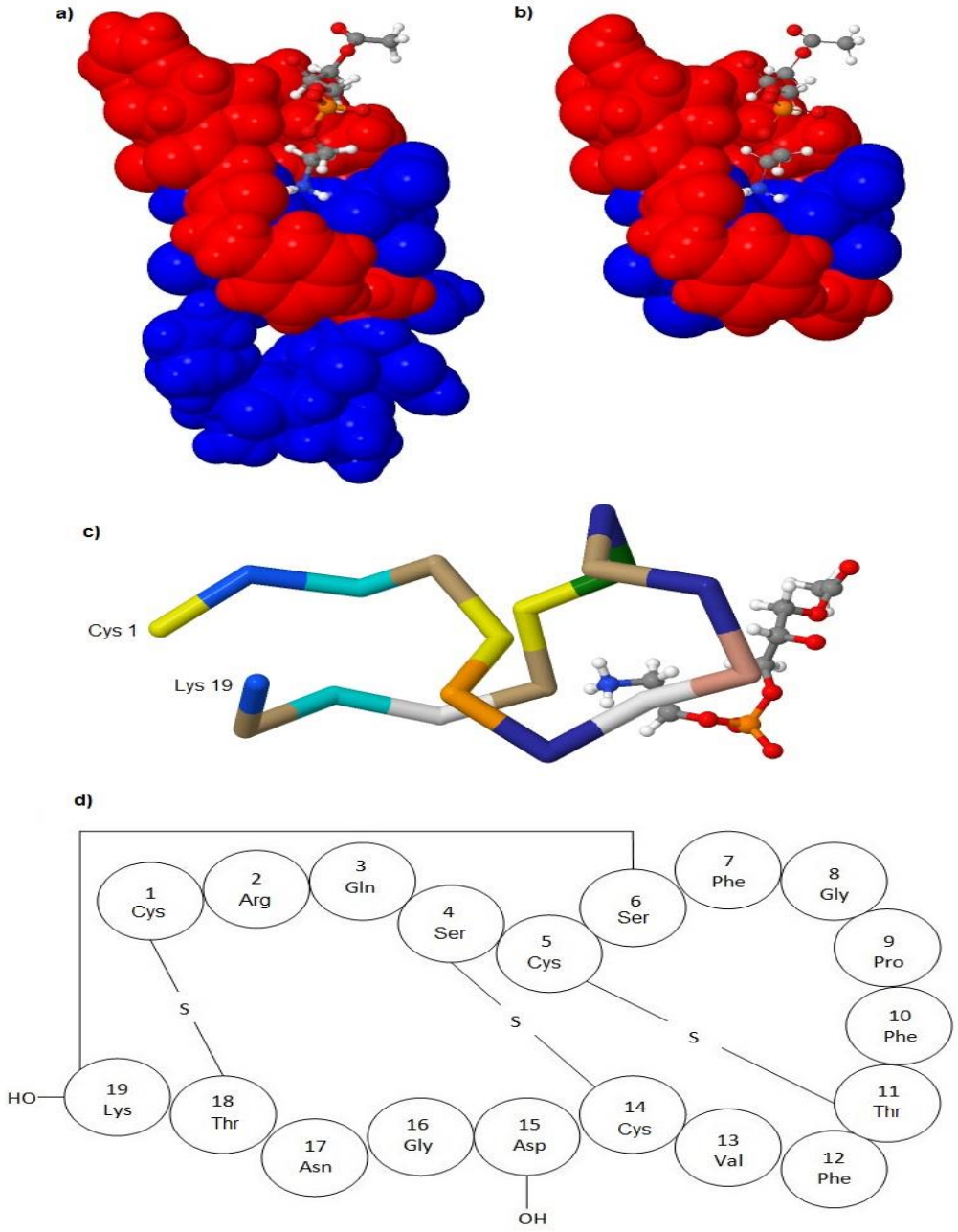

Figure 1.3: Structure and binding site of cinnamycin.

a) Space-fill model of the peptide cinnamycin with lysophosphatidylethanolamine (lyso-PE) as its ligand showing hydrophobic residues (red) and hydrophilic residues (blue). PE is most likely synthesised from its precursor lyso-PE by catalysis with an acyl-CoA-dependent acyltransferase (LPEAT)[33]. The space-fill model was originally drawn using MolScript (Avatar Software) by Hosoda *et al*.[69] from the 10 lowest energy structures from an NMR ensemble that had been used in the determination of the cinnamycin-lyso-PE complex structure. b) Space-fill model of the hydrophobic PE binding cleft of cinnamycin. c) Backbone structure of cinnamycin showing amino acid sequence and lyso-PE binding position. d) Amino acid sequence of cinnamycin pro-peptide. Images from the Protein Data Base (PDB), Research Collaboratory for Structural Bioinformatics (www.rcsb.org) of PDBID: 2DDE (Hosoda K, Ohya M, Kohno T, Maeda T, Endo S, Wakamatsu K. Journal of biochemistry. 1996;119(2):226-30) using JSmol: an open-source Java viewer for chemical structures in 3D (http://www.jmol.org/). Accessed 10 Nov, 2016.

Duramycin binds to the membrane phospholipid PE which it specifically recognises through interactions with the ethanolamine polar headgroup. Early evidence of duramycin's recognition of PE was found in duramycin resistant *Bacillus subtilis*[70]. Duramycin was shown to inhibit ATP-dependent calcium ion (Ca^{2+}) uptake in sarcoplasmic vesicles and inhibit the bacteriorhodopsin proton pump only when reconstituted in lipid vesicles formed from PE. However duramycin had no effect on the Ca^{2+} uptake or proton secretion in the duramycin-resistant *B. subtilis* strain. It was found that the lipid composition of the resistant strain was different to its parent strain as it contained no PE. Additionally duramycin resistant *Bacillus firmus* was observed to have reduced PE levels compared to its non-resistant counterpart[71]. Increased amounts of other phosphoethanolamine containing lipids such as plasmenylethanolamine and lysophosphatidylethanolamine (lyso-PE) were present in the resistant strain, perhaps taking the functional place of PE. However they did not contribute to the organisms' resistance and thus it was concluded that the plasmalogen and monodeacylated forms of phosphoethanolamine were unlikely to contribute to duramycin sensitivity.

NMR studies involving cinnamycin[69] and further studies involving duramycin revealed that the recognition site for PE was conserved between the two structurally similar lantibiotics. Duramycin's and cinnamycin's binding site for PE is situated within the hydrophobic portion of the peptide: Phe 7 through to Ala 14[66], as shown by the interaction between cinnamycin and lyso-PE (figure 1.3). The binding site is in the form of a hydrophobic cleft (figure 1.3b) in which the hydrophobic residues, Gly 8, Pro 9 and Val 13, are involved in the binding to the glycerol moiety of PE. The fatty acid chains of PE can be concealed within this hydrophobic cleft. The 2 Phe side chains that protrude from the loop region of the cleft anchor the peptides to the hydrophobic core of the plasma membrane[64]. Additionally, an ionic interaction between the carboxylate group of Asp 15 and the ammonium group of PE further stabilises the interaction[69, 72]. The size of the hydrophobic cleft is 8-10 methylene segments which was found to be the required amount for maximal binding interaction between lyso-PE and cinnamycin[72]. The specific interactions that exist between the duramycin-type lantibiotics and PE confer a binding ratio of 1 molecule of peptide to 1 molecule of PE (a stoichiometry of 1:1)[72]. It also means that their dissociation constant is in the low nanomolar range (4-6 nM)[65, 66, 73].

1.3.2 Duramycin conjugates

The N-terminal of duramycin, which consists of 2 primary amino acids (cysteine and lysine), is situated away from the PE binding site (figure 1.3c) so that it offers a potential location for conjugation. Duramycin has no unique spectroscopic properties[72] which is why this conjugation site has been utilised in a number of studies to produce various fluorescently labelled imaging compounds. Some of these studies attached duramycin to a reporter molecule such as a biotin and then the biotinylated form was subsequently conjugated to a fluorescently-labelled streptavidin molecule. Duramycin attached to the NHS-ester of a biotin molecule (DLB) and duramycin attached to the near infrared fluorophore 800CW (Dur-800CW) were used to characterise and image the exposure of PE on tumour vasculature[59]. Both compounds were able to bind to phospholipid-coated 96 well plates and thus were shown to retain their ability to bind to PE. DLB was shown to lyse 50% of murine red blood cells (RBCs) at 80 µM compared to 20 µM for unconjugated duramycin. Thus it was shown that biotinylation could reduce the haemolytic ability of duramycin. This was also observed in a biotinylated cinnamycin compound in which the biotinylation abolished the cytotoxic potential against Chinese hamster ovarian cells[50]. Intravenous injection of DLB into tumour bearing mice showed localisation of DLB to tumour blood vessels in all tumours investigated (including prostate, breast and lung carcinoma and melanoma from both mice and human species) as shown by immunohistochemical stains[59]. The exposure of PE on the blood vessels was seen to co-localise with the exposure of PS. Uptake of the intravenously injected DLB was not observed in any other tissue of the mice save the kidney due to the urine being the main excretory route of duramycin[64]. Investigation into the possibility of using duramycin to image PE exposure *in vivo* revealed that Dur-800CW localised to the tumour vasculature of prostate tumour bearing mice and no other tissue with the exception of the kidneys[59]. Along with showing that duramycin could be a useful imaging agent this study highlighted that PE could be a promising broad tumour marker for a wide variety of malignancies.

The development of radiolabelled duramycin conjugates has been reported in the literature though these studies have been more focused on the imaging and detection of cell death rather than with cancer. Duramycin conjugated to technetium (^{99m}Tc-duramycin) showed good pharmacokinetic and biodistribution properties when intravenously injected into rats[64]. Duramycin was rapidly cleared from the blood, with a half-life of 4 minutes, and was predominately excreted in the urine where it was recovered intact and therefore had not been metabolically degraded. Hepatic and gastrointestinal uptake was low and the

duramycin conjugate was successfully used to image acute cardiac cell death. As an improvement upon this study the research group developed a single-step labelling technique for ^{99m}Tc to hydrazinonicotinamide (HYNIC)-duramycin which increased the purity of the compound and was shown to retain its ability to localise to the infarcted site in rat cardiac tissue and also localise to PE exposed on the luminal surface of aortic endothelium[74, 75]. Further studies have been published by this research group with regards to the expansion of ^{99m}Tc-duramycin's application and its improvement as a probe for cell death[63, 76-81]. An interesting development was the demonstration of a use for ^{99m}Tc-duramycin in the early detection of apoptosis following paclitaxel treatment of a breast carcinoma xenograft[63]. Other studies have also utilised ^{99m}Tc-duramycin and SPECT as a tool to image early apoptotic response to chemotherapy in tumours[62, 82]. A novel positron emission tomography (PET) probe was developed using duramycin ([^{18}F]FPDuramycin) through conjugation to duramycin's lysine residue at position 2[83]. *In vitro* binding studies showed that the radiotracer bound to apoptotic and necrotic Jurkat cells and did not bind to healthy Jurkat cells. Tumour-bearing mice were treated with cyclophosphamide or cisplatin chemotherapy and the tumours visualised using small animal PET imaging. [^{18}F]FPDuramycin was seen to localise to the tumour site and immunohistochemical stains showed that it was bound to apoptotic and necrotic regions. Therefore duramycin conjugates have been shown to be potentially effective probes for assessment of early response to chemotherapy and for the detection of cell death in disease.

1.3.3 Effect of duramycin on ion transport and plasma membranes

Duramycin has been reported in the literature to have an effect on a variety of ion transport channels and pumps in many different cell types. Duramycin was shown to inhibit the sodium-potassium (Na^+-K^+) ATPase pump, purified from dog kidney, by inhibiting phosphorylation and causing hydrolysis of the phosphoenzyme[84]. This effect was completely reversed upon addition of phospholipids. Duramycin was shown to inhibit the function of a proton translocating ATPase pump and its linked chloride ion (Cl^-) transporter in clathrin-coated vesicles[85]. The inhibitory effect on the clathrin-coated vesicles was found to be determined by the ratio of duramycin to membranes rather than the final duramycin concentration. At lower ratios of duramycin (5 µg/ 100 µg protein) to clathrin-coated protein the proton pump activity was blocked through Cl^- inhibition and the process could be reversed through the addition of valinomycin (a K^+ transporter). At higher ratios (20 µg duramycin/ 100 µg protein) the proton pump itself was inhibited. Within a narrow concentration range of 0.2-5 µM duramycin had a sustained effect on increased short

circuit current due to Cl^- secretion in canine tracheal epithelium over a 75 minute period[86]. A concentration dependent effect for duramycin was also seen in airway epithelial cells where lower duramycin concentrations (0.1 μM) caused an increase in intracellular calcium ion concentration ($[Ca^{2+}]_i$) through Ca^{2+} release from internal stores[87]. It was thought that higher concentrations (1-5 μM) caused the rise in $[Ca^{2+}]_i$ through intracellular Ca^{2+} release an extracellular influx. In sarcoplasmic reticulum (SR) vesicles duramycin inhibited the ATP-dependent uptake of Ca^{2+} though it was observed that neither the hydrolysis of ATP nor the Ca^{2+} permeability of the vesicles was effected[70].

Though earlier studies suggested that duramycin had specific action on ion channels and pumps themselves it is currently theorised that the effect that duramycin has on cellular ions is due to the formation of non-selective pores in membranes. Monolayer cultures of colonic epithelial cells were treated with duramycin and cinnamycin and subsequent ion transport was measured as changes in short circuit currents[88]. The majority of the changes in current were found to be due to Na^+ absorption however an outward movement of Cl^- occurred with duramycin treatment and both peptides increased $[Ca^{2+}]_i$. It was theorised that the increase in $[Ca^{2+}]_i$ was due to pores formed in the epithelial cell membranes which allowed the influx of Ca^{2+}. This was then demonstrated using black lipid (PC/PE) membranes (nanometre thick lipid bilayers) which showed relatively large conductance fluctuations (for Na^+, Cl^-, Mg^{2+} and Ca^{2+}) upon treatment with duramycin (>2 μM)[89]. This occurred only in bilayer membranes and not in thick films which was suggested to mean that pores were formed rather than the specific activation of ion carriers. In epithelial cells the conductance changes revealed that both Na^+ absorption and Cl^- secretion occurred which furthered the idea that non-selective pores were formed. The effect of duramycin was investigated on various voltage-gated channels including hERG K^+ channels in human embryonic kidney cells (HEK293), Ca^{2+} channels in mouse cardiomyocytes and Cl^- channels in HEK293, cardiomyocytes, neuroblastoma cells and skeletal muscle cells[90]. Duramycin >0.3 μM reduced the amplitude of the currents measured in all of the cell types. It was suggested that this could have been a result of duramycin-induced changes to the biophysical properties of the cell membranes, through interaction with PE, and a consequent indirect action on the perturbation of ion channels. At higher concentrations (>3.3 μM) leak currents were induced which were consistent with the formation of non-selective pores[90]. Additionally, duramycin induced Ca^{2+} release from human cystic fibrosis bronchial epithelial cells (CFBE) at 1-3 μM and in their normal (non-cystic fibrosis) counterparts at 3 μM[91]. Efflux of Cl^- was also observed in CFBE cells in a narrow concentration range of 1 μM.

Higher duramycin concentrations (>100 µM) inhibited Cl^- efflux which was suggested to be due to duramycin-induced cell membrane damage. It was theorised that the damage to the plasma membrane had effected Ca^{2+}-activated Cl^- (CaCC) channels which made the membranes permeable and resulted in non-selective ion efflux[91].

As well as the formation of pores and the effect on ion transport duramycin has been shown to cause shape changes to plasma membranes. Duramycin, in a concentration dependent manner (40-500 µM), caused PE-containing multilamellar vesicles to change shape resulting in the formation of rod-like structures[73]. These rod-like structures were found to be hollow tubules consisting of lipid bilayers in which duramycin was able to penetrate into the hydrophobic interior region. The binding to the PE-containing vesicles was dependent upon membrane curvature in which there was a preference for small vesicles with highly curved membranes over large liposomes. Cinnamycin has been shown to be able to induce transbilayer lipid movement in PE-containing model membranes[39]. Thus it is theorised that duramycin has the potential to promote its own binding to cell surfaces through the induction of PE exposure and an increase in the curvature of membranes. A study into the interaction between duramycin and PE-containing monolayers showed that disruption to cell membranes by duramycin occurs through a reduction in lipid order, a weakening of water hydrogen bonding around PE and a reduction in line tension[92]. Reduction in line tension can occur if there is a significant change in the curvature in the boundary between a lipid raft and its surrounding lipid bilayer. Duramycin reduced line tension between two different lipid phases in PE monolayers which caused one of the phases to change from circular to horse-shoe like[92].

1.3.4 Duramycin and Cystic Fibrosis

Duramycin was shown to have an effect on Cl^- transport in airway epithelia[86, 87], specifically through action on the CaCC anoctamin 1 (ANO1)[93]. ANO1 is a potential target in cystic fibrosis (CF) therapy due to its ability to induce fluid secretion. Lung epithelial cells that express the CF transmembrane conductance regulator (CFTR) defective in patients with CF also express ANO1, this has been shown to be important in Cl^- secretion in trachea epithelia. ANO1 can be activated by duramycin through an increase in $[Ca^{2+}]_i$ as a result of duramycin-formed Ca^{2+}-permeable pores in cell membranes. Thus duramycin was viewed as a potential therapeutic for CF. While in clinical trials (ClinicalTrials.gov identifier NCT00671736)[94, 95] its biodistribution in mice, rats[96] and beagle dogs[97] was assessed using radiolabelled duramycin. The absorption of radiolabelled duramycin was poor in rats after

oral administration, inhalation and intratracheal instillation and in mice after oral administration[96]. However good retention was seen in lung tissue and this was taken as evidence to support the use of duramycin as a respiratory disease treatment. A dose of ^{14}C-Moli1901 (radiolabelled duramycin) was given to dogs by instillation into the left cranial lobe of the lung[97] and distribution was monitored using accelerator MS analysis of blood, plasma, urine and faeces samples and homogenised lung tissue. It was found that the main form of excretion was through the faeces and that the highest distribution of ^{14}C-Moli1901 occurred in the lung and kidney. ^{14}C-Moli1901 became associated with RBCs and its removal from the blood was slower than its addition. It was theorised that this was due to duramycin's binding to exposed PE on the RBCs. It was also suggested that binding to PE explained the retention of the duramycin compound in the lung however problems with absorption due to the globular 3D structure of duramycin were also implicated. This study showed that theoretically radiolabelled duramycin could be used to analyse the biodistribution of duramycin in clinical trials with humans.

Good results were obtained from the Phase I[94] and Phase II[95] clinical trials in which subjects were given duramycin (Moli-1901) in the form of an inhaled aerosol. Duramycin stimulated the secretion of Cl^- in CF patients at a concentration of 3 μM and in healthy volunteers at 1-10 μM[94]. However, as far as the author is aware, there has been no further development in clinical trials with duramycin in regards to CF[98]. This may be because a study on airway epithelium showed that duramycin did not selectively effect Cl^- but rather disrupted cell membranes which resulted in non-selective ion movement[91]. Thus the hypothesis that duramycin stimulated Cl^- secretion through action on alternative Cl^- channels was discredited. Additionally, duramycin was found to increase conductance of Cl^- in the human airway epithelial cell line Calu-3 yet no selective increase in Cl^- permeability was found[99].

1.4 Importance of calcium ions

1.4.1 Calcium ion transport

Calcium signalling and Ca^{2+} are a key component of cellular life and have diverse roles in the alteration of cellular transcription, cell cycle regulation, cell proliferation, cell motility and programmed cell death[100]. In excitable cells Ca^{2+} can be used to propagate signals, for example in the production of action potentials in muscle tissue[101]. These processes rely on and are influenced by $[Ca^{2+}]_i$ and the gradient between the intracellular environment and the extracellular Ca^{2+} concentration. Cells invest a large amount of energy in the maintenance of low $[Ca^{2+}]_i$, which is usually in the range of ~100 nM compared to the

extracellular environment which ranges from ~1.2 mM to 2 mM. This equates to a ~20,000 fold gradient between intracellular and extracellular Ca^{2+} [102]. Thus, upon cell activation, $[Ca^{2+}]_i$ can undergo rapid change due to a relatively steep concentration gradient and, dependent upon the stimulus, the $[Ca^{2+}]_i$ can reach ~1 μM[100]. In resting cells low cytosolic Ca^{2+} concentration is maintained by various ATP-dependent mechanisms that either i) chelate Ca^{2+} which removes free Ca^{2+} either for use in cellular processes or expulsion from the cell later, ii) compartmentalise Ca^{2+} into organelles such as the sarco/endoplasmic reticulum, mitochondria[102] and, to a lesser extent, the golgi apparatus, lysosomes and the nuclear envelope[103] which act as temporary buffers before expulsion of Ca^{2+} or iii) immediate removal of Ca^{2+} from the cytoplasm through various pumps[100]. The pumps responsible for the transport of Ca^{2+} into and out of the cell are P2-type ATPases, members of the P-type ATPase pump family. Sarco/endoplasmic reticular Ca^{2+} ATPase (SERCA) removes two Ca^{2+} from the cytoplasm into the endoplasmic reticulum (ER) lumen per cycle in exchange for 2-3 protons in the opposite direction[47]. Similarly the plasma membrane pumps Ca^{2+} ATPase (PMCA) transports one Ca^{2+} per ATP hydrolysed[100]. The secretory pathway Ca^{2+} ATPase (SPCA) transports Ca^{2+} into the golgi apparatus and, unlike the structurally similar PMCA and SERCA, is also responsible for the removal of manganese ions. The SERCA, PMCA and SPCA are the primary pumps responsible for $[Ca^{2+}]_i$ maintenance. A secondary mechanism for the transport of calcium is through the P2-type ATPases Na^+/Ca^{2+} exchangers (NCX) and Na^+/Ca^{2+}-K^+ (NCKX) exchangers. These exchange one Ca^{2+} for three Na^+ or co-transport one K^+ with one Ca^{2+} for four Na^+, respectively. NCX and NCKX are responsible for rapid changes in Ca^{2+} concentration, for example those required in action potentials in neurons, whereas the primary pumps, particularly PCMA, maintain low $[Ca^{2+}]_i$ over longer durations[102]. The transient receptor potential (TRP) channels are, usually, non-selective ion channels[100] though some have a more specific role in Ca^{2+} transport such as TRPV6 found in the small intestine, kidneys, colon and exocrine tissues[104]. By far the fastest Ca^{2+} signalling proteins are the voltage-gated Ca^{2+}-selective channels (VGCC) in which one channel can conduct ~1 million calcium ions/ second. A few thousand VGCC per cell can increase $[Ca^{2+}]_i$ by more than 10 fold within milliseconds[100]. The VGCC open pores in the cell membrane of cells undergoing Ca^{2+} signalling by a change in voltage. In addition to this pores can be formed by ligand binding (TRP channels) and store operated Ca^{2+} influx through Stim/Orai channels. Store operated Ca^{2+} influx occurs in non-excitable cells where a depletion in ER Ca^{2+} stores and a loss of Ca^{2+} from cells through PMCA results in the activation of Ca^{2+} influx[105]. The principle components of store operated

Ca^{2+} influx are the endoplasmic Ca^{2+} depletion sensor STIM1 and the pore forming calcium channel sub-unit ORAI1[106]. Additionally, in response to low $[Ca^{2+}]_i$ inositol trisphosphate receptors (IP_3R) in the ER and ryanodine receptors (RyRs) in the ER and SR can be stimulated to release Ca^{2+} into the cytoplasm.

1.4.2 Calcium ions, cancer and cancer cell death

Tumour cells utilise the same calcium channels and pumps as non-tumour cells. However the Ca^{2+} transport mechanisms in tumour cells are usually modified and their expression levels, cellular localisation and function have been observed to be altered[105]. The primary pumps, SERCA and PMCA, have been seen to be both up- and down-regulated to differing amounts in thyroid, colon, lung and breast cancer and in squamous cell carcinoma[100]. IP_3R mRNA levels were upregulated in non-small cell lung cancer and gastric cancer and RyRs mRNA levels were downregulated in thymus cancer[107-109]. The mRNA and protein expression of the TRP channel TRPV6 is upregulated in some cancers and, though not yet fully defined, has been linked to tumour progression and invasiveness in prostate cancer and cancer cell survival in breast cancer[104]. In non-tumour cells the Ca^{2+}-permeable TRPM8 channel is involved in the cellular response to temperature[110] however expression in a wide variety of cancer types has been linked to cancer proliferation, invasion and survival[110]. TRPM8 was found to be overexpressed in a number of pancreatic cancer cell lines (MIA PaCa-2, PANC-1, Panc 02.03, PL45, BxPC-3, Capan-1 and HPAF-II) and was found to be required for uncontrolled growth and progression of the cancer cells[111]. A recent meta-analysis of microarray sets investigating the overexpression of VGCC found that many different VGCC channels are present in a large variety of malignancies, some of which were theorised to have an important role in cancer development and metastasis[112]. Alterations in the flux of Ca^{2+} across cell membranes and the control of $[Ca^{2+}]_i$ can confer cell survival properties to the tumour cell and, importantly, can aid in the evasion of apoptotic cell death[113]. Additionally, the increased expression of anti-apoptotic BCL2 family proteins, commonly found in tumour cells, can reduce Ca^{2+} flux from the ER through the inhibition of SERCA or by binding to IP_3R[114]. BCL2 expression can also decrease mitochondrial Ca^{2+} uptake and increase the ability of the mitochondria to accumulate more Ca^{2+} [115]. Phosphorylation of IP_3R in glioblastoma cells (U87) resulted in decreased Ca^{2+} transport from the ER to the mitochondria and a subsequent reduction in the response to pro-apoptotic signals[116].

One potential reason for why cells homeostatically maintain a low resting $[Ca^{2+}]_i$ is that Ca^{2+} can be cytotoxic[117]. A prolonged increase in cytosolic Ca^{2+} concentration can stimulate Ca^{2+} overload, mitochondrial permeability, mitochondrial ATP depletion and ROS production[118]. If the majority of mitochondria in a cell maintain the ability to synthesise ATP then any loss in ATP may favour apoptotic cell death. However, if ATP depletion is too severe for the activation of apoptosis the cell can potentially undergo necrotic cell death[118]. The targeting of $[Ca^{2+}]_i$ has been suggested to be a possible anti-cancer therapy[100]. Cancer cell lines, Chinese hamster lung fibroblast (DC-3F), human leukaemia (K-562) and a murine lung carcinoma (Lewis Lung Carcinoma), were made permeable to Ca^{2+} through electroporation with isotonic calcium[118]. Cell proliferation was assessed 24 and 48 hours later in which a significant ($p < 0.01$) dose-dependent reduction was observed compared to non-electroporated cells. The ATP levels were measured in the DC-3F cell line following the calcium electroporation in which an immediate drop in ATP levels was observed which remained low at 10.3% ($p < 0.0001$) of the controls at 8 hours post-treatment. Nude mice were then transfected with a human small cell lung cancer cell line (H69) and subjected to the treatment. Reduction in tumour volume occurred in the Ca^{2+}-electroporated tumours which was significantly different ($p < 0.0001$) to the non-electroporated tumours and histological analysis revealed that complete tumour necrosis occurred 6 days post treatment. Thus Ca^{2+} overload is potentially an effective mechanism for the inducement of cancer cell death.

1.5 Photodynamic Therapy

1.5.1 Mechanisms of action

Photodynamic therapy (PDT) is a minimally invasive treatment which can be used to deliver selective phototoxic effect towards a specific target, for example in the treatment of tumour tissue. There are three essential components of PDT - a photosensitising drug, light irradiation and molecular oxygen[119]. A photosensitiser (PhtS) is a light absorbing chemical which, when excited with light at a specific wavelength, elicits a photochemical cytotoxic reaction (table 1.1). The therapeutic light used in PDT is usually in the wavelength range of 600-800 nm. In this wavelength range the energy of each photon of light is high enough (1.5 eV) to excite the PhtS and low enough that the light will sufficiently penetrate into tissue[120]. When a PhtS absorbs a photon of electromagnetic radiation from light energy an electron can be promoted to a higher energy orbital which takes the PhtS from its ground state (S_0) to an electronically excited state (S_n) (figure 1.4). The PhtS can then rapidly lose

energy by decaying through vibrational sub-levels (S_n) via internal conversion (IC) to occupy the first excited singlet state (S_1) before entering into the ground state (S_0)[121]. This decay from S_1 to S_0 occurs via fluorescence. An alternative route can occur in which the excited singlet state electron (S_1) undergoes spin inversion to populate the lower energy first excited triplet state (T_1) via intersystem crossing (ISC)[121, 122]. The excited electron can experience a second spin inversion and depopulate T_1 by decaying to the ground state (S_0) via phosphorescence[120]. The transition of the PhtS from the triplet state (^{3}PhtS*) to the singlet state (^{1}PhtS) is spin forbidden and thus the lifetime of the species in phosphorescence is longer than that in fluorescence. This means that the PhtS in the triplet state exists for a sufficiently long enough time to interact with biological molecules.

After activation of the PhtS with the correct wavelength of light the production of cytotoxic ROS occurs in biological tissue or the cellular environment (i.e. *in vitro* cell culture). Excited PhtS can produce ROS through two mechanisms known as Type I and Type II reactions[121, 122]. Type I reactions involve the transfer of electrons from a substrate molecule to the excited PhtS, either ^{1}PhtS* or ^{3}PhtS*, (oxidation) (Type I(i)) or the transfer of a hydrogen atom to the PhtS (reduction) (Type I(ii)). The radicals formed in these reactions react with molecular oxygen ($^3O_2$) to form a complex mixture of oxygen derivatives (see table 1.1). Type II reactions involve the direct reaction between the PhtS in the excited triplet state (^{3}PhtS*) with $^3O_2$. When the ^{3}PhtS* collides with $^3O_2$ spin inversion of one of $^3O_2$ outer electrons occurs which simultaneously produces singlet oxygen ($^1O_2$) and causes the PhtS to decay to its ground state (S_0) (figure 1.4). The highly reactive $^1O_2$ species then causes cellular damage via apoptotic or necrotic cell death[121]. Type II reactions are widely regarded to be the predominant mechanism of cell damage in PDT.

Table 1.1: Definitions of some of the compounds and species involved in PDT.

Photosensitiser (PhtS)	A light absorbing compound that initiates a photochemical reaction.	Agostinis *et al*. 2011.[119]
Ground state	A state of particles with the lowest energy in a system, this is the usual (singlet) state of most molecules. Molecular oxygen in its ground state, however, is a triplet and can be converted to a higher energy singlet state during PDT.	Agostinis *et al*. 2011.[119] Josefsen and Boyle 2008.[121]
Triplet state	A molecule or free radical in a state in which there are two unpaired electrons.	Agostinis *et al*. 2011.[119]
Singlet oxygen ($^1O_2$)	An excited form of molecular oxygen ($^3O_2$) that has a pair of electrons with opposite spin. More reactive and unstable than $^3O_2$.	Agostinis *et al*. 2011.[119]
Reactive oxygen species (ROS)	ROS is a collective term and includes oxygen radicals ($OH^{\cdot}$, $O_2^{\cdot -}$ etc.) and some non-radical oxygen derivatives (H_2O_2, HOCl, O_3, $^1O_2$ etc.).	Rajendran 2015.[123]
Light fluence rate	The number of particles (photons) that intersect an area in a given time, usually measured in W/m^2.	Rajendran 2015.[123]

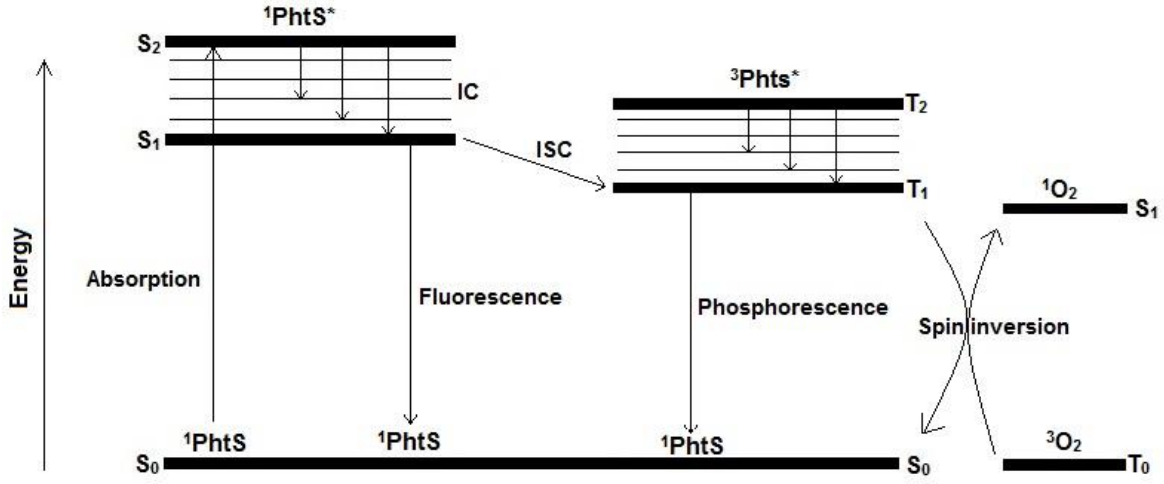

Figure 1.4: Modified Jablonski energy diagram.

A PhtS becomes excited when it absorbs a photon of electromagnetic radiation from light energy causing it to transition from its ground state (S_0) to a higher energy state (S_n). The excited PhtS can then rapidly decay to a lower level singlet excited state (S_1) via IC and return to S_0 by fluorescence or populate the lower energy first excited triplet state (T_1) via ISC. Decay from T_1 to S_0 occurs by phosphorescence. The excited triplet state of the PhtS (^{3}PhtS*) can react directly with molecular oxygen ($^3O_2$) to produce highly reactive singlet oxygen ($^1O_2$). Image modified from Josefsen LB, Boyle RW. Metal-based drugs. 2008;2008: 276109.

1.5.2 Photodynamic therapy and cancer

PDT can be used to deliver targeted anti-cancer therapy to tumours[119]. A photosensitising drug can be delivered to the tumour by intravenous injection or topical application and light can be guided to specific areas within the body using flexible optical fibres. The theory of using PDT as an anti-cancer therapy is based on the aim of increasing ROS accumulation in tumour tissue to over the tolerance threshold so that cell death is induced[124]. Tumour cells have a higher basal level of ROS than non-tumour cells and thus, theoretically, would be easier to bring to the cell-death threshold[124]. As well as direct cytotoxic/ phototoxic action on tumour cells PDT can enhance the chance of cell death through the induction of the inflammatory response and damage to tumour vasculature. PDT induced tumour cell injury promotes an inflammatory response in the body in a similar manner to damage to non-tumour cells so that the inflammatory response and innate immune system work to remove dead and irreparable tumour cells[125, 126]. PDT has been used in the treatment of abundant vessel growth in age-related macular degeneration[127] as preferential damage to vasculature can be manipulated through the use of a short drug-light interval. This is the time between administration of the photosensitising drug and the application of light irradiation. When introduced intravenously the PhtS is present in the vasculature and thus application of light treatment a short interval later (highly dependent on a PhtS pharmacokinetics) can localise damage to blood vessels. This method could potentially be applied to cancer therapy as a target for tumour angiogenesis or vasculature in the tumour vicinity.

PDT has clinical approval in the United States, Canada and European Union for the treatment of a variety of premalignant and malignant conditions such as skin cancers (actinic keratosis, Bowen's disease, basal cell cancer)[128, 129], localised head and neck cancers (oral cavity, pharynx and larynx carcinomas)[11, 130], oesophageal cancer (and Barrett's oesophagus)[131], prostate cancer, bladder cancer, brain tumours and non-small cell lung cancer[119]. The assessment of the effectiveness of PDT treatment in many other cancer types at the pre-clinical and clinical trial stages has been reported in the literature.

As the focus of this study was ovarian and pancreatic cancer the reports for these cancers will be concentrated on here. A panel of gemcitabine-non-responsive pancreatic cancer cell lines, consisting of AsPC-1, BxPC-3, Capan-1, Capan-2 and PANC-1, was PDT treated with a benzoporphyrin derivative (BPD) PhtS known as verteporfin[132]. The cell viability of the cancer cell lines was measured after light irradiation and was found to be reduced in both

a light fluence and total BPD-PDT dose dependent manner. The response was cell line specific, with AsPC-1 and PANC-1 being more resistant than the other cancer cell lines, however a total dose of ~6 μM·J/cm^2 was enough to reduce cell viability of all cell lines to 0%. Interestingly, the relatively high expression of the anti-apoptotic factor Bcl-xL was shown to decrease in response to PDT and a shift towards pro-apoptotic factors (Bax) was observed. PDT has also been shown to be effective against the *in vitro* cell cultures of ovarian cancer using different culture techniques. OVCAR5 ovarian cancer cells were cultured as 3D micronodules and treated with verteporfin so that the effect of PDT on total volume and live volume of the *in vitro* tumours could be assessed[133, 134]. Fluorescent imaging revealed that the PhtS was able to penetrate through the entirety of the nodules and that uptake occurred in a concentration dependent manner. A reduction in the live volume and thus viability of the nodules occurred at a total verteporfin-PDT dose of 10 μM·J/cm^2. A high density culture film of OVCAR5 cells was used to assess the effect of simultaneous delivery of PhtS and singlet oxygen, via a fibre-optic probe, on PDT outcome[135]. As PDT is dependent on a supply of molecular oxygen its effectiveness can be reduced in areas of hypoxia[136] especially in the hypoxic tumours of the peritoneal cavity. Thus a system which can deliver PhtS, oxygen and light irradiation to hard to reach tumours could potentially be beneficial in the clinical setting. Irradiation of the cell cultures for 1 hour reduced their cell viability by 60±5% and no cell damage was observed through force of the fibre-optic probe.

Murine models, transplanted with ovarian cancer (OVCAR3) and pancreatic cancer (AsPC-1 and PANC-1), have also been used in the pre-clinical assessment of PDT. Treatment with an immunoconjugated PhtS, that is a PhtS attached to a monoclonal antibody (mAb), which recognised a specific antigen on OVCAR3 cell surfaces significantly increased median survival in PDT treated mice compared to untreated (non-irradiated) control mice ($p = 0.0006$)[137]. Verteporfin-PDT, in increasing light doses of 10, 20 and 40 J/cm, was used to treat AsPC-1 and PANC-1 transplanted SCID mice[138]. MRI analysis revealed a positive relationship between increased light dose and increased tumour volume which was found to be due to PDT-induced inflammation of the surrounding tissue. An exception was the 40 J/cm treated AsPC-1 tumours which were decreased in volume due to extensive necrosis in the tumour and surrounding tissue. In addition, histological analysis showed that, while 40 J/cm induced complete necrosis in AsPC-1, less extensive cell death occurred in PANC-1 tumours. Thus this study highlighted that PDT effect in clinical trials may show a

heterogeneous range of results and individual treatment effect would need to be considered[138].

A phase I trial involving 16 patients with inoperable pancreatic adenocarcinoma was conducted using Foscan® (*meta*-tetrahydroxyphenylchlorin, *m*THPC)-PDT and a percutaneous delivery of light irradiation using fibres that were delivered to the tumour by CT guidance[139]. Application of light treatment was performed 3 days after PhtS administration. Extensive necrosis of all the pancreatic tumours was observed by CT scan though response to treatment varied between patients with the area of necrotic tissue ranging from 9-60 cm^3 (median 36 cm^3). In an attempt to improve upon the relatively long drug-light interval applied in the above study, Huggett *et al*.[140] used a verteporfin PhtS which required only a 60-90 minute interval in a Phase I/II trial involving 15 patients with inoperable pancreatic adenocarcinoma. Though a light dose of 40 J/cm consistently produced lesions of 12 mm in all tumours imaged by CT, the volume of necrosis varied considerably between patients (range 0-23 cm^3, mean 3.5 cm^3). However, the verteporfin PhtS had a fast accumulation in the tumour tissue, hence the shorter drug-light interval, and a fast clearance by excretion in the bile was observed. Therefore prolonged photosensitivity was not a problem as in the study involving Foscan®-PDT[139].

In addition to direct anti-cancer application PDT has been used as an alternative/ synergistic approach to other major anti-cancer therapies; chemotherapy, radiotherapy and surgery[15, 141, 142]. For example, PDT in combination with gemcitabine treatment of pancreatic cancer (SW1990) xenograft tumours in nude mice showed a significantly enhanced reduction in tumour volume compared to the PDT treated and chemotherapy treated only control groups ($p < 0.05$)[141]. An advantage of PDT as an anti-cancer therapy is that it does not compromise the effect of chemotherapy, radiotherapy or surgery and thus can be used in conjunction with these treatments, as a first-line treatment before major therapies for example in the case of highly localised tumours, or after treatment to improve patients' quality of life when other therapies have failed[119]. PDT has also been shown to produce good cosmetic outcomes in skin cancer and provide retained functional abilities in localised head and neck tumours due to minimal fibrosis in normal tissue[11, 143]. However, the clinical outcome of PDT can vary between patient (and cancer cell line/ tumour type or specific area of tissue), largely due to differences in the optical properties of tissues, and a uniform effect is difficult to achieve due to the complex tumour microenvironment[138, 139, 144]. The main drawback of PDT treatment with regards to oncology is the lack of specificity

of PhtS to tumour tissue. Accumulation of PhtS in non-tumour tissue has led to prolonged photosensitivity in patients and damage to surrounding normal tissue[119].

1.5.3 Photosensitisers

The majority of PhtS used in cancer therapy are based on the tetrapyrrole structure similar to the protoporphyrin in haemoglobin[119]. The best characterised class of PhtS are the porphyrins, discovered over 150 years ago, though there are a large number of different PhtS classes including texapyrins, phthalocyanines, chlorin derivatives and the less well characterised antracens, chlorophyll derivatives, porphycenes, purpurins, hypocrellins and hypericin[122, 145]. The first clinically approved PhtS was haematoporphyrin derivative (HPD) which was a complex mixture of porphyrin monomers and oligomers. Partial purification of the most active oligomers by HPLC[122] lead to the commercially available porfimer sodium compound (Photofrin®) which gained clinical approval for the treatment of early stage lung cancer in 1998 and Barrett's oesophagus in 2003[120]. Photofrin® has some major disadvantages which limited its successful clinical application. Firstly, it is not selective to tumour tissue and so results in significant uptake in cutaneous tissue for 4-10 weeks post-administration. Thus it has resulted in prolonged photosensitivity with patients having to avoid direct sunlight[122, 145]. Secondly, the absorption band most often used to excite the PhtS is its weakest (630 nm) which has limited its depth of tissue penetration[120] and thus relatively high doses and high fluence rates are required to stimulate the same effect as newer PhtS. An effort has been made to develop second generation PhtS which have longer wavelength absorptions and more rapid clearance from the skin. Several criteria for the 'ideal' PhtS have been proposed[119, 122, 145] to name a few; a PhtS should be chemically pure to allow manufacturing reproducibility and a known composition, be stable in storage, have a high absorption peak (600-800 nm), high capacity to form ROS upon irradiation, no dark toxicity, preferential tumour retention, fast tumour accumulation and a relatively fast clearance from normal tissue. While no PhtS has met all these criteria the second generation of PhtS have offered significant improvements over the HPDs.

One of the most promising second generation PhtS is 5-aminolevulanic acid (ALA) (Levulan®) and its esters (methyl ester (Metvix®) and hexyl ester (Hexvix®)[120]. ALA itself is not a PhtS but is a pro-drug that requires mitochondrial conversion into the naturally occurring PhtS protoporphyrin IX (PpIX). ALA was clinically approved for the treatment of actinic keratosis in 1999 and later basal cell skin carcinoma[120, 145]. Another promising PhtS is BPD monoacid A (BPD-MA) or verteporfin which was approved for the treatment of age-

related macular degeneration in 2000[120] and has shown promising results in a number of pre-clinical and clinical oncological studies[132, 133, 138, 140] though has not yet gained clinical approval. *m*-THCP (Foscan®) is a chemically pure chlorin derivative and a relatively potent PhtS requiring both low doses (0.1 mg/kg) and low fluence rates (10 J/cm^2)[145]. *m*-THCP has been shown to have short skin photosensitivity (~15 days), produce a high yield of singlet oxygen and be considerably more effective than Photofrin® PDT[146]. It was approved for the treatment of head and neck cancers in 2001 and has shown promising results in clinical trials with prostate, pancreatic and oesophageal cancer and mesothelioma[120].

1.5.3.1 Porphyrin

Porphyrins are highly conjugated heterocyclic tetrapyrroles that were first investigated for their PhtS-PDT properties over 45 years ago[147]. Porphyrins are found naturally, for example as haem in animals (conveying the red colour) and chlorophyll in plants (green colour)[148]. Free porphyrin derivatives, such as PpIX and haem, can cause oxidative stress and subsequent cell injury in tissue and so cells utilise a number of mechanisms to maintain low levels such as haem degradation, rapid consumption in haemoprotein synthesis and the extracellular transport of free porphyrins[148]. As synthesised cyclic tetrapyrroles are inherently similar to those found in nature they have little cytotoxicity in the absence of light[121]. The heterocyclic macrocycle, known as a porphine, is at the heart of the porphyrin skeleton and can become a porphyrin when substituted with non-hydrogen atoms or groups at either the meso- or β-hydrogen positions (figure 1.5). Due to their heterocyclic structure porphyrins typically have absorption in the visible light range and tend to have a characteristic ultraviolet-visible (UV-vis) spectrum. Usually porphyrins display an intense, relatively large, absorption band at ~400 nm known as the Soret band and then four weaker bands at ~450-700 nm known as the Q bands (figure 1.6a)[121]. The Soret band is the result of the transition of (porphyrins) electrons from the ground state (S_0) to the second excited singlet state (S_2)[121] (figure 1.6b). Whereas the Q bands are the result of a weaker transition to the first excited singlet state (S_1). The dispersion of energy via IC is so rapid that fluorescence can only be observed when the porphyrin transitions from S_1 to S_0. Porphyrins are very efficient at undergoing ISC and therefore have a high possibility of being converted into the excited triplet state (^{3}PhtS*) and reacting with $^3O_2$ to produce $^1O_2$ making them attractive PhtS in PDT.

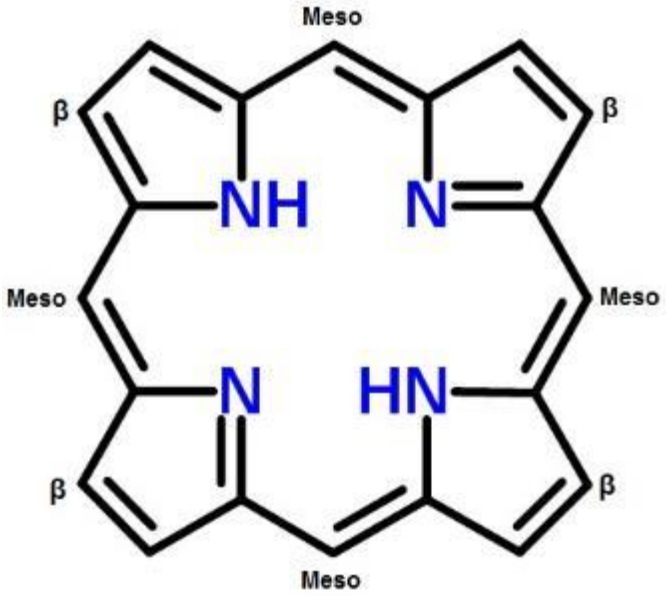

Figure 1.5: Porphine macrocycle structure.

The porphine is the heart of the porphyrin skeleton and can be substituted at the meso- and β-hydrogens to form a variety of porphyrins. Image adapted from ChemSpider, Royal society of Chemistry CSID: 10447586, (http://www.chemspider.com/Chemical-Structure.10447586.html). Accessed Nov 11, 2016.

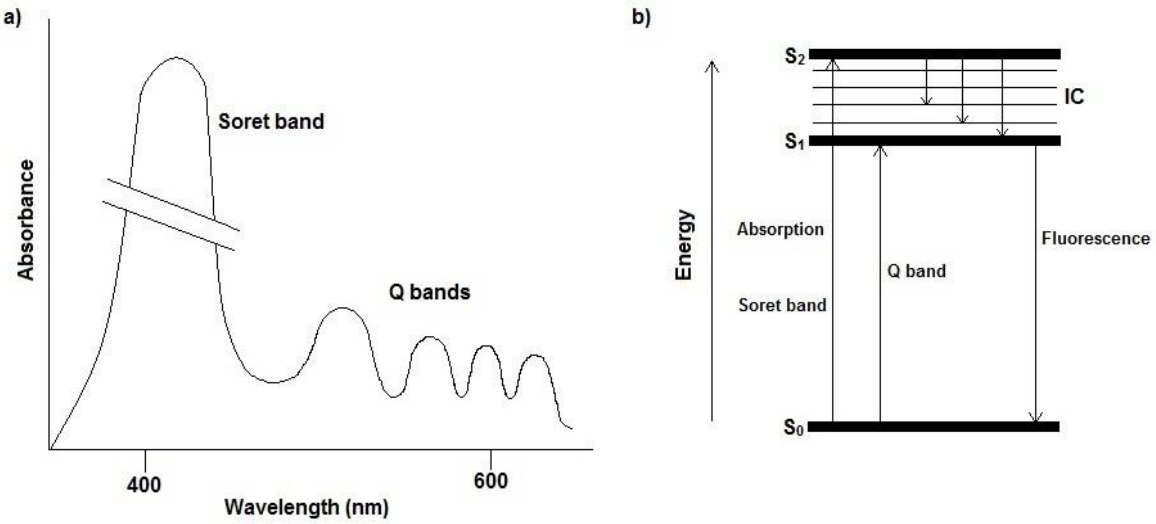

Figure 1.6: Soret and Q bands of porphyrin.

a) Typical UV-vis spectrum of a porphyrin. b) Jablonski energy diagram for a porphyrin's Soret and Q bands. Images modified from Josefsen LB, Boyle RW. Metal-based drugs. 2008;2008:276109.

Porphyrins have been reported in the literature to be effective PhtS in the PDT treatment of cancer. The porphyrins TTP (5,10,15,20-tetra-p-tolyl porphyrin) and THNP (5,10,15,20-tetra-p-naphthyl-porphyrin) were incubated with a melanoma cell line (WM35) for 24 hours before irradiation with 4.5 J/cm^2 red light (630 nm)[149]. Both of the porphyrins were shown to reduce cell proliferation in a concentration dependent manner and TTP significantly reduced the cell proliferation compared to non-irradiated controls at 0.1 μg/ml ($p \leq 0.003$) and THNP at 1 μg/ml ($p \leq 0.02$). A relatively high cytotoxic effect occurred in the irradiated cells at 100 μg/ml for TTP and 500 μg/ml for THNP though no dark toxicity was observed for either PhtS. Recently, primary epithelial cells cultured from patients with prostate cancer were PDT light treated using the porphyrin 5-[aminobutyl-N-oxycarbonyl)phenyl]phenyl]-10,15,20-tris(N-methyl-4-pyridinium) porphyrin trichloride.[150] Treatment was shown to reduce cell survival by 80-90% at the highest concentration (50 μM). The half maximal inhibitory concentration (IC_{50}) values ranged from 13-18 μM. The porphyrin was then assessed for its ability to prevent colony forming of the prostate epithelial cells in which this ability was completely eliminated at concentrations >37.5 μM. The production of ROS (H_2O_2) was detected only in cells that had been both PhtS treated and light irradiated and the production was seen to increase in a PhtS concentration dependent manner. The major route of cell death following the treatment was found to be necrosis with a number of cells also undergoing autophagy, apoptosis was not observed in any of the cells[150]. The porphyrin 5-[4-(N-succinimidyloxycarbonyl)phenyl]-10,15,20-tris(4-methylpyridinium) porphyrin trichloride has been shown to exhibit antibacterial properties, be an efficient cytotoxic after 5 minutes of light treatment and be stable against photodegradation[151]. This PhtS was chosen for use in this study as it was a promising candidate for the production of PDT-induced cytotoxicity in cancer cells.

The main disadvantage of PDT in regards to oncology is the lack of specificity that most PhtS have towards tumour tissue. An accumulation of PhtS in non-tumour tissue has led to prolonged photosensitivity and damage to normal tissue[119]. Additionally, the low targeting of tumour tissue means that some PhtS need a long time to reach sufficient levels in the tumour and so a relatively large dose can be required[152]. To overcome this there has been the development of PhtS conjugated to biological molecules that can specifically target tumours via binding to structural features overexpressed or enhanced in tumours. A number of porphyrin PhtS were developed by Sutton *et al*.[153] which allowed conjugation to biological molecules under mild conditions through direct reaction with an isothiocyanate group on the porphyrin and the primary amino group on the side chain of lysine residues.

Using this method the single chain Fv (scFv) antibody fragment LAG3 was conjugated through its lysine residue to the porphyrin 5-(4-isothiocyanatophenyl)-10,15,20-tris(N-methyl-4-pyridinium) porphyrin trichloride[154]. LAG3 was identified as an antibody fragment that specifically recognises colorectal cancer cells. Its *in vitro* binding ability to the colorectal cancer cell line Caco-2 was shown to be unaffected by the conjugation. After treatment with 15 J/cm^2 light irradiation a concentration of 0.85 μM was seen to induce 30% cell inhibition. No effect on cell proliferation was observed using the negative scFv control (anti-NIP), unconjugated LAG3 scFv or dark control (i.e. non-irradiated) PhtS conjugate. Treatment with LAG3 at a low lethal dose (LD_{25}) revealed that apoptosis and necrosis were stimulated in the cancer cells. Due to their relatively small molecular size scFv fragments tend to have a rapid blood clearance which means that they tend not to accumulate in non-target tissues[152]. Thus as carriers for a PhtS they could offer the advantage of a low risk of damage to non-tumour tissue. Another example of the conjugation of a porphyrin to a carrier with tumour-selectivity is the chlorin-e6 (Ce-6) (a porphyrin derivative) low-density lipoprotein (LDL) conjugate (Ce-6-LDL)[155]. Uptake of the LDL-conjugated Ce6 was analysed using the retinoblastoma cell line Y79 which expressed receptors for the LDL. Uptake occurred in a time and temperature dependent manner and was saturable at ~1 hour. The uptake of the conjugate was shown to be significantly enhanced over the free and mixed (unconjugated Ce-6 and LDL) Ce-6 compounds. Light irradiation (10 J/cm^2) of Ce-6-LDL treated cancer cells reduced cell survival by 80% compared to 10-20% in the mixed Ce-6 treated cells and 0% in the free Ce-6 treated cells[155]. Recently, derivatives of 5,10,15,20-tetrakis(carboxyphenyl) porphyrin (TCPP) were conjugated to silicon resin nanoparticles[156]. Before conjugation to the nanoparticles the redox-responsive (responds to ROS stimuli) TCPP derivatives were shown to be able to produce $^1O_2$ in response to different doses of both white (400-700 nm, 41 mW/cm^2) and red light (630-700 nm, 89 mW/cm^2). Both UV-vis and fluorescence spectroscopy analysis revealed that encapsulation of the control and redox-responsive TCPP into nanoparticles had no effect on the photophysical properties of the PhtS. The redox-responsive PhtS produced higher amounts of $^1O_2$ than the control PhtS however the conjugation to nanoparticles had reduced the efficiency at which $^1O_2$ was produced. Irradiation of HeLa cancer cells with red light for 20 minutes showed that the redox-responsive porphyrin-nanoparticles significantly reduced cell survival compared to the non-irradiated cells and the control PhtS at concentrations as low as 0.01 μM (IC_{50} was 0.1 μM). However there was some phototoxicity produced by the control porphyrin-nanoparticles at concentrations

>0.5 μM[156]. These studies showed that by conjugating PhtS to biological molecules or carriers it is possible to produce a more specific reaction against cancer cells during PDT.

1.6 Chorioallantoic membrane

1.6.1 Chick embryo and chorioallantoic membrane development

The chick embryo and chorioallantoic membrane (CAM) is an established method to study treatment effect on embryo development, viability of the embryo/ CAM and on tumour xenografts implanted either on the CAM or in the chick embryo. Due to the transparency of the CAM (figure 1.7a) treatment effect can be observed and imaged as it progresses, a benefit gained from the CAM model over more complex mammalian models that require more difficult and expensive imaging techniques. Chick embryo development lasts 21 days before hatching[157]. During this time three extraembryonic membranes are formed; the yolk sac membrane, the amnion and the CAM, which enclose and support the developing embryo. The CAM is formed on the 3rd-4th day of embryo incubation and is produced from the fusion of the chorion and the allantois. The CAM consists of three layers, the ectoderm, mesoderm and endoderm. The ectoderm is the most exterior layer of the CAM and is composed of an epithelial layer from the chorion. The mesodermal layer, formed from the allantois, is a highly vascularised mesenchyme that is supplied by a set of paired allantoic arteries and paired allantoic veins. These are connected to the chick embryo's blood circulation and are associated with lymphatic vessels[158]. The endodermal layer is also formed from the allantois and is comprised of allantoic epithelium[157]. The CAM increases in size over chick embryo development, from ~6 cm^2 on the 6th day of incubation to ~65 cm^2 on the 14th day and becomes closely pressed against the egg shell membrane and covers the majority of the yolk sac by the 16th day (figure 1.7b)[157]. The main function of the CAM is to serve as a gas exchange membrane which receives oxygen and eliminates carbon dioxide through pores in the egg shell. The CAM also plays an important role in the storage of excretions, the transport of sodium and chloride from the allantoic sac[158] and the movement of calcium from the egg shell to the chick embryo and yolk[159].

Chick embryos are naturally immunodeficient in the earlier periods of incubation and an immune system is not developed until the 2nd week of incubation[157, 158]. Alike to other vertebrates chickens are protected by a dual immune response consisting of T and B lymphocytes which can be first detected on the 11th and 12th day of incubation, respectively. Also on the 12th day monocytes and macrophages can be found in various sites including the yolk sac, liver, spleen, bursa, gut and thymus[160]. The chick immune

system (along with the vascular system) is fully established on the 18th day of incubation and thus the chick becomes immunocompetent[161]. The CAM contains extracellular matrix proteins such as laminin, fibronectin, collagen and some of their integrin receptors[22]. Several of these characteristics change during embryo development such as the degree of differentiation of endothelial cells and blood vessels, the extracellular matrix composition and the location of blood vessels within the CAM[158]. Thus careful consideration of the developmental stage of the chick embryo must be made in CAM model experiments with an emphasis on the use of eggs at the same day of incubation otherwise comparisons between experiments become difficult.

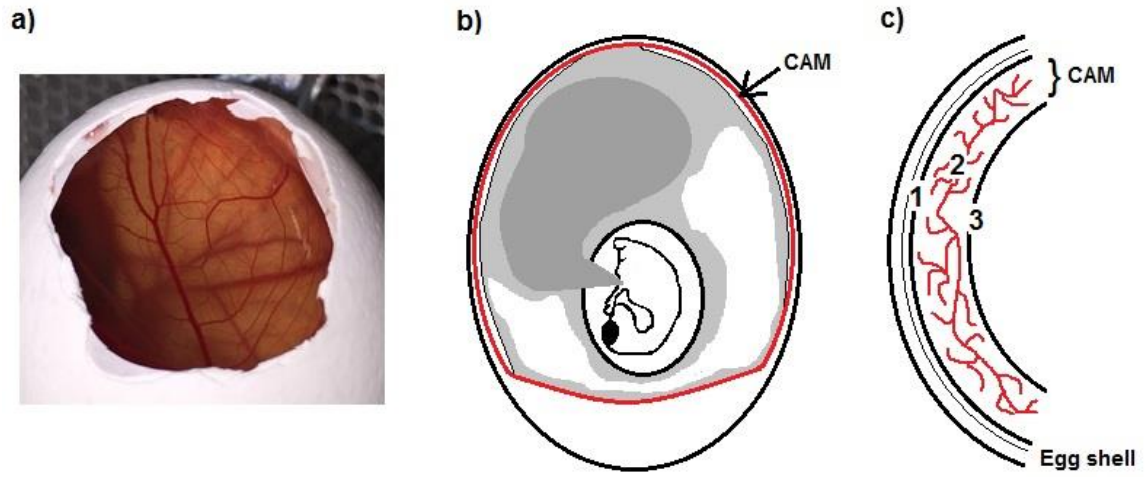

Figure 1.7: The chorioallantoic membrane.

a) Image of CAM from opening in egg shell. b) Position of CAM (red) around chick embryo and in contact with the egg shell. c) Cross-sectional illustration of the CAM, 1 – ectoderm, 2 – vascularised mesoderm and 3 – endoderm.

1.6.2 Chorioallantoic membrane and cancer

The natural immunodeficiency of the chick embryo in the early stages of development means that the conditions for tissue rejection are not yet present and thus the CAM provides an excellent model for the study of tumour xenografts. The successful transplantation of tumour tissue onto the CAM was first described in the literature in 1912 by Murphy and Rous[162]. Though the reason for this was quickly suggested to be due to a lack of 'natural defence'[163] an understanding of the immune response and immune system development in the chick embryo was defined around 50-60 years later[161, 164]. Tumour cells grown on the CAM display many *in vivo* characteristics such as angiogenesis, mass development and metastasis[158]. Tumour xenografts are typically formed 2-5 days after cells are implanted on the CAM and a visible mass can be seen. In this time the tumour

xenografts stimulate angiogenesis of the CAM blood vessels, often observed as a spoke-wheel pattern surrounding the tumour, which penetrate the tumour mass[157]. Due to the presence of extracellular matrix components the CAM model can provide a mimicry of the physiological tumour microenvironment[22].

The CAM model has been utilised in oncological research for the assessment of anti-cancer agents, primarily with a focus on their antiangiogenic effects. Anti-cancer agents can be assessed on the CAM through a number of physiologically relevant delivery routes; applied topically to the CAM, intravenously injected into the CAM blood supply, amnion or yolk sac and intraperitoneally injected within the body of the chick embryo. The CAM can offer a relatively easy and cost effective model for the gain of early information about drug biodistribution, toxicity, activity and pharmacokinetics before application to more complex *in vivo* mammalian models[158]. Microspheres consisting of poly(D,L-lactic acid) (PLA) and ethylene-vinyl acetate (EVA) polymers were loaded with paclitaxel, an anti-cancer drug with antiangiogenic properties[165]. On the 6th day of embryo incubation the paclitaxel microspheres (0.6% w/v) were applied topically to the CAM. A zone of avascularity, taken to mean angiogenesis inhibition as a result of vessel occlusion, regression and disruption, occurred on all of the CAM (9/9) around the area of treatment application (2 days post-application). Whereas the CAM treated with the paclitaxel-free control microspheres had normal blood vessel architecture. Another study looked at the effect of two metal based anti-cancer agents (ruthenium(II)-*p*-cymene complexes) on ovarian tumours (A2780) on the CAM[166]. The intravenous injection of the compounds into the CAM vasculature resulted in significant changes ($p = 2.8x10^{-5}$) to blood vessels compared to untreated controls in particular to the number of branching points in larger vessels. Tumour growth was reduced by both of the compounds when administered separately and in combination (63-88%) compared to untreated controls. Histological analysis revealed a reduction in blood vessel density within the treated ovarian tumours. Graphene oxide treatment of a glioblastoma cancer cell line (U87) grown as tumour xenografts on the CAM reduced tumour volume by 43% and weight by 41% compared to untreated controls[167]. While the blood vessels in the treated group appeared smaller compared to the controls no direct antiangiogenic effect was proposed and tumour reduction was associated with graphene oxide-induced apoptotic cell death and a reduction in cell proliferation. A toxicological study investigated whether the CAM could be used as a predictive model for acute drug toxicity studies[168]. The LD_{50} of 10 approved anti-cancer agents (paclitaxel, carmustine, camptothecin, cyclophosphamide, vincristine, cisplatin, aloin, mitomycin C, actinomycin-D and melphalan)

were determined on CAM and then compared to the LD_{50} values gained from rodent models reported in the literature[168]. A moderate correlation was found between the LD_{50} of all the intravenously injected drugs between CAM and mice models (Pearson's correlation coefficient $r = 0.68$, $p < 0.005$) and CAM and rat models ($r = 0.42$, $p < 0.05$). Interestingly, though administered via different routes, the intravenous injection of the drugs in CAM also had moderate correlation with intraperitoneally injected mice ($r = 0.50$, $p < 0.05$) and rats ($r = 0.55$, $p < 0.05$). Therefore the CAM may be a viable model for the screening of anti-cancer agents before full toxicological studies are undertaken in rodents or other animal models.

The CAM model can also be used to study tumour metastasis and cancer cell invasion properties. Tumour cells can migrate from the original CAM tumour site into the mesodermal layer where they can actively enter the vasculature and migrate to secondary tissues and organs[157]. Therefore important information can be gained on the ability of different cancer cell lines to penetrate the chorion epithelium, invade the mesenchyme, survive in the circulation, arrest in vasculature and proliferate in distant organs[157]. Post-mortem examination was performed on chicks that had squamous cell carcinoma transplanted onto the CAM or injected subcutaneously into the chick embryo[164]. Metastatic tumours were found only in CAM transplanted chicks. Those that hatched from the egg with tumours over 4x4 mm had a median survival of 8 days (range 1-29 days) and widespread metastases were found in tissues with filtering capacity; heart, liver, kidneys, brain, and other sites including skeletal muscle, subcutaneous connective tissue, eye, beak and gastrointestinal tract. Tumour cells that have migrated from the original transplantation site can be seen directly on the CAM through the visualisation of tumour micro-nodules close to the original site. This was seen with osteosarcoma (MNNG-HOS) tumour xenografts which formed multiple nodules on the underside of the CAM[169]. The migration and invasive properties of three ovarian cancer cell lines (OV-90, OVCAR3 and SK-OV-3) were compared by histological analysis of the CAM layers[22]. Invasion of the cancer cells into the mesoderm was assessed on the 14th day of chick embryo incubation. The cancer cell lines destroyed the ectodermal layer and invaded and proliferated in the mesodermal layer to varying degrees with the most invasive being OV-90 and the least OVCAR3. The CAM model closely resembled the *in vivo* invasion of ovarian cancer cells in the peritoneum. The RNA silencing of CD147, a glycoprotein associated with poor prognosis in malignancy, in MIA PaCa-2 CAM xenografts resulted in a reduction in invasiveness (91% of tumours with no CD147 silencing had invasion of the CAM compared to 50% of CD147

silenced tumours)[170]. Thus the CAM model showed that CD147 is potentially important in the invasiveness of pancreatic adenocarcinoma.

1.6.3 Chorioallantoic membrane and photodynamic therapy

The CAM model has been used in PDT studies with regards to the assessment of PhtS antiangiogenic effects and their anti-cancer potential. A number of porphycene PhtS were incorporated into liposomes, which were used as delivery vehicles, and applied to the CAM[171]. Uptake of the PhtS into the CAM was shown to increase over time with rapid uptake occurring in the first 15 minutes and then a slower period of uptake up to 40 minutes and was independent of the liposome vehicle used (egg PC or dipalmitoylphosphatidylcholine). Non-cancerous fibroblastic tumours grown on the CAM surface were systemically treated, through injection into the yolk sac, with the PhtS at 5 µg/G chick embryo body weight 24 hours prior to a 30 minute irradiation period. The irradiated tumours were reduced to 10% of their original area and were less proliferative compared to the non-irradiated tumours. The reduction in tumour area was proposed to be due to tumour cell necrosis. Complete tumour regression occurred ~100 hours post-irradiation. Direct treatment of the CAM plus PDT light irradiation caused changes to blood vessel morphology and optical density (OD). Changes in OD were measured by subtracting the OD of a perfused vessel from the CAM background. During irradiation small arterioles were seen to darken which was associated with constriction of the vessels, reduced by 55% of their original width. Venules were rapidly blanched (4-16 minutes) during irradiation due to emptying of the vessels and larger arterioles were observed to be occluded 3-4 hours post-irradiation[171]. Thus the CAM was effective in monitoring the effect of PDT treatment, both in real-time and post-irradiation, on blood vessels and tumour. Another study that incorporated porphycene PhtS into liposomes revealed differences in toxicity between *in vitro* cell culture and the *in vivo*-like CAM environment[172]. The porphycenes resided at different depths in the liposomes dependent on hydrophilic side chains which influenced the effect PDT had on cultured canine epithelial cells (MDCK). The deeper the embedded PhtS the less damage was caused. The depth of the PhtS was not, however, an influential parameter on the blood vessel damage observed in the CAM. It was theorised that this difference was a result of the fusing of liposomes to epithelial membranes *in vivo* which delivered the PhtS more effectively to the tissue. Thus the CAM model could potentially be used to evaluate any differences in drug delivery mechanisms between *in vitro* and *in vivo* tumour models. The CAM was used to assess the efficacy of PDT effect of a number of topically applied PhtS; Photofrin®, ALA, verteporfin, lutetium texaphyrin (lu-tex) and

chloro-aluminium phthalocyanine ($AlPcS_n$)[173]. The effect of different PDT parameters on the inducement of vessel damage by the different PhtS was investigated in which it was found that the order of importance of each parameter was unique to each PhtS. However, similar trends were observed for all PhtS where vessel damage was increased with increased light dose (5 J/cm^2 compared to 10 J/cm^2), longer irradiation time (30 minutes compared to 90 minutes), power density (33 mW/cm^2 compared to 100 mW/cm^2) and increased drug dosage (0.1-5 μg/cm^2). With the exception of verteporfin, vessel damage was observed to occur more frequently in arteries than veins, similar to results observed in PDT treated rats[174]. The CAM model provides a relatively simple means of assessment for the topical application of PhtS. However intraperitoneal injection into the chick embryo allows the PhtS to be delivered to the tumour via the CAM blood circulation and therefore mimics the application of PhtS to non-surface tumours *in vivo*. The intraperitoneal injection of the PhtS used in the previous study (ALA, $AlPcS_n$, verteporfin and lu-tex), plus light irradiation, was found to produce higher vascular damage in the CAM than the topical application[175]. Intraperitoneal injection of ALA into the chick embryo and its uptake into an ovarian tumour xenograft (NuTu-19) was monitored via fluorescence microscopy[176]. Higher vascular damage in the CAM occurred with an increase in PDT light dose. Increase in uptake in both the tumour xenograft and blood vessels occurred in a time dependent manner. The increase in fluorescence showed that the chick embryo was able to convert the non-fluorescent ALA into its photoactive form PpIX. The CAM model was used in the evaluation of nanoparticles as a drug delivery system for a hydrophobic porphyrin, these PhtS can be difficult to administer intravenously in their free form due to their lipophilicity[177]. The porphyrin derivative, meso-tetra(*p*-hydroxyphenyl)porphyrin (*p*-THPP), in poly(D,L-lactide-*co*-glycolide) (PLGA) nanoparticles and the free form (free- *p*-THPP) was injected into the CAM vasculature. Fluorescent angiographies showed that both forms became rapidly (5 seconds post-administration) distributed within the intravascular spaces while the extravascular space remained free from fluorescence. However, the nanoparticle bound form had an enhanced ability to remain within the vasculature for up to 25 minutes post-administration whereas the free- *p*-THPP had already been extravasated. Irradiation of the *p*-THPP-PLGA nanoparticles resulted in the closure of small CAM vessels (<30 μM) and the partial closure of higher order vessels. This effect was increased with increased PhtS dose. In all light dose and PhtS dose conditions the PDT effect of the nanoparticle bound *p*-THPP was significantly greater than the free- *p*-THPP ($p = 0.024$).

1.7 Aims

The overall aim of this project was to gain an understanding of the effect that duramycin had on tumour cells so that it could be characterised as a potentially novel cancer targeting agent. Thus the initial aim of this project was to characterise the PE detection abilities of duramycin on a number of different cancer cell lines and also to assess its cytotoxic abilities. Additionally, the anti-proliferative effects of duramycin were evaluated on both 2D and 3D cancer cell cultures. The mechanism through which duramycin causes cell death is yet to be elucidated in detail. Therefore, another aim of this project was to investigate whether the necrotic and apoptotic cell death induced by duramycin, as had been observed in earlier experiments, was a result of some form of Ca^{2+} overload. Another aim of this project was to develop a duramycin-PhtS conjugate that would potentially have an enhanced anti-cancer effect over both the unconjugated free PhtS and unconjugated duramycin. Finally, a preliminary investigation into the anti-cancer effect of the newly synthesised duramycin-PhtS conjugate on *in vivo* tumours was performed using ovarian and pancreatic tumour xenografts on the CAM. The aim of these experiments were to provide early evidence for whether duramycin plus light irradiation had the ability to effect tumour viability.

1.7.1 Objectives

- To address the initial aim of the project (the characterisation of duramycin's PE detection and cytotoxic abilities) a number of cancer cell lines representing different cancer types were analysed for PE expression by flow cytometric detection of fluorescently labelled (fluorescein isothiocyanate (FITC) labelled tertiary antibody) duramycin.
- Flow cytometry was also used for the determination of cell viability of ovarian and pancreatic cancer cell lines following duramycin treatment.
- The anti-proliferative effects of duramycin treatment on 2D and 3D cancer cell cultures was then evaluated using a colourimetric cell proliferation assay.
- To address whether duramycin-induced cell death was due to Ca^{2+} overload the $[Ca^{2+}]_i$ of ovarian and pancreatic cancer cell lines, following the addition of duramycin, was measured via a spectrofluorometric method and subsequently by confocal microscopy.
- In addition, an effect on cancer cell membrane integrity was explored. This avenue was followed as the literature had reported that duramycin could affect cell membranes by creating non-selective pores[88, 89, 178, 179] and effect ion transport[70, 84, 86, 87, 91] and that its derivative cinnamycin could cause haemolysis of erythrocytes[180].

- In this study, cell surface PE detection and a reduction in cell viability with duramycin was observed in a normal endothelial cell line. Thus, to be an effective anti-cancer agent an increase in the specificity of duramycin's damage to tumour cells was theorised to be advantageous. PDT is an effective anti-cancer therapy and yet arguably is under-utilised in the clinical setting. PDT light therapy has been shown in oncological research to be able to bring about specific damage to tumour cells when PhtS are bound to biological molecules that have tumour-specific receptors or markers[154-156]. Therefore duramycin was conjugated to a porphyrin PhtS and the subsequent novel duramycin-porphyrin conjugate was used to treat ovarian and pancreatic cancer cell lines which were PDT treated using visible red light. PDT effect was then assessed using a colourimetric cell proliferation assay.
- A preliminary investigation into the anti-cancer effect of the duramycin-porphyrin conjugate on *in vivo* tumours was performed using ovarian and pancreatic tumour xenografts on the CAM. The effect of duramycin-PDT on the CAM xenografts was subsequently assessed by histological analysis.

Chapter 2 Materials and Methods

2.1 Cell culture

2.1.1 American Type Culture Collection cell lines

The cell lines that were used in this study were AsPC-1, Caco-2, Colo320, HCT116, JJN3, LoVo, MCF7, MDA-MB-231, MIA PaCa-2, MM.1S and U266B1. AsPC-1 is a human pancreatic adenocarcinoma derived from metastatic cells from the ascites of a 62 year old Caucasian female patient with pancreatic cancer[181]. Caco-2 are human epithelial cells from colon tissue taken from a 72 year old Caucasian male with colorectal adenocarcinoma[182]. Colo320 is a human colorectal adenocarcinoma from a 55 year old Caucasian female[183]. HCT116 is a human colorectal carcinoma isolated from an adult male with colorectal carcinoma[184]. JJN3 is a sub-clone of the parental cell line JJN1 which originated from the bone marrow of a 57 year old female patient with plasma cell leukaemia[185]. LoVo is a human colorectal adenocarcinoma derived from a supraclavicular region metastasis in a 56 year old Caucasian male patient[186]. MCF7 is a human breast adenocarcinoma derived from the metastatic site of a pleural effusion in a 69 year old Caucasian female[187] as is MDA-MB-231 however this cell line is from a 51 year old Caucasian female[188]. MIA PaCa-2 is a pancreatic carcinoma derived from pancreatic tumour tissue from a 65 year old Caucasian male[189]. MM.1S is a human multiple myeloma derived from the parental cell line MM.1 which is from the peripheral blood of a 42 year old Black female multiple myeloma patient who had become resistant to steroid-based therapy[190]. U266B1 is a human multiple myeloma taken from the peripheral blood of a 53 year old male myeloma patient[191].

2.1.2 Public Health England Culture Collection cell lines

The cell lines that were used in this study were A2780, HL-60, Jurkat E6.1, SK-OV-3, T47D and U937. A2780 is a human ovarian carcinoma established from ovarian tumour tissue from an untreated patient[192]. HL-60 is a human promyelocytic leukaemia derived from peripheral blood leukocytes from a 36 year old Caucasian female with acute promyelocytic leukemia[193]. Jurkat E6.1 are human leukaemic T cell lymphoblasts[194]. SK-OV-3 is a human ovarian adenocarcinoma derived from the ascitic fluid of a 64 year old Caucasian female with ovarian cancer[182]. T47D is a human breast tumour established from the pleural effusion of a ductal carcinoma in a 54 year old female[195]. U937 is a human lymphoma derived from a pleural effusion in a 37 year old Caucasian male with histiocytic lymphoma[196].

2.1.3 PromoCell cell line

The PromoCell cell line used in this study was human umbilical vein endothelial cells (HUVECs) which had been taken from the vein of the umbilical cord from up to 4 different donors and pooled.

2.1.4 Maintenance of cell lines

All tissue culture plastics used in this study were purchased from Sarstedt, UK except for the Corning® tissue culture flasks used to grow HUVECs which were purchased from VWR, UK. Cell cultures were grown in 25 cm^3 or 75 cm^3 tissue culture flasks and were stored in an incubator at 37°C in a 5% CO_2 atmosphere (except MDA-MB-231 which required a 0% CO_2 atmosphere). The cell lines were sub-cultured when in the logarithmic phase at 70-90% confluence to ensure optimal cell density for continued growth. Cell culture medium was refreshed every 48 hours. The cancer cell lines were physically removed from the surface of flasks via scraping with a cell scraper and pelleted using centrifugation at 320g for 3 minutes. The supernatant was then discarded and the cell pellet re-suspended in appropriate volume of fresh medium and transferred to a new flask. Cell viability was assessed using the Trypan Blue exclusion test (section 2.2). HUVECs were removed from flask surfaces via trypsinisation with trypsin-ethylenediaminetetraacetic acid (EDTA) (Lonza, UK) for 5 minutes. The cells were washed with phosphate buffer solution (PBS) prior to trypsinisation and subsequently with an excess of media before centrifugation at 210g for 5 minutes. The cell pellet was then re-suspended in medium and a cell count performed using the Trypan Blue exclusion test. Cells ($4x10^5$) were then seeded in 75 cm^3 flasks and fresh media added.

The media used for cell culture differed between cell lines due to the specific growth requirements of the different cell lines. A2780 and AsPC-1 were cultured using Roswell Park Memorial Institute 1640 medium (RPMI) supplemented with 10% foetal bovine serum (FBS) (Bio-Sera, UK) and (v/v); 100 units/mL penicillin, 100 µg/mL streptomycin (P/S) (Lonza, UK). AsPC-1 media was also supplemented with 1% sodium pyruvate solution and 1% HEPES buffer solution (Lonza, UK). MIA PaCa-2 was cultured using Iscove's Modified Dulbecco's Medium (IMDM) plus 10% FBS, 1% P/S and 2.5% horse serum (Bio-Sera, UK). SK-OV-3 were cultured in McCoy's 5a Medium Modified supplemented with 15% FBS and 1% P/S. Media for the cancer cell lines was purchased from Scientific Laboratory Supplies Limited, UK. HUVECs were cultured in Endothelial Cell Basal Medium plus Endothelial Cell Growth Medium Supplement Mix (PromoCell, UK). All serum, P/S and buffers added to media were

filtered through a 0.2 µm filter before addition. Between uses all media was stored at 2-8°C and before addition to cell culture warmed to 37°C in a water bath. The cell lines Caco-2, Colo320, HCT116, HL-60, JJN3, Lovo, MCF7, MDA-MB-231, MM.1S, T47D, U266B1 and U937 were cultured and maintained by Dr Jessica Hall and the cell line Jurkat E6.1 by Dr He Liang at The University of Hull, Hull, UK and were generously donated when required.

All media preparation, cell culture and maintenance of cell lines was performed in a Class II Biological Safety Cabinet with laminar air flow to avoid contamination and provide sterile working conditions. The cabinet was disinfected before and after use with Virkon disinfectant (Scientific Laboratory Supplies Limited, UK) and 70% ethanol. The incubator where cell lines were stored and the 37°C water bath used for the incubation of media and other materials was disinfected with Virkon and 70% ethanol at regular intervals. All equipment was sprayed with 70% ethanol prior to insertion into the biological safety cabinet. All cell lines were checked monthly for mycoplasma infection using EZ-PCR Mycoplasma Test Kit (Geneflow Ltd., UK).

2.1.5 Culture of 3D tumour spheroids

Culture of 3D tumour spheroids was performed using the cancer cell lines A2780, AsPC-1, MIA PaCa-2 and SK-OV-3. BioReagent agarose (Sigma-Aldrich, UK) was added to an appropriate volume of distilled water (dH_2O) and autoclaved to make a non-adhesive 1.5% agarose gel. Once cooled to 50-60°C agarose gel (100 µl) was added to wells in 96 well sterile tissue culture plates (Sarstedt, UK). The agarose was allowed to set in a biological safety cabinet and PBS (200 µl) was added to all unused wells to limit evaporation during incubation. Cells were removed from flasks using method 2.1.4 and counted using method 2.2. Cells ($2x10^4$/100 µl media) were then seeded into agarose containing wells. The 96 well plates were incubated at 37°C in a 5% CO_2 atmosphere for 72 hours. If spheroids were to be drug treated the plate was centrifuged at 320g for 3 minutes after which the supernatant was removed and duramycin in solution with PBS (100 µl), at the required concentration, was added. After 24, 48 or 72 hours incubation at 37°C in a 5% CO_2 atmosphere the plates were then centrifuged again. Either media was added to wells or a cell proliferation assay was performed using method 2.4.2. Spheroids were imaged using a GelCount™ colony counter (Oxford Optronix, UK) and spheroid size was measured using ImageJ software (National Institute of Health, US).

2.1.6 Cryopreservation

Cells at a low passage number were removed from flasks using the method 2.1.4 and an aliquot (10 µl) was taken to assess cell number and cell viability using method 2.2. To ensure recovery after thawing cells were cryopreserved only if viability was >90%. Cells were centrifuged at 320g for 3 minutes and re-suspended in freezing medium (90% FBS: 10% dimethyl sulphoxide (DMSO) (Sigma-Aldrich, UK)) and aliquoted into 1 mL cryovials. The cryovials were frozen slowly, in a -80°C freezer, at approximately 1°C per minute using a Nalgene® cryofreezing container (Sigma-Aldrich, UK). After 24 hours cryovials were transferred to liquid nitrogen. Cryopreserved cells were recovered by rapid thawing at 37°C in an incubator and then sprayed with 70% ethanol including the rim just below the cap of the cryovial before being placed into the biological safety cabinet. Cells were then transferred to a 50 mL centrifuge tube containing appropriate medium (10 mL) and centrifuged at 320g for 3 minutes to remove the freezing medium. The supernatant was discarded and the cell pellet re-suspended in medium and placed in a 25 cm^3 tissue culture flask until confluent enough to be transferred to a 75 cm^3 flask.

2.2 Cell count and Trypan Blue exclusion test

Trypan Blue can be used in the determination of cell viability as the dye is unable to permeate the membrane of viable cells (no stain/ appear clear) but can enter through the damaged membrane of dead cells (stain blue). Cells suspended in PBS (10 µl) were mixed with 0.4% w/v Trypan Blue (10 µl) (Sigma-Aldrich, UK) in a 0.5 mL polypropylene tube until a homogenous solution was achieved. Cell solution (10 µl) was pipetted onto an improved Neubauer haemocytometer (depth of 0.1 mm, 1/400 mm^2) (Hawksley, UK). The solution spread evenly under the cover slip by capillary action. Cells were counted using a 20x magnification on a phase contrast microscope. All cells visible in the centre 25 square grid were counted and total cell count (cells/mL PBS) and cell viability was calculated using the following formulae;

Total cell count (cells/mL) = (cell count of viable and non-viable cells x dilution factor) x volume of chamber

Percentage cell viability = (viable cells/mL / total cells/mL) x 100

Cells were then diluted in the required volume of media dependent on the cell count needed for the experiment. Cells were discarded if their viability was calculated to be <70%.

2.3 Flow cytometry

2.3.1 Detection of cell viability using Annexin V: FITC assay

The Annexin V: FITC Apoptosis Detection Kit I (BD Biosciences, UK) was used to assess cell viability by flow cytometry. Annexin V, in the presence of calcium, binds to cell surface phosphatidylserine (PS)[197] which is exposed on the outer cell membrane during physiologically active processes such as apoptosis[42]. Propidium iodide (PI) is able to permeate the damaged cell membranes of cells that are necrotic and stains the DNA in the nucleus of necrotic cells. The Annexin V: FITC assay can be used to identify populations of cells that are viable or are undergoing apoptosis and necrosis through the detection of both annexin V and PI negative cells (viable), annexin V only stained cells (apoptosis) and both annexin V and PI positive cells (necrosis). Cells ($2x10^5$) suspended in PBS (50 µl) in 5 mL polypropylene tubes were treated with duramycin at required concentration for 30 minutes and then centrifuged at 320g for 3 minutes. The supernatant was discarded and the cell pellet was re-suspended in Annexin V Binding Buffer (100 µl) (1:10 dilution with dH_2O) and then annexin V (5 µl) and PI (5 µl) were added. The tubes were incubated for 15 minutes in the dark at room temperature. For control cells; 1 tube was left unstained (cells only), 1 tube contained only annexin V and 1 tube contained only PI. These controls were used in the setup of the flow cytometer for compensation and quadrant parameters. After incubation binding buffer (300 µl) was added to the tubes and cells were analysed by flow cytometry.

2.3.2 Detection of phosphatidylethanolamine

2.3.2.1 Duramycin

Phosphatidylethanolamine (PE) on the surface of cell lines was detected using duramycin by flow cytometry. Cells ($2x10^5$) were suspended in PBS (50 µl) in a 5ml polypropylene tube and incubated with either duramycin (duramycin from *Streptoverticillium cinnamoneus*, Sigma-Aldrich, UK) at the required concentration or normal rabbit serum (Thermo Fisher Scientific Inc., UK) (1:5000 dilution, 0.2% v/v) which was used as a negative control to account for any non-specific binding. After incubation (which differed in length depending on experiment) at room temperature, the cells were washed with PBS (1 mL), centrifuged at 320g for 3 minutes and then the cell pellet was re-suspended in PBS (300 µl). Cells were then incubated with a secondary (rabbit) anti-duramycin antibody (Abcam, UK) (final dilution 1:600, final concentration estimate of whole antiserum un-purified antibody from Abcam ~1.3-13 µg/µl) at room temperature for 30 minutes. After this the cells were

washed, centrifuged and re-suspended as before and then incubated with a tertiary sheep anti-rabbit IgG: fluorescein isothiocyanate (FITC) antibody (Bio-Rad, UK) (final dilution 1:600, final concentration ~1.6 µg/µl) in the dark at room temperature for 30 minutes. After cells were washed and centrifuged they were re-suspended in PBS (300 µl) and then analysed using the 488 nm argon laser on a BD FACScalibur (BD Biosciences, UK) with BD CellQuest™ Pro software (version 5.1, BD Biosciences, UK). This was the flow cytometer used for all flow cytometric analysis in this study. Level of PE expression was given as median fluorescence intensity ratio (MFIR) calculated using the formula;

MFIR = MFI value of the positive sample / MFI value of the negative control sample

This indicated the level of shift in fluorescence intensity of duramycin labelled cell populations. All readings were performed in duplicate to gain average MFIR and standard deviation (SD).

2.3.2.2 Duramycin-porphyrin conjugate

Detection of PE was also performed using the duramycin-porphyrin conjugate. Cells ($2x10^5$) were suspended in PBS (50 µl) in a 5 mL polypropylene tube and incubated with the conjugate at required concentration in the dark, at room temperature, for 30 minutes. Cells were then washed with PBS (1 mL), centrifuged at 320g for 3 minutes to remove excess conjugate and re-suspended in PBS (300 µl). The cells were then analysed by flow cytometry. There was no requirement for a fluorescently labelled antibody as the porphyrin moiety of the conjugate had a wide ultraviolet-visible (UV-vis) spectrum with bands of 422 nm, 521 nm, 560 nm, 580 nm and 645 nm and was detectable using the flow cytometers 635 nm red diode laser. Levels of PE expression were given as median fluorescence and were performed in duplicate to attain average median fluorescence and SD.

2.3.3 Analysis of the light scatter of cancer cell lines

Forward scatter (FSC) and side scatter (SSC) are measurements of laser light scatter and are generally correlated with cell size and internal cell complexity and granularity, respectively. They are detected when laser light from the 488 nm argon laser in the flow cytometer hits the single stream of cells and is diffracted in different directions with the light that carries on the forward path hitting the FSC detector. SSC is measured at 90° to the cell and relies on the presence of internal cellular structures that change the refractive index of light in order to measure intracellular granularity. Data for the effect of duramycin and the duramycin-porphyrin conjugate on the FSC and SSC of cancer cell lines was collected from cells processed using methods 2.3.1 and 2.3.2.2, respectively.

2.4 Cell proliferation assays

2.4.1 MTT assay

MTT (3-[4,5-dimethylthiazol-2-yl]-2,5- diphenyltetrazolium bromide; thiazolyl blue) cell proliferation assays were performed by Mrs Huguette Savoie at The University of Hull, Hull, UK. MTT is a soluble tetrazolium salt that forms a yellow solution when dissolved in PBS and added to media. The soluble yellow dye is converted to the insoluble purple formazan through cleavage of the tetrazolium ring by dehyrdrogenases present in the mitochondria of living cells. Conversion of the dye cannot be performed by dead cells. In this way MTT can be used as a colourimetric detection assay of cell viability as the amount of converted purple dye, thus its absorbance, is assumed to be proportional to metabolically active cells, and thus the viable cell population. Cells were treated as described in method 2.9.1 and then incubated for 24 hours at 37°C in a 5% CO_2 atmosphere. After this MTT reagent (10 µl) (Sigma-Aldrich, UK) in solution with PBS (final concentration 12 mM) was added to wells in the 96 well plate and incubated (37°C, 5% CO_2) in the dark for 4 hours. The media was then discarded and the resultant insoluble formazan crystals were dissolved by adding acid-alcohol mixture (150 µl) (0.04 mol/L HCl in absolute 2-propanol). The plates were then analysed at 570 nm using a BioTek ELX800 Universal Microplate Reader (Corgenix Ltd., UK). All readings were performed in triplicate to gain the average absorbance. The average absorbance value for the blank was then subtracted. Percentage cell proliferation was expressed relative to untreated control cells.

2.4.2 MTS assay

Cell proliferation was assessed using MTS reagent (3-[4,5-dimethylthiazol-2-yl]-5-[3-carboxymethoxyphenyl]-2-[4-sulfophenyl]-2H-tetrazolium) in combination with the electron coupling reagent phenazine ethosulfate using the commercially available kit; CellTiter AQ_{ueous} One Solution (Promega, UK). MTS reagent is a soluble yellow coloured tetrazolium compound that is enzymatically converted by mitochondrial dehydrogenases in metabolically active cells into a soluble purple formazan product. This colourimetric assay can be used to determine cell proliferation as described in method 2.4.1. Cells ($2x10^4$) in media (180 µl) were transferred to wells in 96 well sterile tissue culture plates. The plates to be treated for 24, 48 or 72 hours with duramycin were drug treated with duramycin (20 µl) at required concentration and then placed in the incubator (37°C, 5% CO_2) for 24, 48 and 72 hours. However plates to be treated with duramycin for 30 minutes were first incubated (37°C, 5% CO_2) overnight before drug treatment commenced. After incubation

plates were centrifuged at 320g for 3 minutes and supernatant removed. Fresh medium (180 µl) was then added followed by MTS reagent (20 µl) and plates incubated (37°C, 5% CO_2) for 2 hours. The plates were then read at 490nm using a microplate reader (BioTek, UK). When this method was performed on tumour spheroids the plates were first centrifuged at 320g for 3 minutes and supernatant (100 µl) was transferred to a fresh 96 well plate before reading. This was so the absorbance reading taken would not be affected by the agarose gel and spheroid present at the bottom of the well. All drug dilutions were replicated 4 times for the cancer cell line cultures and 8 times for the tumour spheroids so that average absorbance and SD could be calculated. Percentage cell proliferation was expressed relative to untreated controls.

2.5 Calcium ion assay

The calcium indicator Fluo-3, AM selectively binds to divalent cations such as Ca^{2+} and, once bound, undergoes an increase in fluorescence. As the Ca^{2+}-indicator complex is formed inside cells its fluorescent signal can be detected using spectrofluorometry. Thus changes in intracellular calcium ion concentration ($[Ca^{2+}]_i$) can be measured. The acetoxymethyl (AM) ester derivative of Fluo-3 confers cell membrane permeability to the non-permeating Fluo-3 salt. Once inside the cell non-specific esterases cleave the ester leaving the salt form behind. To prevent leakage of Fluo-3 out of cells the anion transport inhibitor sulphinpyrazone is added to the cell suspension. The calcium ionophore A23187 causes rapid increase in $[Ca^{2+}]_i$. It can also increase cell membrane permeability to Ca^{2+} as it selectively binds to divalent cations and allows their transport across the hydrophobic portion of plasma membranes. Additionally it induces the release of Ca^{2+} from intracellular stores, for example the mitochondria, and allows a relatively small influx of Ca^{2+} through native Ca^{2+} channels

Media was removed from cell cultures and the cells washed with PBS which was then discarded. Cells were then incubated with HEPES-buffered saline EDTA (2 mL) (10 mM HEPES pH7.4, 155 mM NaCl, 1.7 mM EDTA) for 5 minutes at 37°C in a 5% CO_2 atmosphere. The cells were then washed with PBS (3 mL), lifted off the flask with gentle agitation and transferred to a 25 mL universal tube to be centrifuged at 320g for 5 minutes. The cell pellet was re-suspended in fresh media (0.5 mL) to which sulphinpyrazone (1.3 µl, 100 mM) and Fluo-3, AM (5 µl, 2.19 mM) (Life Technologies, UK) was added. The cells were incubated for 30 minutes at room temperature on a rotating shaker. After incubation PBS (4.5 mL) was added and the universal tube centrifuged at 320g for 5 minutes. Cells were re-suspended

in room temperature calcium buffer (150 mM NaCl, 3 mM KCl, 10 mM glucose, 20 mM HEPES and 2.5 µM sulphinpyrazone, adjusted to pH 7.5). When the experiment required the presence of extracellular calcium the buffer contained calcium chloride ($CaCl_2$) (1.5 mM). Cells (100 µl, $1x10^5$) were added to a cuvette containing calcium buffer (1.9 mL) and placed in a spectrofluorometer. Duramycin (20 µl) at required concentration or calcium ionophore A23187 (12 µl) (Sigma-Aldrich, UK) was added to the cuvettes. The cells were analysed using a Photon Technology International (PTI) 814 photomultiplier detection system interfaced with a desktop computer (PTI, UK) coupled to FeliX GX software (PTI, UK). The increase in $[Ca^{2+}]_i$ in duramycin treated cells was calculated as a percentage of the total increase in $[Ca^{2+}]_i$ in the control A23187 treated cells. The assay was performed in duplicate with each duramycin concentration repeated in duplicate and the A23187 control in triplicate.

2.6 Pro-thrombin time coagulation assay

Clotting time was measured via a prothrombin time assay using a Thrombotrack SOLO Coagulometer (Axis-Shield, UK) steel ball coagulometer. The coagulometer measures clotting time by the magnetic rotation of a steel ball within a cuvette containing a liquid cell solution, once a solid fibrin clot is formed the steel ball ceases to rotate and can no longer be detected by the magnetic sensor and the timer stops. A sample is recorded as 'did not clot' if the timer does not stop before 600 seconds. The coagulometer was allowed to warm to 37°C before use which was detected by the machine (approximately 10 minutes). Normal control plasma (Norm-Trol 1, Helena BioSciences Europe, UK), which contains a source of coagulation factors, was reconstituted in 1 mL dH_2O and placed in a cuvette in the coagulometer, along with a cuvette containing 1 mL 25 mM calcium chloride ($CaCl_2$), to warm to 37°C. Cell sample (100 µl, $4x10^5$ cells) was incubated in a cuvette in the coagulometer for 2 minutes prior to the addition of 100 µl $CaCl_2$ after which a 3 second countdown was initiated which started the rotation of the steel ball and 100 µl normal control plasma was added.

2.7 Confocal microscopy

2.7.1 Increase in intracellular calcium ion concentration

Confocal microscopy was used to image the increase in $[Ca^{2+}]_i$ in duramycin treated cancer cells. Cells ($1x10^6$) were suspended in PBS (1 mL) in a 5 mL polypropylene tube. To this sulphinpyrazone (2.6 µl, 100 mM) and Fluo-3, AM (10 µl, 2.19 mM) was added and the tube was incubated in the dark for 30 minutes at room temperature on a rotating shaker. Cells

were washed with PBS (1 mL), centrifuged at 320g for 3 minutes and then re-suspended in warm (37°C) PBS (1 mL) and a cell count was once again performed. Cells, adjusted to $8x10^5$ in warm PBS (1 mL), were incubated with 1x CellMask™ Orange plasma membrane Stain (Life Technologies, UK) for 10 minutes in the dark at 37°C in a 5% CO_2 atmosphere. Cells were washed, centrifuged and re-suspended in PBS as before and then transferred to lumox® dish 35 dishes (Sarstedt, UK) ($2x10^5$ cells in 250 µl PBS). Cells were treated with 50 µM duramycin (10 µl) and imaged live using a TimeSeries of 1 image/minute for 30 minutes. Imaging was performed using a Zeiss LSM 710 confocal microscope and Zen software version X (Zeiss, UK).

2.7.2 Uptake of propidium iodide

Confocal microscopy was used to image the effect of duramycin on cell viability and cell membrane appearance using the CellVue® Jade Cell Labelling Kit (eBioscience, UK) and PI (BD Biosciences, UK). Preliminary experiments were performed where the cell membrane dye CellVue® Jade was incubated with cells for 3, 4 and 5 minutes. This is because CellVue® Jade partitions itself into cell membranes so while longer incubations can result in higher fluorescence the cell membrane integrity can become adversely affected. The optimum incubation time for the cancer cells used in this study was found to be 3 minutes. Cells ($2x10^7$) in PBS (1 mL) were placed in a 5 mL polypropylene tube and centrifuged at 320g for 3 minutes. The supernatant was discarded and the pellet re-suspended in Diluent C (500 µl) and then further Diluent C (500 µl) containing 4 µM CellVue® Jade dye solution was added. This cell suspension was incubated for 3 minutes at room temperature in the dark with gentle, periodic manual agitation. PBS (1 mL) was used to wash the cells and the tube was centrifuged as before and cells counted to adjust to $8x10^5$/ mL. Cells in PBS (250 µl) were then incubated with PI (12.5 µl) in the dark at room temperature for 15 minutes. The suspension was then transferred to lumox® dishes and cells were treated with 50 µM duramycin (10 µl) and imaged live using a TimeSeries of 1 image/minute for 20 minutes. Imaging was performed using a Zeiss LSM 710 confocal microscope.

2.8 Synthesis of the duramycin-porphyrin conjugate

The duramycin-porphyrin conjugate was synthesised and analysed by Dr Francesca Giuntini at Liverpool John Moores University, Liverpool, UK. A solution of duramycin (10 mg, $4.97x10^{-3}$ mM) (Sigma, UK) in DMSO (2 mL) plus trimethylamine (TEA) was treated with 5-[4-(N-succinimidyloxycarbonyl)phenyl]-10,15,20-tris(4-methylpyridinium) porphyrin trichloride[151] (8 mg, $9.94x10^{-3}$ mM). The resultant solution was mixed on a rotating shaker

at room temperature for 24 hours. The crude material was recovered by addition of dichloromethane (5 mL) and filtration through paper. The solid was dissolved in 0.1% aqueous trifluoroacetic acid (TFA) (1 mL) and the 1:1 duramycin-porphyrin conjugate was isolated and purified by semi-preparative high performance liquid chromatography (HPLC). The purified conjugate was then analysed using electrospray ionising mass spectrometry (ESI-MS). Recovery of 4.8 mg of the conjugate was achieved which equated to a 34.4% yield.

2.8.1 Purification and analysis of duramycin-porphyrin conjugate

Reversed phase HPLC photodiode array (RP-HPLC-PDA) analyses were performed on an Agilent 1200 HPLC system (Agilent, Germany) equipped with a G1312B BinPump SL, G13798 degasser, G1367D HiP ALS SL plus autosampler, a G1316B column compartment (set at 35°C), and a G1315C diode array detector (acquisition rate, 80Hz; scan rate: 380-600 nm, step: 1 nm), using a Gemini C18, 5µ, 150 x 4.6 mm, 110 Å column (Phenomenex, UK), equipped with a SecurityGuard C18 (ODS) 4 x 3.0 mm ID guard column (Phenomenex, UK). The injection volume was 20 µL, and the flow rate was 1 mL/minute. Mobile phase consisted of a mixture of 0.1% TFA in deionised water (18.2 MΩ, Elga Purelab Ultra ULXXXGEM2), solvent A, and 0.1% TFA in HPLC-grade acetonitrile, solvent B. The gradient for the elution was as follows: 0-2 minutes, 5% B; 2-7 minutes, B to 95%; 7-12 minutes, 95% B; 12-12.1 minutes, B to 5%. Duramycin R_t = 7.32, porphyrin R_t = 7.01, conjugate R_t = 6.20 min. RP-HPLC purifications were carried out on a Jasco HPLC system equipped with a PU-1580 LC pumps, HG-1580 degasser, AS-1555 autosampler and MD-1515 array UV-visible detector, using a Luna C18, 5 µ, 250 x 10 mm, 110 Å (Phenomenex, UK), at a flow rate of 2.5 mL/minute. Mobile phase consisted of a mixture of 0.1% TFA in deionised water (18.2 MΩ, Elga Purelab Ultra ULXXXGEM2), solvent A, and 0.1% TFA in HPLC-grade acetonitrile, solvent B. The gradient for the elution was as follows: 0-8.5 minutes, 5% to 51% B; 8.5-13 minutes, 51% B; 13-14 minutes, 51 to 95% B; 14-18 minutes, 95% B, 18-18.1 minutes, 95 to 5% B. Conjugate R_t = 6.20 min. Quadrupole time-of-flight MS (Q-TOF-MS) data were acquired in positive mode scanning from 400 to 3000 *m/z* with and without auto MS/MS fragmentation. Ionization was achieved with an Agilent JetStream electrospray source and infused internal reference masses. Agilent 6540 Q-TOF-MS parameters: gas temperature, 325°C; drying gas, 10 L/minute; and sheath gas temperature, 400°C. ESI-MS (+): 675.66 $[(M+4H^+)/4]^{4+}$ (expected: 675.67). Conjugate R_t = 7.34.

2.8.2 Synthesis of the capped porphyrin control

The capped porphyrin control (unconjugated porphyrin) was synthesised and analysed by Dr Francesca Bryden at The University of Hull, Hull, UK[150]. The capped porphyrin control, 5-[Aminobutyl-*N*-oxycarbonyl)phenyl]phenyl]-10,15,20-tris(*N*-methyl-4-pyridinium) porphyrin trichloride, was produced by adding 5-[4-(succinimide-*N*-oxycarbonyl)phenyl]-10,15,20-tris-(4-*N*-methylpyridimiumyl) porphyrin trichloride (50 mg, 0.055 mM) in DMSO (5 mL) to butylamine (50 mg, 0.68 mM) and mixed on a rotating shaker at room temperature overnight. Ammonium hexafluorophosphate and water (20 mL) was then added to the solution until a precipitation was seen which was collected by filtration. The precipitate was re-dissolved in acetone and tetrabutylammonium chloride was added until precipitation occurred which was again collected by filtration. The crude porphyrin was then purified by precipitation from diethyl ether over methanol[150]. Using this method the NHS ester group, used in the conjugation of porphyrin to duramycin, was reacted to butylamine so that non-specific binding was prevented.

2.8.3 Concentration determination of photosensitiser containing compounds

The photosensitiser (PhtS) containing compounds were lyophilised (freeze-dried) and kept, protected from light, at -20°C until required. The lyophilised duramycin-porphyrin conjugate and the capped porphyrin control were re-suspended in DMSO (600 µl and 2 mL, respectively). Their final concentrations were determined using UV-vis spectrophotometry and Beer-Lambert Law;

Absorbance (A) = absorption coefficient in H_2O at 422 nm (ε) x path length (*l*) x concentration of solution (*c*)

The final concentrations of the duramycin-porphyrin conjugate was found to be 2.75 mM (7.41 mg/mL) and 1.41 mM (3.8 mg/mL) for the first batch and the second batch of conjugate, respectively. The amount of conjugate recovered from the conjugation procedure for both batches was 4.8 mg (34.4% yield) however 4.45 mg of lyophilised powder from the first batch and 2.28 mg from the second batch was given to the author (the remainder was used for analysis by Dr Francesca Giuntini) which accounted for the differences in final concentration. The final concentration of the capped porphyrin control was determined to be 1.89 mM (1.44 mg/mL). The absorption spectra of the capped porphyrin control determined the porphyrin's Q bands to be 521 nm, 559 nm, 588 nm and 645 nm and the Soret band as 422 nm.

2.9 Photodynamic light treatment

The photodynamic light treatment experiments were performed in part by Mrs Huguette Savoie and in part by the author at The University of Hull, Hull, UK.

2.9.1 Cancer cell lines

Cells were cultured and removed from flasks as described in method 2.1.4 (except with serum free media) and cell count and viability attained using method 2.2. Cells (8 x 10^5) in medium (800 µl) were added to 5 mL polypropylene tubes to which either unconjugated duramycin, capped porphyrin control or duramycin-porphyrin conjugate (200 µl) at required concentration was added. The tubes were then incubated in the dark at 37°C in a 5% CO_2 atmosphere for 5 minutes. Cells were washed with media (3 mL) to remove any unbound conjugate and centrifuged at 320g for 10 minutes. The pellet was then re-suspended in media (1 mL) and the cell suspension (100 µl, 8x10^4 cells) was transferred to the wells of a 96 well sterile tissue culture plate. This was incubated in the dark at 37°C in a 5% CO_2 atmosphere for 5 minutes. The PDT light supply (figure 2.1), a 9x14 LED light array designed by Professor Andrew Beeby of Durham University, Durham, UK, was allowed to stabilise for 5 minutes. The 9x14 LED array emits red light in the wavelength range 620-660 nm with peak emittance at 650 nm. After the light array was stabilised the irradiance reading was taken using a R203 Macam radiometer (Irradian Ltd. UK). The following equation was used to calculate the length of time required to deliver a light fluence rate of 7.5 J/cm^2 to the cancer cell lines:

$$\text{Length of time (min)} = (7.5\ \text{J/cm}^2 / \text{irradiance reading (W/m}^2)) \times 1000 / 60$$

The answer attained from the above calculation can result in a decimal. The numbers after the decimal point can be transformed using the following equation to determine the time in seconds required for light irradiation, in addition to the time in minutes:

$$\text{Length of time (secs)} = (\text{numbers after decimal} / 100) \times 60$$

After incubation one plate was irradiated and an identical plate was kept in the dark at room temperature for the duration of the light treatment (non-irradiated/ dark toxicity control plate). After light treatment 5 µl FBS was added to the wells of both plates. The plates were incubated at 37°C in a 5% CO_2 atmosphere for 24 hours before being analysed for cell proliferation using method 2.4.1.

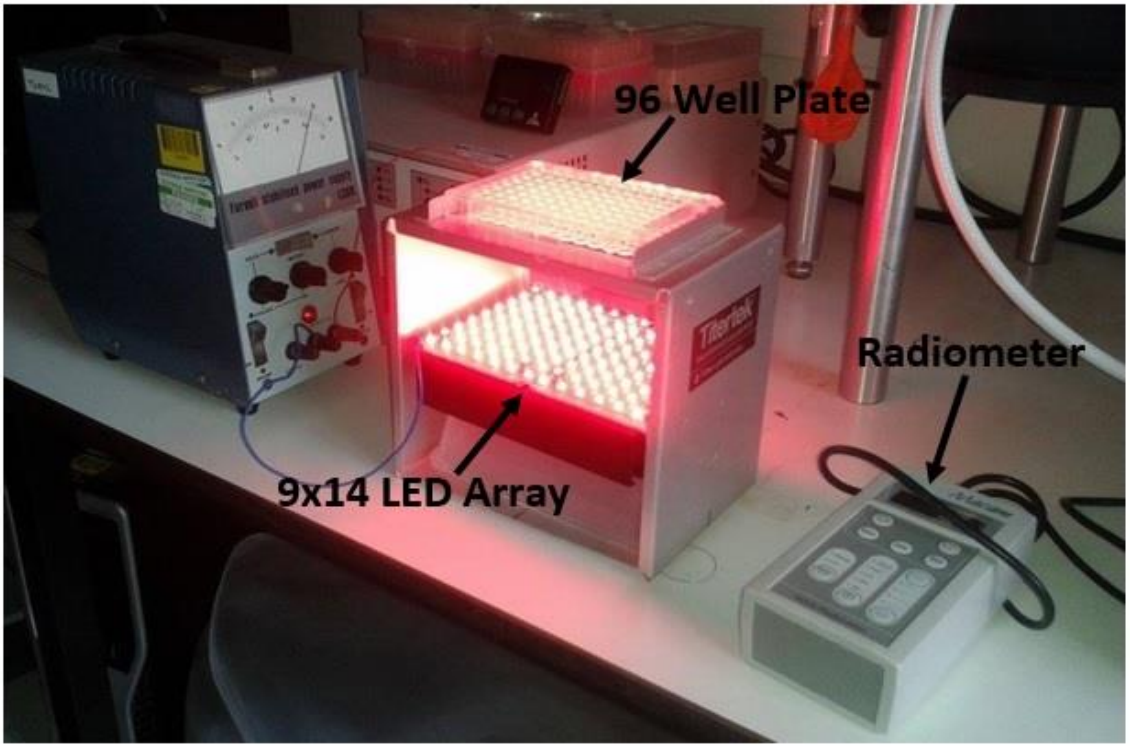

Figure 2.1: Setup of the equipment used in the photodynamic therapy treatment of cancer cell lines.

The red light emitted from a 9x14 LED light array was used to deliver a 7.5 J/cm^2 light dose to cancer cell lines treated with either duramycin-porphyrin conjugate, unconjugated duramycin or the capped porphyrin control.

2.9.2 Tumour xenografts

The PDT treatment of tumours grown on the CAM of chicken eggs (section 2.10) was performed under the supervision of Dr Yu-Pei Xiao at The University of Hull, Hull, UK. Tumour xenografts were irradiated with light using the setup in figure 2.2. The tumour xenografts were drug treated topically (pipette application) with unconjugated duramycin or duramycin-porphyrin conjugate (10 µl, 50 µM) in subdued lighting. The eggs were then returned to the incubator (37°C, 70% humidity) for 5 minutes. After incubation the eggs were treated with 7.5 J/cm^2 light dose using a Paterson Lamp BL1000A light system (Phototherapeutics Ltd., UK) equipped with a red filtered beam (GLEN S100 367 0134, flat response 620-642 nm). The light irradiance was measured using a R203 Macam radiometer and the required time to deliver 7.5 J/cm^2 light dose (found to be 4 minutes and 41 seconds) was calculated using the equations in method 2.9.1. In total there were 4 chicken eggs used for the PDT experiments in which 1 xenograft was treated with unconjugated duramycin plus light irradiation, 2 xenografts were treated with duramycin-porphyrin conjugate plus light irradiation and 1 xenograft was treated with the conjugate but not irradiated which

served as the dark control. The tumour xenografts were treated over a 4 day time course (drug treated/ irradiated at 0, 24, 48 and 72 hours) with an image of the tumours taken before and after each treatment, except the dark control which was kept in the dark in the incubator for the duration of the experiment. At 72 hours the tumours were dissected from the CAM following method 2.10.4. Eggs were out of the incubator for a maximum of 5 minutes at a time to limit damage to the chick embryo and to prevent dehydration of the CAM.

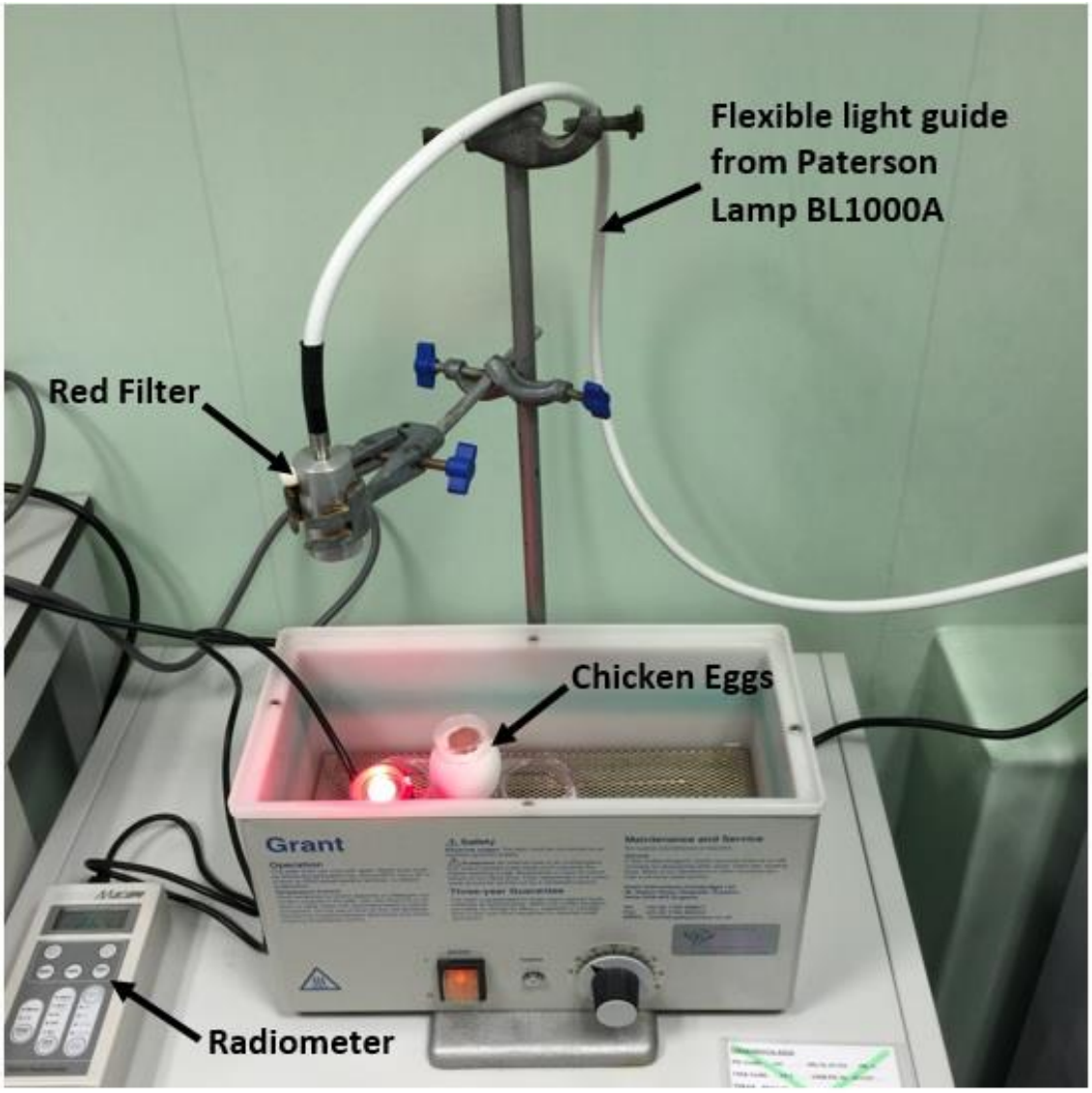

Figure 2.2: Setup of the equipment used in the photodynamic therapy treatment of tumour xenografts on the CAM.

The chicken eggs were supported on a rack immersed in a 37°C water bath to keep the chick embryo at the correct temperature while it was outside of the incubator. The red light beam measured 38 mm across which adequately covered the opening in the shell of the chicken egg. To achieve this beam size the flexible light guide was held in place 19 cm above the eggs.

2.10 Tumour xenografts on the chorioallantoic membrane

2.10.1 Ethical considerations and maintenance of chicken eggs

The maintenance of the chicken eggs used in this study along with the transplantation of cancer cells onto the CAM, drug treatment and dissection of tumours was performed by Dr Yu-Pei Xiao. The research is covered by the project licence PPL 40/3564 which was granted on 12th January 2012. This project licence was reviewed by the Home Office inspector, the NVS (Named Veterinary Surgeon) and the NACWO (Named Animal Care and Welfare Officer) in its initial stages. It was then reviewed and approved by The University of Hull AWERB committee (Animal Welfare Ethical Review Board) and finally approved and granted by the Animals in Science Licensing Division of the Home Office (ASRU), UK.

The chicken eggs used in this study were Extra-Large Size Fertilized White Leghorn Chicken Eggs purchased from Henry Stewart & Co Ltd, UK. Upon arrival the eggs were washed with dH_2O and transferred to an incubator (37°C, 70% humidity atmosphere) and allowed to incubate for 7 days. The shell over the air sac and the shell membrane were removed to expose the CAM on the 5^{th} day of incubation. A plastic cap was used to cover the opening to prevent the membrane drying out and to reduce the risk of contamination. To keep the incubator and CAM moist dH_2O mist was sprayed into the incubator every time it was opened and periodically throughout the day. All eggs remained outside of the incubator for a maximum of 5 minutes at a time to eliminate the risk of damage to the chick embryo.

2.10.2 Transplantation of cancer cells

The cancer cell line used for the CAM xenografts was the ovarian cancer cell line SK-OV-3 which was cultured and removed from tissue culture flasks as described in method 2.1.4 and cell counts performed using method 2.2. Cells ($1x10^6$) were suspended in Matrigel (Cultrex® Basement Membrane Extract) (10 µl) (Trevigen® Inc., UK) which was pipetted onto the CAM of the chicken eggs on the 8^{th} day of incubation. The SK-OV-3 cells were allowed to establish into a visible tumour on the CAM and promote angiogenesis of CAM blood vessels for 3 days. After which drug treatment experiments were performed with duramycin (section 2.10.3) and the duramycin-porphyrin conjugate (section 2.9.2).

2.10.3 Duramycin treatment

In total 3 batches of chicken eggs were used for duramycin treatment of SK-OV-3 xenografts. The results presented in this study (Chapter 7) were performed using the third batch of eggs which included 5 eggs treated with duramycin (50 µM) and 2 eggs treated

with ‘neat’ duramycin (4.97 mM). The first and second batches were controls to establish method 2.10.2 and that given below. The first batch of eggs were transplanted with SK-OV-3 cells ($1x10^6$) and included 2 non-graft controls and 3 treated eggs; 1 PBS control, 1 with 50 µM duramycin and 1 with 4.97 mM duramycin, for 24 hours. The second batch of eggs were transplanted with SK-OV-3 cells ($2x10^6$) and included 2 eggs treated with 50 µM duramycin and 1 with 4.97 mM duramycin, for 24 hours. The resultant tumours in the second batch stimulated excessive angiogenesis and the high amount of vascularisation obscured view of the tumour. The tumours also grew too thick for adequate penetration of duramycin. It was therefore found that the optimal number of cells required for transplantation was $1x10^6$. The tumours treated with 50 µM in the control batches appeared viable at 24 hours and so it was decided to extend drug treatment to 72 hours.

Duramycin treatment of SK-OV-3 xenografts was performed on the 11^{th} day of embryo incubation. Eggs were removed from the incubator and placed in a plastic storage rack and the plastic cap was removed from the opening in the egg shell. Duramycin (10 µl) at required concentration was applied to the tumour xenograft topically by pipetting directly onto the tumour. The tumours were drug treated with duramycin at 0, 24 and 48 hours (corresponding to the 11^{th}, 12^{th} and 13^{th} day of incubation) with images taken using a light microscope at 0 hours (pre-treatment) and 24, 48 and 72 hours. Re-application of duramycin was required due to the penetration of CAM blood vessels into the tumour which could have removed duramycin away from the vicinity of the tumour and thus potentially reduce its concentration.

2.10.4 Dissection of tumours

Following the PDT light treatment of SK-OV-3 tumour xenografts (section 2.9.2) the chicken eggs were kept at 4°C for 4 hours in order to cull the chick embryos. The tumour was then dissected from the CAM and placed in an excess of RNA*later*® (Sigma-Aldrich, UK) in 0.5 mL polypropylene tubes. These were stored at 2-8°C for 1 hour prior to being snap frozen (section 2.10.5).

2.10.5 Cryostat sections

The dissected tumours were removed from RNA*later*® and placed on a square piece of cork to dry. The tumour was then covered with Tissue-Tek® O.C.T. Compound, Sakura® Finetek (VWR, UK) and immersed into a measuring cup of cooled 2-methylbutane (Sigma-Aldrich, UK) which was submerged in liquid nitrogen. Once frozen (~30 seconds after immersion) the tumour was removed and stored in air tight bags at -20°C until required. To section the

tissues excess Tissue-Tek® was removed from the outside of the tumours using a scalpel and then more precisely trimmed in 20 µM sections using a Leica Cryostat CM1950 (Leica Biosystems, UK). The cryostat had been allowed to cool and was set at -30°C for the sample block and -25°C for the chamber. Once the sample had become exposed the sections were taken at 12 µM with each section being picked up from the microtome block using a labelled glass microscope slide. The tumour sections were allowed to dry and then the microscope slides were stored at 2-8°C until required.

2.10.6 Haematoxylin and Eosin stain

The oxidation product of haematoxylin, haematin, in complex with aluminium ions forms the active staining ingredient haemalum. Haemalum is a basic dye which binds to basophilic cell structures such as RNA and DNA in the nucleus and RNA in ribosomes of the rough endoplasmic reticulum which appear blue or violet in colour. The counterstain Eosin Y is an acidic dye and therefore binds to acidophilic cell structures such as the cytoplasm (which is positively charged due to the abundance of the amino acids lysine and arginine present in cytoplasmic proteins), blood cells, cell membranes and some extracellular structures which appear pink to red in colour.

A resin ring was drawn around tumour sections on microscope slides using a PAP pen for immunostaining (Sigma-Aldrich, UK) so that the haematoxylin and eosin dyes were localised to the tumour sections. Using a Pasteur pipette the sections were covered with Haematoxylin Solution, Mayer's (filtered before use) (Sigma-Aldrich, UK) for 1 minute. The slide was then rinsed with running tap water until the water ran clear. The sections were then covered with Eosin Y (dissolved in ethanol to produce a 1 mg/mL solution) (Sigma-Aldrich, UK) for 2 minutes and the slide was rinsed as before. The tumour sections were dehydrated in increasing concentrations of ethanol made up in solution with dH_2O in 50 mL centrifuge tubes. The ethanol solutions and times were as follows; 50% ethanol for 2 minutes, 70% ethanol for 2 minutes, 80% ethanol for 1 minute, 90% ethanol for 1 minute and 100% ethanol for 2 minutes. The slides were then immersed in Histo-Clear (National Diagnostics, UK) for 1 minute after which the slide was allowed to dry at room temperature. Histomount (National Diagnostics, UK) was used to cover the sections and a cover slide placed on top. This was left to dry at room temperature overnight and the slides stored at 2-8°C until required. Interpretation of the stained tumour sections was performed in a blinded fashion by Dr Justin Cooke at Hull Royal Infirmary, Hull, UK. Images of the sections were taken by the author using a phase contrast microscope and an Olympus DP70 digital

microscope camera (Olympus, UK) at 10x magnification and Image-Pro Plus software (Media Cybernetics, UK) at The University of Hull, Hull, UK.

2.11 Statistical analysis

Correlation coefficients were calculated using the Pearson Correlation Coefficient and the Spearman's Rank Correlation. Statistical significance for differences between experimental conditions were calculated using the T-test for unequal variances (heteroscedastic), after an F-test had been performed to confirm unequal variances, and a p value of <0.05 was considered statistically significant.

Chapter 3 Characterisation of Duramycin

Papers and posters published in support of this chapter:

Broughton LJ, Crow C, Maraveyas A, Madden LA. Duramycin-induced calcium release in cancer cells. *Anti-Cancer Drugs*. 2016; 27(3):173-82.

Broughton L, Maraveyas A, Madden L. Targeting phosphatidylethanolamine on tumour cells using duramycin. *Thrombosis Research*. 2014; 133(S2):S213.

3.1 Introduction

Duramycin is a 19-amino acid polycyclic peptide, isolated from the bacterium *Streptoverticillium cinnamoneus*, which exhibits weak antimicrobial activity against gram-positive organisms[65]. Initial analyses of its structure were performed using high performance liquid chromatography (HPLC) which revealed the presence of ten common amino acids; asparagine, glutamine, proline, glycine (2), valine, phenylalanine (3) and lysine all in the L-form and the uncommon amino acids; β-methyllanthionine (2), meso-lanthionine, lysinoalanine and β-hydroxyaspartic acid[65]. Due to the presence of these amino acids in its structure duramycin is classed as a type B lantibiotic. The duramycin-type lantibiotics (duramycin, duramycin B, duramycin C and cinnamycin) are characterised by the presence of a lysinoalanine bridge between the C-terminal lysine (Lys 19) and an L-alanine (Ala 6) and the presence of 2 β-methyllanthionine and 1 meso-lanthionine thioether bridges[66]. The restrictive nature of the bridging system means that the duramycin-type compounds have a rigid globular formation which confers to them a stable and defined three-dimensional (3D) structure. As a result of the almost circular nature of duramycin's structure the lack of a free peptide terminus means that duramycin is resistant to proteolytic degradation[65, 66]. It has been reported that radiolabelled duramycin did not suffer metabolic degradation and was recovered intact from the urine of intravenously injected rats[64]. Duramycin is an amphipathic molecule with its hydrophobic residues existing together on one side and its hydrophilic residues on the other[66] (figure 1.3a). As cinnamycin is structurally similar to duramycin, differing by only one amino acid (figure 3.1), it also shares this unusual amphipathic structure.

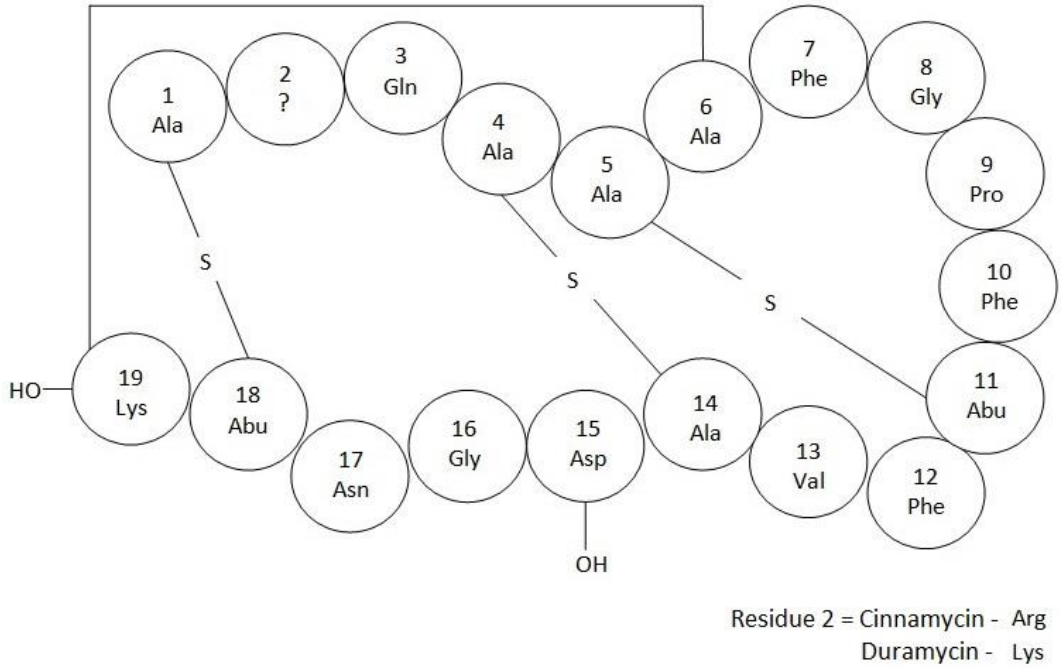

Figure 3.1: The structure of duramycin and cinnamycin.

Duramycin and cinnamycin are 19-amino acid peptides that share a conserved structure differing only at residue 2. The lantibiotics undergo a high amount of post-translational modification resulting in the presence of the uncommon amino acids; Ala-Abu – β-methyllanthionine, Ala-Ala – meso-lanthionine, Ala-Lys – lysinoalanine. Asp-OH – β-hydroxyaspartic acid.

Duramycin specifically recognises and binds to the polar headgroup of the membrane phospholipid phosphatidylethanolamine (PE). Some of the earlier evidence that duramycin specifically recognises PE was seen in duramycin resistant *Bacillus subtilis* which were found to have significantly reduced levels of PE in their membrane lipids[70]. Additionally duramycin resistant *Bacillus firmus* had reduced PE levels compared to its non-resistant counterpart[71]. The binding of radiolabelled duramycin to Jurkat cells was competitively diminished by PE-containing liposomes in a liposome concentration dependent manner[64]. However phosphatidylserine (PS), phosphatidylcholine (PC) and phosphatidylglycerol-containing liposomes were unable to competitively reduce the binding. NMR studies involving cinnamycin[69] and further studies involving duramycin revealed that the binding to PE is conserved between the two structurally similar lantibiotics. The PE binding pocket consists of the hydrophobic residues Phe 7 through to Ala 14[66]. The hydrophobic residues, Gly 8, Pro 9 and Val 13, are involved in the binding to the glycerol moiety of PE. The fatty acid acyl chains of PE can be concealed in the hydrophobic cleft of duramycin and cinnamycin (right side of structure, figure 3.1). The size of the hydrophobic cleft is that of 8-10 methylene segments which was found to be the required amount for maximal binding

interaction between lyso-PE and cinnamycin[72]. The binding pocket formed fits so exactly over the PE polar headgroup that anything other than a glycerophosphoethanolamine would not fit[69]. Additionally 2 Phe side chains protrude from the loop region of the hydrophobic cleft which anchors the lantibiotics to the hydrophobic core of the plasma membrane[64]. An ionic interaction between the carboxylate group of Asp 15 and the ammonium group of PE further stabilises the interaction[69, 72]. The exactness of duramycin's and cinnamycin's binding pocket in the recognition of PE confers their stoichiometry binding ratio of 1:1[72] and results in a dissociation constant in the low nanomolar range[65, 66, 73].

PE is the second most abundant phospholipid in mammalian cell membranes constituting 20-50% of the total phospholipids, dependent on tissue and organ[33]. It is well established that phospholipids are distributed asymmetrically between the bilayer of most eukaryotic cell membranes including the plasma membrane and the golgi, secretory vesicles and endosomal membranes[34, 35]. This feature is most evident in the plasma membrane where the majority of the choline-containing lipids such as sphingomyelin and PC reside on the outer (non-cytosolic) membrane. The majority (>80%)[33] of the aminophospholipids PS and PE reside on the inner (cytosolic) membrane[36]. The asymmetrical distribution of the phospholipids (most commonly the loss of it) contributes to the regulation of many biological processes such as the initiation of coagulation[56, 198, 199], exposure of PE during cytokinesis[50, 51], the activation of apoptosis[48, 82] where the exposure of PS provides a signal for phagocytosis and the regulation of autophagy[37]. The thermodynamic barrier to the passive transbilayer movement of phospholipids prevents spontaneous loss of membrane asymmetry[38]. The half time of the translocation of phospholipids is highly dependent upon cell type though ranges from hours to days. Thus the rapid movement of phospholipids in the maintenance and loss of membrane asymmetry must be sustained by more than the thermodynamic barrier. The unidirectional inward transport of phospholipids is controlled by a group of P4-type ATPases known as the aminophospholipid translocases (APTLs), often referred to as flippases[41]. These are members of the P-type ATP pump superfamily which is divided into five sub-families the first three of which transport small cations or metal ions across the membrane such as the calcium ion (Ca^{2+})-ATPase and the sodium potassium (Na^{+}/ K^{+})-ATPase[35, 43]. Along with the P4-type ATPases the flippases include the erythrocyte specific magnesium (Mg^{2+})-ATPase[38]. Flippases are specific for PE, PC and PS and are ATP and Mg^{2+} dependent[44]. Unidirectional outward transport of phospholipids is controlled by a number of proteins from four families of the ATP-binding cassette (ABC) transporter

group and are often referred to as the floppases. The ABC transporters can be specific or non-specific for certain phospholipids[38], transporting a variety of phospholipids across membranes. Bidirectional phospholipid transport is controlled by the phospholipid scramblases (PLSCRs or just scramblases) which are ATP-independent[33]. The flippases and floppases require an input of energy (ATP) to allow them to pump against a concentration gradient but the scramblases are ATP-independent due to the existence of a transbilayer lipid gradient[45]. It is widely believed that scramblases function to remove membrane asymmetry upon activation such as in apoptosis rather than to assist in the maintenance of membrane asymmetry[46, 47]. Cell injury, cell activation, apoptosis and malignant transformation can all have an effect on the activity of phospholipid transporters. They can also be affected by an increase in intracellular Ca^{2+} concentration ($[Ca^{2+}]_i$) which can inhibit flippases and stimulate some of the floppases and scramblases. At physiological Ca^{2+} concentrations phospholipid membrane asymmetry is maintained by activated flippases and floppases and inactivated scramblases[200]. An increase in physiological $[Ca^{2+}]_i$ results in the outward movement of PE and PS which can lead to the activation of many of the physiological processes mentioned above. The cell surface exposure of PE and PS that preceded apoptotic cell death in reperfused ischaemic myocytes was thought to be connected to the Ca^{2+} overload and decreased ATP often observed in ischaemic myocardium[44]. It was thought that the translocation of PE and PS could have been caused by inhibited flippases.

The exposure of cell surface PE has also been seen to occur on tumours, tumour vasculature and tumour-derived microparticles[49, 59-61] and in response to chemotherapy[62, 63]. PE expression on the surface of endothelial cells, detected using biotinylated duramycin via flow cytometry, was shown to be upregulated in response to treatment with irradiation, reactive oxygen species (ROS), low pH and hypoxia[59]. Using the same duramycin compound it was show that PE becomes exposed on the vascular endothelium of tumours where it is most prominent in areas of hypoxia[59]. The level of cell surface PE expression, detected by duramycin, was increased on the pancreatic cancer cell lines AsPC-1 and CFPAC-1 when they were apoptotic compared to untreated viable cells and was further increased when the cells were necrotic[49]. It has recently been shown that PE was expressed in higher abundance in xenografts from a variety of tumour types compared to their normal tissue counterparts[61].

A number of studies have utilised the externalisation of PE on activated cells and the specificity of duramycin for the phospholipid. The N-terminal of duramycin, which consists of 2 primary amino acids (cysteine and lysine), is situated away from the PE binding site so that it offers a potential location for conjugation[68]. Duramycin conjugates were used to characterise and image the exposure of PE on tumour vasculature[59]. Duramycin attached to the NHS-ester of a biotin molecule (DLB) and duramycin attached to the near infrared fluorophore 800CW (Dur-800CW) were shown to retain their binding ability and to specifically recognise PE over other phospholipids. Intravenous injection of DLB into tumour bearing mice showed localisation of DLB to tumour blood vessels in all tumours investigated (prostate, breast and lung carcinoma and melanoma from both mice and human species). The exposure of PE on the blood vessels was seen to co-localise with PS exposure. Dur-800CW localised to the tumour vasculature of prostate tumour bearing mice and no other tissue with the exception of the kidneys, the main excretory route for duramycin[59]. This study highlighted that PE could possibly be used as a broad tumour marker for many different malignancies. Biotinylated duramycin has also been used to assess the level of PE compared to PS in the membrane of microparticles (MPs) derived from a variety of cells (breast cancer cells, endothelial cells and red and white blood cells)[60]. A higher level of PE than PS was detected on the MPs from all cell types. Duramycin (≤0.5 μM) did not bind to the cells that the MPs were derived from which was thought to indicate the lack of cell surface PE expression on the viable cells.

Other studies in the literature have largely focused on duramycin as a molecular probe for the imaging and assessment of acute cell death. Duramycin was covalently modified with HYNIC to either Cys 1 or Lys 2 and subsequently radiolabelled with technetium (^{99m}Tc)[64]. *In vitro* experiments showed that the cellular binding of ^{99m}Tc-duramycin to Jurkat cells was significantly enhanced in apoptotic cells compared to viable cells. The binding was competitively reduced in the presence of PE-containing liposomes. *In vivo* imaging of rats by single-photon emission computed tomography (SPECT) that had been intravenously injected with ^{99m}Tc-duramycin showed specific uptake in the infarcted region of the myocardium. As an improvement upon this study the research group developed a single-step labelling technique for ^{99m}Tc to HYNIC-duramycin which bettered the purity of the compound and was shown to retain its ability to localise to the infarcted site in rat cardiac tissue and also localise to PE exposed on the luminal surface of aortic endothelium[74, 75]. Further studies have been published by the same group with regards to the expansion of ^{99m}Tc-duramycin's application and its improvement as a probe for cell death[63, 76-81]. An

interesting development was the demonstration of a possible use for ^{99m}Tc-duramycin in the early detection of apoptosis following paclitaxel treatment of a breast carcinoma xenograft[63]. Other studies have also utilised ^{99m}Tc-duramycin and SPECT as a tool to image early apoptotic response to chemotherapy in tumours[62, 82]. A novel positron emission tomography (PET) probe was developed using duramycin ([^{18}F]FPDuramycin) that localised to the tumour site, specifically the apoptotic and necrotic regions, following cyclophosphamide or cisplatin chemotherapy[83]. Thus duramycin has been utilised in a number of ways to take advantage of the cell surface exposure of PE.

Duramycin has been shown to effect PE-containing membranes through the inducement of transbilayer lipid movement and changes in the shape of the membrane[73, 92]. Duramycin, in a concentration dependent manner (40-500 μM), caused PE-containing multilamellar vesicles to change shape resulting in the formation of rod-like structures. These rod-like structures were found to be hollow tubules consisting of lipid bilayers in which duramycin was able to penetrate into the hydrophobic interior region[73]. Furthermore, duramycin has been shown to induce pore formation in membranes[88, 89], increase membrane permeability[178, 179], effect ion transport[70, 84, 86, 87, 91] and cause haemolysis of erythrocytes[180]. Additionally, the duramycin-type lantibiotics can indirectly interfere with enzyme activity through the blocking of PE leading to the inhibition of phospholipase A2[201]. At the time of the investigations undertaken in this chapter duramycin was recognised as a potential probe for cell surface exposed PE[59, 64], which was a potential biomarker for tumours[59, 61] and cell death[64], and although duramycin's ability to effect cell membranes was acknowledged in these studies its cell death-inducing effects were not fully appreciated. Therefore the work in this chapter was undertaken with the aim of assessing the cytotoxic effects of duramycin on tumour cells and to characterise its ability to detect PE in order to establish whether duramycin could be used as a novel direct anti-cancer agent. However, at the time of writing the literature had begun to take into consideration the cytotoxic potential of duramycin when developing it as a novel conjugate for the targeting of PE[202].

3.2 Results

3.2.1 Phosphatidylethanolamine detection on cancer cells by flow cytometry

The detection of PE was investigated using a series of duramycin concentrations (0.1-1000 µM) on the 2 ovarian cancer cell lines, A2780 and SK-OV-3, and the 2 pancreatic cancer cell lines, AsPC-1 and MIA PaCa-2. Briefly, cells ($2x10^5$) in PBS were incubated for 30 minutes at room temperature with either duramycin or normal rabbit serum (1:5000 dilution) which was used as the negative control to account for non-specific binding. Preliminary experiments using A2780 and MIA PaCa-2 showed that there was no difference in the level of PE detection by duramycin (50 µM) at different incubation times (0, 2, 5, 15 and 30 minutes) (Appendix A, figure A.1). However different incubation times (0, 15, 30 and 60 minutes) with duramycin (50 µM) did result in a difference in the amount of necrotic cell death in 3 out of the 4 cancer cell lines assessed (Appendix A, figure A.2). The percentage of cells that were necrotic increased with longer incubation times. An incubation time of 30 minutes was chosen to allow consistency with future experiments that would have the aim of using duramycin as an anti-cancer (cell death inducing) agent. After incubation cells were washed with PBS, centrifuged and re-suspended in PBS (300 µl) at which point they were incubated for 30 minutes at room temperature with an anti-duramycin antibody. Once they had been washed and re-suspended as before the cells were incubated with a sheep anti-rabbit IgG:FITC antibody for 30 minutes in the dark at room temperature. After the cells had been washed and re-suspended they were analysed by flow cytometry with an argon laser at 488 nm. PE expression was given as the median fluorescence intensity ratio (MFIR) of the median fluorescence of the positive (duramycin treated) cells over the negative control (rabbit-serum treated) cells.

Duramycin detected the expression of PE on the surface of all 4 of the cancer cell lines in a concentration dependent manner (figure 3.2). The level of PE expression was similar for all 4 cancer cell lines at duramycin concentrations 0.1-10 µM however at concentrations ≥25 µM a difference in PE expression emerged between the cell lines. The order of the cancer cell lines from the lowest PE expression to the highest was MIA PaCa-2 ≤ SK-OV-3 < A2780 < AsPC-1. The duramycin concentration that detected the highest level of PE expression differed between the cancer cell lines. For A2780 and MIA PaCa-2 this concentration was ≥200 µM, for SK-OV-3 it was 500 µM and for AsPC-1 it was 1 mM. Thus in order to detect the optimal level of PE expression in these 4 cancer cell lines a duramycin concentration of ≥200 µM is required.

a)

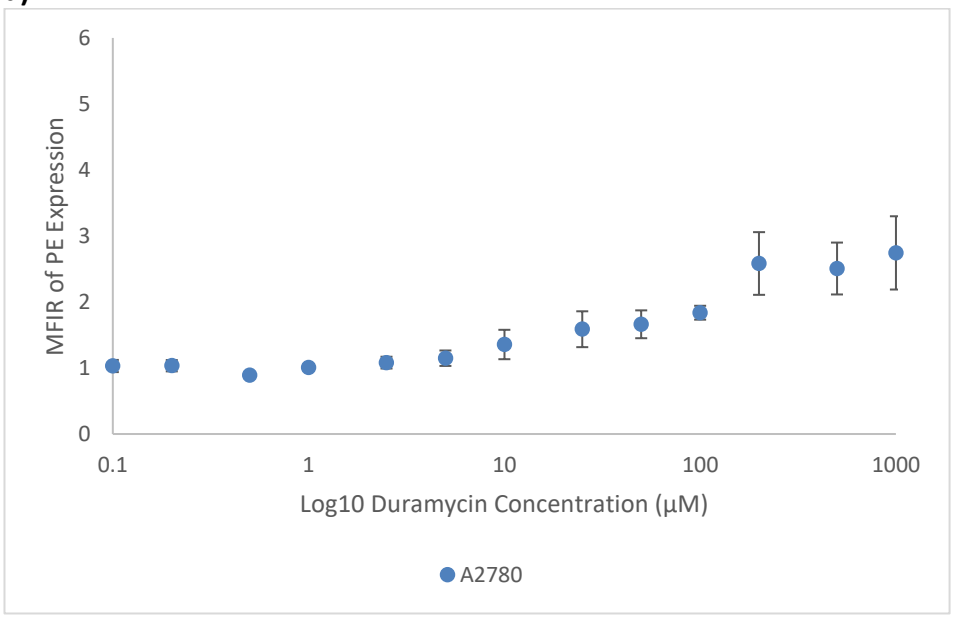
MFIR of PE Expression
0
1
2
3
4
5
6
0.1
1
10
100
1000
Log10 Duramycin Concentration (µM)
A2780

b)

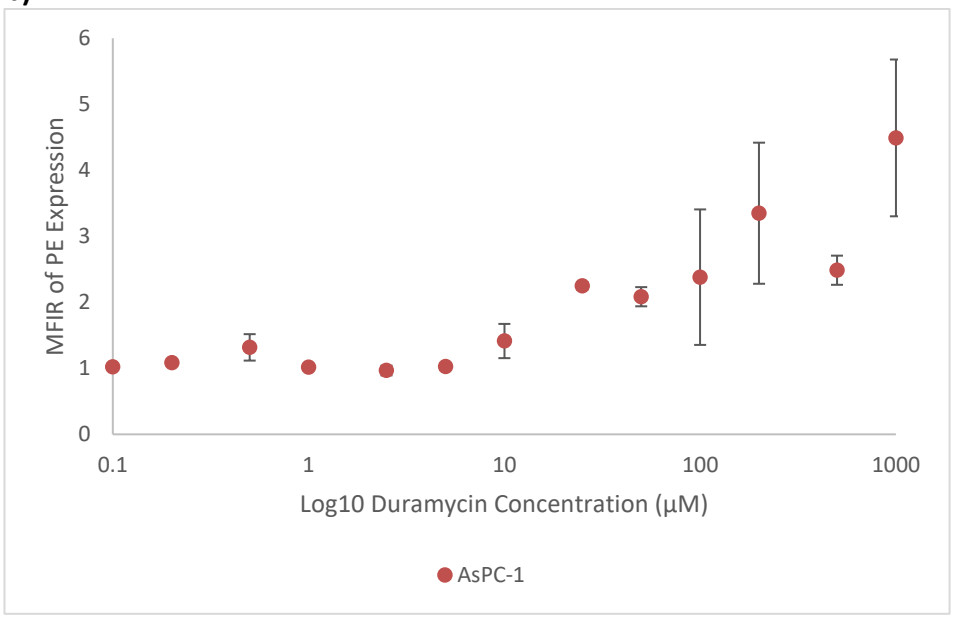
MFIR of PE Expression
0
1
2
3
4
5
6
0.1
1
10
100
1000
Log10 Duramycin Concentration (µM)
AsPC-1

c)

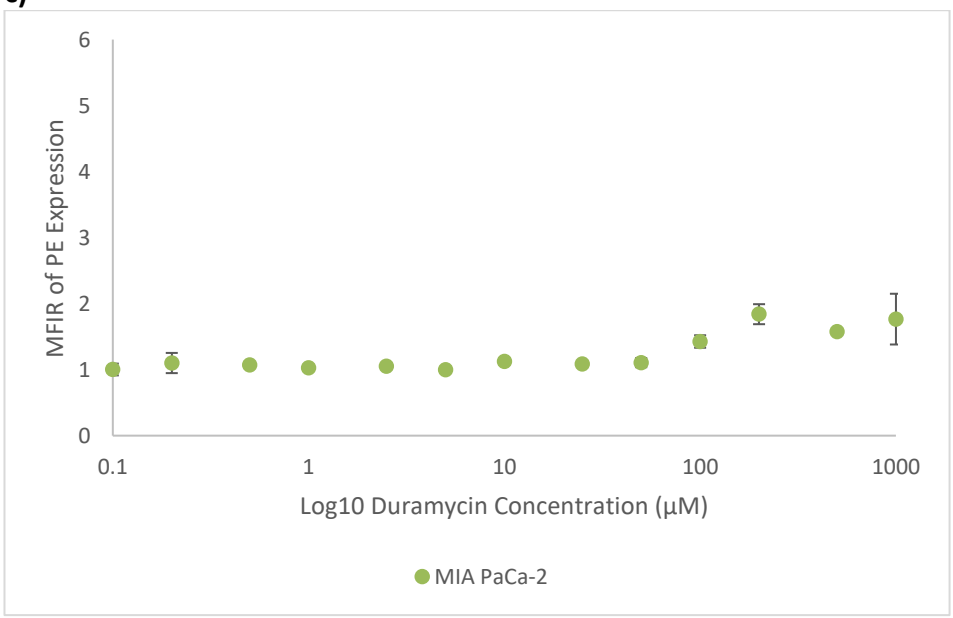
MFIR of PE Expression
0
1
2
3
4
5
6
0.1
1
10
100
1000
Log10 Duramycin Concentration (µM)
MIA PaCa-2

d)

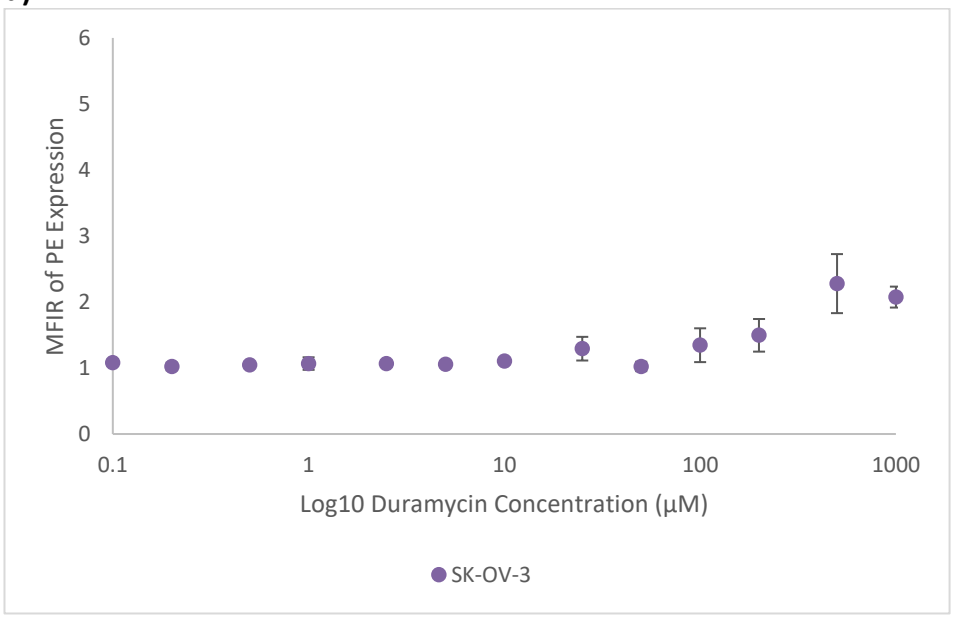

e)

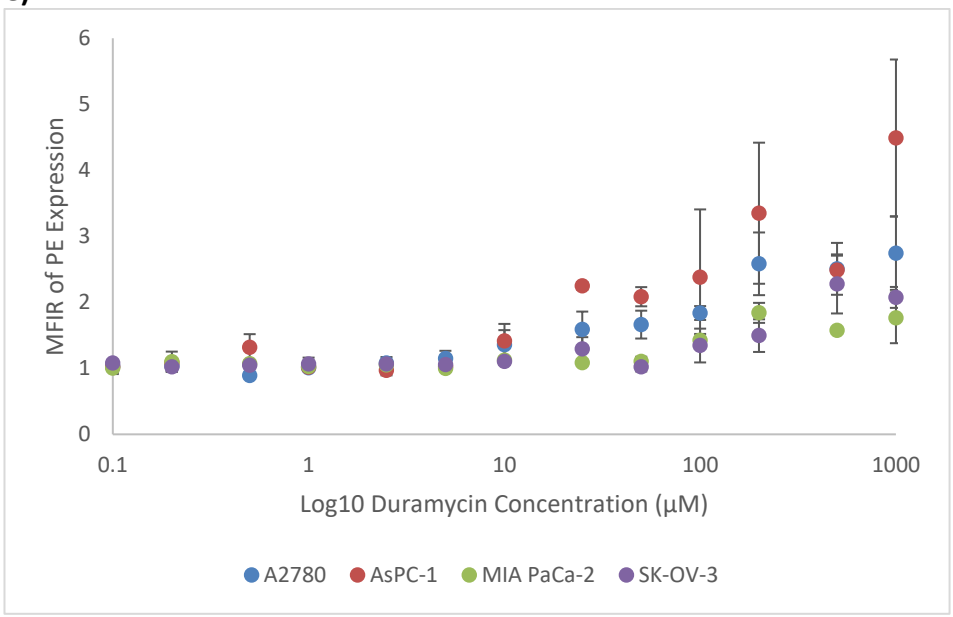

Figure 3.2: Detection of PE on the surface of cancer cells by duramycin.
The detection of cell surface PE was duramycin concentration dependent for all 4 cancer cell lines a) A2780, b) AsPC-1, c) MIA PaCa-2 and d) SK-OV-3. Optimal PE detection occurred at duramycin concentrations ≥200 µM. e) Comparison of the cancer cell lines. PE expression was given as the MFIR. Error bars represent standard deviation (SD) of 2 replicates.

3.2.2 Effect of duramycin on the viability of cancer cells

To investigate whether duramycin had an effect on the viability of tumour cells the cancer cell lines A2780, AsPC-1, MIA PaCa-2 and SK-OV-3 were treated with 0.1-1000 µM duramycin and assessed by flow cytometry using the Annexin V: FITC Apoptosis Detection Kit I. Briefly, cells ($2x10^5$) in PBS were treated with duramycin for 30 minutes at room temperature and then washed with PBS, centrifuged and re-suspended in Annexin V binding buffer (100 µl) (1:10 dilution). The cells were then incubated with propidium iodide (PI) (5 µl) and Annexin V (5 µl) for 15 minutes in the dark at room temperature. Subsequently, Annexin V binding buffer (300 µl) was added and the cells were analysed by flow cytometry. As PI is able to permeate damaged plasma membranes it is used to stain the DNA in the nuclei of cells that are necrotic. Annexin V binds to cell surface expressed PS on cells that are undergoing apoptosis. Through dual staining it was possible to identify populations of cancer cells that were healthy, apoptotic or necrotic (figure 3.3) and express the number of cells in each population as a percentage of the total number of cells.

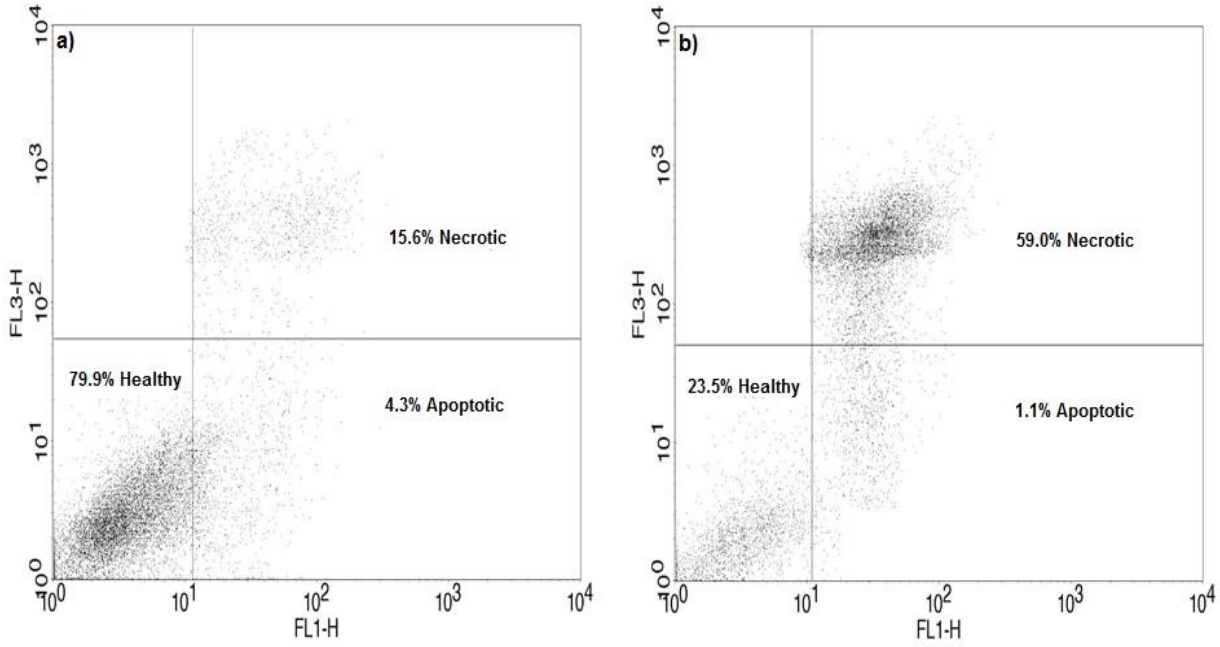

Figure 3.3: Flow cytometry quadrant graphs for annexin V: FITC and PI.

Dual stain using annexin V: FITC (FL1-H) and propidium iodide (FL3-H) was used to determine the percentage of cells that were healthy, apoptotic or necrotic in duramycin treated cancer cell lines. a) A2780 cells treated with 10 µM duramycin. b) A2780 cells treated with 100 µM duramycin. Controls were used to setup the quadrant parameters for each cell line, these controls were; 1 flow cytometer 5 mL tube containing unstained cells (cells only), 1 tube containing cells plus annexin V only and 1 tube containing cells plus PI only.

3.2.2.1 Healthy

Duramycin reduced the number of cells in the healthy cell population in all 4 cancer cell lines A2780, AsPC-1, MIA PaCa-2 and SK-OV-3 in a concentration dependent manner (figure 3.4). Duramycin at 500 µM and 1 mM was able to reduce the population of healthy cells to <5% in A2780 and AsPC-1 and <10% in MIA PaCa-2 and SK-OV-3. The reduction in the healthy cell population followed a similar trend for all the cancer cell lines. However the concentration of duramycin required to reduce the healthy cell population compared to the untreated (PBS treated) control cells differed between the cancer cell lines. This concentration was >25 µM for A2780. For example the percentage of healthy cells in the untreated control was 86.4±2.9% compared to 76.1±7.8% in 25 µM duramycin treated cells and 49.1±2.9% in 50 µM duramycin treated cells. The concentration required for the reduction of healthy cells compared to the untreated control was >10 µM for AsPC-1 and MIA PaCa-2 and >2.5 µM for SK-OV-3. AsPC-1 had a naturally lower cell viability than the other cancer cell lines and the healthy population of cells in the untreated AsPC-1 control equated to 58.1±3.6%.

a)

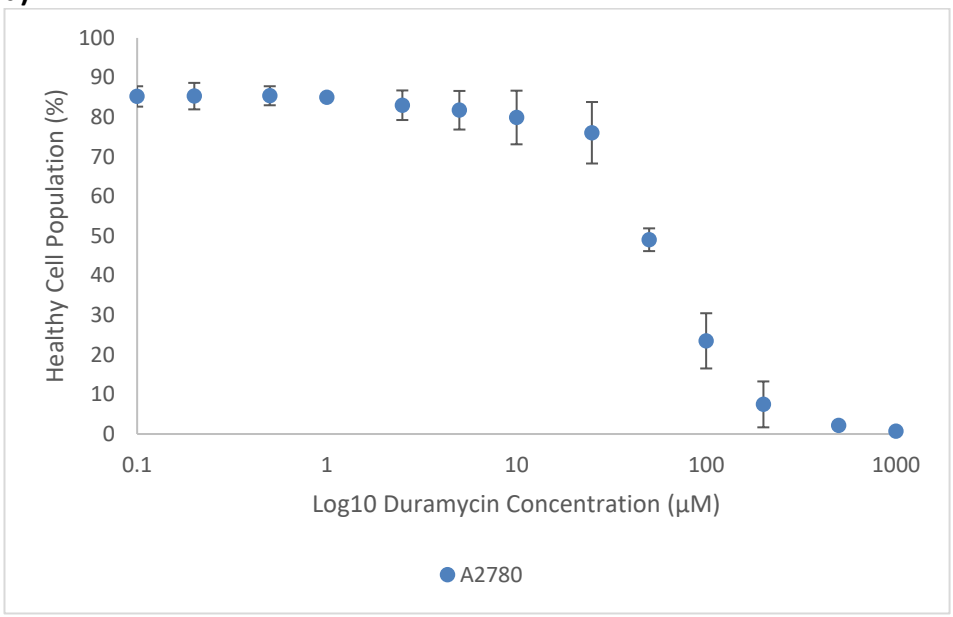
Healthy Cell Population (%)
100
90
80
70
60
50
40
30
20
10
0
0.1
1
10
100
1000
Log10 Duramycin Concentration (µM)
A2780

b)

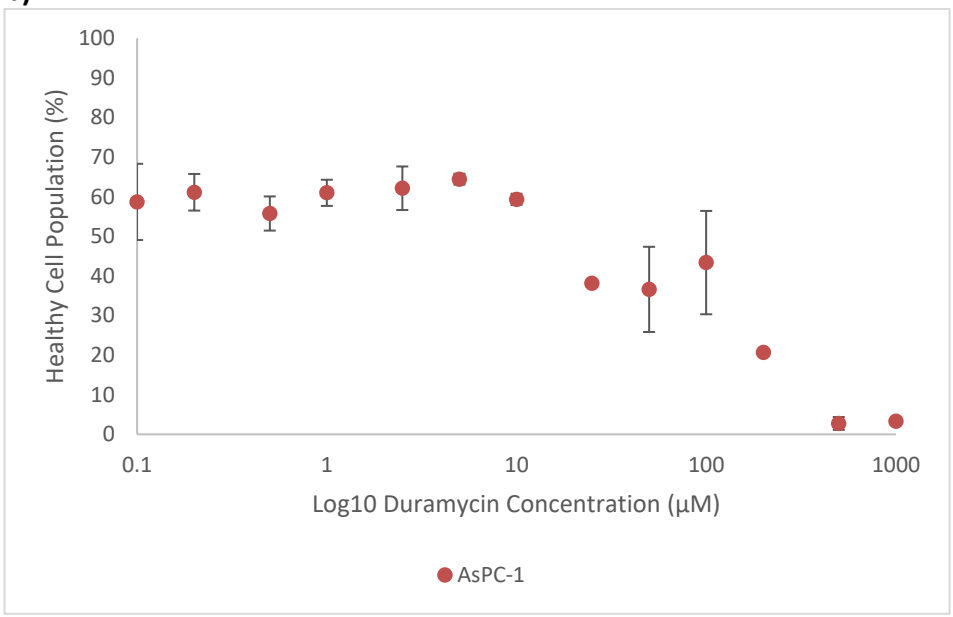
Healthy Cell Population (%)
100
90
80
70
60
50
40
30
20
10
0
0.1
1
10
100
1000
Log10 Duramycin Concentration (µM)
AsPC-1

c)

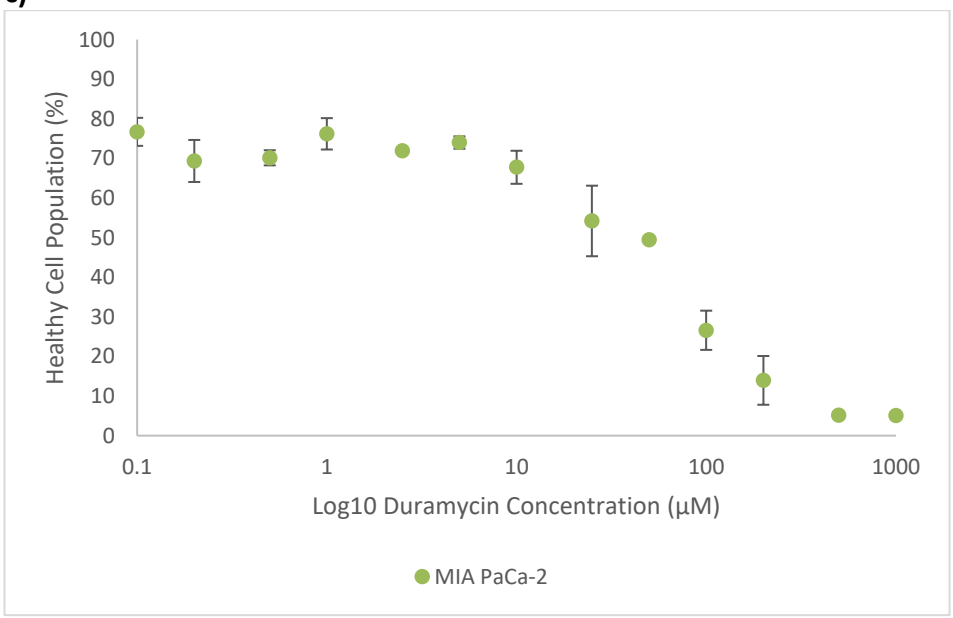
Healthy Cell Population (%)
100
90
80
70
60
50
40
30
20
10
0
0.1
1
10
100
1000
Log10 Duramycin Concentration (µM)
MIA PaCa-2

d)

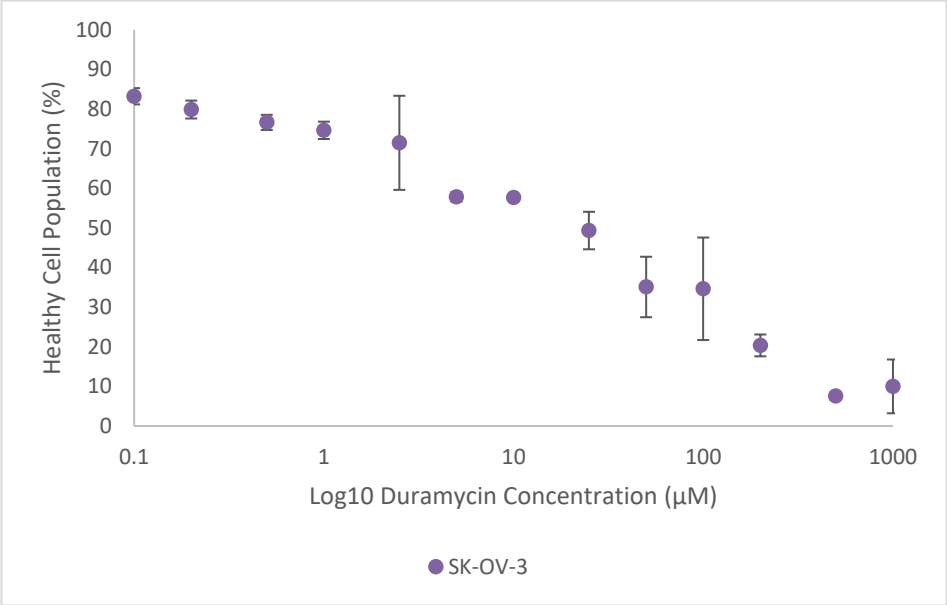

e)

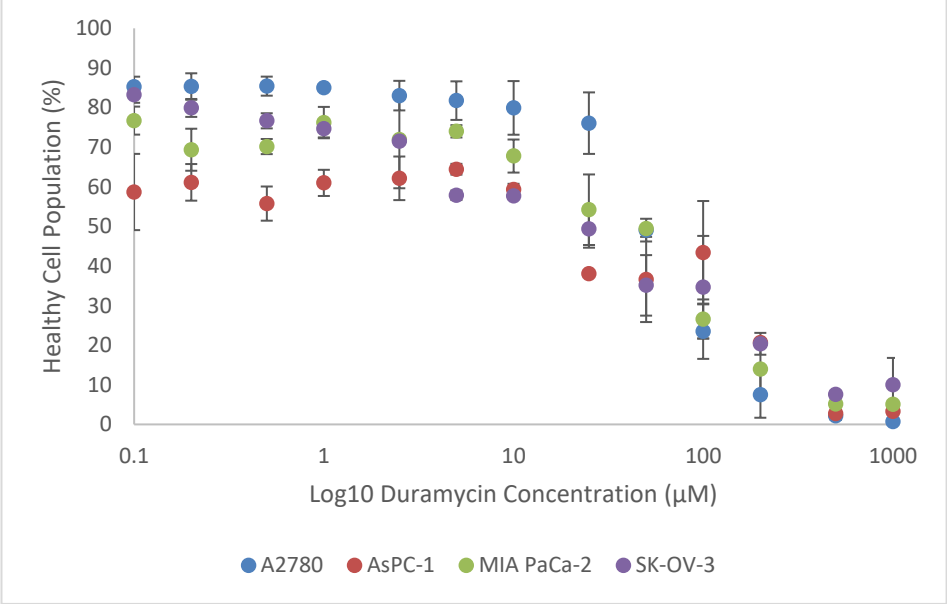

Figure 3.4: The effect of duramycin on the cell viability (healthy cell population) of cancer cells.

Duramycin reduced the percentage population of cells that were healthy in a concentration dependent manner for all 4 cancer cell lines a) A2780, b) AsPC-1, c) MIA PaCa-2 and d) SK-OV-3. e) The reduction in the healthy cell population followed a similar trend for all the cancer cell lines. However a difference in sensitivity to duramycin was observed between the cell lines. Reduction in the healthy cell population compared to the untreated controls occurred at a) >25 µM, b) and c) >10 µM and d) >2.5 µM. Error bars represent SD of 2 replicates.

3.2.2.2 Apoptotic

Duramycin had a different effect on the percentage of cells in the apoptotic cell population for the 4 cancer cell lines (figure 3.5). The apoptotic population of cells was small (<10%) in the A2780 and AsPC-1 cell lines and this number was not effected (within SD) by duramycin concentration nor was it greatly different to the untreated control cells (3.0±1.2% and 3.9±1.5%, respectively). For MIA PaCa-2 there was a population of apoptotic cells present at duramycin concentrations ≤10 μM. However this was also not different to the number in the untreated control cells (13.2±4.6%). It is therefore possible that duramycin does not induce apoptosis in these cancer cell lines. The number of apoptotic cells in MIA PaCa-2 was reduced at concentrations >10 μM which corresponded to a higher level of cells in the necrotic cell population (section 3.2.2.3). As with the above results there was an apoptotic cell population present in SK-OV-3 cells that did not differ from the untreated control cells (15.1±4.4%) at duramycin concentration ranges of 0.1-2.5 μM and 25-200 μM. As with MIA PaCa-2 there was a reduction in the apoptotic population >200 μM which corresponded to a high level of necrosis. However there was a larger population of apoptotic cells at duramycin concentrations of 5 μM and 10 μM. Here the percentage of cells that were apoptotic were 30.2±3.6% and 28.5±4.8%, respectively.

a)

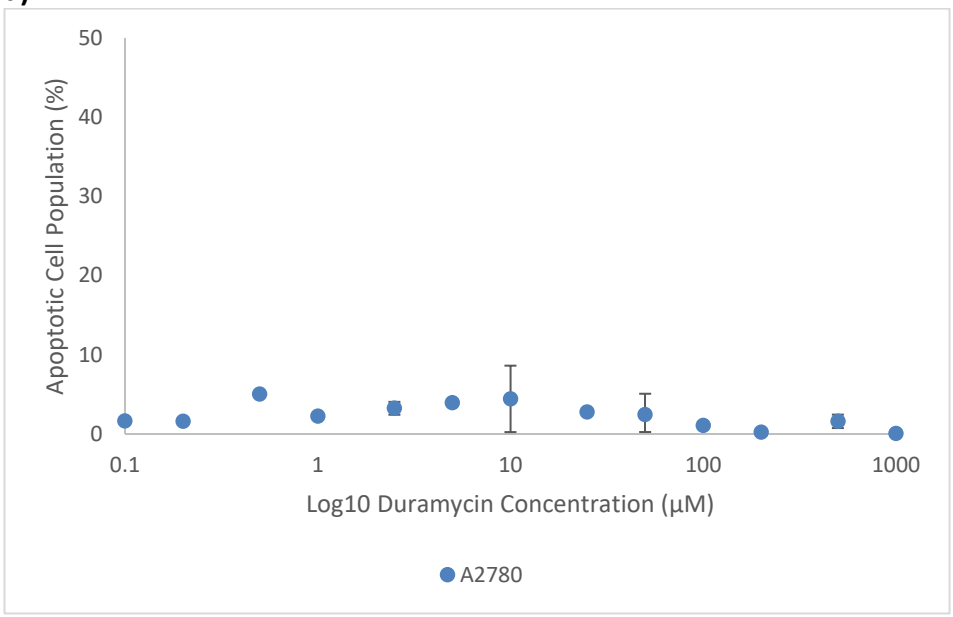
50
40
30
20
10
0
Apoptotic Cell Population (%)
0.1
1
10
100
1000
Log10 Duramycin Concentration (µM)
A2780

b)

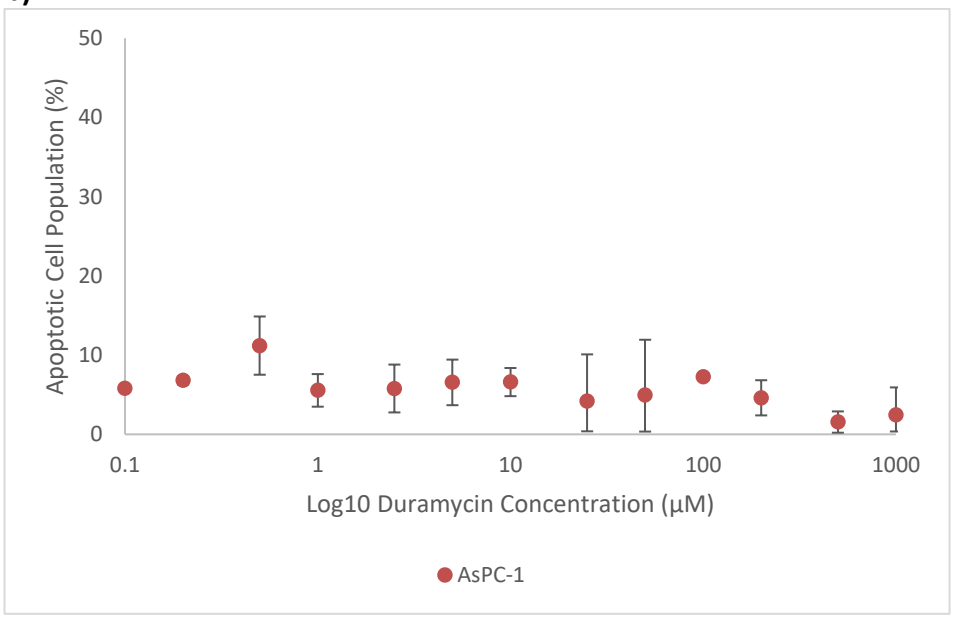
50
40
30
20
10
0
Apoptotic Cell Population (%)
0.1
1
10
100
1000
Log10 Duramycin Concentration (µM)
AsPC-1

c)

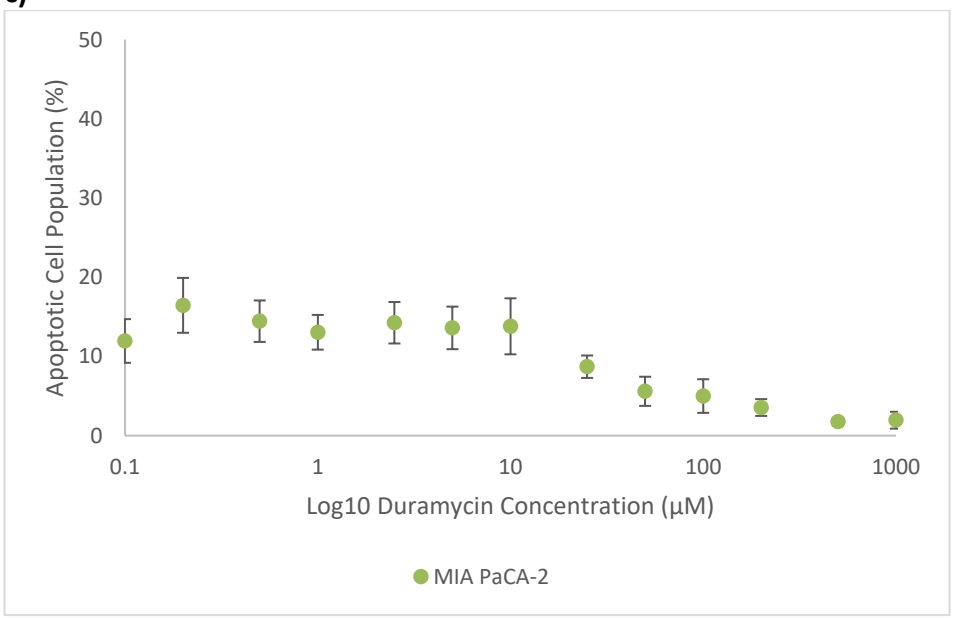
50
40
30
20
10
0
Apoptotic Cell Population (%)
0.1
1
10
100
1000
Log10 Duramycin Concentration (µM)
MIA PaCA-2

d)

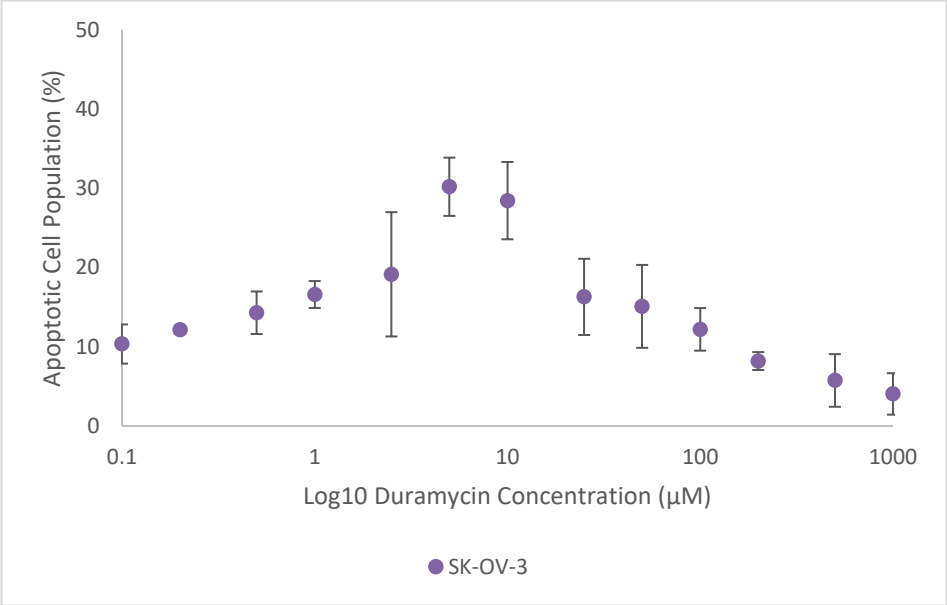

e)

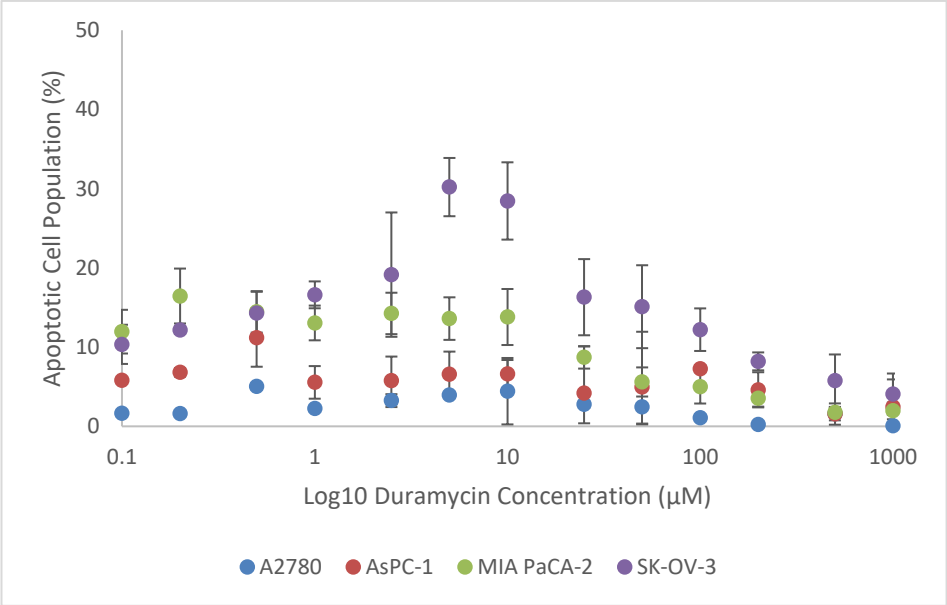

Figure 3.5: The effect of duramycin on the cell viability (apoptotic cell population) of cancer cells.

Duramycin treatment did not affect the number of cells in the apoptotic cell population in a) A2780, b) AsPC-1 and c) MIA PaCa-2. Duramycin at 5 µM and 10 µM resulted in a larger population of apoptotic cells in d) SK-OV-3 cells. e) Comparison of the cancer cell lines. Error bars represent SD of 2 replicates.

3.2.2.3 Necrotic

Duramycin treatment increased the number of cells in the necrotic cell population in all 4 cancer cell lines A2780, AsPC-1, MIA PaCa-2 and SK-OV-3 in a concentration dependent manner (figure 3.6). The majority of cells were necrotic at duramycin concentrations of 500 µM and 1 mM where >95% of cells were necrotic in A2780, >90% in AsPC-1 and MIA PaCa-2 and >85% in SK-OV-3. The increase in the number of necrotic cells followed a similar trend for all 4 cancer cell lines. However the concentration required to increase the necrotic cell population from that of the untreated control cells was >25 µM for A2780 and >10 µM for the other 3 cancer cell lines. AsPC-1 had a naturally lower cell viability than the other cancer cell lines and the necrotic population of cells in the untreated AsPC-1 control equated to 35.9±2.1%.

a)

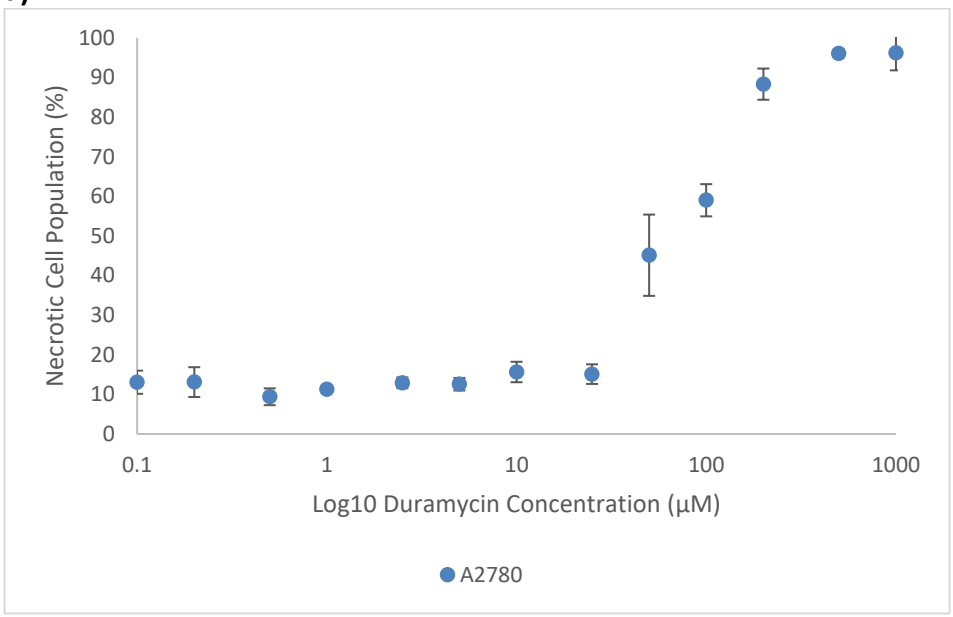
Necrotic Cell Population (%)
100
90
80
70
60
50
40
30
20
10
0
0.1
1
10
100
1000
Log10 Duramycin Concentration (µM)
A2780

b)

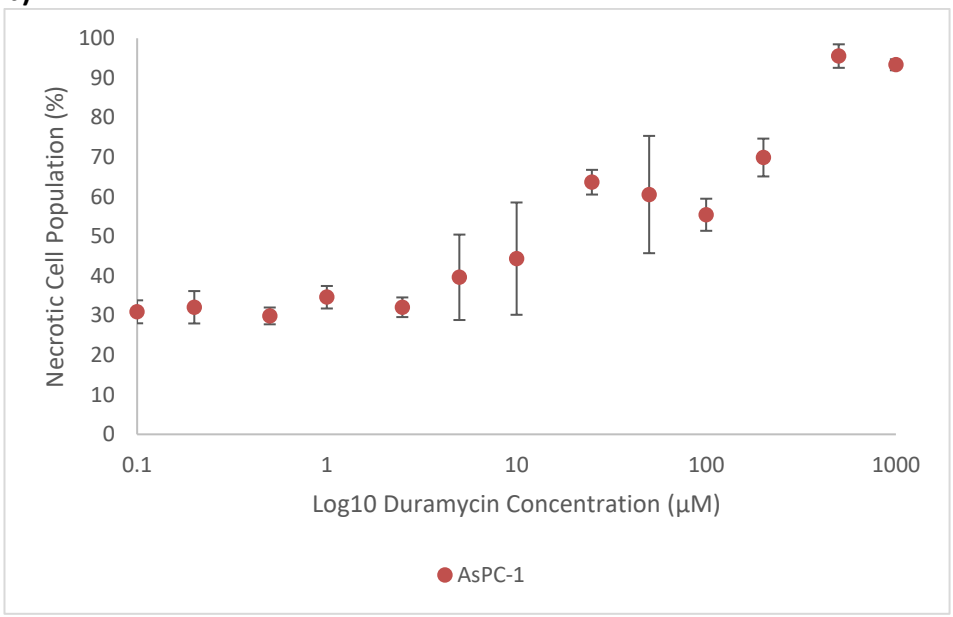
Necrotic Cell Population (%)
100
90
80
70
60
50
40
30
20
10
0
0.1
1
10
100
1000
Log10 Duramycin Concentration (µM)
AsPC-1

c)

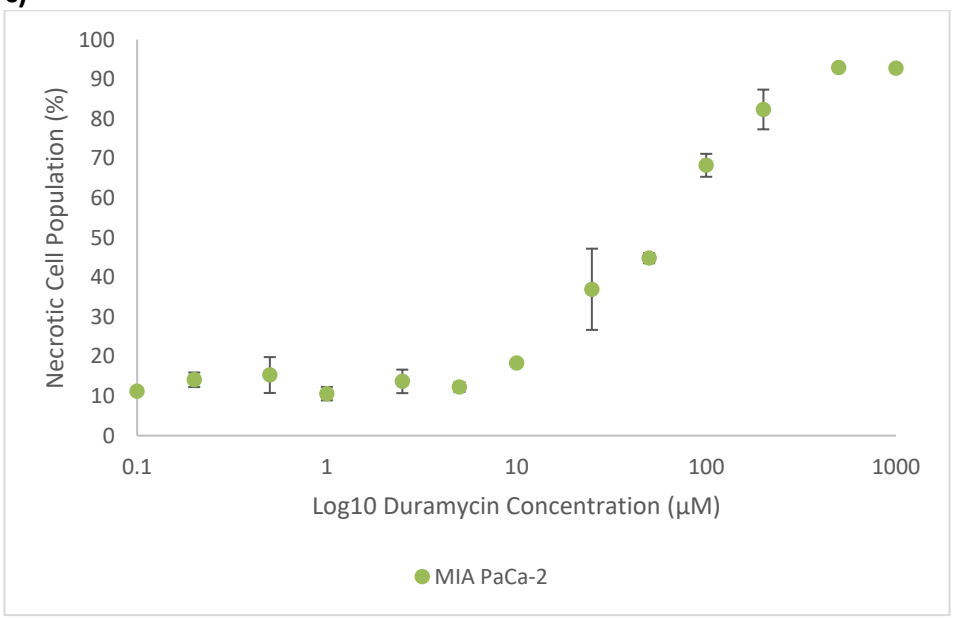
Necrotic Cell Population (%)
100
90
80
70
60
50
40
30
20
10
0
0.1
1
10
100
1000
Log10 Duramycin Concentration (µM)
MIA PaCa-2

d)

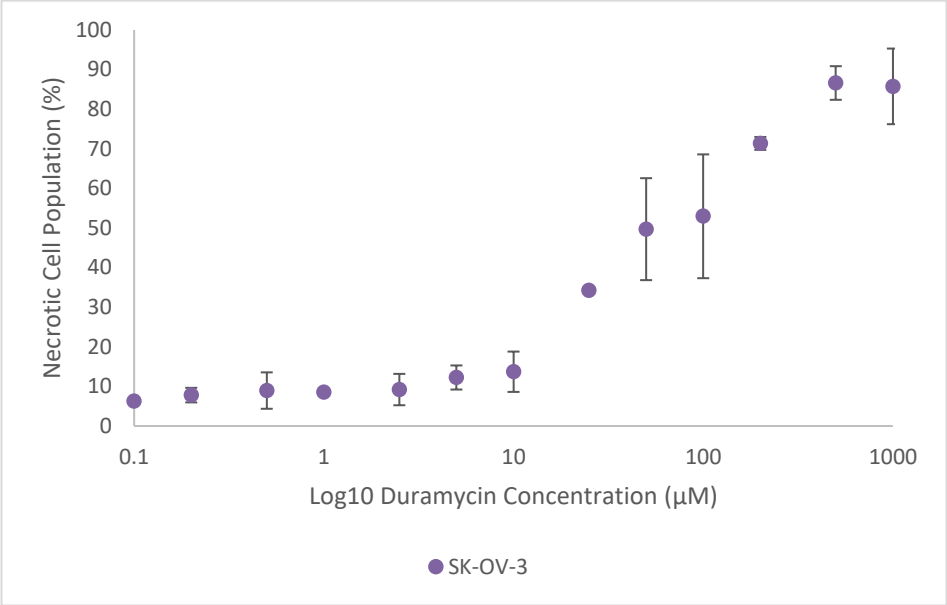

e)

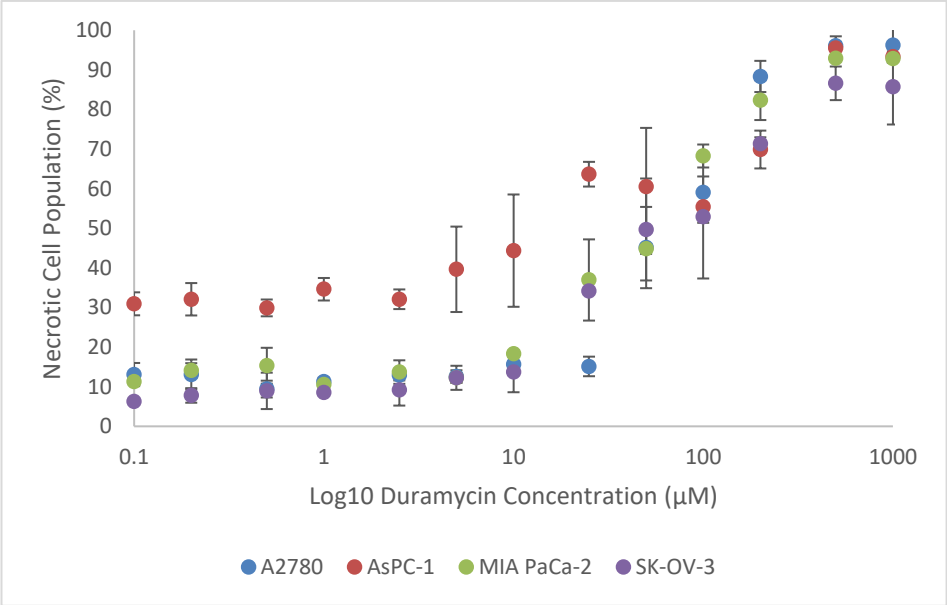

Figure 3.6: The effect of duramycin on the cell viability (necrotic cell population) of cancer cells.

Duramycin induced necrotic cell death in all 4 cancer cell lines a) A2780, b) AsPC-1, c) MIA PaCa-2 and d) SK-OV-3 in a concentration dependent manner. The duramycin concentration which produced a necrotic cell population differed between cancer cell lines where >10 µM induced necrosis in AsPC-1, MIA PaCa-2, SK-OV-3 and >25 µM induced necrosis in A2780. E) Comparison of the cancer cell lines. Error bars represent SD of 2 replicates.

In summary, 30 minute treatment with duramycin was able to reduce the number of healthy cancer cells and induce cancer cell death, primarily through necrosis, in a concentration dependent manner. Duramycin <10 µM had little to no effect on the cell viability of A2780, AsPC-1 and MIA PaCa-2 whereas concentrations >10 µM induced necrosis. SK-OV-3 cells are potentially more sensitive to duramycin treatment as the concentration that did not affect cell viability was ≤2.5 µM. While necrosis was induced >10 µM similar to the other cancer cell lines, ~30% of cells were apoptotic in SK-OV-3 when treated with 5 µM and 10 µM duramycin. Therefore the concentration of duramycin that could be used to detect cell surface expressed PE on tumour cells and not affect cell viability was found to be 2.5 µM.

3.2.2.4 Effect of duramycin on cancer cell viability at longer incubation times

It was shown that duramycin at concentrations <10 μM had little effect on the cell viability of cancer cells. Therefore it was investigated whether these relatively low concentrations had an effect on the viability of cancer cells after longer incubation times. Briefly, cells ($1x10^5$) in appropriate media (400 μl) were treated with duramycin in PBS (100 μl) at required concentration (0.1-10 μM) in 24-well plates. The cells were then incubated at 37°C in a 5% CO_2 atmosphere for 24, 48 or 72 hours. Cells were removed from wells by trypsinisation and the resultant solution was then centrifuged. Cells were then re-suspended in Annexin V binding buffer (100 μl) and analysed for cell viability by flow cytometry using the Annexin V: FITC Apoptosis Detection Kit I. It had been previously reported that relatively low concentrations of duramycin after 48 hours treatment resulted in apoptotic and necrotic cell populations in pancreatic cancer cell lines[49]. Thus it was investigated whether this was found in the pancreatic and ovarian cancer cell lines used in this study.

Duramycin elevated the number of cells in the apoptotic cell population in all 4 cancer cell lines A2780, AsPC-1, MIA PaCa-2 and SK-OV-3. In general there was no difference between the 24, 48 and 72 hour incubation times. The exceptions to this were: a larger population of apoptotic cells at 2.5 μM duramycin at 24 hours for AsPC-1 and MIA PaCa-2 and a smaller population at 10 μM duramycin at 24 hours for A2780 and AsPC-1. To evaluate whether the number of apoptotic cells in the duramycin treated cancer cell lines was different to the untreated control cells the values for the 3 incubation time conditions were averaged. The duramycin concentrations that increased the number of apoptotic cells in the cancer cell lines, compared to the untreated control cells, were 5 μM for A2780 and SK-OV-3, 10 μM for MIA PaCa-2 and 5 μM and 10 μM for AsPC-1 (figure 3.7).

Duramycin also elevated the number of cells in the necrotic cell population in all 4 cancer cell lines A2780, AsPC-1, MIA PaCa-2 and SK-OV-3 (figure 3.8). For example, dependent on cell line, 50-82% of cells were in the necrotic cell population at 10 μM duramycin treatment. In general there was no difference between the 24, 48 and 72 hour incubation time conditions with the exception of larger populations of necrotic cells in AsPC-1 at 5 μM and 10 μM at 24 hours. Duramycin at 5 μM and 10 μM increased the number of necrotic cells in A2780, AsPC-1 and SK-OV-3 compared to the untreated controls. This increase occurred only at 10 μM for MIA PaCa-2 cells. Therefore, while 30 minute duramycin treatment using concentrations <10 μM did not have an effect on cell viability (with the exception of

apoptosis in SK-OV-3), treatment with duramycin ≥5 µM for ≥24 hours was able to reduce the cell viability of the cancer cell lines.

a)

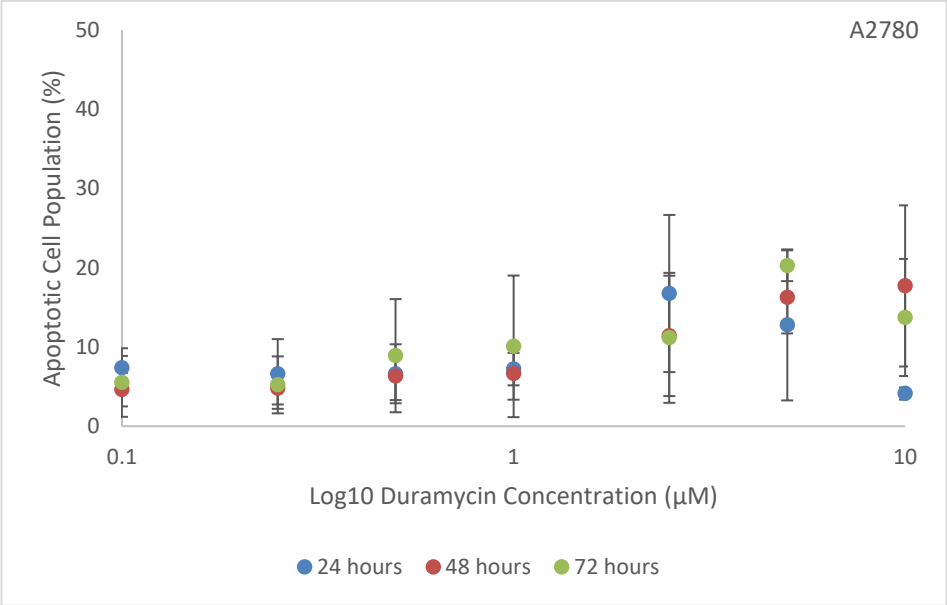

b)

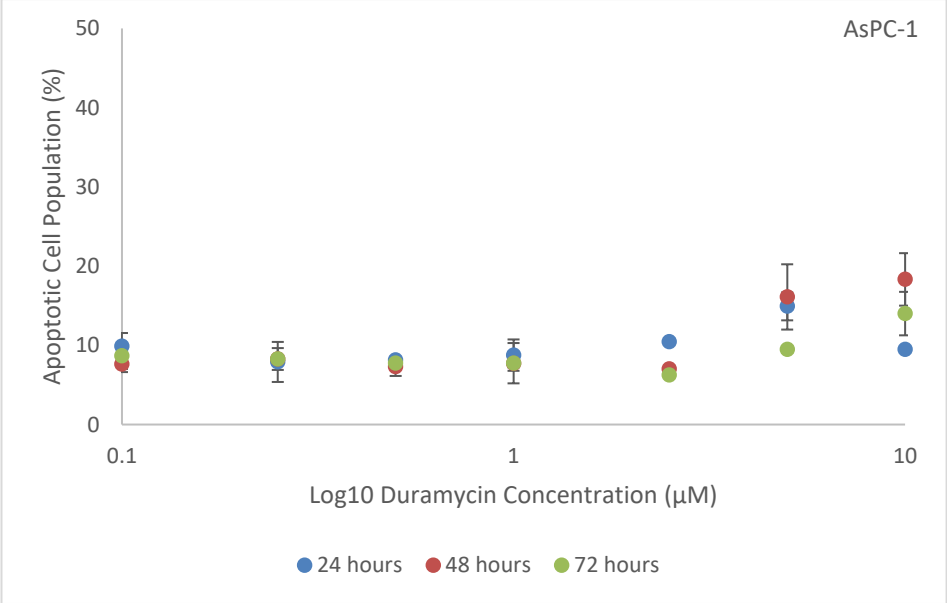

c)

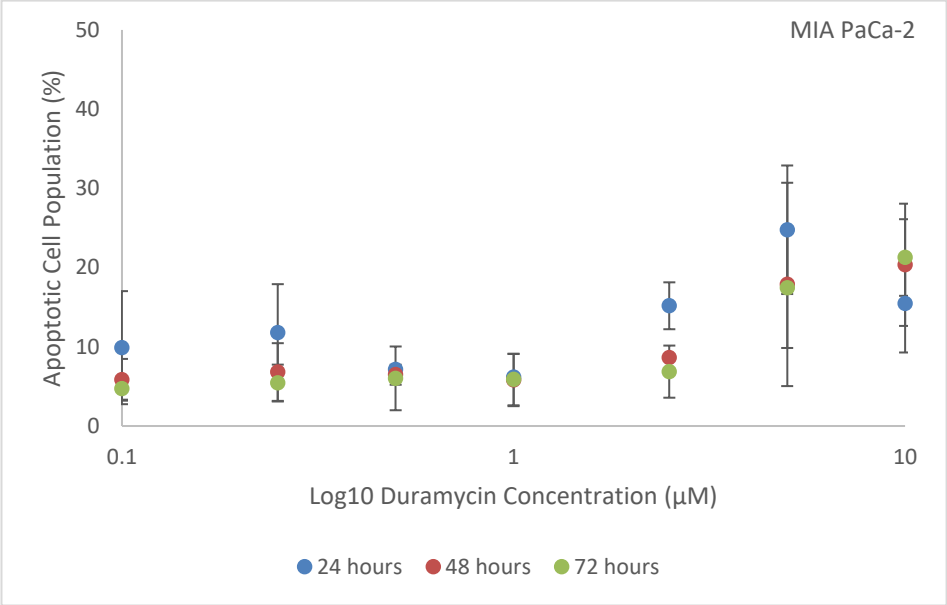

d)

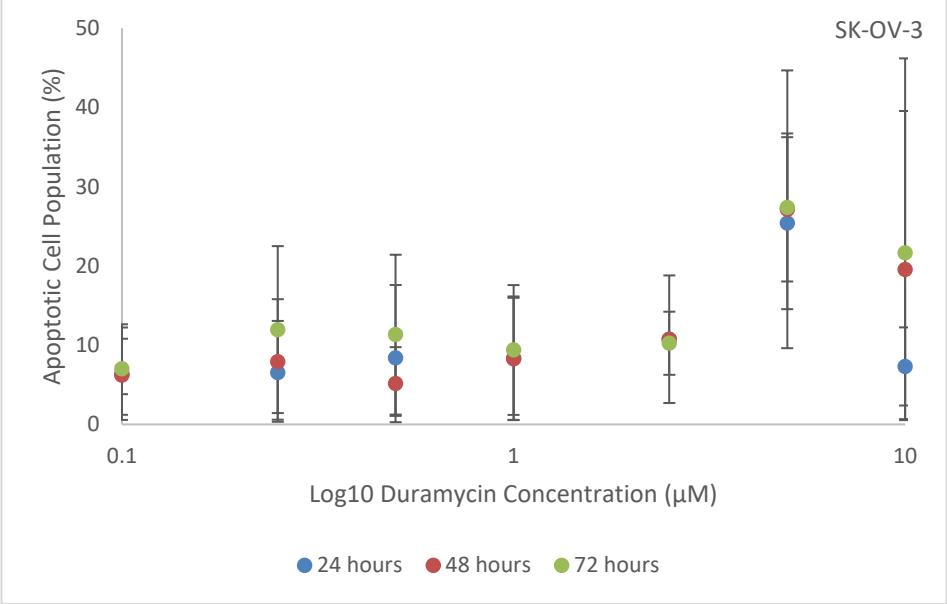

Figure 3.7: The effect of duramycin on the cell viability (apoptotic cell population) of cancer cells >24 hours.

In general, there was no difference between the 24, 48 and 72 hour duramycin treatment conditions for all 4 cancer cell lines a) A2780, b) AsPC-1, c) MIA PaCa-2 and d) SK-OV-3. Duramycin at 5 µM produced a larger population of apoptotic cells in a) A2780 and d) SK-OV-3. This larger population occurred at 5 µM and 10 µM for b) AsPC-1 and 10 µM for c) MIA PaCa-2. Error bars represent SD of 2 replicates.

a)

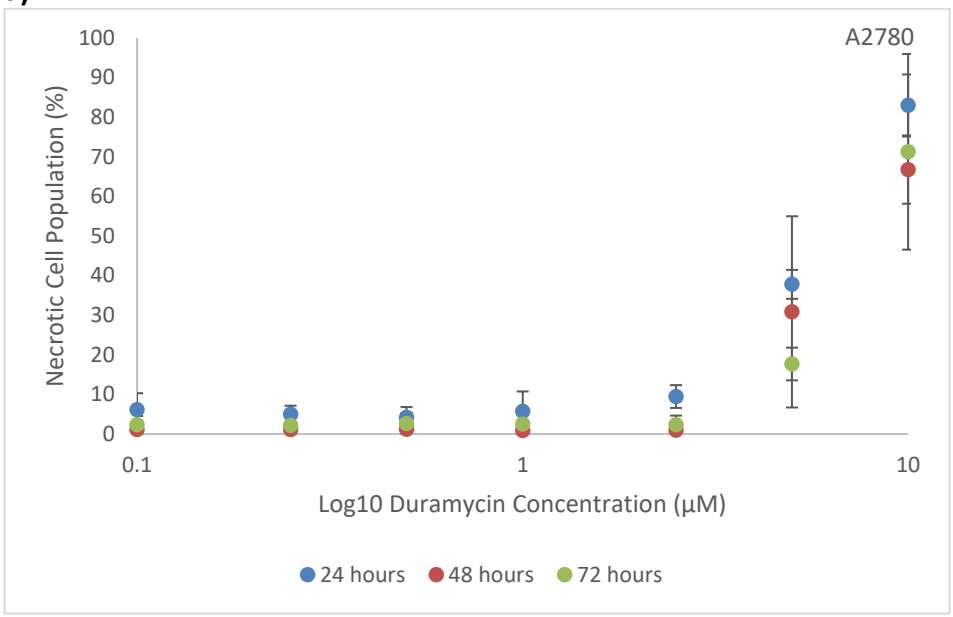
A2780
Necrotic Cell Population (%)
100
90
80
70
60
50
40
30
20
10
0
0.1
1
10
Log10 Duramycin Concentration (µM)
24 hours
48 hours
72 hours

b)

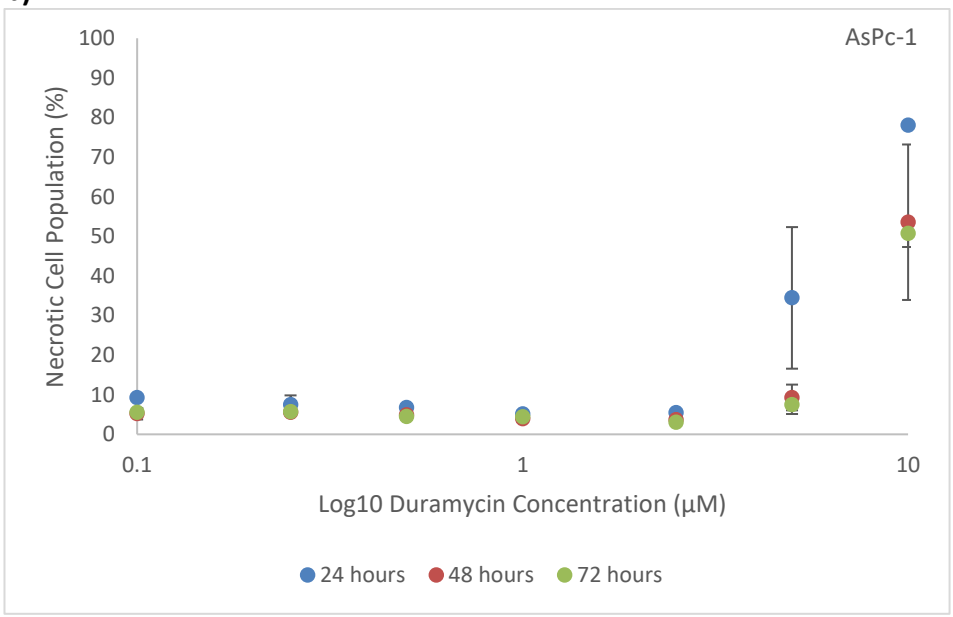
AsPc-1
Necrotic Cell Population (%)
100
90
80
70
60
50
40
30
20
10
0
0.1
1
10
Log10 Duramycin Concentration (µM)
24 hours
48 hours
72 hours

c)

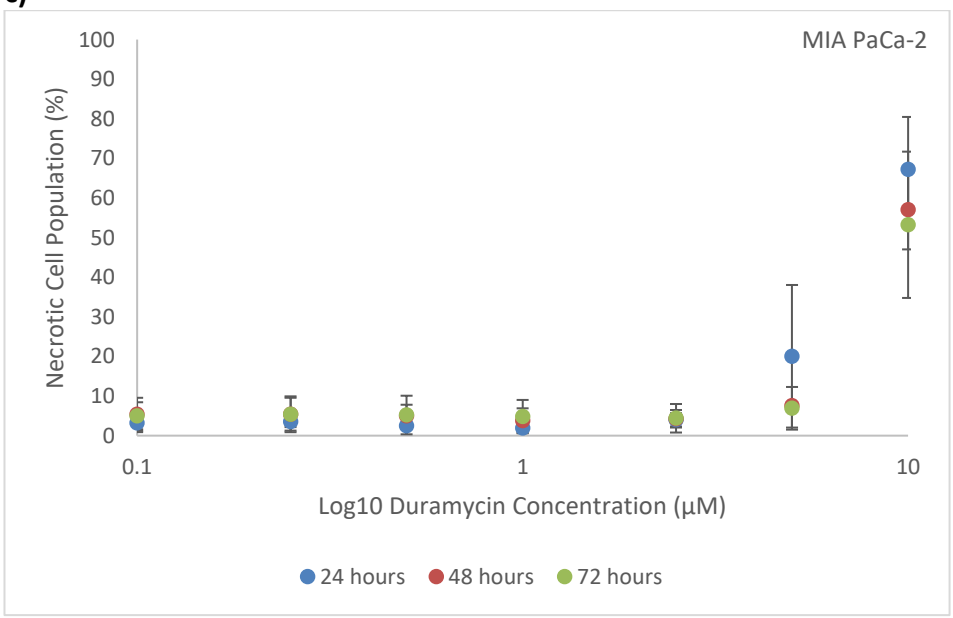
MIA PaCa-2
Necrotic Cell Population (%)
100
90
80
70
60
50
40
30
20
10
0
0.1
1
10
Log10 Duramycin Concentration (µM)
24 hours
48 hours
72 hours

d)

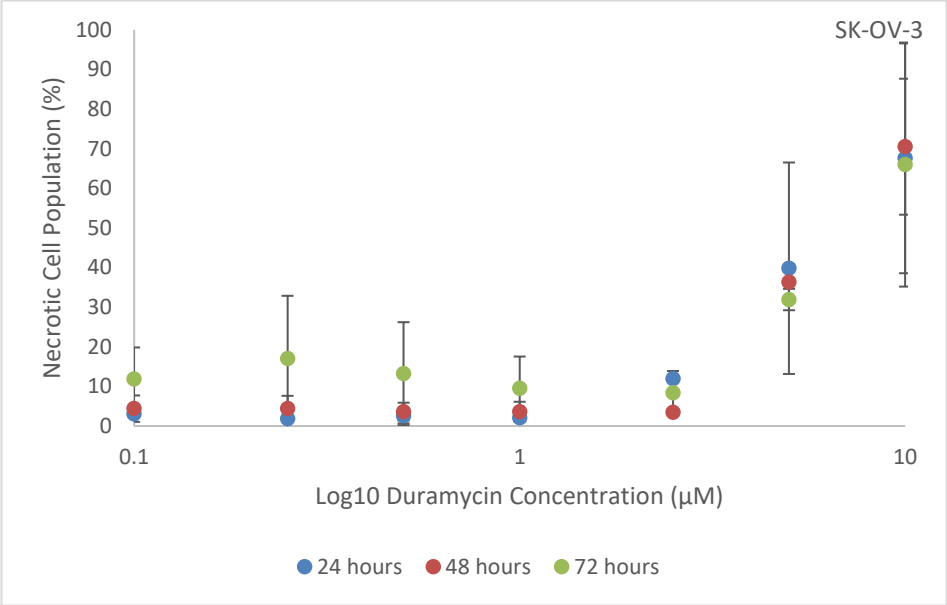

Figure 3.8: The effect of duramycin on the cell viability (necrotic cell population) of cancer cells >24 hours.

In general, there was no difference between the 24, 48 and 72 hour duramycin treatment conditions for all 4 cancer cell lines a) A2780, b) AsPC-1, c) MIA PaCa-2 and d) SK-OV-3. Duramycin concentrations ≥5 µM produced a necrotic cell population in a) A2780, b) AsPC-1 and d) SK-OV-3 however this was not seen in c) MIA PaCa-2 until 10 µM. Error bars represent SD of 2 replicates.

3.2.3 Screen for phosphatidylethanolamine expression on cancer cell lines

To assess whether PE was expressed on the surface of a variety of tumour cells a number of cancer cell lines were incubated with duramycin and PE expression was determined by flow cytometry. The PE screen on cancer cell lines was initially performed using 1 mM duramycin however this was later repeated using 2.5 µM duramycin once it was evident that concentrations >2.5 µM resulted in cancer cell death (section 3.2.2). PE expression was detected on all 17 of the cancer cell lines screened which included 2 ovarian, 2 pancreatic, 3 breast, 4 colon, 1 lymphoma, 2 multiple myeloma and 3 leukaemia cancer cell lines (figure 3.9). The MFIR for 13 of the cancer cell lines was between 1.0 and 2.0 which was considered as a relatively low expression of PE (a ratio of <1.0 would indicate no expression). This is likely due to the relatively low duramycin concentration used (see section 3.2.1). The 4 cancer cell lines with relatively higher levels of PE expression (MFIR >2.0) were all non-adherent cancer cell lines. However this was not consistently seen throughout the non-adherent cell lines as 2 out of the 6 had a MFIR of <2.0. It must be stated that though this trend was observed there was not a large variation seen between the different cancer cell lines.

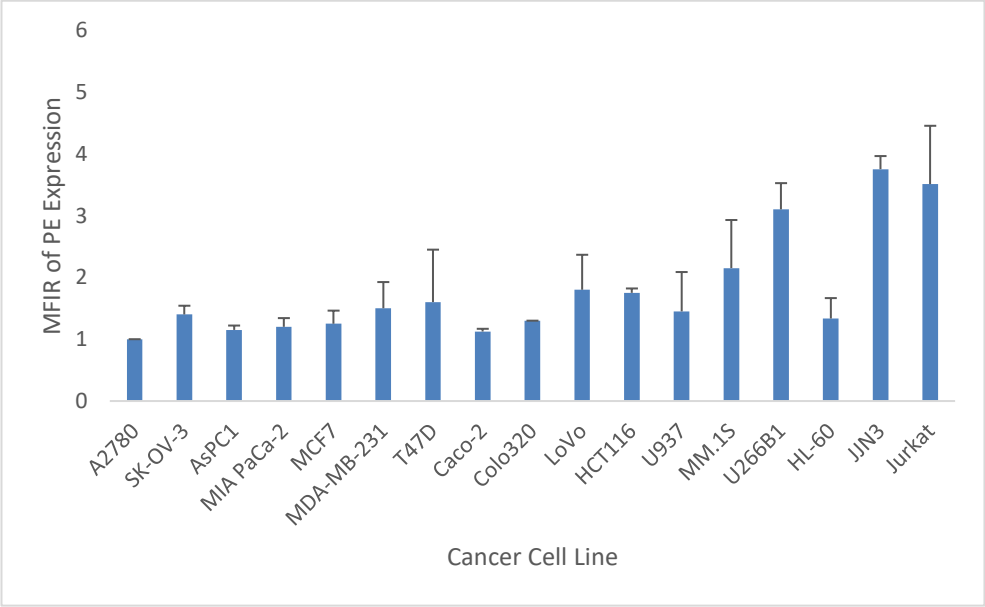

Figure 3.9: PE expression on cancer cell lines detected by 2.5 µM duramycin.
A number (17) of cancer cell lines of a variety of cancer types (ovarian, pancreatic, breast, colon, lymphoma, multiple myeloma and leukaemia) were screened for the expression of cell surface PE using 2.5 µM duramycin. Level of PE expression varied between the cancer cell lines with a general trend that the non-adherent cell lines expressed a higher level of PE than the adherent cell lines. PE expression was given as the MFIR. Error bars represent SD of 2 replicates.

3.2.4 Effect of duramycin on the light scattering properties of cancer cells

Light scatter by cells can be measured by flow cytometry and forward scatter (FSC) can usually be taken as an indicator of cell size and side scatter (SSC) as an indicator of internal cell complexity and granularity. It was investigated whether duramycin (2.5 µM-1 mM, 30 minutes treatment) effected the light scatter properties of cancer cells. The data for this was collected from cells that had been processed using the method described in section 2.3.1.

Duramycin increased the FSC of AsPC-1 and SK-OV-3 in a concentration dependent manner at concentrations ≥50 µM (figure 3.10). The FSC for untreated control AsPC-1 cells was 349.5±2.3 which increased to 432.8±29.6, 463.4±29.3 and 531.9±5.2 for 50 µM, 200 µM and 1 mM duramycin treatment, respectively. The increase in FSC for SK-OV-3 cells was less pronounced and was increased from 479.8±21.8 in the control cells to 561.2±15.9, 540.5±7.3 and 592.6±0.14 for 50 µM, 200 µM and 1 mM treatment, respectively. The FSC of A2780 and MIA PaCa-2 cells was not affected by duramycin treatment.

The SSC of all 4 of the cancer cell lines was increased when treated with duramycin concentrations of 200 µM and 1 mM (figure 3.11). The greatest increase was seen in 1 mM treated cancer cells. However, duramycin treatment increased the SSC of the cancer cell lines to different extents in which AsPC-1 cells saw the highest increase in SSC of 286.3 (untreated control cells = 237.9, 1 mM treated cells = 524.2). The increase in SSC at 1 mM duramycin treatment in SK-OV-3 was 277.0 (249.9-526.8), in MIA PaCa-2 192.5 (245.95-438.4) and in A2780 182.9 (338-520.85).

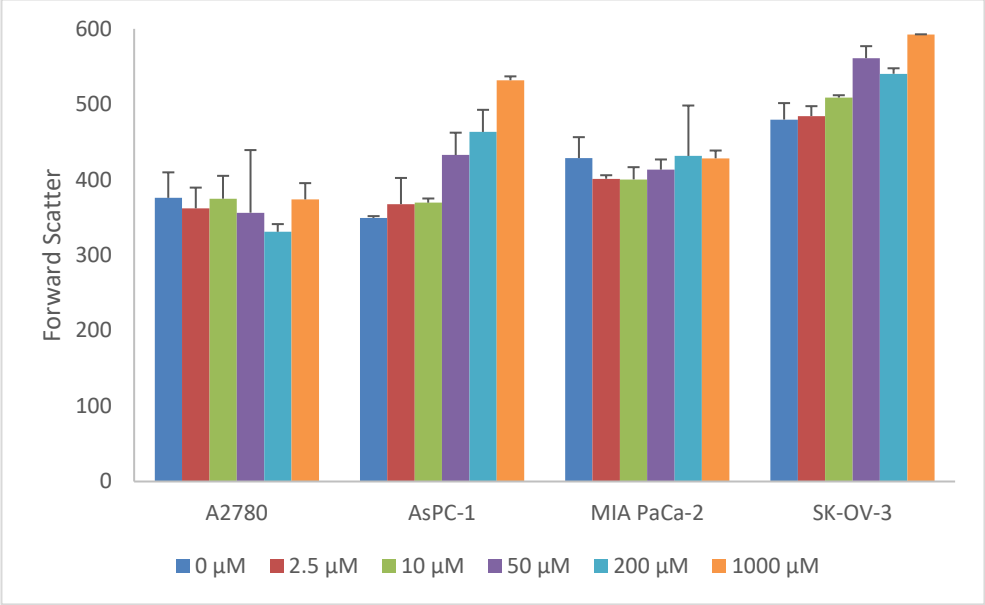

Figure 3.10: The effect of duramycin on the forward scatter of cancer cells. Duramycin treatment did not affect the FSC of A2780 and MIA PaCa-2. Duramycin concentrations ≥50 µM increased the FSC of AsPC-1 and SK-OV-3 cells. Error bars represent SD of 2 replicates.

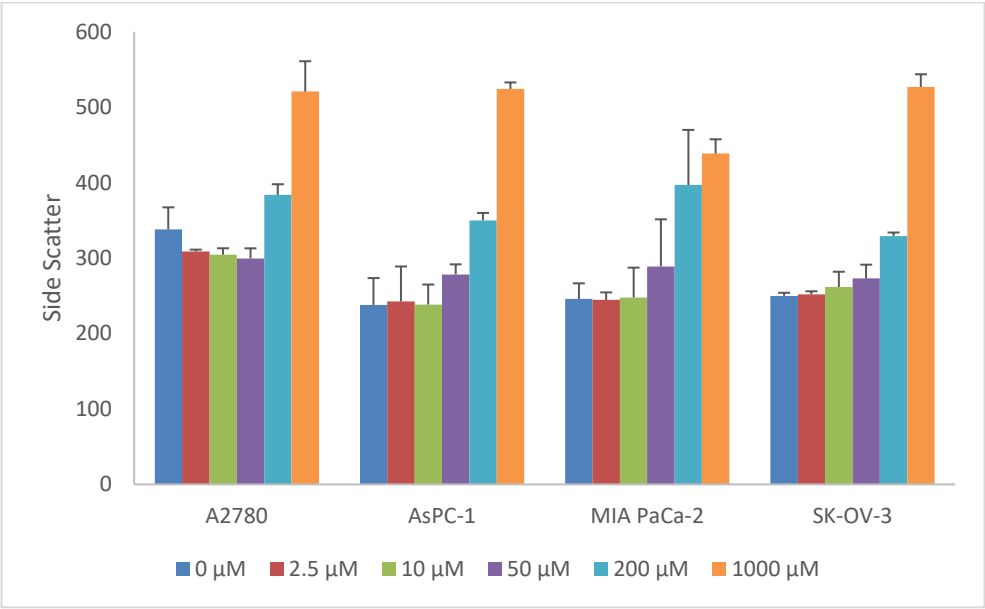

Figure 3.11: The effect of duramycin on the side scatter of cancer cells. Duramycin treatment at concentrations ≥200 µM increased the SSC of all 4 cancer cell lines A2780, AsPC-1, MIA PaCa-2 and SK-OV-3. Error bars represent SD of 2 replicates.

3.2.5 Effect of duramycin on the cell proliferation of cancer cells

It was investigated whether duramycin (0.1-100 µM) had an effect on the cell proliferation of the ovarian cancer cell lines A2780 and SK-OV-3 and the pancreatic cancer cell lines AsPC-1 and MIA PaCa-2. Briefly, cells ($2x10^4$) in appropriate media (180 µl) were transferred to 96 well plates and incubated overnight at 37°C in a 5% CO_2 atmosphere. After incubation duramycin (20 µl) at required concentration was added to the wells and the plates were incubated for 30 minutes (37°C, 5% CO_2 atmosphere). The plates were then centrifuged and after the supernatant was removed fresh media (180 µl) was added to the wells along with MTS reagent (20 µl). The plates were then returned to the incubator for 2 hours and subsequently read at 490 nm using a microplate reader. Cell proliferation was expressed as a percentage of the proliferation of untreated control cells. It had been shown that 30 minutes of duramycin treatment could reduce the cell viability of cancer cell lines through the induction of necrotic cell death (section 3.2.2). The aim of this experiment was to assess whether duramycin had an effect on cell proliferation as it was possible that a reduction in cell viability would be accompanied by a loss in metabolically active cancer cells.

Duramycin reduced the cell proliferation of all 4 cancer cell lines A2780, AsPC-1, MIA PaCa-2 and SK-OV-3 in a concentration dependent relationship (figure 3.12). The reduction in cell proliferation followed a similar trend for all the cancer cell lines (figure 3.12e) however differences in sensitivity to duramycin were observed. The half maximal inhibitory concentration (IC_{50}) values were calculated from the cell proliferation data. MIA PaCa-2 had the highest IC_{50} value of the cancer cell lines of 18.5 µM which may indicate that MIA PaCa-2 is the most resistant cancer cell line to a reduction in cell proliferation by duramycin. This was not so in the cell viability experiments (section 3.2.2) in which the most resistant cancer cell line was found to be A2780. A2780 had the next highest IC_{50} value of 10.0 µM followed by AsPC-1 at 7.1 µM. SK-OV-3 was found to be the most sensitive to a reduction in cell proliferation by duramycin with an IC_{50} of 3.4 µM. This would agree with the cell viability data (section 3.2.2) as duramycin treatment >2.5 µM resulted in the induction of apoptotic (5 µM and 10 µM) and necrotic (>10 µM) cell death in SK-OV-3.

a)

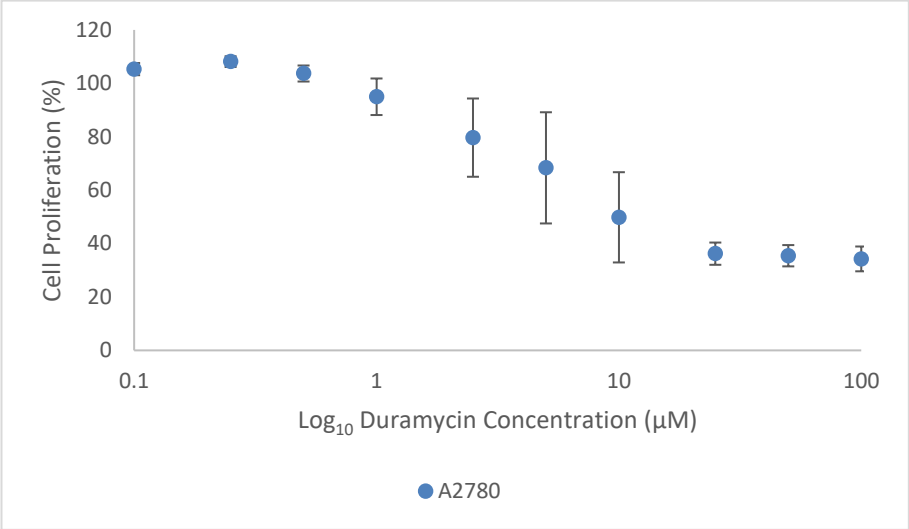
120
100
80
60
40
20
0
Cell Proliferation (%)
0.1
1
10
100
Log10 Duramycin Concentration (µM)
A2780

b)

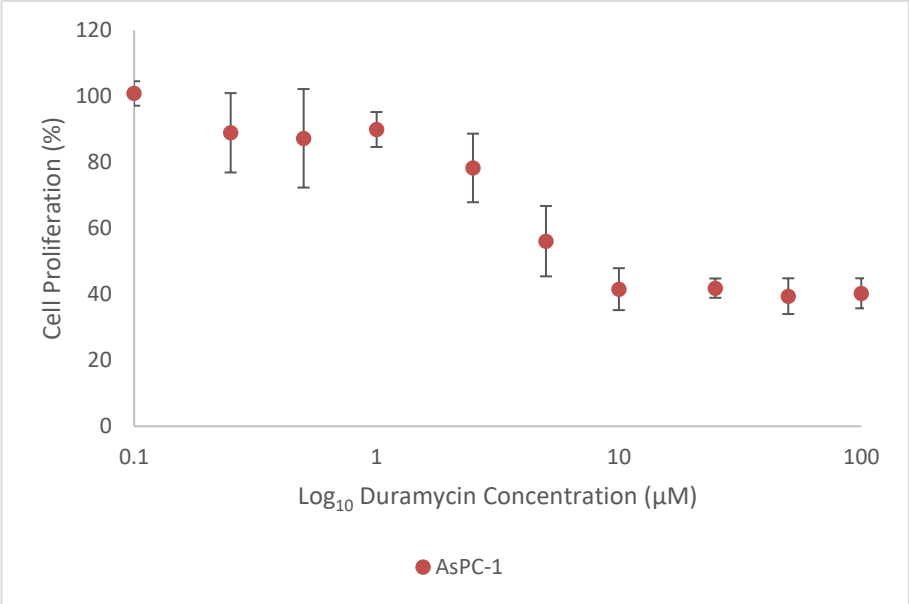
120
100
80
60
40
20
0
Cell Proliferation (%)
0.1
1
10
100
Log10 Duramycin Concentration (µM)
AsPC-1

c)

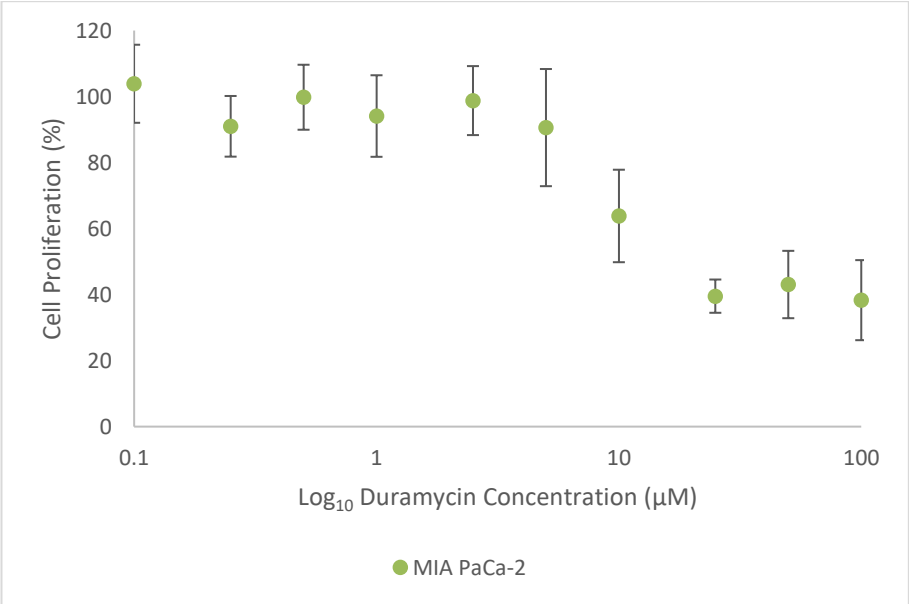
120
100
80
60
40
20
0
Cell Proliferation (%)
0.1
1
10
100
Log10 Duramycin Concentration (µM)
MIA PaCa-2

d)

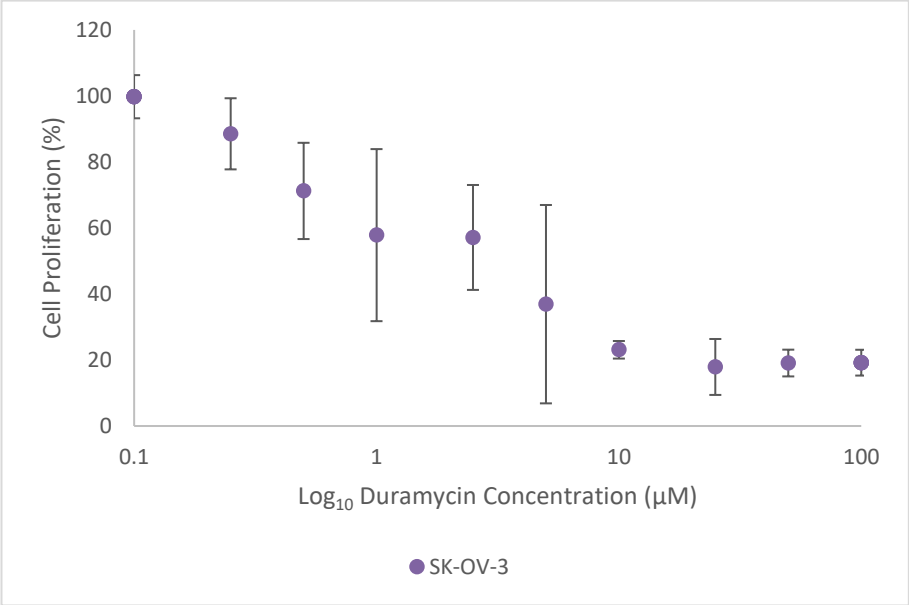

e)

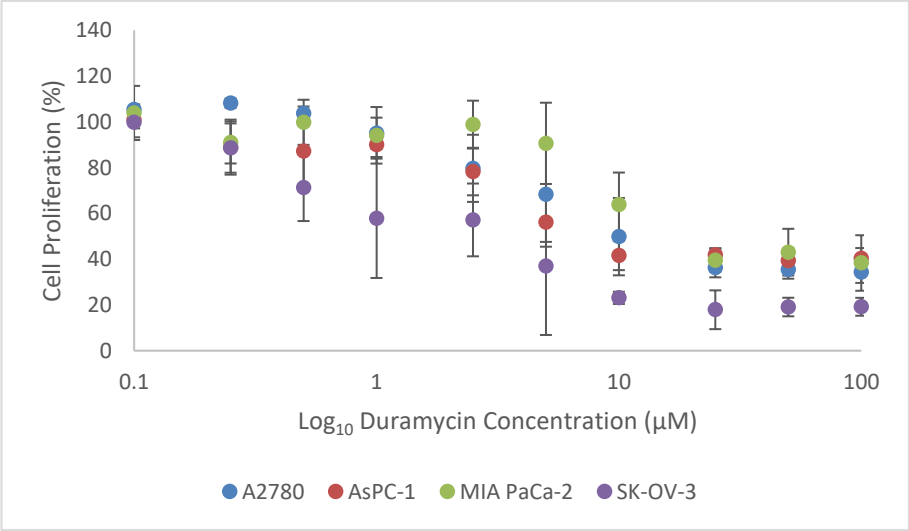

Figure 3.12: The effect of duramycin on the cell proliferation of cancer cells. Duramycin reduced the level of cell proliferation in all 4 cancer cell lines a) A2780, b) AsPC-1, c) MIA PaCa-2 and d) SK-OV-3 in a concentration dependent manner. IC_{50} values showed that a difference in sensitivity to duramycin occurred between the cancer cell lines. The cell lines in order of least sensitive to most sensitive to duramycin treatment was MIA PaCa-2 < A2780 < AsPC-1 < SK-OV-3. e) Comparison of all 4 cancer cell lines. Cell proliferation was calculated as a percentage of the untreated control cells. Error bars represent SD of 4 replicates.

The reduction in cell proliferation by duramycin was negatively correlated with the extent of necrosis induced by (30 minutes) duramycin treatment (figure 3.13). Pearson rank correlation coefficient (*r*) values showed a strong negative relationship between cell proliferation and the percentage of cells in the necrotic cell population for all 4 cancer cell lines where *r* = -0.67, -0.93, -0.88 and -0.74 for A2780, AsPC-1, MIA PaCa-2 and SK-OV-3, respectively.

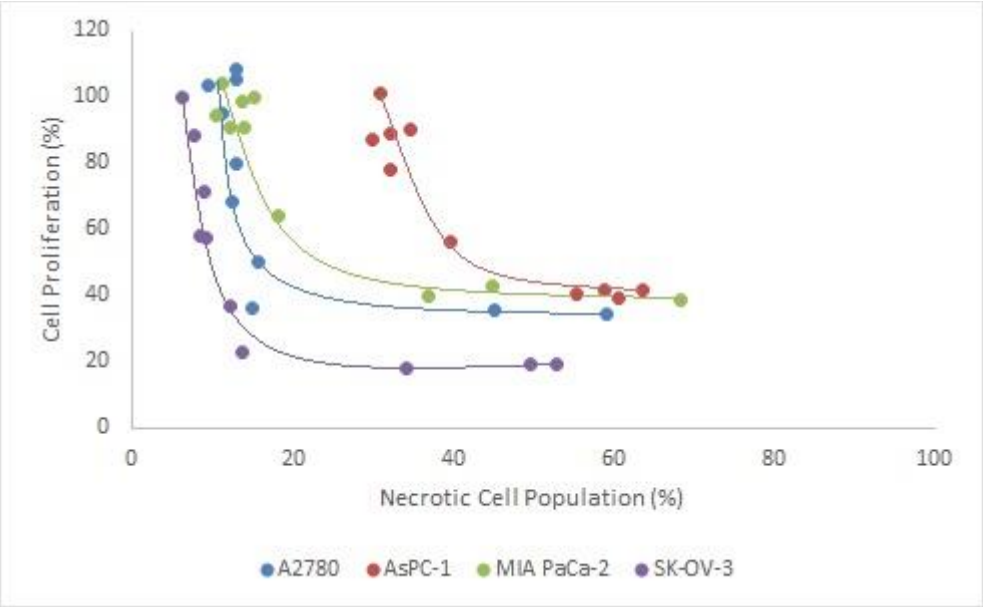

Figure 3.13: Duramycin induced necrotic cell death and reduction in cell proliferation in cancer cells.

There was a negative correlation between duramycin-induced reduction in cell proliferation and the extent of necrotic cell death in all 4 of the cancer cell lines. Trend lines are an illustration of this relationship.

3.2.6 Effect of duramycin on normal endothelial cells

It was investigated whether duramycin (0.1-1000 µM) had an effect on the normal endothelial cell line human umbilical vein endothelial cells (HUVECs). To evaluate if HUVECs expressed PE and whether this was detectable using duramycin the HUVECs were analysed by flow cytometry using the method described in section 2.3.2. The Annexin V: FITC Apoptosis Detection Kit I was used for analysis of the effect of duramycin on the cell viability of HUVECs (section 2.3.1). Duramycin had been shown, in this study, to exhibit cytotoxic (section 3.2.2) and anti-proliferative (section 3.2.5) properties and had been shown in the literature to be a potential anti-cancer agent[49]. A selective effect on tumour cells over normal healthy cells is an ideal characteristic of any anti-cancer agent. The aim of this

experiment was to determine whether duramycin had an effect on a normal (non-tumour) cell line.

Duramycin detected the cell surface expression of PE on HUVECs in a concentration dependent manner (figure 3.14a). Optimal PE detection occurred at 1 mM duramycin. The level of PE expression detected was similar to that detected on the cancer cell lines (figure 3.14b).

Duramycin increased the necrotic cell population present in the HUVECs in a concentration dependent manner (figure 3.15a). Concentrations >25 μM increased the number of HUVECs in the necrotic cell population. At the highest duramycin concentration (1 mM) the necrotic cell population was 84.4±10.4%. The increase in necrosis followed a similar trend to that of the cancer cell lines (figure 3.15b) and HUVECs had a similar sensitivity to duramycin treatment as the ovarian cancer cell line A2780. The amount of necrotic cell death was consistently lower in the HUVECs than in the cancer cell lines at duramycin concentrations 50-500 μM.

a)

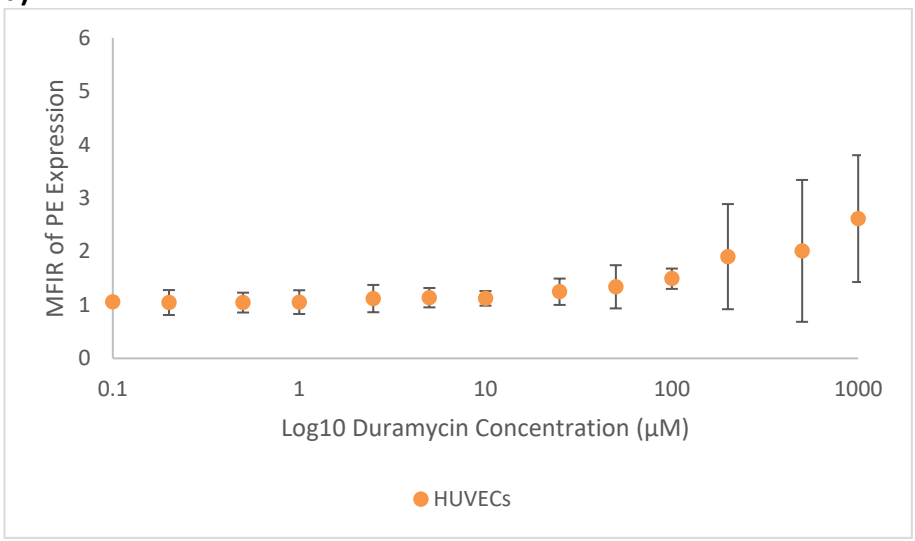

b)

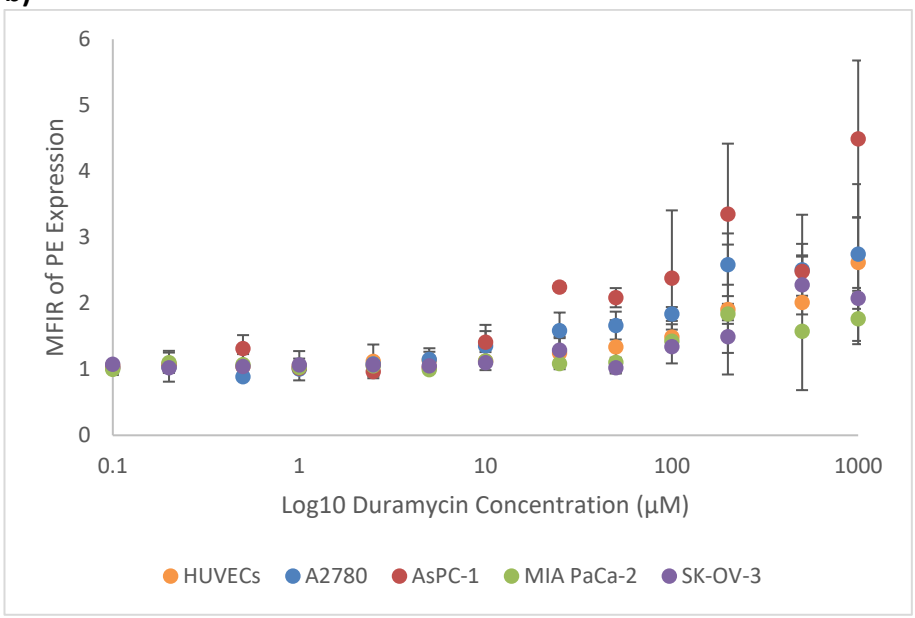

Figure 3.14: Detection of PE on the surface of normal endothelial cells (HUVECs) by duramycin.

a) Duramycin detected cell surface expression of PE on HUVECs in a duramycin concentration dependent manner. b) The level of PE detected on the HUVECs by duramycin was similar to that of the cancer cell lines. PE expression was given as MFIR. Error bars represent SD of 2 replicates.

a)

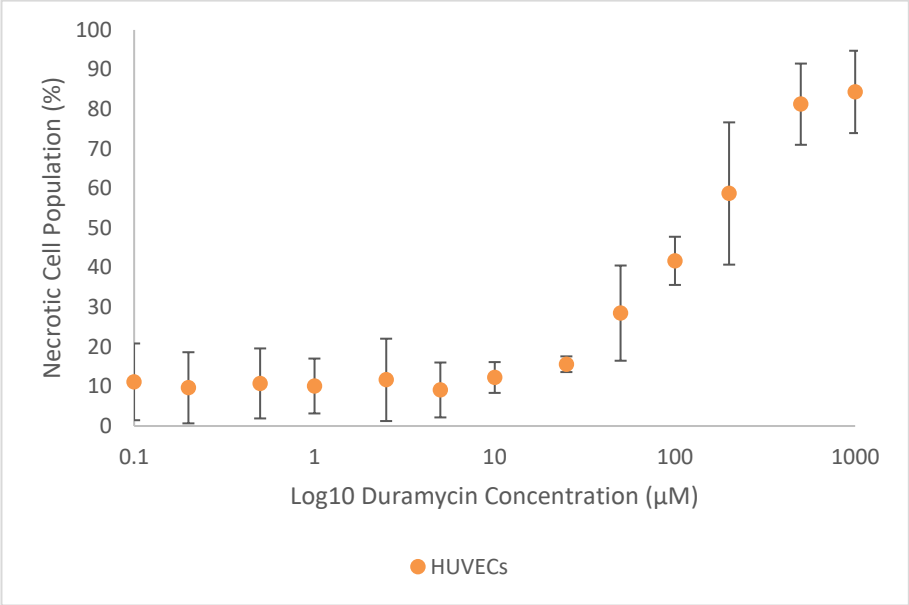

b)

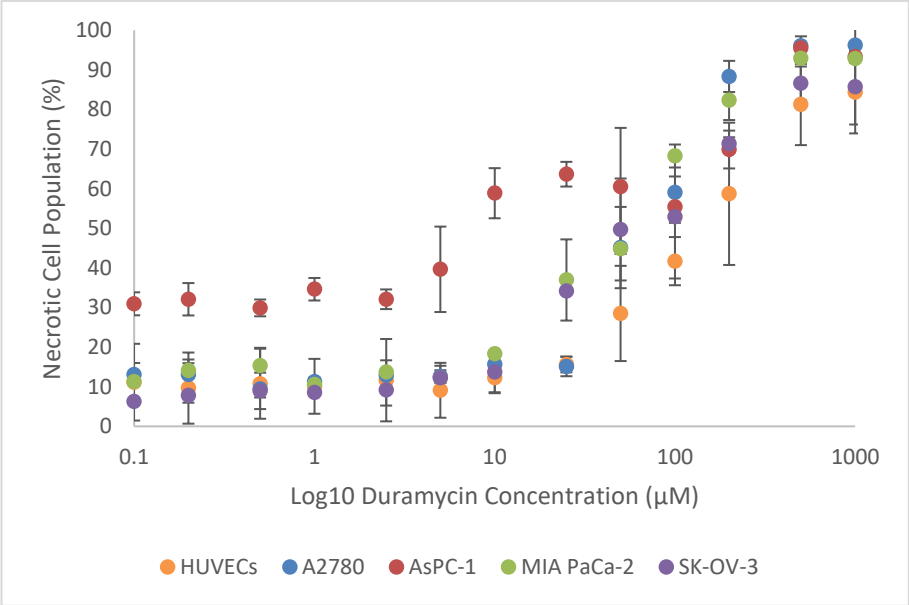

Figure 3.15: The effect of duramycin on the necrotic cell death of normal endothelial cells (HUVECs).

a) Duramycin induced necrosis in the HUVECs in a concentration dependent manner at concentrations >25 µM. b) The level of duramycin-induced necrosis in HUVECs followed the same trend as the cancer cell lines. However a smaller population of necrotic cells were seen in the HUVECs compared to the cancer cell lines between 50-500 µM duramycin. Error bars represent SD of 2 replicates.

3.3 Discussion

The aim of this chapter was to characterise the effect of duramycin on cancer cells in order to establish whether it could be a potential anti-cancer agent. It was first necessary to investigate whether cell surface PE was expressed on a variety of cancer cell lines. PE expression was indeed detected on the surface of all 17 of the cancer cell lines that were screened which included 7 different cancer types (ovarian, pancreatic, breast, colon, lymphoma, multiple myeloma and leukaemia) of which 4 were adherent types and 3 were suspension cultures. These results can potentially be applied to the *in vivo* setting as recently it was shown that PE was in much higher abundance in xenografts formed from a number of different tumour types (lung, colon, pancreatic and glioblastoma) than in their normal tissue counterparts[61]. In this study, the level of PE expression was presented as the MFIR which gave an indication of the level of shift in fluorescence that occurred between the control cells and those that had been fluorescently labelled with duramycin. Thus a high MFIR value would imply that a greater amount of duramycin molecules were bound to the surface of the cancer cells due to a high level of PE expression. A relatively low expression of PE (MFIR 1.0-2.0) was detected on the majority of the cancer cell lines (13/17) which was most likely a result of the low concentration (2.5 µM) of duramycin used for the PE screen. The concentration that would have yielded optimal PE detection (≥200 µM) was compromised for one that would not have a cytotoxic effect on the cancer cell lines. The 4 cancer cell lines (2 multiple myeloma and 2 leukaemia) that had a higher MFIR than 2.0 were non-adherent cell lines. Yet this was not a trend consistently seen with the non-adherent cancer cell lines as 2 of the cell lines (1 lymphoma and 1 leukaemia) had a MFIR of <2.0. The incubation time for cancer cell lines with duramycin was chosen as 30 minutes. A radiolabelled duramycin compound was able to image acute cell death in a porcine model of myocardial infarction 30 minutes after its injection[80]. This could potentially mean that the incubation times used for the binding of duramycin to PE in the *in vitro* experiments in this study could be applicable for its binding *in vivo*.

Once it had been established that cancer cell lines expressed cell surface PE and that it could be detected by flow cytometry the effect of duramycin concentration on PE detection was investigated. For this the 2 ovarian cancer cell lines A2780 and SK-OV-3, the 2 pancreatic cancer cell lines AsPC-1 and MIA PaCa-2 and the normal endothelial cell line HUVECs were treated with duramycin concentrations 0.1 µM-1 mM. Duramycin detected PE expression in a concentration dependent manner on all 4 of the cancer cell lines and likewise on the normal endothelial cell line. The level of PE expression on the HUVECs was

comparable to that on the cancer cell lines. Concentrations of duramycin <10 µM detected a low level of PE that was similar for all 4 cancer cell lines. A difference in the level of PE expression on the cancer cell lines occurred at duramycin concentrations ≥25 µM. Here it was shown that MIA PaCa-2 and SK-OV-3 had the lowest PE expression of the cancer cell lines and that AsPC-1 had the highest level of expression. There are a number of potential explanations as to why a higher level of PE was detected as duramycin concentration increased. At higher duramycin concentrations it is possible that there were more duramycin molecules available to bind to cell surface PE molecules (duramycin binds to PE at a 1:1 ratio[72]) and thus a higher level of PE expression was detected. Yet it is possible that higher concentrations of duramycin had an effect on the cancer cells once bound which effected the exposure of PE on the cell surface. For example, a duramycin-effect on the cell membrane could result in a loss of phospholipid asymmetry which may alter the amount of PE expressed on the surface of the cells. Cinnamycin was seen to induce cell surface exposure of PE and PS on HeLa cells and this event preceded cell lysis[39]. It was also seen to induce non-specific transbilayer membrane movement of phospholipids in model membranes where both PE and PC were translocated to the outer membrane[39]. The re-organisation of the membranes was associated with cinnamycin-induced cell death. It is therefore possible that duramycin self-promotes its own binding to cells by inducing the movement of PE molecules from the inner to the outer membrane. If so this event could affect the detection of cell surface PE. Cell surface PE expression is upregulated in apoptotic and necrotic cell death[49, 64] and so duramycin-induced cell death could have increased the levels of PE expression on the cancer cells. However, AsPC-1 had a naturally lower cell viability than the other 3 cancer cell lines whereby ~36% of cells were necrotic at duramycin concentrations <25 µM. Yet at these lower duramycin concentrations a higher level of PE expression was not detected on AsPC-1 compared to the other cancer cell lines. This could provide evidence that the necrosis that occurs at the higher duramycin concentrations does not necessarily result in a higher expression of PE. Yet, it is more likely that this was an indication that at lower duramycin concentrations the binding of PE on cell surfaces is sub-saturated.

Cinnamycin at the relatively low concentration of 5 µM was shown to induce 50% haemolysis in erythrocytes from a variety of animal species in just 4 minutes[180] and its binding to HeLa cells ultimately lead to their lysis and death[39]. Duramycin at 20 µM lysed 50% of murine erythrocytes[59]. In this study the effect of duramycin on cell viability and cell death was investigated using the cancer cell lines A2780, AsPC-1, MIA PaCa-2 and SK-OV-3

and HUVECs. Treatment with duramycin for 30 minutes resulted in a reduction in the population of healthy cells and an increase in the population of necrotic cells in all 4 cancer cell lines. Both of these trends were duramycin concentration dependent and relatively high duramycin concentrations (500 µM and 1 mM) resulted in the necrosis of the majority of cancer cells (85-95%). The cancer cell lines exhibited differences in sensitivity to duramycin treatment in which concentrations <25 µM had no effect on A2780 cell viability and concentrations >25 µM resulted in necrosis. This effect was seen at the lower concentration of 10 µM for AsPC-1 and MIA PaCa-2 and at the even lower concentration of 2.5 µM for SK-OV-3. Cell death did not proceed directly through necrosis for SK-OV-3 as it did for the other cancer cell lines in which cells were viable until a threshold and then became necrotic. Instead SK-OV-3 cells underwent apoptosis within the narrow duramycin concentration range of 5-10 µM. Necrosis was then the mechanism of cell death at concentrations >10 µM. Thus it was shown that duramycin could be an effective cytotoxic anti-cancer agent. A desirable property of anti-cancer agents is a selective effect on tumour cells over non-tumour cells. Duramycin reduced the cell viability of HUVECs in a concentration dependent manner in a much similar way to the ovarian cancer cell line A2780. Duramycin >25 µM resulted in necrotic cell death and at the highest concentration (1 mM) ~85% of the HUVECs were necrotic. These results appear to replicate the findings of the toxicity of duramycin and cinnamycin to other normal cells such as erythrocytes[59, 180]. This effect of duramycin on cell death of non-tumour cells may not translate clinically and animal testing would be required to assess the impact of duramycin on normal tissue. However, it is possible that duramycin would not be able to be utilised as a direct anti-cancer agent if damage to normal tissue surrounding the tumour occurred *in vivo*. If this were the case then some form of modification to duramycin would likely be required that would allow for targeted tumour treatment. Conversely, if it were discovered that there was a tumour that had a very high sensitivity to duramycin treatment and there were tolerable side-effects from toxicity to normal cells duramycin could potentially be an effective anti-cancer agent on its own.

Previously it was found that treatment of cancer cell lines with relatively low duramycin concentrations for >48 hours resulted in apoptotic (duramycin ≤0.625 µM) and necrotic cell death (duramycin ≥1.25 µM) of the pancreatic cancer cell lines AsPC-1 and MIA PaCa-2[49]. In this study, duramycin treatment ≥24 hours at ≥5 µM resulted in larger populations of apoptotic and necrotic cells in the cancer cell lines A2780, AsPC-1, MIA PaCa-2 and SK-OV-3 compared to untreated controls. At these longer treatment periods MIA PaCa-2 appeared

to be slightly more resistant to duramycin-induced necrosis than the other cancer cell lines as necrosis did not occur until 10 µM. Herein it was further shown that 2.5 µM duramycin does not affect cancer cell viability, even over longer treatment periods.

Along with a cytotoxic effect duramycin was also shown to have an anti-proliferative effect on the pancreatic cancer cell lines AsPC-1, CFPAC-1 and MIA PaCa-2 at relatively low concentrations (0.125-12.5 µM) >48 hours[49]. In this study, it was investigated whether cell proliferation of cancer cell lines was effected in the shorter time period of 30 minutes due to its ability to reduce cell viability in this time. Duramycin reduced the cell proliferation of all the cancer cell lines A2780, AsPC-1, MIA PaCa-2 and SK-OV-3 in a concentration dependent manner. While a similar trend in the reduction of cell proliferation occurred for all of the cancer cell lines, for example duramycin at the highest concentration (100 µM) reduced cell proliferation to ≤40%, differences in sensitivity to duramycin treatment were shown. With an IC_{50} of 18.5 µM MIA PaCa-2 was the most resistant cell line to a duramycin-induced reduction in cell proliferation. It had been previously shown that MIA PaCa-2 had a higher IC_{50} (1.32 µM, >48 hours) for duramycin treatment than AsPC-1 (0.82 µM, >48 hours)[49]. A2780 and AsPC-1 had IC_{50} values of 10.0 µM and 7.1 µM, respectively. SK-OV-3 was the most sensitive cell line with a relatively low IC_{50} of 3.4 µM. This was in agreement with the cell viability experiments in which duramycin >2.5 µM resulted in apoptotic or necrotic cell death in SK-OV-3. The effect of duramycin on cell proliferation had a strong negative correlation with the extent of necrosis induced by duramycin treatment in all 4 cancer cell lines. As was theorised the reduction in cell proliferation by duramycin, indicating a loss in metabolically active cells, was accompanied by a greater number of necrotic cells. Interestingly, the relative sensitivities to duramycin treatment were not related to PE expression. MIA PaCa-2 and SK-OV-3 had very similar levels of PE expression, lower than both A2780 and AsPC-1, yet MIA PaCa-2 had the highest IC_{50} value and SK-OV-3 the lowest. If larger amounts of PE exposed on the cancer cell surface meant that a higher amount of duramycin bound to the cells and this in turn resulted in a larger effect on cell viability/ proliferation then duramycin sensitivity may be expected to correlate with PE expression levels. Therefore the mechanism of action by which duramycin produces cell death, which is currently not fully established, may rely upon more than binding to PE and a successive effect on the cell membrane.

Duramycin increased the FSC of the cancer cell lines AsPC-1 and SK-OV-3 at concentrations ≥50 µM and the SSC of all 4 cancer cell lines at concentrations ≥200 µM. Changes in cells

light scattering properties have been connected to apoptotic and necrotic cell death. The swelling of cells and increased granularity that occurs during necrosis have been associated with an increase in FSC and SSC, respectively[203]. An increase in intracellular granularity in synthetic androgen R1881 treated prostate cancer cells (LNCaP) was detected as a concentration dependent increase in SSC[204]. Cyclosporine treatment of the renal proximal tubular epithelial cell line LLC-PK1 at low concentrations resulted in apoptotic cells that had an increased SSC and a decreased FSC[205]. At higher cyclosporine concentrations necrotic cell death occurred and the cells had an increased FSC and decreased SSC. The decrease in SSC in the necrotic cells was theorised to be due to a release of cellular organelles through ruptured cell membranes. Additionally, the increased SSC in early apoptotic human B-cell lymphoma cells was associated with condensation of the cell nucleus and cytoplasm during cell shrinkage which lead to enhanced light refraction[206]. The results from this study appear to be slightly contradictory to the literature. Increased FSC occurred only in AsPC-1 and SK-OV-3 at duramycin concentrations ≥50 µM yet it was shown that necrosis occurred in all 4 cancer cell lines when treated with duramycin >10 µM. Increased SSC, usually associated with apoptosis, occurred in all 4 of the cancer cell lines although at 30 minutes duramycin treatment it was shown that only SK-OV-3 experienced apoptotic cell death. It must be taken into account that morphological and cell size changes measured by light scatter should be considered as supportive rather than as definitive evidence of cell death. This is especially true as an increase in granularity and therefore SSC has also been linked with an increased number of mitochondria[204], terminal differentiation[207], cellular senescence[208] and the accumulation of intracellular membranous organelles during autophagy[204].

In conclusion, duramycin was shown be effective in the detection of PE on cancer cell lines and on endothelial cells and also to be an effective cytotoxic and anti-proliferative agent. The concentration of duramycin that did not affect cell viability or proliferation and could detect low level PE expression was identified as 2.5 µM. Through the manipulation of duramycin concentration and incubation time it is theoretically possible that apoptosis and necrosis could be induced in cancer cells to different extents. However, it was shown that apoptosis of cancer cells occurred only within a narrow concentration range of 5-10 µM when cells were treated for ≥24 hours. The major form of duramycin-induced cell death was through necrosis. Duramycin has the potential to be an effective anti-cancer agent but has a narrow therapeutic window, to be successfully applied to the clinical setting some form of enhancement to its cytotoxic effect on tumour cells that would limit its effect on non-tumour cells would be required.

Chapter 4 The Effect of Duramycin on 2D and 3D Cell Cultures

4.1 Introduction

The standard *in vitro* model used in anti-cancer drug testing is the two-dimensional (2D) monolayer culture of cancer cells, usually on the flat surface of plastic tissue culture vessels. However 2D monolayer cell cultures do not accurately represent the three-dimensional (3D) environment of solid tumours[209]. Monolayer cultures lack the hypoxic and necrotic areas present in naturally occurring tumours, they do not include interactions between the extracellular matrix and are usually composed of a homogenous mixture of cells. Additionally, *in vivo*, anti-cancer agents must penetrate the tumour mass which is not a factor in 2D cultures and thus can lead to discrepancies in effective drug concentration[210]. To overcome these limitations many forms of 3D cell culture have been applied in oncological research[209]. One form of 3D cell culture is the multicellular tumour spheroid defined as aggregates of cancer cells that grow into spherical structures and are capable of growth in isolation[211, 212]. Tumour spheroids provide an *in vitro* model for small tumours due to the cell-cell and cell-matrix interactions that occur within them[213-215]. Spheroids also have diffusion gradients for glucose, oxygen and other nutrients which decrease towards the core of the spheroid. A higher build-up of waste products exists at the core of spheroids along with a hypoxic environment[211]. Glioblastoma cells cultured as 2D and 3D systems were evaluated for their glycolytic activity via their lactate production[216]. The 3D spheroid cultures exhibited higher amounts of lactate production than the 2D monolayer cultures. The enhanced lactate production was theorised to be a result of acidosis of the cells in the interior of spheroids, confirmed by pH probe. The core of the spheroids were found to be significantly lower in pH than the exterior. The hypoxia and acidosis in the spheroids core stimulated angiogenic factors (vascular endothelial growth factor (VEGF) and platelet-derived growth factor (PDGF)) that were expressed in much higher amounts than in the 2D system[216].

The 3D spheroid model can more accurately mimic the *in vivo* tumour environment. For example, in ovarian cancer, cancer cells can become detached from the tumour and subsequently migrate into the peritoneal cavity. Metastasised implants in the peritoneum and other body sites are dependent on the ovarian cancer cells migration, adhesion and invasion abilities[214]. These 'free' cancer cells have been shown to exist as both single cells and multicellular aggregates (*in vivo* tumour spheroids) in patients' ascites fluid. The multicellular aggregates in the ascitic fluid of 6 ovarian carcinoma patients were found to

be similar in appearance to OVCAR5 cultured spheroids and had similar resistance to physical manipulation and trypsinisation[214]. Desjardens *et al*.[18] found that ovarian carcinoma spheroids (OVCAR3, OVCAR4 and SK-OV-3) expressed the molecule versican, a peptidoglycan protein with a wide variety of roles in the promotion of tumour migration, adhesion, proliferation and metastasis, in much higher quantities than their monolayer cell cultures. Knockdown of versican resulted in the reduction of the spheroids ability to adhere to peritoneal mesothelial cells, disaggregate and subsequently migrate. These observations were also made in *in vivo* SK-OV-3 xenografts in athymic nude mice where effected veriscan expression resulted in a much lower rate of metastasis[18]. Therefore the tumour spheroid model was shown to accurately mimic *in vivo* ovarian tumour behaviour. Additionally, ovarian cancer cell lines grown as spheroids showed a high level of histological differentiation that was not seen in their 2D counterparts[217]. Furthermore, many cancer biomarkers and proteins often expressed in ovarian tumours including increased E-cadherin, PAX8, CA125 and cytokeratin, decreased MIB1 and vimentin expression[217], extracellular matrix proteins (laminin, fibronectin and collagen) and their integrin receptors[214, 215] have been observed in 3D spheroids. Thus cultured tumour spheroids can be an intermediate between *in vitro* cell culture and *in vivo* tumours[210] and can more accurately reflect the condition of *in vivo* tumours than 2D cell culture.

One reason for the similarities between 3D tumour spheroid models and *in vivo* tumours is their growth pattern. The culturing of cancer cells can theoretically continue indefinitely in 2D monolayers provided that there is an unlimited supply of nutrients such as oxygen and glucose[218]. This is because the cells at the boundary of the growth area have enough space and nutrients to adequately proliferate. When there is not enough space for growth the cancer cells stop proliferating which is known as contact inhibition. This set up is different when cancer cells are cultured as 3D tumour spheroids. In the 3D model contact inhibition occurs in conjunction with a lack of nutrients in the core of the spheroid. This eventually leads to apoptotic and/ or necrotic cell death which means that in the later stages of spheroid growth a necrotic core develops. The core is surrounded by a layer of quiescent but viable (contact inhibited) cells which are further surrounded by a proliferating outer layer of cancer cells (figure 4.1)[218, 219]. This is one more instance of similarity between spheroids and *in vivo* tumours which often have a dense necrotic core and areas of quiescent cells[220]. The density of the non-proliferating cells in spheroids produces a barrier to the diffusion of anti-cancer agents which has often led to spheroids having a higher drug resistance than their 2D monolayer counterparts[216, 221-223].

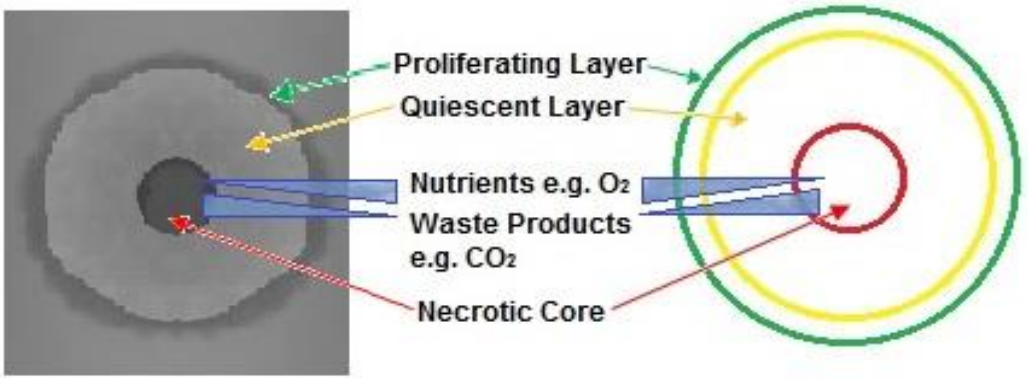

Figure 4.1: Diagram of an *in vitro* 3D tumour spheroid.
As a tumour spheroid grows a diffusion gradient of nutrients and of waste products is established. The build-up of waste products such as carbon dioxide (CO_2) and a lack of nutrients in the core of the spheroid results in the necrotic cell death of tumour cells. The necrotic core is often surrounded by a quiescent layer of cells. A layer of proliferating cells exists on the surface of the tumour spheroid.

The tumour spheroid model was first developed over 45 years ago[224] and subsequently was utilised for investigations into the cellular response to chemotherapy[211, 225]. Here differences in *in vivo* tumour behaviour and types of cell culture were highlighted. The human glioblastoma cell line U251 was cultured as a monolayer or spheroids on a flat substrate and as a monolayer or spheroids suspended in a polymeric scaffold coated with collagen[216]. The scaffold was used as a more realistic representation of the 3D tumour microenvironment. The spheroids suspended in the scaffold had a higher resistance (higher IC_{50} values) to doxorubicin and irinotecan treatment than all of the other culture types. The inhibition of the proliferation of the pancreatic cancer cell line AsPC-1 in response to 5-fluorouracil (5-FU), gemcitabine and oxaliplatin was lower when cultured as 3D spheroids than as 2D monolayers[226]. While the reaction to 3 anti-cancer drugs was shown to be similar between 6 ovarian cancer cell lines in 2D culture differences in sensitivity to the drugs occurred when the cells were cultured as spheroids[221]. The tumour spheroid model has also been used to assess initial reaction to various anti-cancer agents through DNA microarray screening. Ovarian cancer spheroids formed from 6 different ovarian cancer cell lines were treated with 3 chemotherapeutics over 72 hours and then investigated for gene expression changes[221]. Following treatment it was found that 623 genes were commonly down-regulated and 348 genes were commonly up-regulated in all 6 spheroid types. For example genes involved in apoptosis, cell adhesion, the stress response and cell cycle control were

both up- and down-regulated in varying amounts. Genes associated with DNA repair, DNA replication and cell cycle arrest were all exclusively overexpressed.

Additionally, tumour spheroids have been used to assess the procoagulant activity of cancer cells on microfluidic chips[227]. AsPC-1 spheroids were established as tumours using the liquid overlay method of spheroid formation and then transferred to a microfluidic chip. The spheroids were shown to retain continuous procoagulant activity which was speculated to be a result of microparticle release. Spheroids have also been used to investigate the ability of cancer cell lines to invade and migrate into 3D matrices[17]. Therefore tumour spheroids can be a useful model for 3D cell culture in oncological research.

The aim of this chapter was to investigate whether there was a difference in the anti-proliferative effects of duramycin on 2D cancer cell line cultures and 3D tumour spheroid cultures. The precursor to phosphatidylethanolamine (PE), phosphorylethanolamine, was shown to increase slightly during the proliferating stage of T47D spheroids and plateaued when the spheroids reached the stage of necrosis development[228]. As the 4 cancer cell lines used in this study have been shown to express cell surface PE (Chapter 3) it was theorised that PE would be present on the cancer cells once formed as spheroids and subsequently would be accessible to duramycin.

4.2 Results

4.2.1 Effect of duramycin on the cell proliferation of 2D cancer cell cultures

It was investigated whether duramycin (0.1-100 µM) had an effect on the cell proliferation of the ovarian cancer cell lines A2780 and SK-OV-3 and the pancreatic cancer cell lines AsPC-1 and MIA PaCa-2 after 24, 48 and 72 hours of treatment. Briefly, cells ($2x10^4$) in the appropriate media (180 µl) were transferred to 96 well plates and subsequently drug treated with duramycin at the required concentration in a solution with PBS (20 µl). The plates were then incubated at 37°C in a 5% CO_2 atmosphere for 24, 48 or 72 hours. After incubation the plates were centrifuged and the supernatant was removed. Fresh media (180 µl) was added to the wells along with MTS reagent (20 µl). The plates were returned to the incubator for 2 hours and then read at 490 nm using a microplate reader. Cell proliferation was expressed as a percentage of the proliferation of untreated (PBS treated) control cells. Duramycin had been shown to reduce the cell proliferation of the 4 cancer cell lines described above in a concentration dependent manner after 30 minutes (Chapter 3) and had previously been shown to reduce cell proliferation after 48 hours treatment on pancreatic cancer cell lines[49].

Duramycin treatment reduced the cell proliferation of all 4 of the cancer cell lines A2780, AsPC-1, MIA PaCa-2 and SK-OV-3 in a concentration dependent manner (figure 4.2). In general there was no difference between the 24, 48 and 72 hour treatment conditions. There were some exceptions to this, the first being that the cell proliferation of A2780 cells treated with 0.1-1 µM duramycin was lower at 48 hours than the cell proliferation at 24 and 72 hours. The other was the cell proliferation of AsPC-1 which was lower at 24 hours than at 72 hours for 0.1 µM and at 48 hours for 0.5 µM duramycin treatment. Differences in the sensitivity to duramycin treatment were observed between the cancer cell lines. After 24 hour treatment the highest concentration of duramycin (100 µM) reduced cell proliferation to 14.0% and 14.5% in the A2780 and AsPC-1 2D cell cultures, respectively. SK-OV-3 was less affected with a reduction in cell proliferation to 24.9% and MIA PaCa-2 even less so at 34.2%. The concentration of duramycin which reduced cell proliferation compared to the untreated control cells was 2.5 µM for A2780, 10 µM for AsPC-1 and SK-OV-3 and 25 µM for MIA PaCa-2. The IC_{50} values for 24 hour duramycin treatment on the 4 cancer cell lines were found to be 3.6 µM for A2780, 7.1 µM for AsPC-1, 18.4 µM for MIA PaCa-2 and 7.6 µM for SK-OV-3. Therefore the order of sensitivity from most to least sensitive was: A2780 > AsPC-1 > SK-OV-3 > MIA PaCa-2.

a)

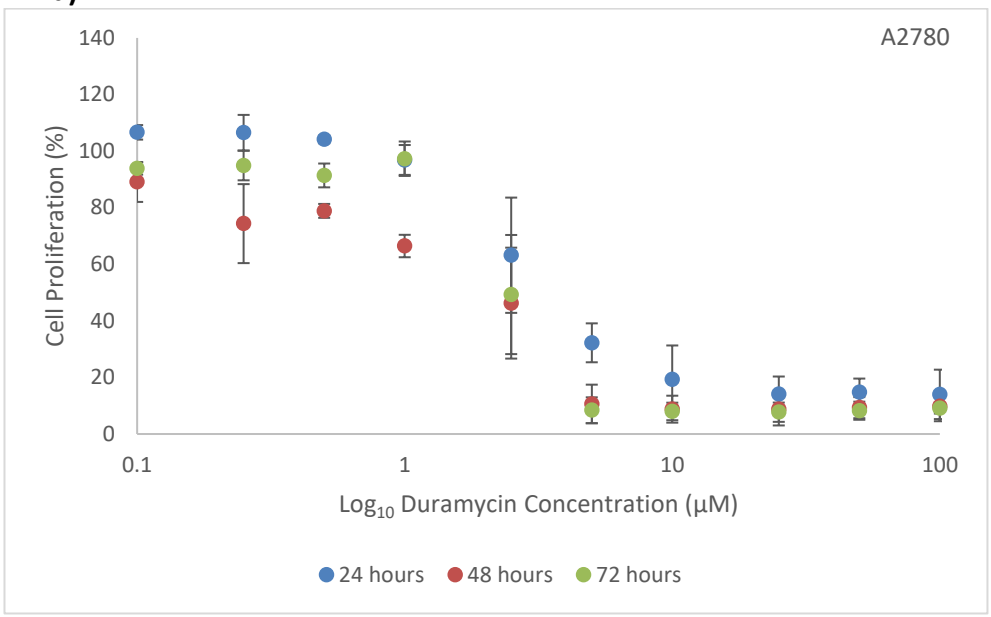
A2780
Cell Proliferation (%)
140
120
100
80
60
40
20
0
0.1
1
10
100
Log10 Duramycin Concentration (µM)
24 hours
48 hours
72 hours

b)

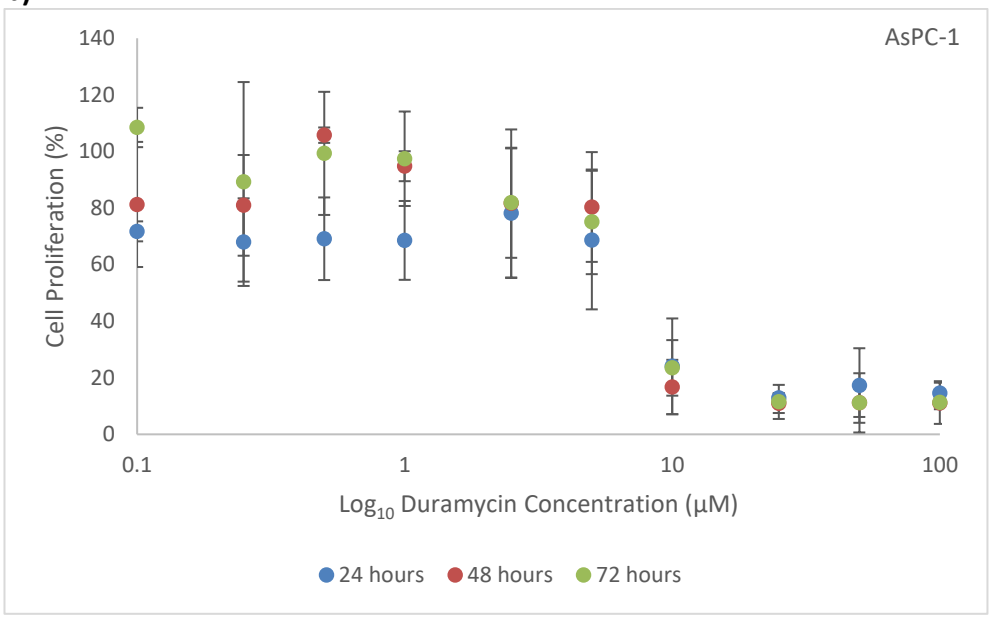
AsPC-1
Cell Proliferation (%)
140
120
100
80
60
40
20
0
0.1
1
10
100
Log10 Duramycin Concentration (µM)
24 hours
48 hours
72 hours

c)

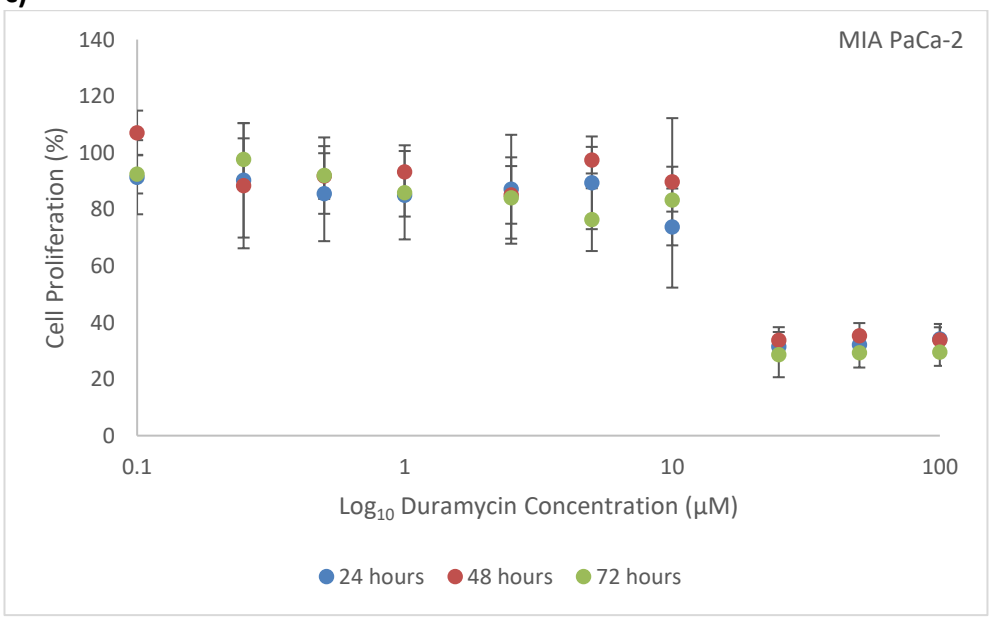
MIA PaCa-2
Cell Proliferation (%)
140
120
100
80
60
40
20
0
0.1
1
10
100
Log10 Duramycin Concentration (µM)
24 hours
48 hours
72 hours

d)

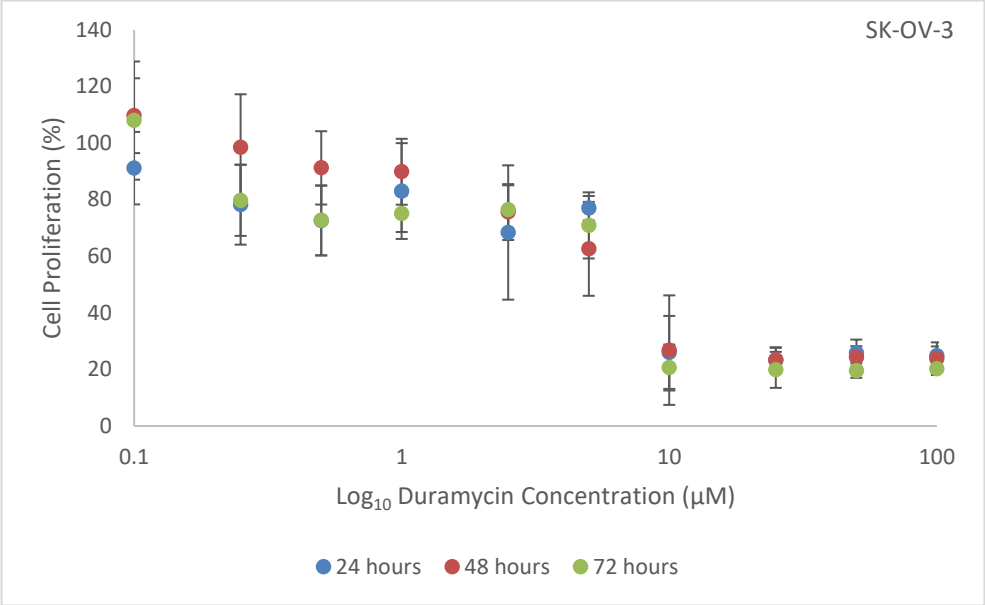

Figure 4.2: The effect of duramycin treatment on the cell proliferation of 2D cancer cell line cultures.

Duramycin reduced the cell proliferation of the cancer cell lines a) A2780, b) AsPC-1, c) MIA PaCa-2 and d) SK-OV-3 in a concentration dependent manner. In general there was no difference between the treatment time conditions (24, 48 and 72 hours). Error bars represent the SD of 4 replicates.

4.2.2 Characterisation of tumour spheroids

It was investigated whether the cancer cell lines A2780, AsPC-1, MIA PaCa-2 and SK-OV-3 were able to form tumour spheroids. The required number of cells to form adequately sized spheroids and the proliferation of the spheroids was assessed. Briefly, 1.5% agarose gel (100 µl) was added to the inside 40 wells of a 96 well plate and allowed to set at room temperature in a sterile biological safety cabinet. PBS (200 µl) was added to all outside wells to prevent evaporation from the plates. After the agarose gel had set either $5x10^3$, $1x10^4$, $2x10^4$ or $5x10^4$ cells in media (100 µl/ well) were added to the wells. The plates were then incubated at 37°C in a 5% CO_2 atmosphere for 72 hours. The plates were set up in duplicate so that after 72 hours of spheroid formation 1 plate was imaged using a GelCount™ colony counter. This plate was then centrifuged and the supernatant was removed and replaced with fresh media (180 µl) to which MTS reagent (20 µl) was added. The plates were incubated (37°C, 5% CO_2) for 2 hours after which they were centrifuged again. Supernatant (100 µl) was removed from each well and pipetted into a fresh 96 well plate. This was so the absorbance reading measured was not affected by the agarose gel and spheroid in the well. The plates were subsequently read at 490 nm using a microplate reader. The media in the duplicate plate was refreshed by removing the old media (100 µl) and adding fresh media (100 µl). This plate was then returned to the incubator for a further 72 hours after which the plate was imaged and read at 490 nm. The size of the spheroids was measured using ImageJ software from the images taken on day 3 and day 6 of the spheroids growth.

All 4 cancer cell lines were seen to form spherical aggregates after 72 hours of growth though the size of the spheroids varied between the cell lines (figure 4.3). The number of cells seeded into the wells strongly correlated with the size of the spheroids (whole area of the spheroid, calculated from values measured using ImageJ software) for all 4 cancer cell lines (Pearson correlation coefficient values ranged from r = 0.96-0.99). The average area for a $5x10^4$ seeded cells spheroid on day 3 was 10.6 mm^2 for A2780, 10.2 mm^2 for AsPC-1, 12.1 mm^2 for MIA PaCa-2 and 1.0 mm^2 for SK-OV-3. As SK-OV-3 formed relatively small spheroids occasionally one of the spheroids became dislodged during the experimental process which resulted in an empty well, as can be seen on figure 4.2. For the A2780, AsPC-1 and MIA PaCa-2 spheroids there was no difference in the size of the spheroids, within SD, between day 3 and day 6 of spheroid growth. The SK-OV-3 spheroids showed no difference in size between day 3 and day 6 for the $5x10^3$ and $1x10^4$ seeded cells spheroids. However the spheroids formed from $2x10^4$ and $5x10^4$ seeded cells were smaller in size on day 6 than day 3.

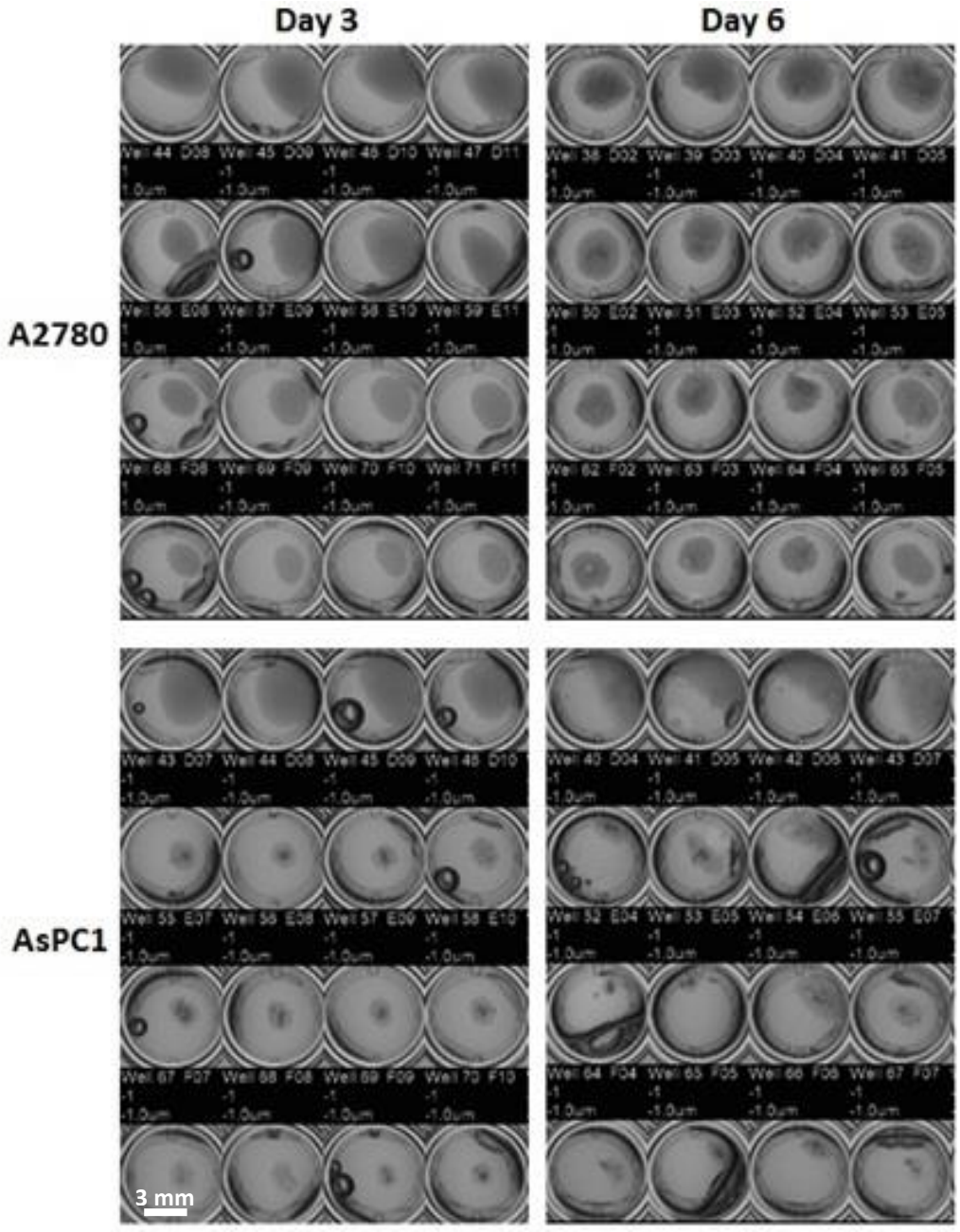
Day 3
Day 6
A2780
AsPC1
3 mm

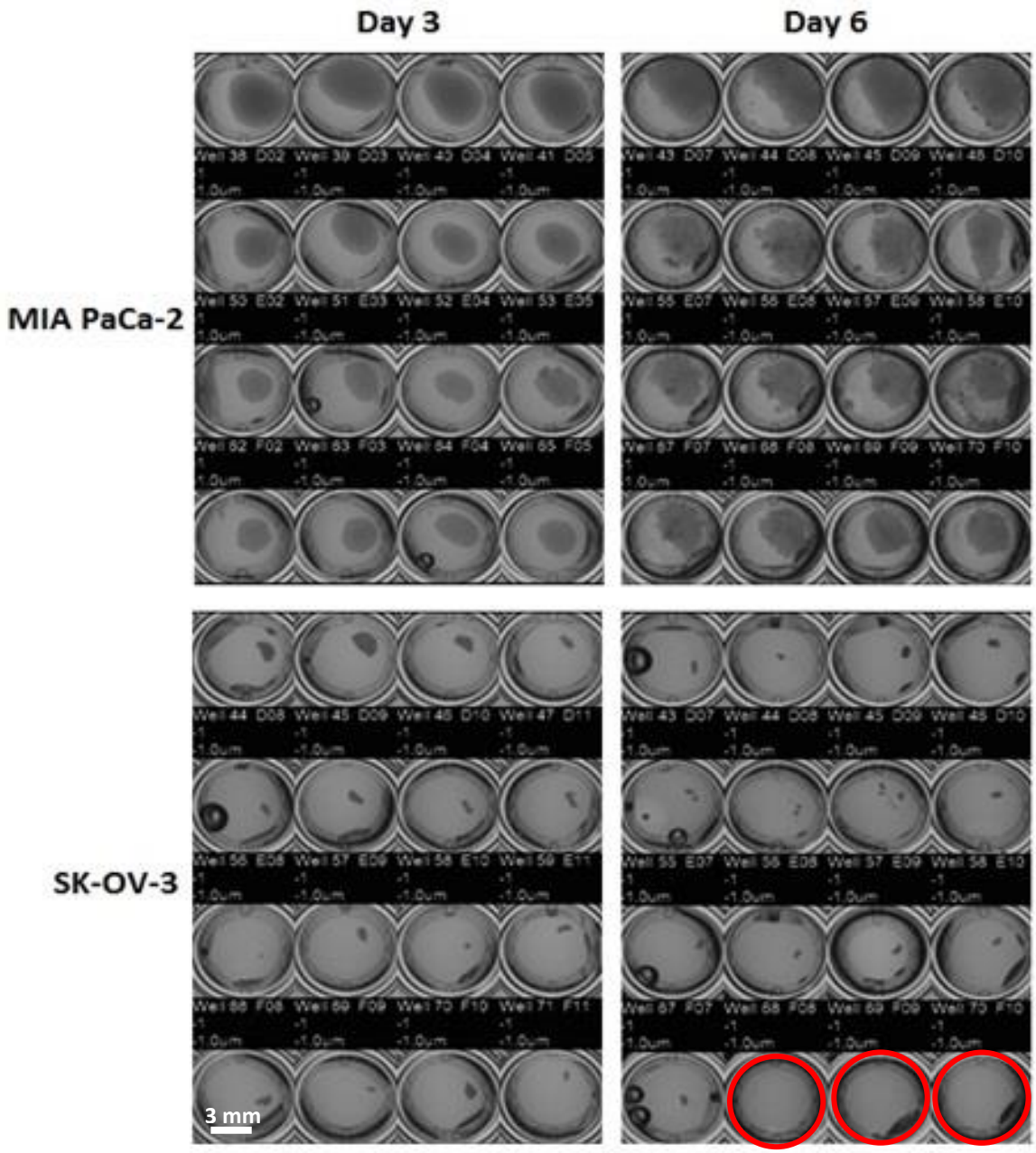

Figure 4.3: The growth of ovarian and pancreatic tumour spheroids.

All 4 cancer cell lines formed tumour spheroids after 3 days of growth and they remained intact as spheroids after 6 days of growth. The number of cells seeded in each row was; 1st row – $5x10^4$ cells, 2nd row – $2x10^4$ cells, 3rd row – $1x10^4$ cells and 4th row – $5x10^3$ cells. The assay was performed with 10 replicates. The images are representative of the spheroid replicates. Empty wells are indicated by red circles. Magnification x2.

The number of cells seeded into the wells was not correlated to the maximal optical density (max OD) (the measurement of the optical density of the MTS reagent, indicative of cell proliferation) for the A2780, AsPC-1 and MIA PaCa-2 spheroids. There was also no correlation between the max OD and spheroid size for these spheroid types. However max OD correlated with both the number of cells seeded into the wells (r = 0.99) and overall spheroid size (r = 0.99) for SK-OV-3 on day 3, though not on day 6. This correlation was effected by the $5x10^4$ cell seeded spheroids which had relatively higher max OD values and were larger in size than the spheroids seeded with a lower number of cells. The max OD was lower on day 6 than day 3 for all 4 of the spheroid types and this was found to be statistically significant (Student's T Test, significance $p < 0.05$) where $p = 0.011$, 0.003, 0.002 and 0.015 for A2780, AsPC-1, MIA PaCa-2 and SK-OV-3, respectively.

The appearance of the A2780, AsPC-1 and MIA PaCa-2 spheroids changed between day 3 and day 6. The spheroids were more permeable to light on day 3 than day 6 which is indicative of a lower level of cell-cell adhesion[217]. The spheroids on day 6 had a dense, dark core and had a rough surface as opposed to the surface on day 3 which was smoother. The SK-OV-3 spheroids were relatively small and appeared dark at all time points during their growth. The appearance of the dense SK-OV-3 spheroids was similar to that seen by Myungjin Lee *et al*.[217].

4.2.3 Effect of duramycin on the cell proliferation of 3D tumour spheroids

It was investigated whether duramycin (0.1-25 µM) had an effect on the cell proliferation of tumour spheroids formed from the cancer cell lines A2780, AsPC-1, MIA PaCa-2 and SK-OV-3 over a 72 hour treatment period. Briefly, agarose gel and PBS were added to 96 well plates as described in the previous section and then cells ($2x10^4$) in appropriate media (100 µl) were added to the wells and incubated for 72 hours. The plates were set up in quadruplicate so that 1 plate was imaged using a GelCount™ colony counter as the pre-treatment plate. The other 3 plates were centrifuged and the supernatant was removed. Duramycin at required concentration in a solution with PBS (100 µl) was added to the wells. The plates were then incubated for 24, 48 or 72 hours at 37°C in a 5% CO_2 atmosphere. After incubation the spheroids were imaged and then the plates were centrifuged. Supernatant was removed and fresh media (180 µl) was added along with MTS reagent (20 µl) and the plate incubated for 2 hours. The plate was then centrifuged and supernatant (100 µl) was removed and added to a fresh plate which was read at 490 nm using a microplate reader. Cell proliferation was calculated as a percentage of the untreated (PBS treated) control spheroids.

Representative images of the duramycin treated 3D tumour spheroids are presented in figure 4.4. All of the SK-OV-3 spheroids appeared to have reduced in size when imaged 24 hours post-treatment. There were no further observable changes over the 72 hour treatment period. At 24 hours post-treatment the A2780 spheroids were all slightly changed in appearance with a less smooth margin at the edge of the spheroid. However there was a noticeable difference in the spheroids treated with 10 µM and 25 µM duramycin and they appeared to be less compact. The reduction in a smooth outside margin and an increase in the breaking up of the spheroid was further enhanced at 48 hours and 72 hours post-treatment. At 24 hours post-treatment the untreated and <10 µM duramycin treated AsPC-1 and MIA PaCa-2 spheroids were not changed in appearance to the pre-treated spheroids. The 10 µM and 25 µM treated spheroids appeared to be less compacted. This trend continued over the 72 hours treatment for MIA PaCa-2 spheroids. However the untreated and <10 µM treated AsPC-1 spheroids appeared to have developed a dark, dense core at 48 and 72 hours. The spheroids treated with duramycin >10 µM appeared to become increasingly less compact at 48 and 72 hours post-duramycin treatment.

Duramycin treatment reduced the cell proliferation of A2780, AsPC-1, MIA PaCa-2 and SK-OV-3 spheroids in a concentration dependent manner (figure 4.5). In general there was no difference between the 24, 48 and 72 hour treatment conditions. The exception to this was that the cell proliferation of SK-OV-3 spheroids treated with 25 µM duramycin was lower at 48 hours than the cell proliferation at 24 and 72 hours. Differences in sensitivity to duramycin treatment were observed between the spheroid types. The highest concentration of duramycin (25 µM) after 24 hour treatment was able to reduce the cell proliferation of A2780 spheroids to 22.3%, AsPC-1 to 16.4%, MIA PaCa-2 to 17.4% and SK-OV-3 to 73.7%. Duramycin at 25 µM reduced the cell proliferation of the 2D cancer cell line cultures to 14.0%, 12.8%, 31.5% and 23.3% for A2780, AsPC-1, MIA PaCa-2 and SK-OV-3, respectively. There was no difference, within SD, between these values for the A2780 and AsPC-1 cell lines. However there was a difference for the MIA PaCa-2 and SK-OV-3 cell lines. The 2D culture of MIA PaCa-2 was more resistant to duramycin treatment than the 3D spheroids. Whereas the 2D culture of SK-OV-3 was substantially more sensitive to duramycin treatment than the 3D spheroid cultures. The concentration of duramycin which reduced cell proliferation compared to the untreated control spheroids was 10 µM for A2780 and AsPC-1 and 25 µM for MIA PaCa-2 and SK-OV-3. This was a higher concentration than what was required for the 2D cultures of the ovarian cancer cell lines A2780 and SK-OV-3 but the same concentration required for the 2D cultures of the pancreatic cancer cell lines AsPC-1 and MIA PaCa-2.

The IC_{50} values for 24 hour duramycin treatment of the tumour spheroids were found to be 9.1 µM for A2780, 7.9 µM for AsPC-1 and 17.2 µM for MIA PaCa-2. As the highest concentration of duramycin (25 µM) reduced the cell proliferation of SK-OV-3 to 73.7% it was not possible to calculate the IC_{50} value for this cell line. Thus it appeared that SK-OV-3 spheroids were relatively resistant to duramycin treatment. The order of sensitivity of the 3D tumour spheroids from most sensitive to least sensitive was: AsPC-1 > A2780 > MIA PaCa-2 > SK-OV-3. This differed from the order of sensitivity for the 2D cultures which was A2780 > AsPC-1 > SK-OV-3 > MIA PaCa-2.

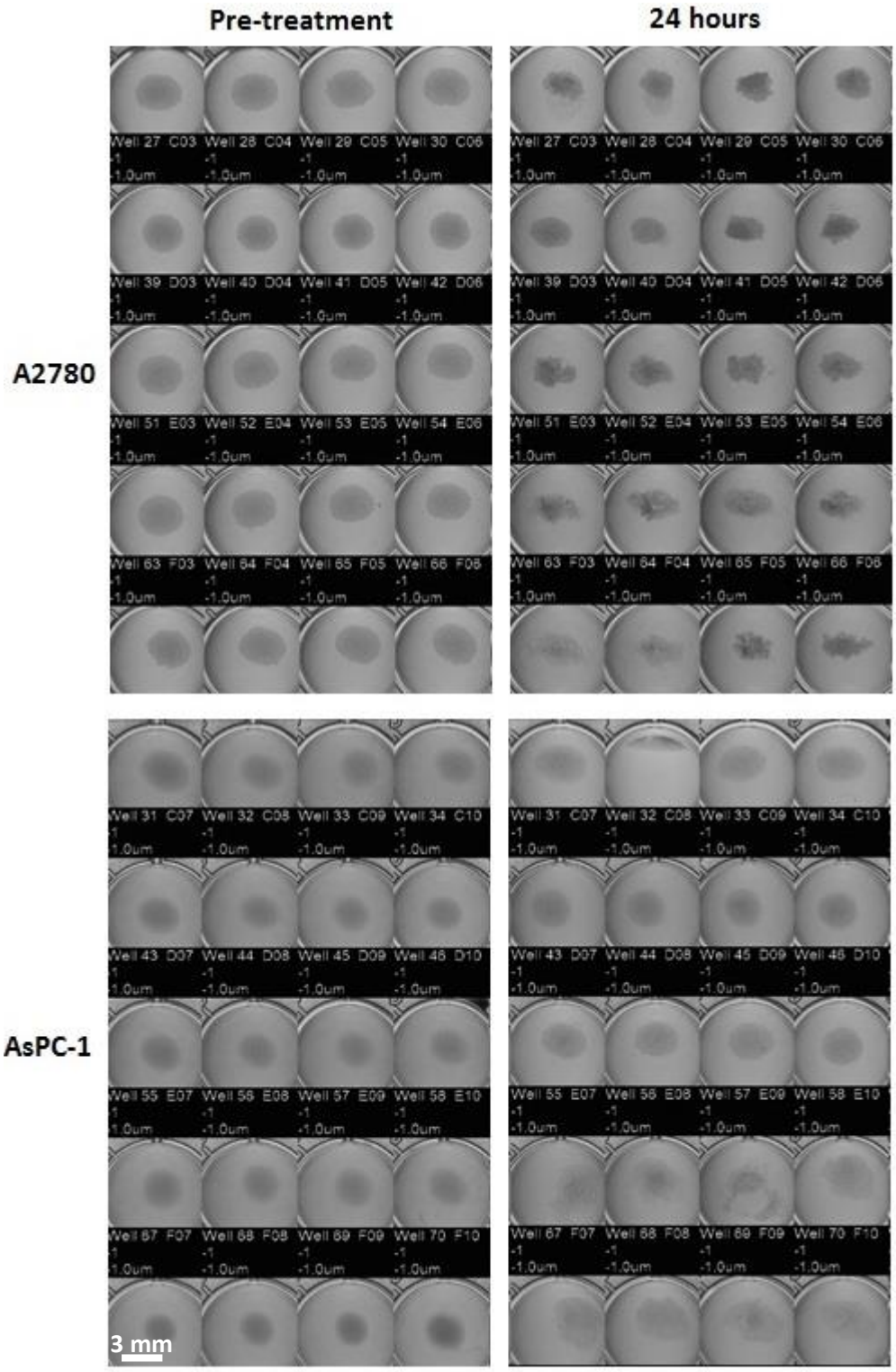
Pre-treatment
24 hours
A2780
AsPC-1
3 mm

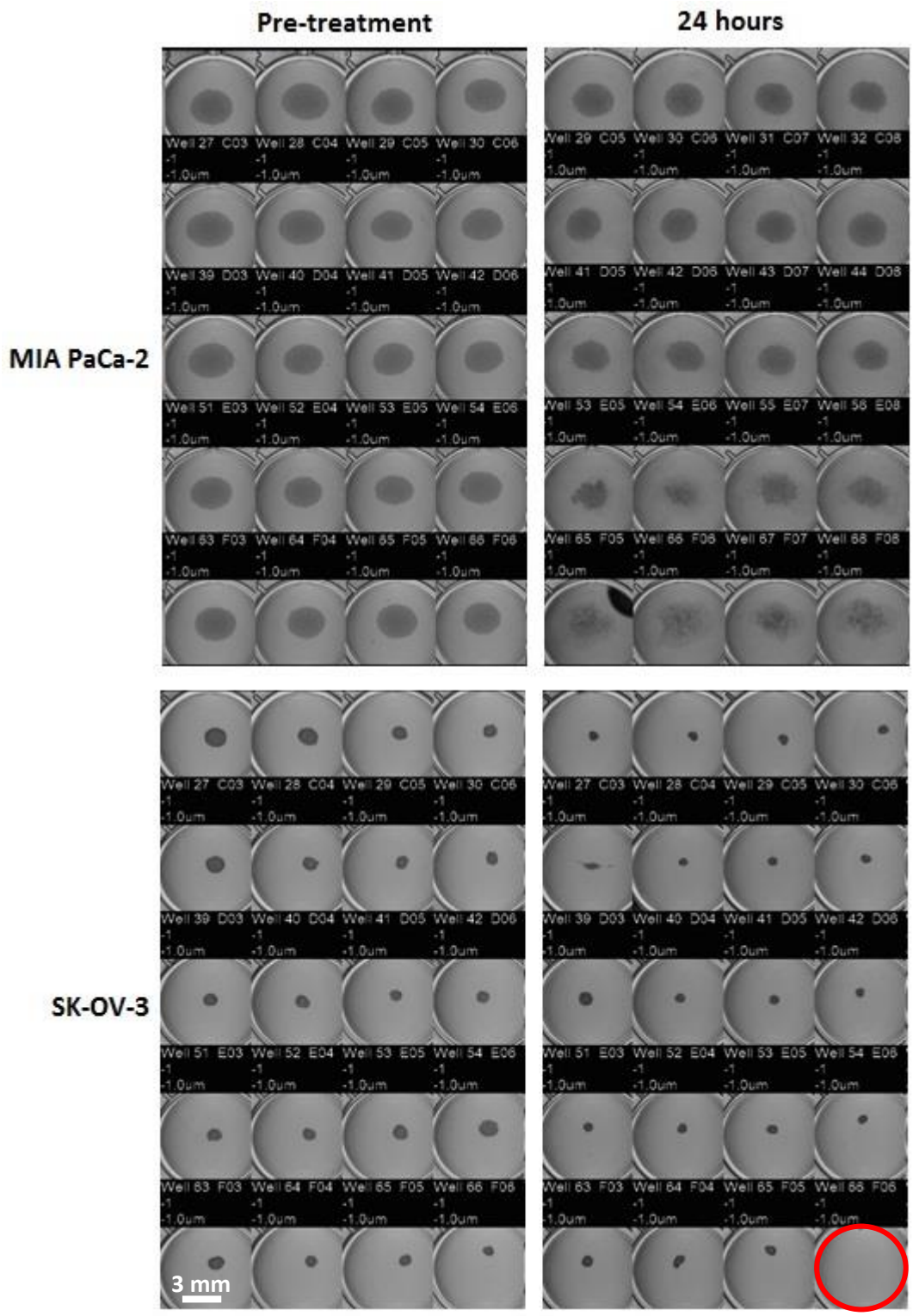

Figure 4.4: The effect of 24 hour duramycin treatment on 3D tumour spheroids. Duramycin had a concentration dependent effect on the A2780, AsPC-1 and MIA PaCa-2 spheroids. As the duramycin concentration increased the spheroids became less compacted. Little effect was observed on SK-OV-3 spheroids though there was a slight reduction in size in the majority of the spheroids. The concentration of duramycin in each row was; 1st row – PBS control, 2nd row – 0.1 µM, 3rd row – 1 µM, 4th row – 10 µM and 5th row – 25 µM. The assay was performed with 8 replicates. The images are representative of the treated spheroids. Magnification x2.

a)

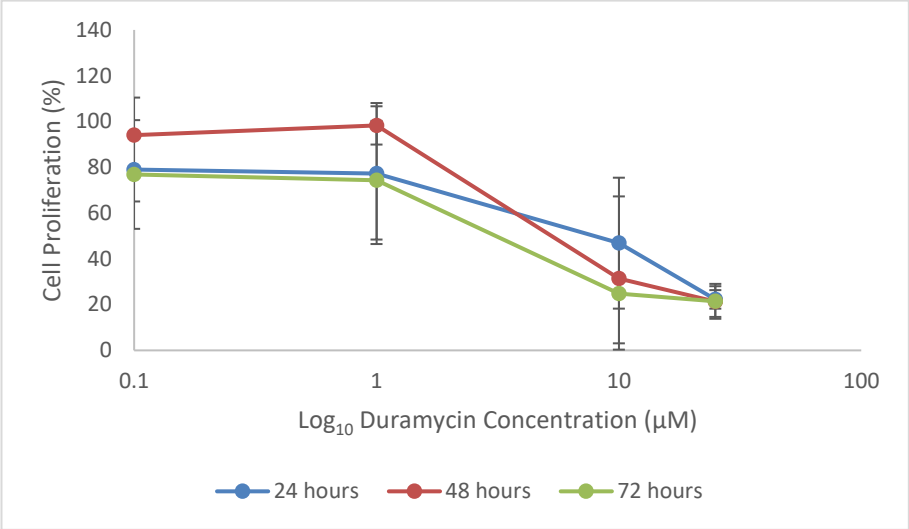
140
120
100
80
60
40
20
0
Cell Proliferation (%)
0.1
1
10
100
Log10 Duramycin Concentration (µM)
24 hours
48 hours
72 hours

b)

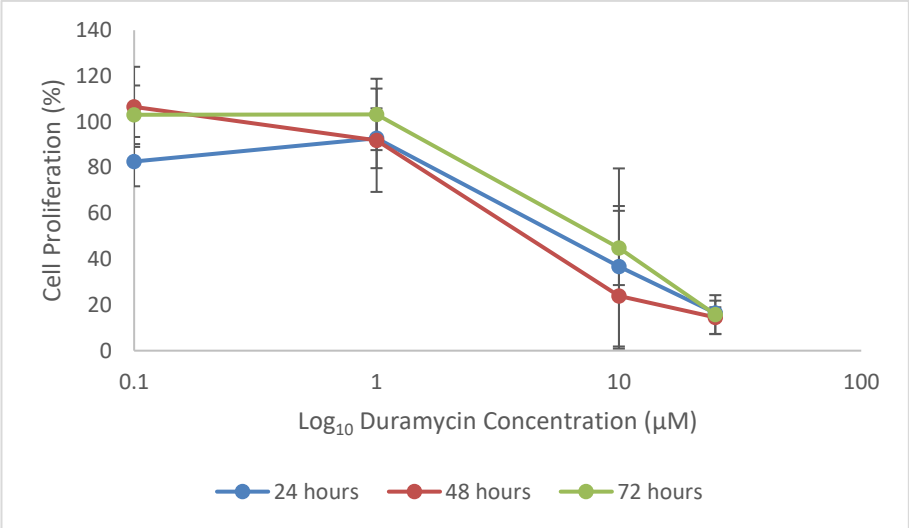
140
120
100
80
60
40
20
0
Cell Proliferation (%)
0.1
1
10
100
Log10 Duramycin Concentration (µM)
24 hours
48 hours
72 hours

c)

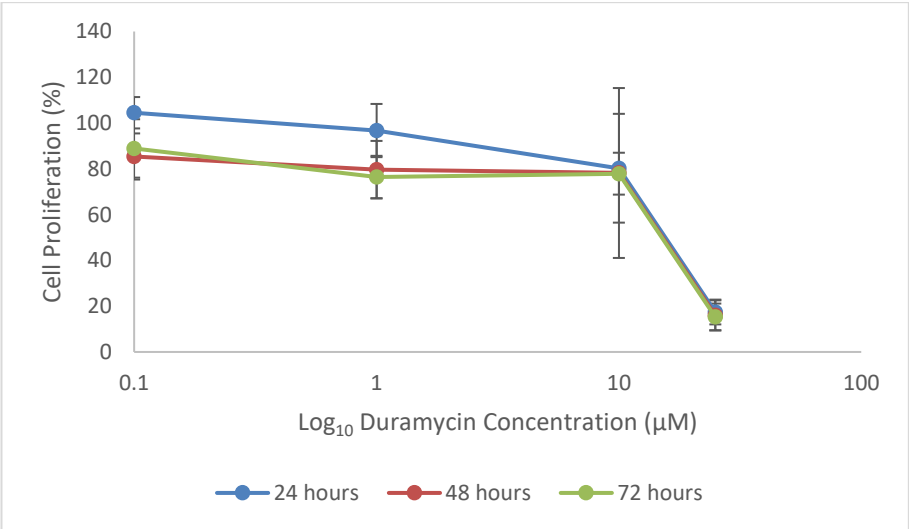
140
120
100
80
60
40
20
0
Cell Proliferation (%)
0.1
1
10
100
Log10 Duramycin Concentration (µM)
24 hours
48 hours
72 hours

d)

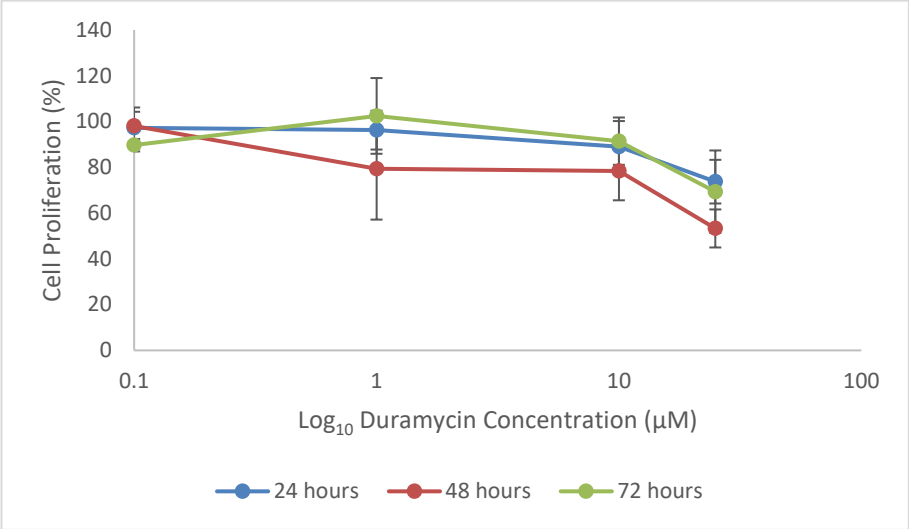

Figure 4.5: The effect of duramycin treatment on the cell proliferation of 3D tumour spheroids.

Duramycin reduced the cell proliferation of the a) A2780, b) AsPC-1, c) MIA PaCa-2 and d) SK-OV-3 tumour spheroids in a concentration dependent manner. In general there was no difference between the treatment time conditions (24, 48 and 72 hours). Error bars represent the SD of 8 replicates.

4.2.4 Comparison of duramycin treated 2D and 3D cell cultures

The effect of duramycin on the cell proliferation of both the A2780, AsPC-1, MIA PaCa-2 and SK-OV-3 2D cell cultures and 3D spheroid cultures is presented in figure 4.6. There was no statistical difference (Student's T Test, significance $p < 0.05$) between the 2 different types of cell culture for the A2780, AsPC-1 and MIA PaCa-2 cultures where the p values (for 24 hour duramycin treatment) were p = 0.93, 0.68 and 0.87, respectively. This same trend was observed in SK-OV-3 for duramycin concentrations <10 µM however concentrations >10 µM had a greater effect on the cell proliferation of the 2D cell culture than the 3D spheroids. Yet this difference was not found to be statistically significant (p = 0.08 for 24 hour treatment).

a)

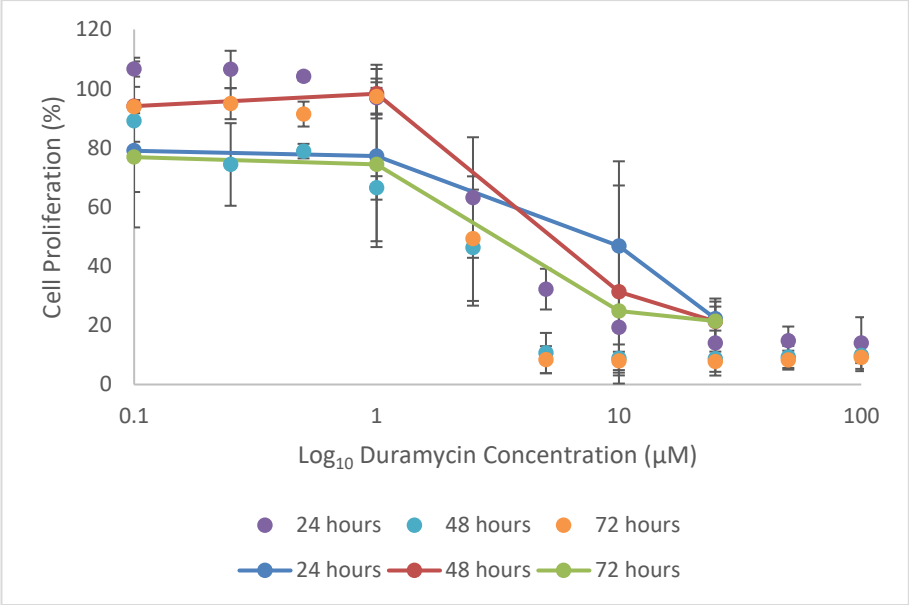

b)

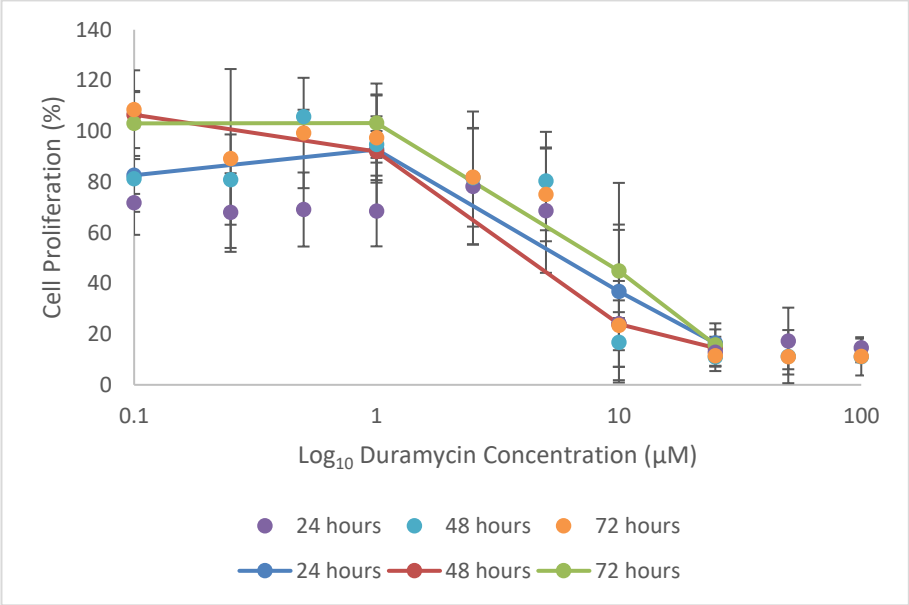

c)

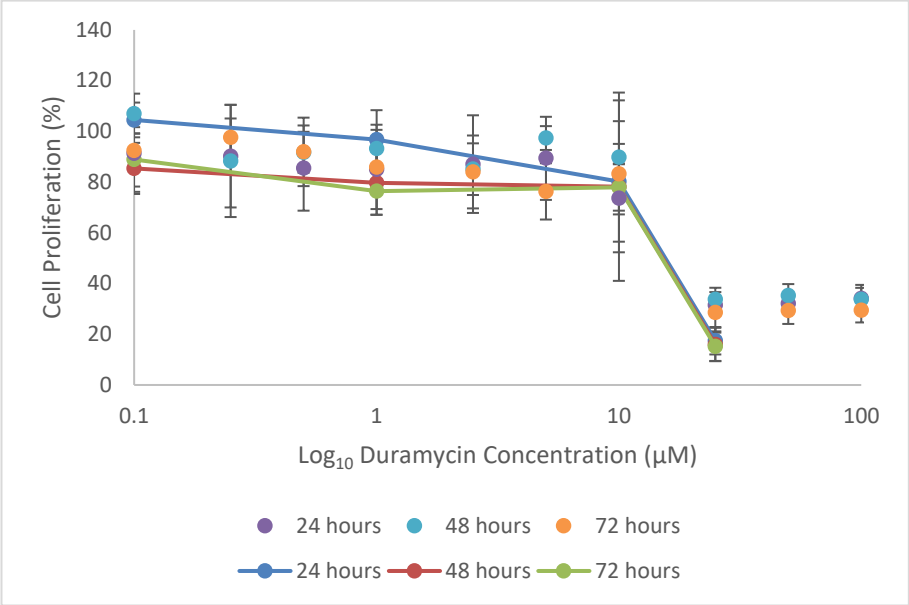

d)

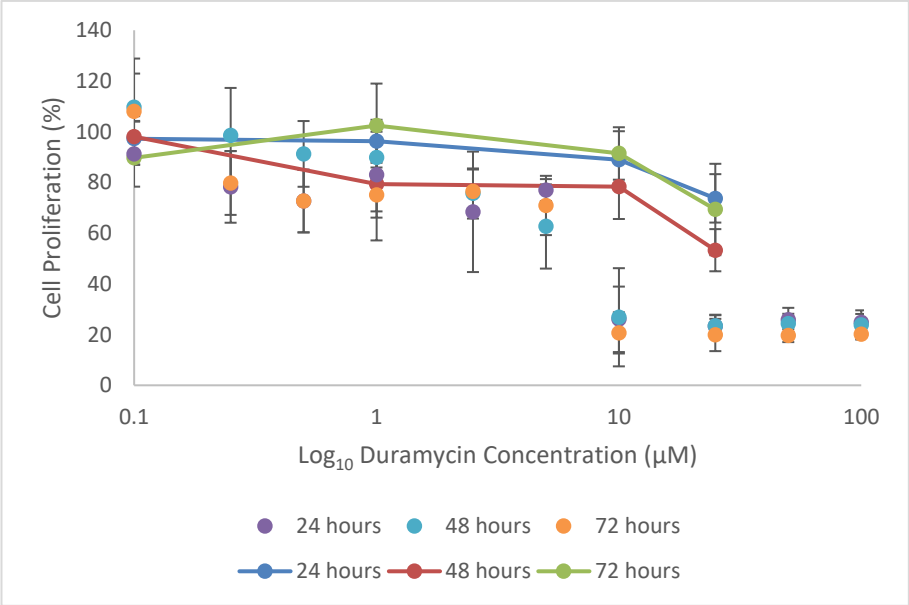

Figure 4.6: The effect of duramycin treatment on 2D vs 3D cell culture.
Duramycin treatment resulted in a similar level of reduction in cell proliferation between the 2D and 3D cell cultures of a) A2780, b) AsPC-1 and c) MIA PaCa-2. This trend was observed in the d) SK-OV-3 cancer cell line between duramycin concentrations 0.1-5 µM. Duramycin >10 µM reduced the cell proliferation of the 2D culture to a larger extent than the 3D spheroid culture though this was not found to be statistically significant (Student's T Test, significance $p < 0.05$). The data points with lines through represent the 3D spheroid cultures and the data points without lines through represent the 2D cell cultures. Error bars represent the SD of 4 replicates for the 2D cell cultures and 8 replicates for the 3D spheroid cultures.

4.3 Discussion

Duramycin treatment after 30 minutes had been previously shown to reduce the cell proliferation of 2D cultures of the cancer cell lines A2780, AsPC-1, MIA PaCa-2 and SK-OV-3 with IC_{50} values of 10.0 µM, 7.1 µM, 18.5 µM and 3.4 µM, respectively (Chapter 3). Thus the order of sensitivity to duramycin was found to be SK-OV-3 > AsPC-1 > A2780 > MIA PaCa-2. The 48 hour duramycin treatment of the pancreatic cancer cell lines AsPC-1 and MIA PaCa-2 revealed that AsPC-1 were more sensitive to duramycin treatment with an IC_{50} value of 0.82 µM compared to 1.32 µM for MIA PaCa-2[49].

In this study, duramycin reduced the cell proliferation of all of the cancer cell lines, A2780, AsPC-1, MIA PaCa-2 and SK-OV-3, in a concentration dependent manner after 24, 48 and 72 hour treatment. No difference was found between these treatment times. Differences in the effect of duramycin on cell proliferation were seen between the cancer cell lines whereby the highest concentration of duramycin (100 µM) reduced AsPC-1 and A2780 cell proliferation to ~14%, SK-OV-3 to ~25% and MIA PaCa-2 to only ~34%. The IC_{50} values revealed that the cancer cell lines had a different sensitivity to 24 hour duramycin treatment than 30 minute treatment. The IC_{50} values were 3.6 µM, 7.1 µM, 18.4 µM and 7.6 µM for A2780, AsPC-1, MIA PaCa-2 and SK-OV-3, respectively. The IC_{50} values found in this study were higher than those seen by Yates *et al*.[49]. It is interesting to note that the same methodology for cell culture and measurement of cell proliferation was used. The discrepancy seen could have been the result of differences between cancer cell line batches or length of time in culture (i.e. number of freeze/ thaw cycles). The cancer cell lines in order of sensitivity to duramycin was A2780 > AsPC-1 > SK-OV-3 > MIA PaCa-2. It may be expected that the concentration required to produce half maximal inhibition of cell proliferation would be lower at longer treatment times as the duramycin has a longer time to effect cells. It was shown that even relatively low duramycin concentrations (5 µM and 10 µM) can induce apoptotic and necrotic cell death in the cancer cell lines after 24 hour treatment (Chapter 3). Thus it is likely that a higher number of dead cells would correspond to a lower number of cells that have metabolically active mitochondria. It is therefore interesting to observe that the IC_{50} value of SK-OV-3 was increased after 24 hour treatment. An explanation for this could be that once the most sensitive cells undergo cell death after 30 minutes treatment those that are left are more resistant to duramycin. The proliferation of these cells is detected at 24 hours and they require a higher concentration of duramycin to produce an anti-proliferative effect. In support of the findings in Chapter 3, duramycin

treatment was shown to have an effect on the cell proliferation of 2D cancer cell line cultures.

Because of the differences between 2D culture and *in vivo* tumours some anti-cancer agents that have been screened thoroughly *in vitro* fail to produce an adequate effect *in vivo*[216] and the majority of drugs fail to make it into clinical trials[217]. Thus 3D spheroid cultures have been applied in anti-cancer drug testing in an attempt to produce a more accurate model of the *in vivo* tumour. The ovarian cancer cell line A2780, cultured in both 2D monolayers and 3D spheroids, was treated with paclitaxel for 24 hours and then assessed for cell proliferation using an MTT assay[229]. The spheroids were shown to be significantly less sensitive to treatment than the 2D cultures ($p < 0.01$). The level of apoptosis was also lower in the spheroids than the 2D cultures which was attributed to a lower level of caspase-3 expression and a higher expression of the anti-apoptotic protein Bcl-2. The overexpression of Bcl-2 was thought to explain the spheroids resistance to paclitaxel as apoptotic cell death may have been inhibited. Spheroids formed from the glioblastoma cell line U87-MG were treated with the cytotoxic agent combretastatin A-4 at different time points (day 2 and day 4) of spheroid formation[230]. Interestingly, the spheroids that were drug treated on day 2 showed a number of dead cells dispersed throughout the spheroid. Yet the dead cells in the spheroids treated on day 4 were confined to the outer layers. Combretastatin A-4 was unable to diffuse into the core of the spheroids in the later growth stages which may have shown that the spheroids had become more compact and had developed a quiescent layer of cells. Spheroids formed from a number of different cancer types (colon, head and neck, bladder, prostate and kidney) were treated with 2 common apoptosis inducing agents, staurosporine and cisplatin, and all but 1 prostate cancer cell line were shown to undergo apoptotic cell death[210]. Recently, the chemotherapeutic treatment of HT29 colon cancer spheroids showed that a number of anti-cancer agents reduced the cell viability of 2D and 3D cultures in a concentration dependent manner[223]. However the IC_{50} values were much higher for the 3D spheroid cultures than the 2D monolayers where the IC_{50} was 15 mM and 5 mM for 5-FU, 500 µM and 90 µM for oxaliplatin and 2 mM and 500 µM for folinic acid, respectively. The sensitivity of spheroids to anti-cancer agents has been shown to resemble the sensitivity of *in vivo* tumours[211]. There are a number of causes for this including the lower proliferative rate of spheroids compared to cell culture[214], altered drug absorption kinetics i.e. lack of diffusion into spheroid cores[214, 229], increased expression of pro-survival factors[17], enhanced anti-apoptotic pathways[229] and the upregulation of genes that confer drug resistance[215, 221].

In this study, tumour spheroids were formed from the ovarian cancer cell lines A2780 and SK-OV-3 and the pancreatic cancer cell lines AsPC-1 and MIA PaCa-2. Initially the spheroids were characterised for the number of cells needed to form adequately sized spheroids and also for their proliferative abilities over a 6 day period. The number of cells seeded into 96 well plates had a strong positive correlation with the overall size (area) of the resultant spheroids. The number of cells chosen for the experiments that followed was $2x10^4$ cells/ well which resulted in relatively large sized spheroids for A2780, AsPC-1 and MIA PaCa-2. At this seeding density the tumour spheroids developed dark, dense and potentially necrotic cores after 3 days of growth for AsPC-1 and MIA PaCa-2 and after 6 days of growth for the A2780 spheroids. It is well established that as *in vitro* tumour spheroids progress through growth that a necrotic core composed of nutrient deficient tumour cells is formed[231, 232]. Breast cancer (MCF7) spheroids that had become dark in appearance after 7-9 days in culture were shown to have a decreased DNA content which was due to an increased level of apoptosis and necrosis[222]. The SK-OV-3 spheroids were smaller than the other cancer cell line spheroids and appeared dark at all time points of their growth (discussed below). After 6 days of growth the A2780, AsPC-1 and MIA PaCa-2 spheroids appeared to have a less smooth periphery compared to day 3. The 'ruffled' edges of MCF7 spheroids seen in the later stages of their growth (5-7 days) was suggested to be due to cell proliferation occurring at the spheroid's periphery[222]. In contrast, drug treated glioblastoma (U87-MG) spheroids had a rough periphery 3 days post-treatment compared to the smooth outer edges of the untreated spheroids[230]. The spheroids were stained for live/ dead cells and imaged where it was shown that the rough edges corresponded to areas of dead cells and that the untreated spheroids remained almost completely alive. Therefore it is possible that the rough periphery of the spheroids seen on day 6 in this study was because they had a lower cell viability than on day 3. This was supported by the statistically significant (Student's T Test, significance $p < 0.05$) (p values were $p \leq 0.02$) reduction in the max OD from day 3 to day 6 for all of the spheroid types. The decrease in max OD was most likely due to a reduction in the number of proliferating cells at the surface of the spheroids. As characterised by the Gompertzian growth model, the amount of proliferating cells in spheroids becomes reduced over time as cancer cells enter into the quiescent layer and dead cancer cells are either removed or become part of the necrotic core[231, 232]. The loss in a linear increase in cell viability, due to the development of a necrotic core, was theorised to be the reason for the reduction in luminescence of the active reagent of a cell viability assay in A549 lung cancer spheroids[233].

Duramycin treatment of the 3D tumour spheroids resulted in a change in their appearance. The A2780, AsPC-1 and MIA PaCa-2 spheroids appeared less compact and became disaggregated when treated with duramycin >10 µM over the 72 hour treatment period. This may be expected as duramycin >10 µM had been shown to induce apoptotic and necrotic cell death in these cancer cell lines (Chapter 3). It is possible that duramycin had an effect on the adherence properties of the spheroids. Duramycin effects the integrity of cell membranes[88, 89, 178, 179] and so could possibly disrupt the expression of cell surface receptors essential in spheroid formation (e.g. α5β1-integrin which was shown to be important in spheroid aggregation[214]). Perhaps it is more likely that the loss of spheroid aggregation was due to cellular death as seen in 2D cell culture at these concentrations (Chapter 3) which would be supported by the reduction in cell proliferation seen in the spheroids. The disaggregation of A549 lung cancer spheroids with increasing drug (fenretinide) concentration was confirmed to be correlated with a reduction in cell viability[233]. The SK-OV-3 spheroids appeared to be relatively small and dark for the duration of the treatment and no observable changes were seen (discussed below).

Duramycin treatment was shown to reduce the cell proliferation of all 4 spheroid types in a concentration dependent manner over 24, 48 and 72 hours. No difference was shown between these treatment times. Differences in the sensitivity to duramycin were observed between the spheroid types whereby the highest duramycin concentration (25 µM) reduced the cell proliferation of A2780 to 22.3%, AsPC-1 to 16.4%, MIA PaCa-2 to 17.4% and SK-OV-3 to only 73.7%. The IC_{50} values for 24 hour duramycin treatment were 9.1 µM, 7.9 µM and 17.2 µM for A2780, AsPC-1 and MIA PaCa-2, respectively. It was not possible to calculate an IC_{50} value for SK-OV-3 as the proliferation was not reduced to ≤50%. Thus the order of sensitivity to duramycin was AsPC-1 > A2780 > MIA PaCa-2 > SK-OV-3. This was different to the order of the sensitivity of the 2D cultures which was A2780 > AsPC-1 > SK-OV-3 > MIA PaCa-2. Another difference observed between the 2D and 3D culture types was the concentration of duramycin required to reduce the cell proliferation compared to the untreated controls. A higher concentration was needed for the 3D cultures (10 µM and 25 µM, respectively) of the ovarian cancer cell lines A2780 and SK-OV-3 than the 2D cultures (2.5 µM and 10 µM, respectively). However, this was not seen with all of the cancer cell lines and the same concentration (10 µM and 25 µM, respectively) was shown to be required for both culture types of the pancreatic cancer cell lines AsPC-1 and MIA PaCa-2. The IC_{50} value for MIA PaCa-2 spheroids was slightly lower than the 2D monolayer (IC_{50} = 17.2 µM compared to 18.4 µM, respectively). There was a trend that the IC_{50} values for

duramycin treated A2780 and AsPC-1 spheroids were slightly higher than their 2D monolayer cultures, which is in agreement with the literature. It is often the case that tumour spheroids are much more resistant to anti-cancer drugs than 2D monolayers. For example, the IC_{50} values for cisplatin, paclitaxel and topotecan treated spheroids formed from 6 different ovarian cancer cell lines, including SK-OV-3, were found to be significantly higher than their 2D culture counterparts[221]. Colon cancer spheroids and cancer cell monolayers (HCT116) were treated with a number of anti-cancer agents[210]. It was found that cisplatin, 5-azacytidine, emodine, mitoxantr and 5-FU had a significantly larger effect on the cell viability of the 2D cell cultures than the 3D spheroids.

Yet, despite the slight differences observed between the 2D and 3D cancer cultures in this study, no statistically significant difference between the 2 culture types was found for duramycin's anti-proliferative effect (Student's T Test, significance $p < 0.05$). For A2780, AsPC-1 and MIA PaCa-2 p values were $p = 0.93$, 0.68 and 0.87, respectively. Duramycin concentrations >10 µM had a greater effect on the cell proliferation of SK-OV-3 2D cell culture than SK-OV-3 3D spheroid culture but again this difference was not found to be statistically significant ($p = 0.08$). Though the usual result is that 3D spheroid cultures have a higher drug resistance than 2D monolayer cultures no differences for drug effect between the culture types have been reported in the literature. A number of anti-cancer agents were observed to have the same effect on the 2D and 3D cultures of HCT116 cancer cells where DMSO and piroxicam did not affect the cell viability of either[210]. Tamoxifen and miconazole reduced the cell viability of the 2D culture to zero and the spheroids to almost zero and pimozide and tetrandine induced complete cell death of both culture types. Additionally, other studies have found no difference in the effect of anti-cancer drugs between 2D and 3D spheroid cultures[234, 235].

A spheroid diameter of >500 µm is often stated as the required size to accurately mimic the conditions found in natural tumour masses[210, 215, 233]. Under these conditions a layer of quiescent cells under the proliferating outer surface can develop and, due to a limited supply of oxygen and nutrients, a necrotic core can form. The average diameter of the spheroids (seeded at $2x10^4$ cells) in this study ranged from 850 µm for SK-OV-3 to ~3 mm for A2780 and MIA PaCa-2 spheroids. Therefore the spheroids would be classified as 'large' spheroids[233]. The quiescent layer is often attributed to the drug resistance exhibited by spheroids and *in vivo* tumours[210, 215]. This is due to the requirement of actively proliferating cancer cells of some anti-cancer agents. Therefore this potentially confounds the finding

that there was no significant difference in the effect of duramycin between the 2D and 3D cultures. However, duramycin may have an advantage over other anti-cancer agents as its anti-cancer effect is exerted through binding to cellular membranes (Chapters 3 and 5) rather than requiring uptake into 'active' cancer cells. In Chapter 5 it was hypothesised that duramycin exerts its cytotoxic effect by disrupting plasma membrane integrity and forming membrane pores that result in ion concentration changes. Also duramycin has been shown to detect a relatively higher level of PE on necrotic pancreatic cancer cells than on viable and apoptotic cells[49] and thus may be able to bind to the necrotic cells. It is therefore possible that duramycin was able to penetrate into the spheroids despite quiescent or necrotic layers. In addition, duramycin is a relatively small peptide, being only 19 amino acids in length[66] and ~2kDa in molecular weight (MW), which could mean that it easily diffused into the spheroids. The lower MW of a radiolabelled duramycin compound, ^{99m}Tc-duramycin, compared to another phospholipid-binding probe, ^{99m}Tc-C2A-GST, contributed to its superior permeability in ischaemic cardiac tissue[76]. Single chain Fv fragments (scFv) of monoclonal antibodies (mAb) have been used in oncological research to produce faster and more enhanced tissue penetration due to their smaller size than mAbs[154]. It has been shown that spheroids have a high resistance to other drugs with a relatively small molecular mass, for example 5-FU[211, 226], however again this is due to its action against 'active' cancer cells rather than a lack of permeability.

The relatively little effect that duramycin had on the cell proliferation of SK-OV-3 spheroids (cell proliferation was not reduced to <70%) compared to the other spheroids could have been due to an initial low viability of the spheroid. As the spheroids appeared dark prior to treatment it is possible that a high number of the cancer cells were already necrotic and/or had a low cell proliferation. Carduner *et al*.[236] found that anchorage-independent growth of SK-OV-3 cells (i.e. grown as spheroids on a non-adherent surface) lead to cell cycle arrest in the G0-G1 phase. The growth arrest was evident in the SK-OV-3 spheroids from the first day of culture. Cell cycle arrest in the G0-G1 phase is a mechanism that cells can employ to evade apoptotic cell death[236]. One of the proteins expressed during this process is the p130 and retinoblastoma protein (p130/Rb) which was shown to increase in expression in the SK-OV-3 spheroids over the first 4 days of growth. It was suggested that the presence of p130/Rb along with the lack of activation of pro-apoptotic pathways meant that SK-OV-3 cells, when cultured as spheroids, become mostly quiescent. Thus if the majority of the cells in the SK-OV-3 spheroids were either dead or in a state of quiescence the duramycin treatment may not have reduced the cell proliferation to a large extent. Alternatively, the

higher resistance to duramycin treatment could have been because SK-OV-3 formed tightly aggregated spheroids. SK-OV-3 were shown to form highly compact spheroids compared to a number of other ovarian cancer cell lines (TOV-112, TOV-21, TOV-155) which formed loosely packed aggregates[221]. Interestingly, genes associated with cell adhesion, metabolism and the negative regulation of cell proliferation, were up-regulated in the compact spheroids compared to the aggregates. Claudin 4, a cellular adhesion molecule overexpressed in ovarian cancer, was shown to increase the rate of ovarian cancer spheroid formation[237]. mRNA analysis showed that the claudin 4 gene was overexpressed in much higher amounts in the SK-OV-3 cell line than in the A2780 cell line. A higher level of claudin 4 expression was associated with a lower permeability of spheroids and was speculated to result in a lower sensitivity to chemotherapy. If claudin 4 was expressed on the ovarian cancer cell lines used in this study it may explain why SK-OV-3 formed densely packed spheroids whereas A2780 formed compact but less dense spheroids. It is possible that the higher resistance of SK-OV-3 was indicative of a diffusion problem faced by duramycin in the more compacted spheroids rather than a resistance due to quiescent or necrotic cells. Additionally, possible inherent differences in protein expression between the cancer cell lines in this study could explain the differences in sensitivity to duramycin observed between the spheroid types.

However, the formation of compact spheroids by SK-OV-3 is not uniformly reported in the literature and they have been shown to form loosely packed aggregates compared to other ovarian cancer cell lines (HEY, OVCA439 and ES-2)[17]. These differences in SK-OV-3 spheroid morphology could partly be due to the method of spheroid formation. There are a number of methods used for the formation of spheroids[233]. The method used in the study above[17] was the hanging drop method whereby cells are suspended in a droplet of liquid which hangs from the lid of a cell culture plate. Through gravity and surface tension cells become compacted at the bottom of the droplet and subsequently form spheroids. The liquid overlay method was used in this study (section 2.1.5) and in the study which observed a more compact formation of SK-OV-3 spheroids[221]. Therefore discrepancies for spheroid morphology (and drug sensitivities[210, 234, 235]) are seen in the literature, which may partly be dependent on the methodology used. Pancreatic cancer cell lines (PANC-1, Aspc-1, Capan-1, Capan-2 and Miapaca-2) were shown to form only weak aggregates using the liquid overlay method[215]. Out of AsPC-1, Capan-2, MIA PaCa-2 and PANC-1 only PANC-1 formed adequately compact and large enough spheroids in polydimethylsiloxane (PDMS) wells. This lack of successful spheroid formation was not observed with the AsPC-1 and MIA PaCa-

2 pancreatic cancer cell lines in this study. Again this may highlight the discrepancies which result between different spheroid formation methods (e.g. PDMS vs. agarose gel).

In conclusion, duramycin had an anti-proliferative effect on both 2D and 3D cancer cell cultures. A treatment time of 24 hours was shown to be efficient enough to produce maximal effect on cell proliferation. The concentration of duramycin required to produce half maximal inhibition of the cancer cell lines' proliferation was lower for 24 hours treatment than the 30 minutes treatment, as shown previously (Chapter 3). As a result of the necrotic cores, limited drug permeability, gene expressions and the inhibition of cell death mechanisms the 3D tumour spheroid model, arguably, offers a more realistic model of cellular drug response than 2D monolayer cultures. There was no statistically significant difference in the effect of duramycin on the cell proliferation of 2D monolayer cultures and the cell proliferation of 3D tumour spheroid cultures. It is therefore possible that the effect of duramycin on cancer cells observed in *in vitro* models of cell culture would translate well into the *in vivo* tumour environment and thus could be a, potentially, successful anti-cancer agent.

Chapter 5 The Effect of Duramycin on Calcium Ion Concentration

Papers published in support of this chapter:

Broughton LJ, Crow C, Maraveyas A, Madden LA. Duramycin-induced calcium release in cancer cells. *Anti-Cancer Drugs*. 2016; 27(3):173-82.

5.1 Introduction

Calcium ions (Ca^{2+}) and Ca^{2+} signalling play an important and diverse role in non-tumour and tumour cellular processes such as the modulation of cellular transcription, cell cycle regulation, cell proliferation, cancer cell differentiation into cancer stem cells, angiogenesis, cell motility and apoptosis[100]. In both non-tumour and tumour cells Ca^{2+} can have a dual purpose as they are a key component of cellular life but Ca^{2+} overload can be an initiator of cell death [112,105]. Cells invest a large amount of energy in the maintenance of a low intracellular Ca^{2+} concentration ($[Ca^{2+}]_i$) (~100 nM) which equates to a 20,000 fold gradient between intracellular and extracellular Ca^{2+} (~1.2-2 mM)[102]. The reason for a homeostatically maintained low level $[Ca^{2+}]_i$ may partly be due to the cytotoxicity of Ca^{2+} to cells[117]. Maintenance of low level cytosolic Ca^{2+} concentration is achieved by various ATP-dependent mechanisms in which Ca^{2+} are chelated, compartmentalised or removed from the cytoplasm[100]. The 'compartments' involved in the removal of Ca^{2+} from the cytoplasm consist of the sarco/endoplasmic reticulum and the mitochondria which act as temporary buffers before expulsion of Ca^{2+} from the cell[102]. In addition, the golgi apparatus, lysosomes and the nuclear envelope have been implicated in the compartmentalisation of Ca^{2+} [103]. The gradient between intracellular and extracellular Ca^{2+} concentration is maintained by ATPase pumps which transfer Ca^{2+} into the endoplasmic reticulum (ER) via sarco/endoplasmic reticular Ca^{2+} ATPases (SERCA) or out of the cell through the plasma membrane pumps Ca^{2+} ATPases (PMCA). A secondary mechanism of Ca^{2+} flux is utilised by cells via Na^+/Ca^{2+} exchangers (NCX) and Na^+/Ca^{2+}-K^+ (NCKX) exchangers which exchange calcium for sodium or co-transport potassium with calcium in exchange for sodium, respectively. NCX and NCKX are responsible for rapid changes in Ca^{2+} concentration whereas PMCA maintain low $[Ca^{2+}]_i$ over longer durations[102]. In excitatory Ca^{2+} signalling pores in the cell membrane are opened by a change in voltage (voltage-gated Ca^{2+}-selective channels; VGCC), ligand binding (transient receptor potential channels; TRP) or by store operated Ca^{2+} influx (Stim/Orai channels). VGCC produce the fastest form of Ca^{2+} signalling in excitatory non-tumour cells where one channel can conduct ~1 million calcium ions/ second. Many different forms of VGCC have been shown to be overexpressed in a wide

variety of malignancies and some have been implicated in playing a key role in cancer cell proliferation[112]. NCX exchangers have been shown to be active in the pancreatic cancer cell lines CFPAC-1, PANC1 and Capan-1 and the pancreatic cancer cell line used in this study, MIA PaCa-2, has been shown to utilise PMCA as its primary Ca2+ efflux pathway[117]. The key components of store operated Ca2+ influx STIM1 and ORAI1 have been shown to be expressed in the ovarian cancer cell line A2780[106].

Tumour cells use the same calcium channels and pumps as non-tumour cells however there are usually modifications to the tumour cells' channels and pumps such as changes in the level of expression, altered cellular localisation and altered function due to post-translational modification[105]. These changes can alter the flux of Ca^{2+} across cell membranes[113]. For example the TRPV6 channel, a highly Ca^{2+} specific ion channel, in health mediates calcium transport in the small intestine, kidneys, colon and exocrine tissues[104] and is inactive in resting cells[103]. Its expression in prostate cancer has been shown to correlate with tumour progression and invasiveness and in breast cancer with cancer cell survival[104]. An increased level of TRPV6 expression has been observed in ovarian cancer tissue compared to normal ovarian tissue[238]. The Ca^{2+}-permeable TRPM8 channel in healthy cells is involved in Ca^{2+} homeostasis and the cellular response to temperature[110]. Yet, in malignancy it has been shown to have an important role in the proliferation, invasion and survival of many different types of cancer[110]. TRPM8 was seen to be overexpressed in all cell lines in a panel of pancreatic adenocarcinoma cell lines, including MIA PaCa-2, where it was required for uncontrolled cancer cell proliferation[111]. The ovarian cancer cell lines A2780 and SK-OV-3 were shown to have an upregulated expression of the mitochondrial Ca^{2+} transporter regulator MICU1 which conferred an enhanced ability to buffer Ca^{2+} compared to normal ovarian endothelial cells[239].

Though Ca^{2+}-mediated cell death is more commonly associated with apoptosis signalling pathways[103, 113] Ca^{2+} also play an important role in programmed necrosis. An increase in $[Ca^{2+}]_i$ by entry of Ca^{2+} through plasma membrane pores or release of Ca^{2+} stored in the ER can activate proteases which cleave the NCX exchangers. This consequently removes cells ability to extrude Ca^{2+} [240]. A prolonged increase in cytosolic Ca^{2+} concentration can stimulate Ca^{2+} overload, mitochondrial permeability, mitochondrial ATP depletion and reactive oxygen species (ROS) production. If a majority of the cells' mitochondria maintain the ability to synthesise ATP the loss in ATP may favour apoptotic cell death. However, if ATP depletion is too severe for the activation of apoptosis the cell is likely to undergo

necrotic cell death[118]. An example of the utilisation of Ca^{2+} in programmed necrosis can be seen with the extracellular ligand N-methyl-D-aspartate (NMDA). NMDA activates the Ca^{2+}-permeable NMDA receptor which plays a significant role in the necrosis of neurons in mammals[240]. Expression of the MEC-4(d) sodium ion channel in *Caenorhabditis elegans* allows influx of Ca^{2+} into neuronal cells and stimulates Ca^{2+} release from the ER which ultimately leads to neuronal necrosis. Additionally, stimulation of cytosolic Ca^{2+}-dependent proteases such as cathepsins or calpains, which activate caspases, can begin the cell death process[240]. There are a number of methods that cancer cells can exploit to evade calcium-induced cell death[113] which mainly include the oncogenic transformation of the ER and mitochondria. The remodelling of mitochondrial Ca^{2+} pathways involved in proliferation, metastasis, angiogenesis and evasion of apoptosis has been shown to occur in cancer cells[100]. Expression of anti-apoptotic members of the BCL2 family can affect mitochondrial Ca^{2+} uptake[115] and reduce Ca^{2+} flux from the ER through inhibition of Ca^{2+} pumps[114]. Phosphorylation of the ER calcium channels inositol trisphosphate receptors (IP_3R) in the glioblastoma cell line U87 resulted in a decrease in Ca^{2+} flux from the ER to the mitochondria and a subsequent reduction in the response to pro-apoptotic signals[116]. Despite these mechanisms Ca^{2+} overload has been shown to be an effective cancer therapy and an inducer of necrosis in cancer cells *in vitro*[117, 118].

Duramycin has been shown to have an effect on a number of ion transport channels and pumps in a variety of cell types. Duramycin was shown to inhibit the Na^+-K^+ ATPase pump by inhibiting phosphorylation by Pi and causing hydrolysis of the phosphoenzyme[84]. Duramycin was also seen to inhibit ATP-dependent Ca^{2+} uptake in sarcoplasmic reticulum (SR) vesicles from rabbit skeletal muscle[70]. An increase in $[Ca^{2+}]_i$ and ion conductance occurred when duramycin was applied to the apical membrane of colonic epithelial cells[88]. Duramycin increased short circuit current and induced chloride (Cl^-) secretion in a narrow concentration range of 0.2-5 µM in tracheal epithelium[86]. An increase in $[Ca^{2+}]_i$ in airway epithelial cells was attributed, at low duramycin concentrations, to release from internal stores and at higher concentrations to both release from internal stores and extracellular calcium influx[87]. Due to its effect on ion channels and, more specifically, its activation of the Ca^{2+}-activated Cl^- channel (CaCC) anoctamin 1 (ANO1)[93] duramycin was investigated as a potential therapeutic in the treatment of cystic fibrosis (CF). Good results were obtained from Phase I[94] and Phase II[95] clinical trials in which subjects were given duramycin in the form of an inhaled aerosol. Within narrow concentration ranges duramycin stimulated Cl^- secretion in CF patients at 3 µM and in healthy volunteers at 1-10 µM[94]. However, there

has been no further development in clinical trials, possibly because the theory that duramycin stimulates Cl^- secretion through action on alternative Cl^- channels was discredited when a study on airway epithelium confirmed that duramycin did not selectively effect Cl^-. Instead duramycin was shown to disrupt cell membranes which resulted in non-selective ion movement[91]. Furthermore, duramycin has been shown to effect artificial and biological membranes[89] through the formation of pores and inducing changes in the shape of membranes[73, 92].

The mechanism through which duramycin induces cell death is yet to be elucidated. The aim of this chapter was to investigate whether the duramycin-induced necrotic cell death of cancer cell lines observed in Chapter 3 was related to a form of Ca^{2+} overload. Therefore the $[Ca^{2+}]_i$ of ovarian and pancreatic cancer cell lines was monitored by spectrofluorometry and confocal microscopy following the addition of duramycin. Due to the numerous reports[87, 89-91, 93, 178, 179] in the literature that duramycin caused non-selective ion movement through the formation of plasma membrane pores and disruption to ATP-dependent membrane ion channels and pumps it was also investigated herein whether duramycin effected cancer cell membrane integrity.

5.2 Results

5.2.1 Effect of duramycin on intracellular Ca^{2+} concentration of cancer cells

To investigate the effect of duramycin on the $[Ca^{2+}]_i$ of tumour cells the ovarian cancer cell lines A2780 and SK-OV-3 and pancreatic cancer cell lines AsPC-1 and MIA PaCa-2 were treated with duramycin (0-50 µM). Briefly, cells were removed from tissue culture flasks with HEPES-buffered saline EDTA, centrifuged and re-suspended in fresh media. To this the anion transport inhibitor sulphinpyrazone and the calcium indicator Fluo-3, AM was added and the cells were incubated in the dark at room temperature for 30 minutes. Cells were then centrifuged and re-suspended in calcium buffer which was supplemented with $CaCl_2$ when the experiment required the presence of extracellular Ca^{2+} (Ca_{ext}). Cells (100 µl, $1x10^5$) were added to a cuvette containing calcium buffer (1.9 mL) and placed into a spectrofluorometer. To this either duramycin (20 µl) or calcium ionophore A23187 (12 µl) was added. A23187 causes a rapid increase in $[Ca^{2+}]_i$ due to release of Ca^{2+} from intracellular stores, this is followed by a rapid clearance of intracellular Ca^{2+} due to increased permeability of the cell membrane to divalent cations such as Ca^{2+}. The maximal increase in Ca^{2+} fluorescence in duramycin treated cells was calculated as a percentage of the maximal Ca^{2+} fluorescence that occurred in the A23187 treated cells. The assay was performed in duplicate with each duramycin concentration done in duplicate and A23187 in triplicate each time.

Duramycin treatment resulted in an increase in $[Ca^{2+}]_i$ in all 4 cancer cell lines A2780, AsPC-1, MIA PaCa-2 and SK-OV-3 in a duramycin concentration dependent manner (figure 5.1). The increase in Ca^{2+} fluorescence (i.e. Fluo-3, AM fluorescence) occurred immediately upon addition of duramycin. Concentrations lower than 5 µM had very little effect on $[Ca^{2+}]_i$ which supported previous findings that showed that relatively low concentrations of duramycin had little effect on cancer cell viability and proliferation (Chapters 3 and 4). The highest concentration (50 µM) induced the greatest percentage increase in $[Ca^{2+}]_i$ in all 4 cancer cell lines. Differences in the effect of duramycin on $[Ca^{2+}]_i$ were observed between the cell lines when treated with 50 µM duramycin. Here the pancreatic cancer cell lines, AsPC-1 (87.0%) and MIA PaCa-2 (84.5%), had a higher percentage increase in Ca^{2+} than the ovarian cancer cell lines A2780 (44.8%) and SK-OV-3 (59.8%) (figure 5.1e). However, this was not found to be statistically significant ($p = 0.16$) (Student's T Test, significance $p < 0.05$). The experiment was performed in either the absence or presence of Ca_{ext}. There was no significant difference observed between the conditions for all the cell lines ($p > 0.05$)

(Student's T Test, significance $p < 0.05$). However, there was a trend that A2780, MIA PaCa-2 and SK-OV-3had a slightly higher percentage increase in $[Ca^{2+}]_i$ in the presence of Ca_{ext} than in the absence at concentrations of duramycin ≥10 µM.

a)

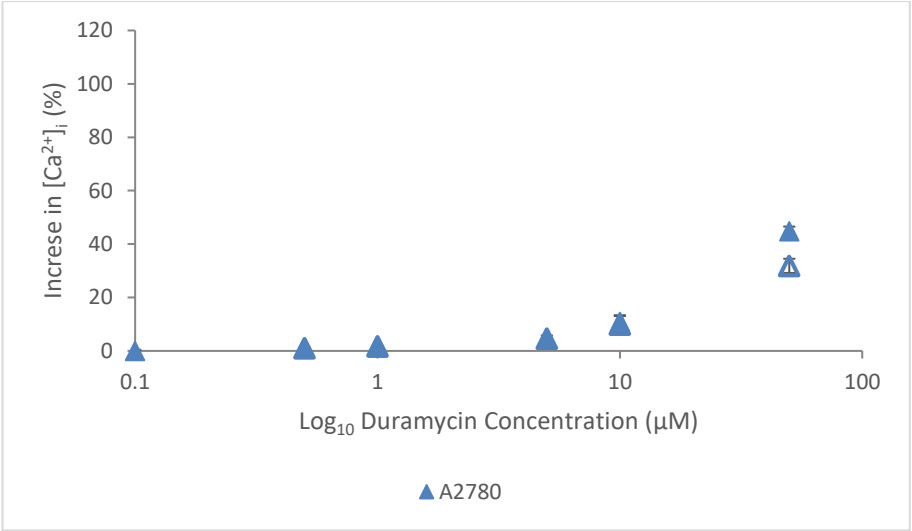

b)

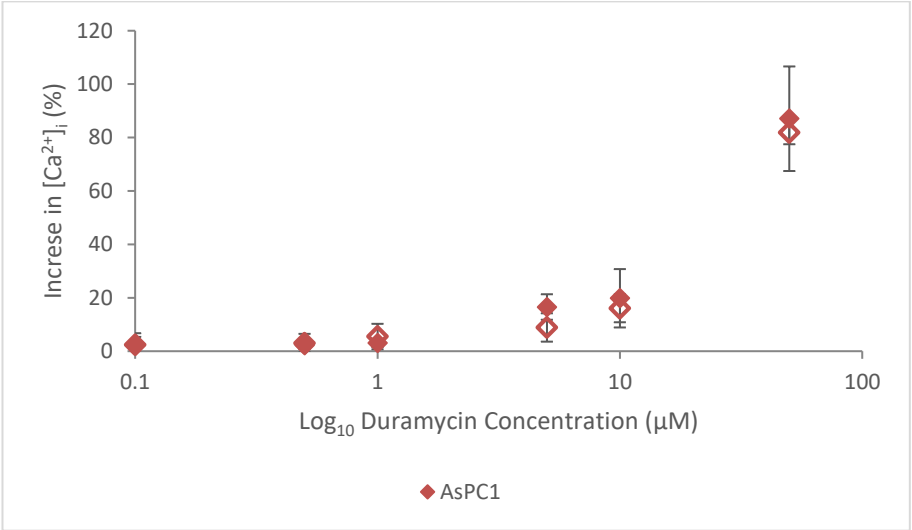

c)

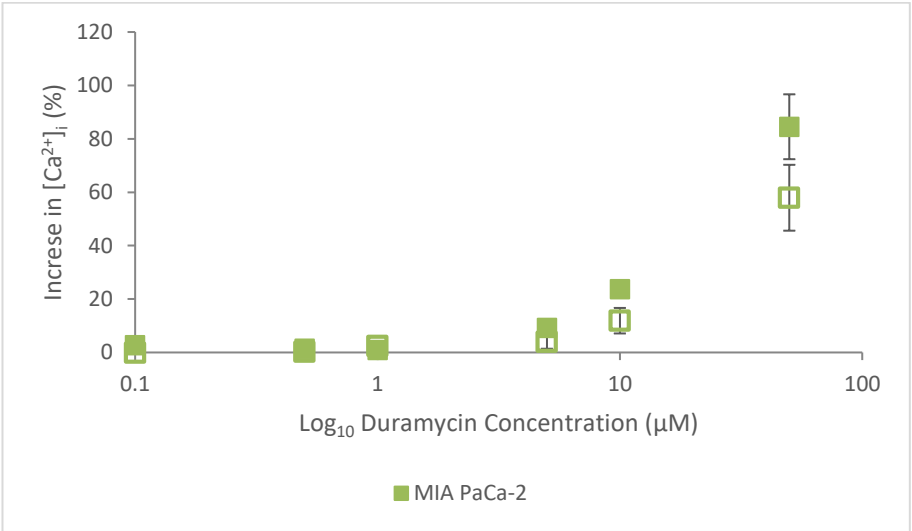

d)

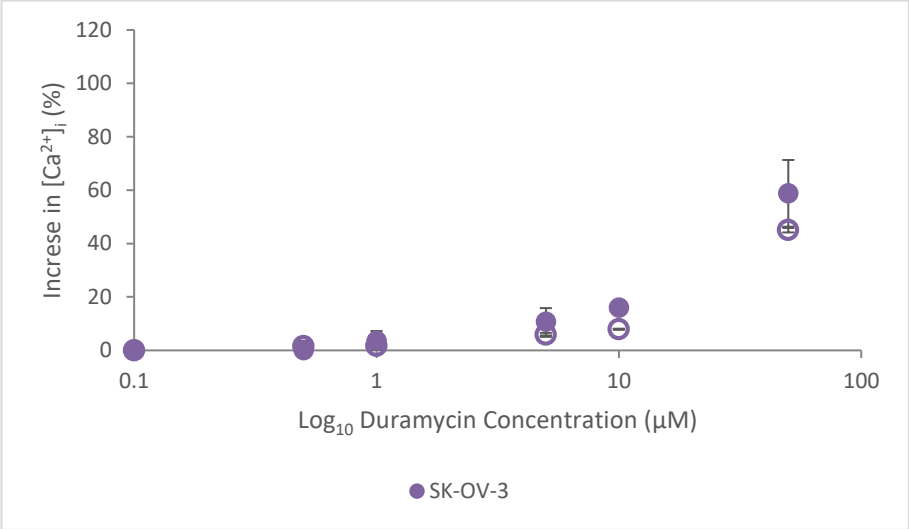

e)

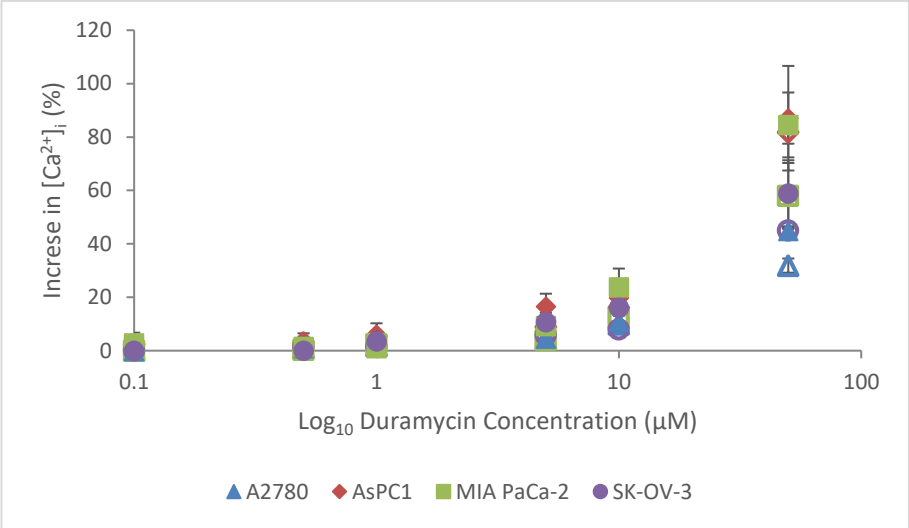

Figure 5.1: Duramycin-induced increase in $[Ca^{2+}]_i$ in cancer cells.

Duramycin increased the $[Ca^{2+}]_i$ in all 4 of the cancer cell lines a) A2780, b) AsPC-1, c) MIA PaCa-2 and d) SK-OV-3 in a duramycin concentration dependent manner. e) The increase in $[Ca^{2+}]_i$ differed between the cell lines with a general trend of the ovarian cancer cell lines having a lower percentage increase than the pancreatic cancer cell lines. There was no significant difference in effect on increased $[Ca^{2+}]_i$ in the presence or absence of Ca_{ext}. No-fill data points represent the absence of Ca_{ext} and filled points the presence. Error bars represent SD of the average value from 2 replicate assays where each duramycin concentration was performed in duplicate.

5.2.1.1 Increase in $[Ca^{2+}]_i$ and necrotic cell death

Duramycin at concentrations >2.5 µM had been observed to induce apoptosis and necrosis in the cancer cell lines A2780, AsPC-1, MIA PaCa-2 and SK-OV-3 (Chapter 3). Necrotic cell death was increased with increased duramycin concentration. Duramycin-induced increase in $[Ca^{2+}]_i$ also occurred in a duramycin concentration dependent manner (section 5.2.1). Therefore, it was hypothesised that the extent of necrosis induced in the cancer cell lines by duramycin treatment may correlate with the amount of increase in $[Ca^{2+}]_i$. The Pearson correlation coefficient (*r*) and the Spearman's rank correlation (ρ) were calculated for these relationships for duramycin concentrations 0-50 µM (table 5.1) and 0-10 µM (table 5.2). The Spearman's rank correlation showed that a strong positive correlation ($\rho > 0.7$) existed between duramycin concentrations 0-50 µM and necrosis in the cancer cell lines A2780, AsPC-1 and SK-OV-3. A lower Spearman's rank correlation value ($\rho = 0.54$) for MIA PaCa-2 may have been a result of the relatively higher resistance to duramycin treatment observed in this cell line (Chapters 3 and 6). The amount of correlation was lower in all 4 cell lines at duramycin concentrations 0-10 µM due to the lesser effect of duramycin on necrosis at these lower concentrations. The Pearson correlation coefficient showed a very strong positive relationship ($r > 0.99$) between duramycin concentrations 0-50 µM and increased $[Ca^{2+}]_i$ in all 4 cancer cell lines (table 5.1) which decreased very slightly for concentrations 0-10 µM (table 5.2).

The extent of duramycin-induced necrotic cell death had a positive correlation with the amount of increase in $[Ca^{2+}]_i$. Pearson correlation coefficient for the cancer cell lines A2780, MIA PaCa-2 and SK-OV-3 showed a strong positive correlation ($r > 0.98$) when treated with 0-50 µM duramycin (table 5.1). AsPC-1 showed a lower value ($r = 0.79$) which may have been influenced by an outlier from the linear regression as shown by the R_2 value for the linear trend line of $R_2 = 0.63$. This was much lower than the other 3 cancer cell lines ($R_2 > 0.97$) (Appendix B, figure B.1). When the highest duramycin concentration of 50 µM was removed from the statistical analyses a weaker correlation was observed (table 5.2). However, a strong positive correlation between necrotic cell death and increased $[Ca^{2+}]_i$ was still seen. The exception to this was AsPC-1 which showed a stronger correlation once 50 µM duramycin was removed. It is possible that this was due to the outlier described above. Spearman's rank correlation, which is less influenced by outlier's than Pearson correlation coefficient, was performed on the data from AsPC-1 which then gave correlation coefficient values of $\rho = 0.79$ for 0-50 µM and $\rho = 0.66$ for 0-10 µM.

Table 5.1: Correlation between duramycin concentration, necrotic cell death and $[Ca^{2+}]_i$ in cancer cell lines treated with 0-50 µM duramycin.

Spearman's Rank Correlation (ρ)				
	A2780	AsPC-1	MIA PaCa-2	SK-OV-3
Duramycin concentration – necrotic cell death	0.714	0.750	0.536	0.793
Pearson Correlation Coefficient (*r*)				
	A2780	AsPC-1	MIA PaCa-2	SK-OV-3
Duramycin concentration – $[Ca^{2+}]_i$ increase	0.999	0.996	0.996	0.993
Necrotic cell death – $[Ca^{2+}]_i$ increase	**0.989**	**0.792**	**0.982**	**0.986**

N.B. Spearman's rank correlation was performed on duramycin concentration-necrotic cell death due to a non-linear relationship. Pearson correlation coefficient was performed on duramycin concentration-$[Ca^{2+}]_i$ increase and necrotic cell death-$[Ca^{2+}]_i$ increase due to linear relationships. The analysis is performed on data for $[Ca^{2+}]_i$ in the presence of Ca_{ext}.

Table 5.2: Correlation between duramycin concentration, necrotic cell death and $[Ca^{2+}]_i$ in cancer cell lines treated with 0-10 µM duramycin.

Spearman's Rank Correlation (ρ)				
	A2780	AsPC-1	MIA PaCa-2	SK-OV-3
Duramycin concentration – necrotic cell death	0.543	0.600	0.257	0.667
Pearson Correlation Coefficient (*r*)				
	A2780	AsPC-1	MIA PaCa-2	SK-OV-3
Duramycin concentration – $[Ca^{2+}]_i$ increase	0.994	0.956	0.983	0.977
Necrotic cell death – $[Ca^{2+}]_i$ increase	**0.802**	**0.841***	**0.912**	**0.927**

N.B. Spearman's rank correlation was performed on duramycin concentration-necrotic cell death due to a non-linear relationship. Pearson correlation coefficient was performed on duramycin concentration-$[Ca^{2+}]_i$ increase and necrotic cell death-$[Ca^{2+}]_i$ increase due to linear relationships. The analysis is performed on data for $[Ca^{2+}]_i$ in the presence of Ca_{ext}.
*An outlier from the linear regression between necrotic cell death and $[Ca^{2+}]_i$ influenced the *r* value for the AsPC-1 data. Spearman's rank correlation performed on this subset of data gave a correlation coefficient of ρ = 0.786 for concentrations 0-50 µM and ρ = 0.657 for concentrations 0-10 µM.

5.2.1.2 Sustained increase of $[Ca^{2+}]_i$ in duramycin treated cancer cells

The calcium ionophore A23187 causes a rapid increase in $[Ca^{2+}]_i$ and also increases cellular permeability to Ca^{2+} through binding to Ca^{2+} and permitting their passage through the hydrophobic section of plasma cell membranes[241]. The rapid peak in $[Ca^{2+}]_i$ fluorescence stimulated by A23187 is detected by spectrofluorometry as an increase in amplitude of the fluorescence of the calcium indicator Fluo-3, AM. For all 4 of the cancer cell lines used in this study the peak in Fluo-3, AM intensity occurred approximately 20 seconds after cells were treated with A23187. The Fluo-3, AM trace then entered a rapid declining phase where the signal returned to basal levels[70, 87]. However, when the cancer cell lines were treated with duramycin this return to the basal level did not occur. Once the peak in Fluo-3, AM intensity had been achieved $[Ca^{2+}]_i$ remained elevated at the same level indicated by a plateau in Fluo-3, AM signal. This occurred when the cancer cell lines were both in the presence and absence of Ca_{ext}. Typical calcium assays were stopped after ~3 minutes so to investigate if the increase in $[Ca^{2+}]_i$ was sustained over time MIA PaCa-2 cells, in the presence of Ca_{ext}, were treated with 50 µM duramycin and analysed over a 60 minute time course. The MIA PaCa-2 cancer cell line was chosen due to its relatively higher resistance to duramycin treatment compared to the other cancer cell lines (Chapter 3). Thus theoretically a higher number of cells would remain viable over the time course.

An increase in $[Ca^{2+}]_i$ in MIA PaCa-2 cells was detected immediately upon addition of duramycin (figure 5.2, green marker) represented by an increase in Fluo-3, AM intensity. At 2 minutes post-duramycin addition maximum Ca^{2+} fluorescence was reached which could be seen as a peak in the frequency of Fluo-3, AM signal. The signal then plateaued (figure 5.2, red marker) and remained constant (within SD) over the remainder of the 60 minute time course. The untreated control cells remained at basal levels of $[Ca^{2+}]_i$ over a 10 minute time course. The A23817 calcium ionophore control produced a rapid increase in $[Ca^{2+}]_i$ followed by a rapid clearance of intracellular Ca^{2+} (figure 5.2) as described above.

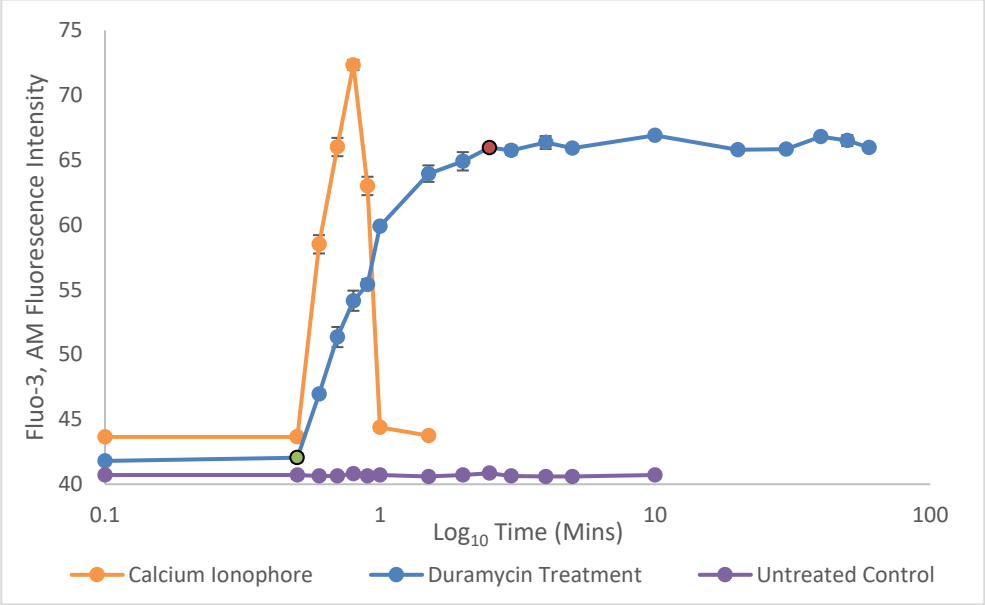

Figure 5.2: Sustained increase in $[Ca^{2+}]_i$ in duramycin treated MIA PaCa-2 cells. Upon addition of 50 µM duramycin (highlighted green marker) $[Ca^{2+}]_i$ was increased in MIA PaCa-2 cells until peak fluorescence was reached at 2 minutes post-duramycin addition (highlighted red marker). Fluo-3, AM signal then remained constant from 2.5-60 minutes suggesting a steady $[Ca^{2+}]_i$. Addition of the A23187 calcium ionophore resulted in a rapid increase in $[Ca^{2+}]_i$ which peaked approximately 20 seconds after addition. A rapid declining phase then followed. The untreated control cells remained at basal levels of $[Ca^{2+}]_i$ over a 10 minute time period. The start time of the assay (0 minutes) is plotted on the Log_{10} Time (Minutes) x-axis as the value 0.1. Error bars represent SD of duplicate assays.

5.2.2 Time taken to reach maximal increase in $[Ca^{2+}]_i$

The time taken to reach maximal increase in $[Ca^{2+}]_i$ was measured as the time interval between the addition of duramycin to the cells and the peak in Fluo-3, AM intensity. The time taken to reach maximal $[Ca^{2+}]_i$ increased in a duramycin concentration dependent relationship for all 4 of the cancer cell lines A2780, AsPC-1, MIA PaCa-2 and SK-OV-3 (figure 5.3). The time to reach maximal $[Ca^{2+}]_i$ was longer in the presence of Ca_{ext} than when in the absence of Ca_{ext} and was cell line and duramycin concentration dependent (>5-50 µM). The effect was most profound at the highest duramycin concentration of 50 µM. When A2780 cells were treated with 50 µM duramycin the time taken to reach maximal $[Ca^{2+}]_i$ in the absence of Ca_{ext} was 63.0 seconds and in the presence 154.0 seconds. The difference was 77.5 and 92.3 seconds, 61.0 and 119.5 seconds and 69.0 and 113.0 seconds for the cancer cell lines AsPC-1, MIA PaCa-2 and SK-OV-3, respectively.

In the absence of Ca_{ext} the time taken to reach maximal $[Ca^{2+}]_i$ was similar for all 4 of the cancer cell lines (figure 5.3e). However in the presence of Ca_{ext} differences between the cell lines emerged when treated with >10 µM duramycin. At 50 µM duramycin in the presence of Ca_{ext} the order of the cell lines to reach maximal $[Ca^{2+}]_i$, from shortest amount of time to longest, was AsPC-1 < SK-OV-3 < MIA PaCa-2 < A2780.

a)

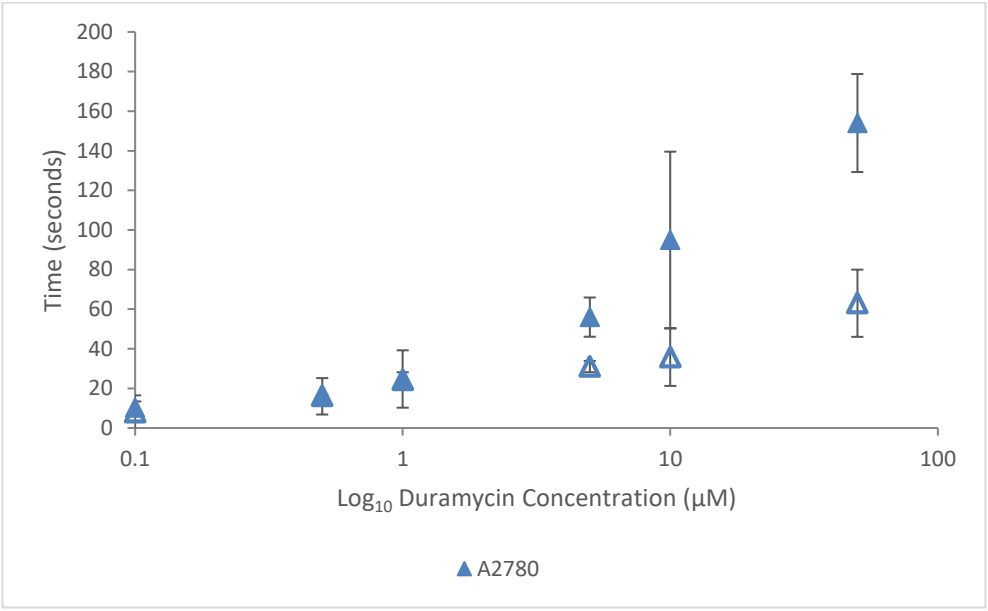
200
180
160
140
120
100
80
60
40
20
0
Time (seconds)
0.1
1
10
100
Log10 Duramycin Concentration (µM)
A2780

b)

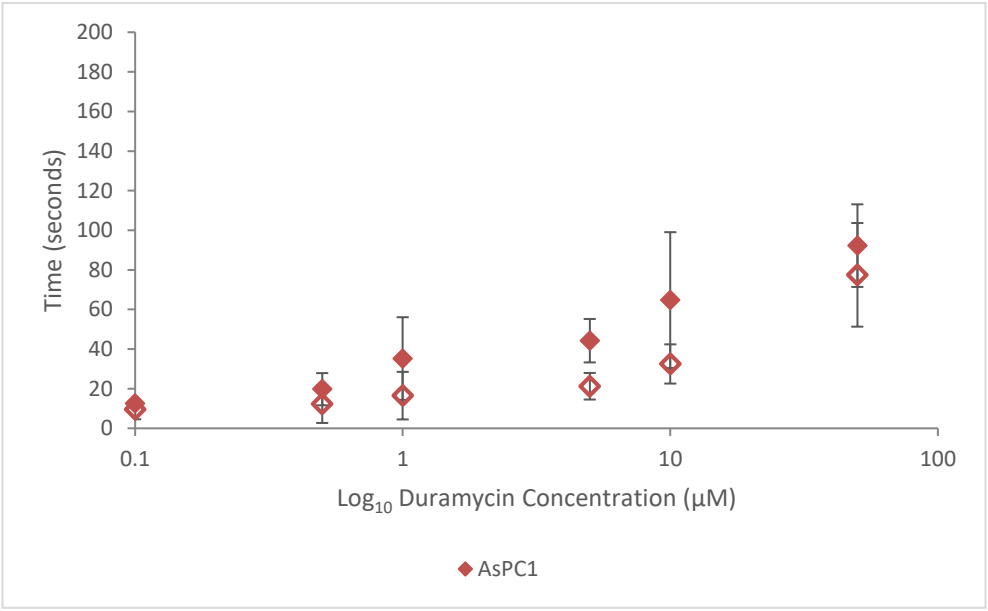
200
180
160
140
120
100
80
60
40
20
0
Time (seconds)
0.1
1
10
100
Log10 Duramycin Concentration (µM)
AsPC1

c)

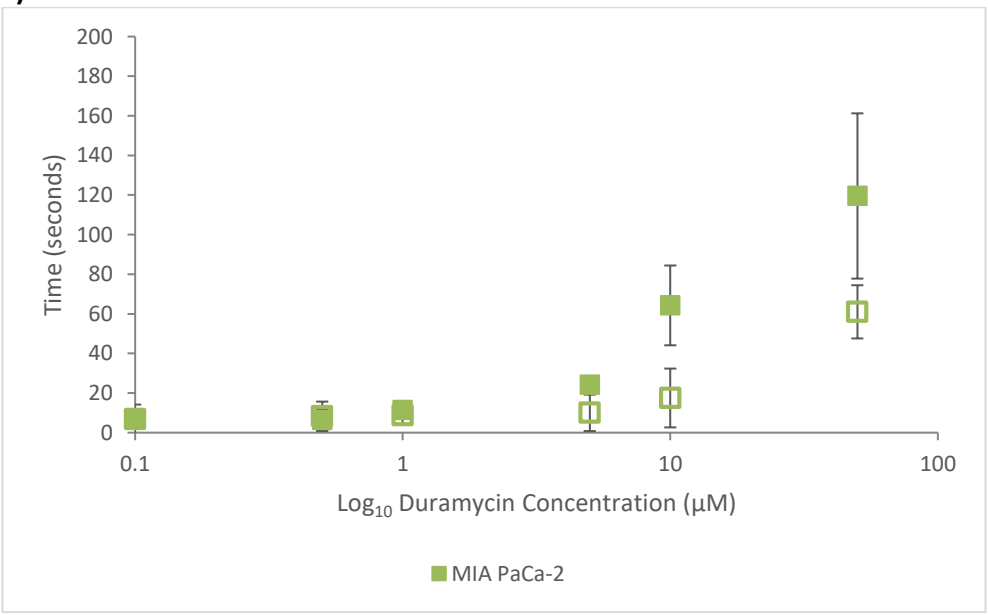
200
180
160
140
120
100
80
60
40
20
0
Time (seconds)
0.1
1
10
100
Log10 Duramycin Concentration (µM)
MIA PaCa-2

d)

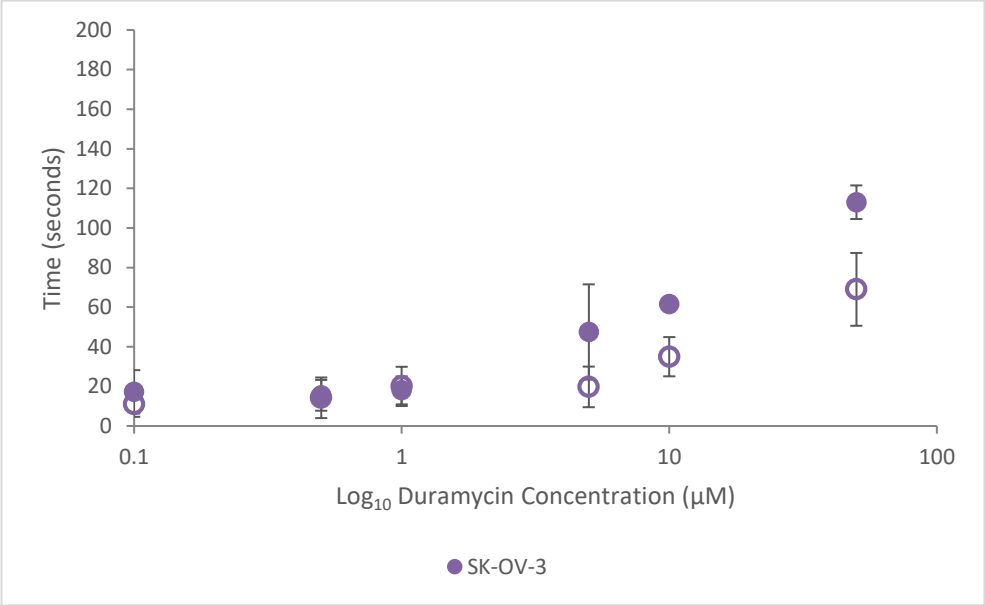

e)

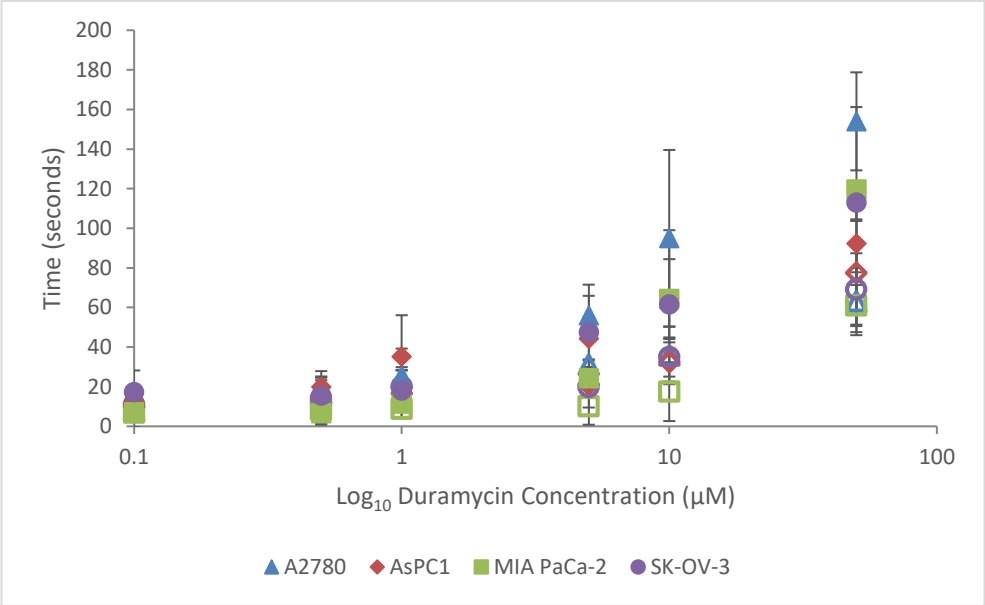

Figure 5.3: Time taken to reach maximal $[Ca^{2+}]_i$ in duramycin treated cancer cells.

The time taken to reach maximal $[Ca^{2+}]_i$ was duramycin concentration dependent in all 4 of the cancer cell lines a) A2780, b) AsPC-1, c) MIA PaCa-2 and d) SK-OV-3. The presence of Ca_{ext} resulted in a longer time to reach peak $[Ca^{2+}]_i$ than the absence of Ca_{ext} at duramycin concentrations >5 µM. e) At 50 µM duramycin treatment the time taken to reach peak $[Ca^{2+}]_i$, in the presence of Ca_{ext}, differed between the cancer cell lines. No-fill data points represent the absence of Ca_{ext} and filled points the presence. Error bars represent SD from 2 replicate assays where each duramycin concentration was performed in duplicate.

5.2.3 Confocal imaging of the effect of duramycin on $[Ca^{2+}]_i$ and the cell membrane of cancer cells

5.2.3.1 Intracellular calcium ion concentration

To further investigate the effect of duramycin on $[Ca^{2+}]_i$ and also to investigate its effect on the release of Ca^{2+} from cancer cells duramycin treated AsPC-1 was imaged using confocal microscopy. AsPC-1 was chosen as it exhibited the highest and quickest increase in $[Ca^{2+}]_i$ (sections 5.2.1 and 5.2.2) and had been shown to be relatively sensitive to duramycin treatment (Chapters 3 and 4). Briefly, cells ($1x10^6$) were suspended in PBS (1 mL) to which sulphinpyrazone (2.6 µl) and Fluo-3, AM (10 µl) were added and then incubated for 30 minutes. After cells were washed, centrifuged and re-suspended the cell number was adjusted to $8x10^5$ cells/ mL warm (37°C) PBS. The cells were then incubated with CellMask™ Orange plasma membrane stain for 10 minutes in the dark at 37°C in a 5% CO_2 atmosphere. Cells were then washed, centrifuged and re-suspended in PBS and cell suspension (250 µl) was transferred to lumox® dishes. Duramycin (50 µM) was added to the AsPC-1 cells and a time series of images were taken at 1 image/ minute over a 30 minute time course. The aim of this experiment was to visualise the increase in $[Ca^{2+}]_i$ in AsPC-1 cells observed in the spectrofluorometry experiments. It was also the aim to visualise any duramycin-induced effect on the cancer cell membranes.

Duramycin treatment of AsPC-1 cells resulted in an increase in $[Ca^{2+}]_i$ and a decrease in cell membrane staining (figure 5.4a). An increase in the fluorescence of the Ca^{2+} indicator Fluo-3, AM was seen 1 minute post-duramycin addition (figure 5.4a) which was most likely due to an increase in $[Ca^{2+}]_i$. The peak in Fluo-3, AM fluorescence in AsPC-1 cells measured by spectrofluorometry occurred at 77.5 seconds (in the absence of Ca_{ext}) post-duramycin addition (section 5.2.2) and so it would seem that these results are in approximate concurrence. From 2 minutes post-duramycin addition there was observed a continual reduction in intracellular Fluo-3, AM fluorescence. A reduction in the fluorescence of the cell membrane dye in some cells 1 minute post-duramycin addition also occurred. This could indicate a loss in cell membrane integrity or the occurrence of cell death. The fluorochromes of the cell membrane and Ca^{2+} dyes were seen to interact upon duramycin addition to give the membrane dye an orange colour (alone the membrane dye appeared red). Cells which retained relatively high membrane dye fluorescence over the time course were likely due to an artefact of fluorochrome interaction as the membranes of these cells were seen to contain areas of yellow colouration (figure 5.4b) indicative of membrane

compartmentalised Fluo-3, AM[243]. Comparison of the cancer cells at the beginning and end of the time course (figure 5.4c) clearly showed the decrease in intensity of intracellular Fluo-3, AM fluorescence and a decrease in cell membrane dye fluorescence in some cells.

a)

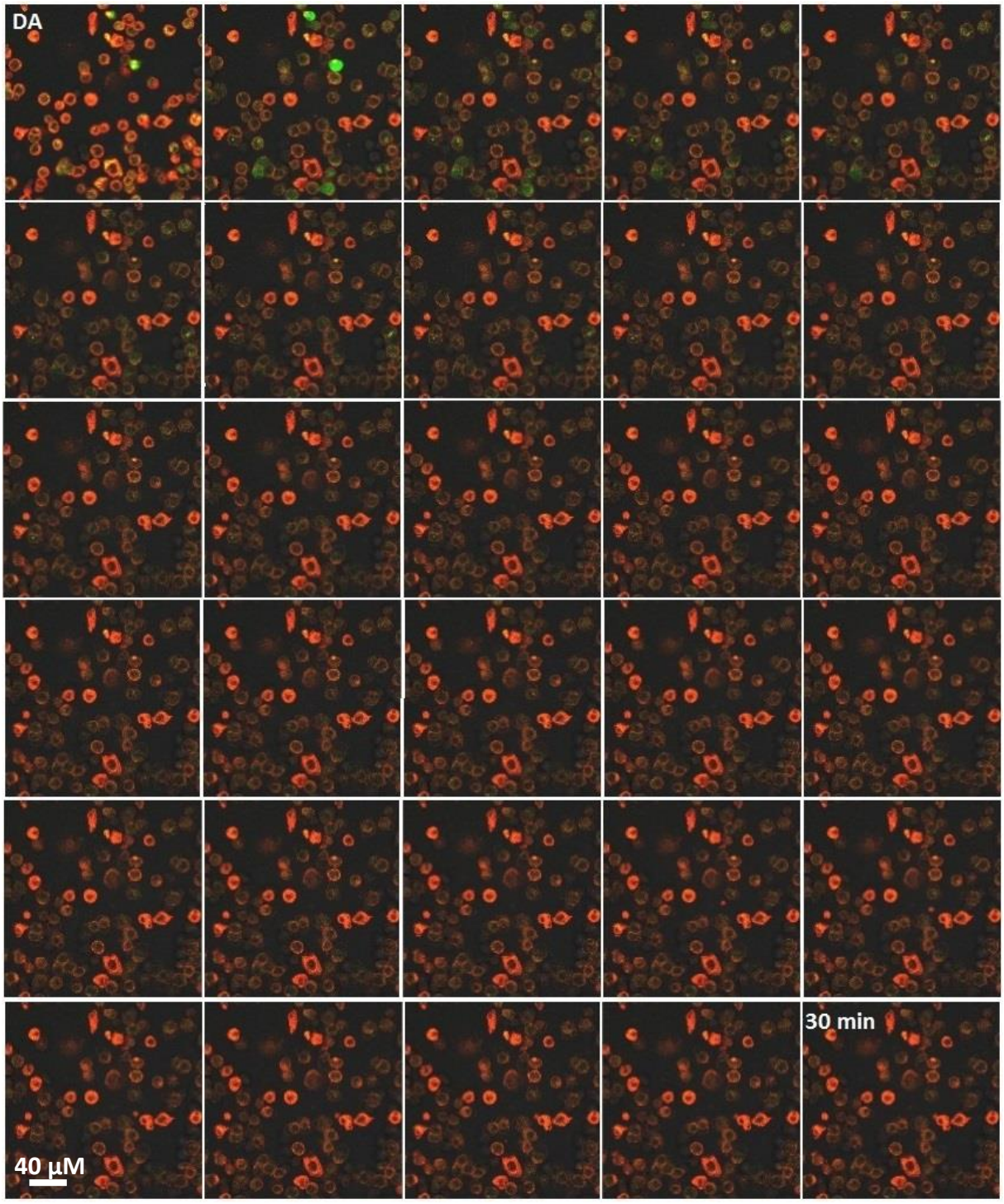

b)

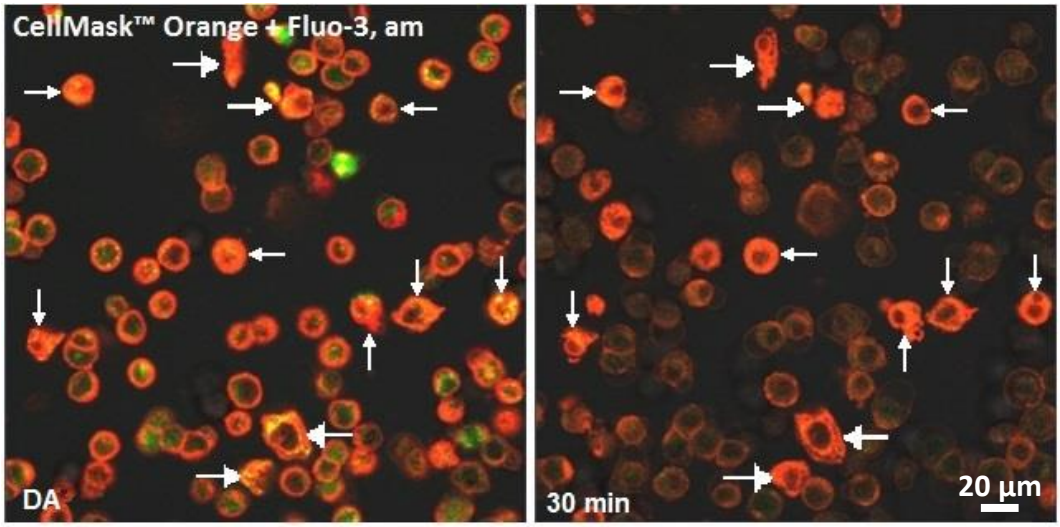

c)

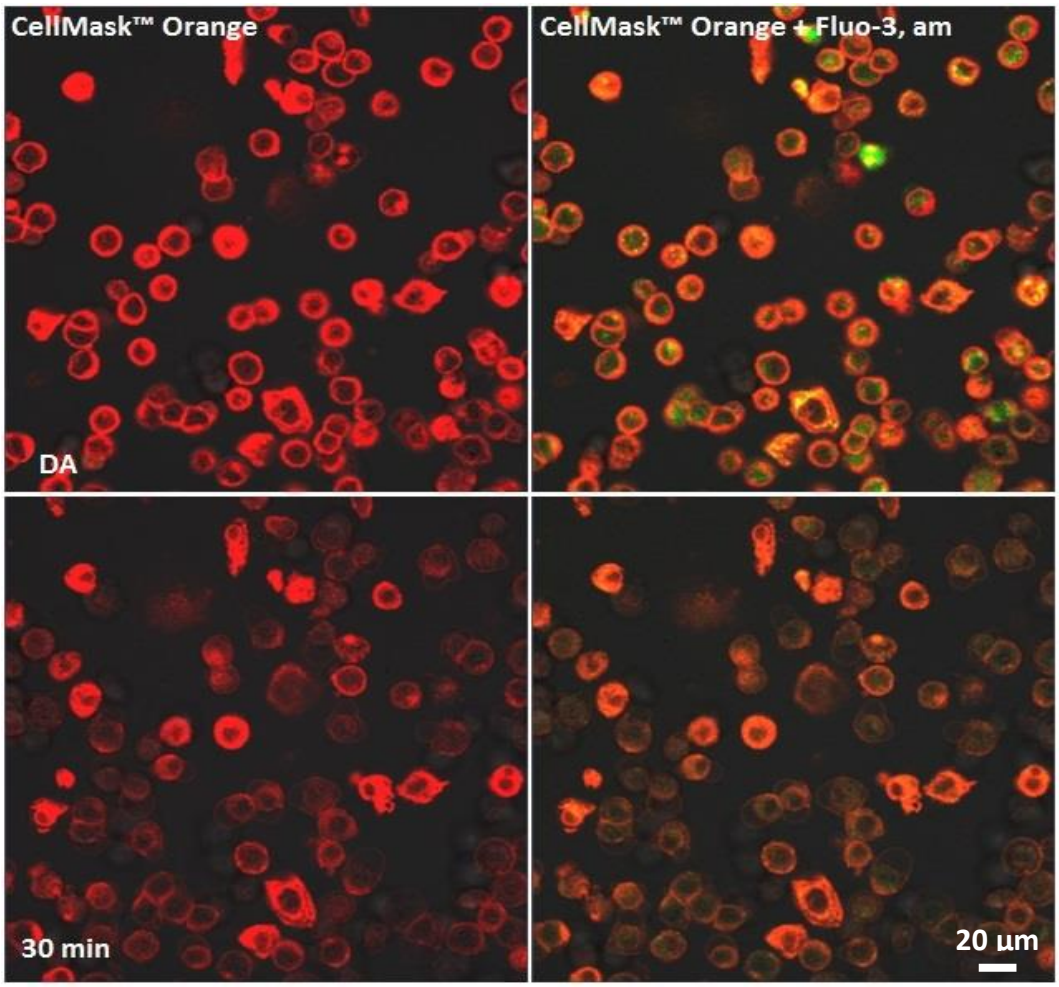

Figure 5.4: Confocal images of duramycin treated AsPC-1 cells.

a) AsPC-1 treated with duramycin (50 µM) was imaged at 1 minute intervals over a 30 minute time course. An increase in Ca^{2+} fluorescence (green, Fluo-3, AM) occurred 1 minute post-duramycin addition after which intracellular fluorescence decreased. Plasma membrane dye: CellMask™ Orange. b) Cells (white arrows) which retained high membrane dye fluorescence at the end of the time course were those that had membrane association of Fluo-3, AM (yellow areas) from the beginning. c) Comparison of duramycin treated AsPC-1 at 0 and 30 minutes showed the reduction in plasma membrane and Ca^{2+} dye fluorescence. DA: time of duramycin addition. 40x magnification.

As a control 2 lumox® dishes that contained untreated AsPC-1 cells, stained for plasma membrane and Ca^{2+}, were imaged at 30 minutes and 60 minutes as time-matched controls to the duramycin treated cells. The control cells were kept under the same conditions as the treated cells. Retention of the Ca^{2+} indicator and the cell membrane dye was seen in both controls (figure 5.5). The cell membrane dye appeared red for most cells unlike in the duramycin treated cells where it appeared orange due to an interaction between the Fluo-3, AM and the plasma membrane dye fluorochromes. Therefore changes to Fluo-3, AM and CellMask™ Orange fluorescence was shown to occur only in duramycin treated cells.

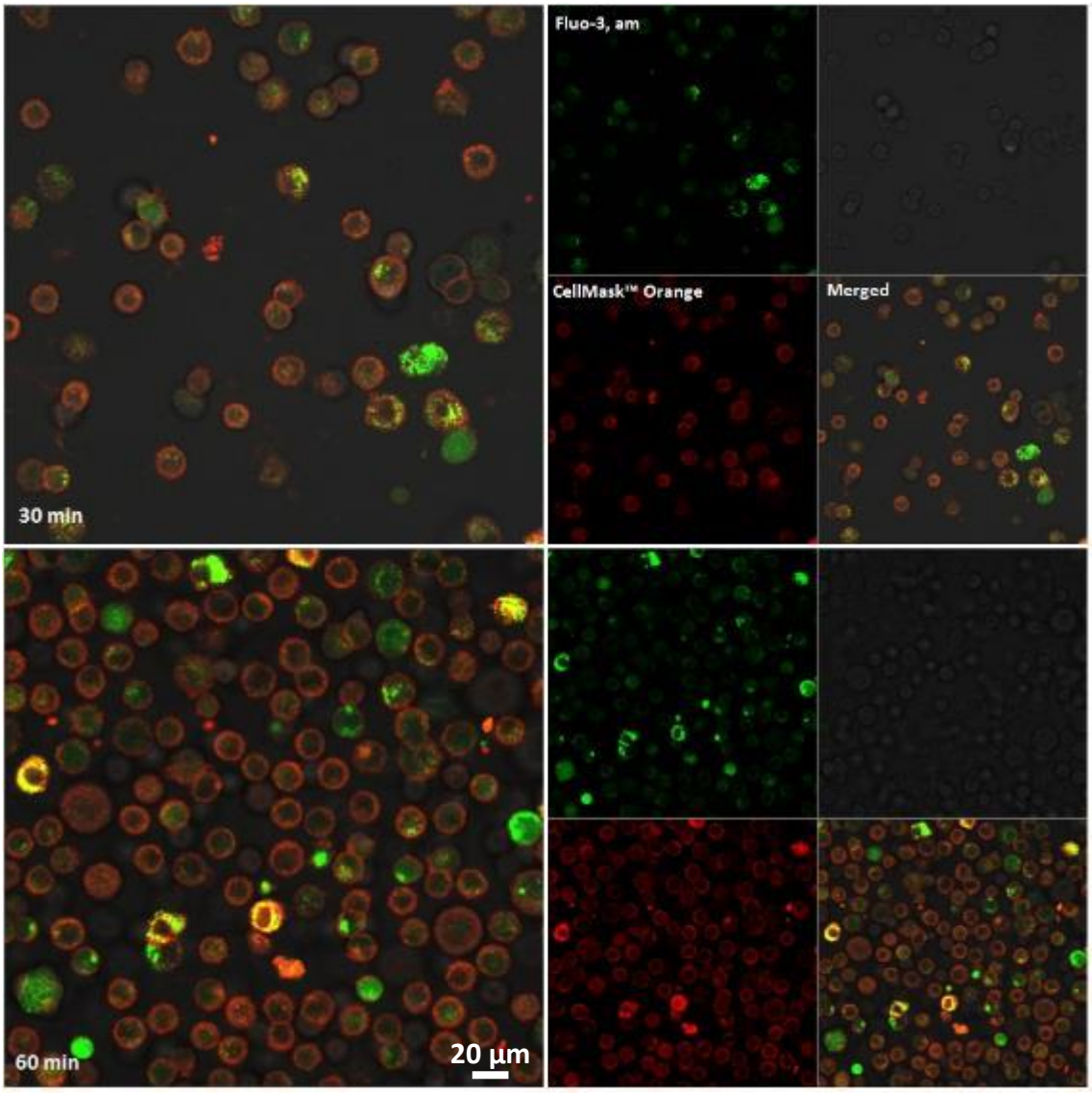

Figure 5.5: Confocal images of untreated control AsPC-1 cells at 30 and 60 minutes.

Untreated control AsPC-1 cells were kept under the same conditions as duramycin treated AsPC-1 cells while they underwent confocal microscopy. Separate dishes of AsPC-1 cells were prepared and imaged at 30 and 60 minutes and retention of plasma membrane stain (red, CellMask™ Orange) and Ca^{2+} indicator (green, Fluo-3, AM) was observed. 40x magnification.

5.2.3.2 Uptake of propidium iodide

Propidium iodide (PI) is commonly used to identify cells that are undergoing late apoptosis or necrosis as its movement into the cell and subsequent staining of the cell nucleus can be an indication of the loss of cell membrane integrity that occurs during cell death. Therefore AsPC-1 were imaged by confocal microscopy for PI uptake following duramycin treatment to investigate its effect on cell membranes. Briefly, cells ($2x10^7$) were suspended in Diluent C (500 µl) to which further Diluent C containing 4 µM CellVue® Jade dye (500 µl) was added. The cell suspension was incubated in the dark at room temperature for 3 minutes with periodic agitation. The cells were then washed, centrifuged and re-suspended in PBS and then cells ($2x10^5$) in PBS (250 µl) were incubated with PI (12.5 µl) in the dark for 15 minutes. The cells were transferred to lumox® dishes and 50 µM duramycin was added. A time series of images was taken at 1 image/ minute over a 20 minute time course.

Duramycin treatment of AsPC-1 resulted in an increase in cell nucleus staining and a decrease in cell membrane staining (figure 5.6). There was a gradual increase in the number of AsPC-1 cells with cell nucleus staining over the 20 minute time course from 1 minute post-duramycin addition onwards. The addition of duramycin therefore resulted in the uptake of PI from the PBS-cell suspension into the AsPC-1 cells. The untreated control cells saw an increase of 1 AsPC-1 cell with cell nucleus staining. A decrease in the number of AsPC-1 cells stained with the plasma membrane dye CellVue® Jade occurred 1 minute post-duramycin addition (figure 5.6a). A reduction in the number of cells that retained the cell membrane dye continued over the remainder of the 20 minute time course. The untreated control AsPC-1 cells also saw a decrease in the number of cells that retained cell membrane stain although to a lesser degree than the duramycin treated AsPC-1 cells. Therefore some loss in cell membrane stain may have been due to a destabilisation of the dye compound. An AsPC-1 cell was observed to increase in size one minute post-duramycin addition, which may indicate cell swelling, there was then changes to the appearance of the cell membrane and the cell became less circular, followed by a shrinking of the cell and eventual loss in membrane stain (indicated by arrows on figure 5.6a). This may have been due to the cell undergoing a form of cell death, likely necrosis. A comparison of the AsPC-1 cells pre-duramycin treatment (0 min) and at the end of the time course (20 min) is presented in figure 5.6b.

a)

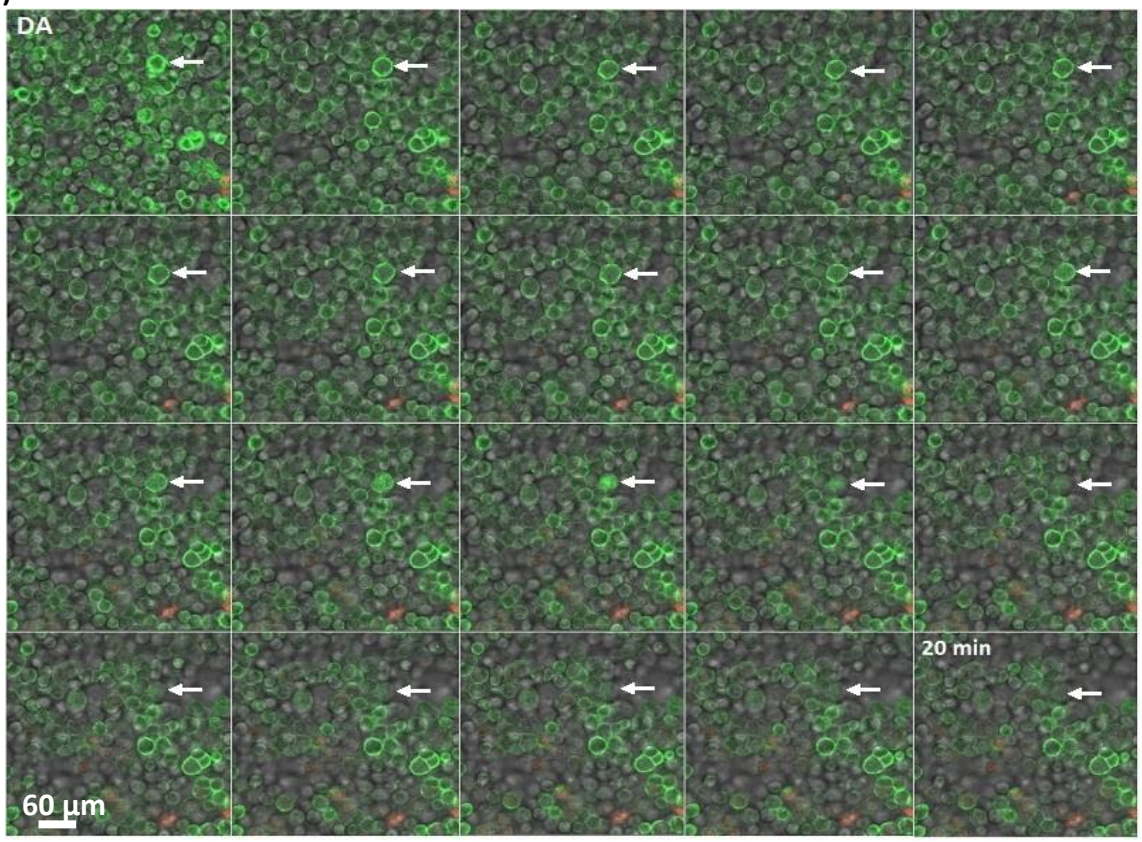

b)

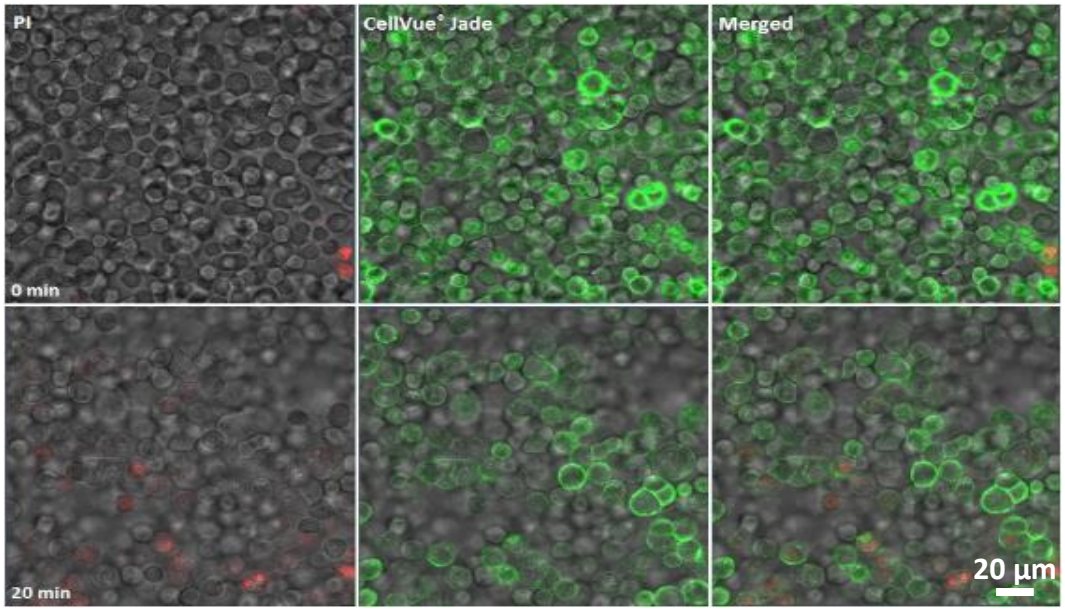

Figure 5.6: Confocal images of duramycin treated AsPC-1 cells over a 20 minute time course.

a) AsPC-1, treated with 50 µM duramycin, were imaged at 1 minute intervals for effect on cell membrane (green, CellVue® Jade) and cell nucleus staining (red, PI). There was an increase in cell numbers with cell nucleus staining over the 20 minutes indicating an uptake of PI from the buffer solution. A reduction in the number of cells stained with the cell membrane dye occurred from 1 min post-duramycin addition onward. Arrows indicate a cell possibly undergoing necrotic cell death. DA: point of duramycin addition. b) Comparison of duramycin treated AsPC-1 cells at 0 and 20 minutes. 40x magnification.

5.3 Discussion

Duramycin has been reported in the literature to have an effect on a variety of ion channels in a number of different cell types. Duramycin inhibited the function of a proton translocating ATPase pump and its linked Cl^- transporter in clathrin-coated vesicles[85]. At low ratios of duramycin to vesicles the proton pump activity was reduced by a duramycin-mediated block in Cl^- uptake. At higher ratios of duramycin to vesicles duramycin was able to directly inhibit the proton pump itself[85]. Duramycin inhibited ATPase-dependent uptake of Ca^{2+} in SR vesicles and impeded the action of a proton pump in the vesicles membranes[70]. The action of duramycin on ion channels is widely regarded to be a result of duramycin-induced cell membrane disruption rather than a selective action on specific ion channels. The efflux of Ca^{2+} and Cl^- in epithelial cells from airway epithelium of non-CF and CF origin was measured following addition of duramycin[91]. Duramycin (1-3 µM) induced Ca^{2+} release from human CF bronchial epithelial (CFBE) cells and their normal counterparts at 3 µM. There was an interesting effect of duramycin concentration on Cl^- efflux in CFBE where 1 µM duramycin induced Cl^- release whereas lower (0.3 µM) and higher (2-10 µM) concentrations did not. Higher concentrations (>100 µM) inhibited Cl^- efflux which was suggested to be due to duramycin-induced cell membrane destruction. It was concluded that disruption to the plasma membranes effected CaCC channels which caused membrane permeability and an non-selective ion efflux[91]. The non-selective pore formation theory is supported by a number of other studies. Duramycin acted on a variety of ion channels in a range of cell types that originated from different species[90]. Concentrations 0.3-3.3 µM reduced the amplitude of all investigated waves (from voltage-gated hERG potassium, sodium and calcium channels) in all of the cell types. Concentrations >3.3 µM were found to induce leak currents that were consistent with pore formation[90]. Duramycin at micromolar concentrations induced ion conductance in colonic epithelial cells[88] as a result of the formation of non-selective pores in both artificial black lipid membranes and biological membranes[89]. It was concluded that the coalescence of small pores into larger ones was the cause of the detectable ion conductance and this led to an ultimate disruption to the cell membrane. Relatively low concentrations of duramycin (<5 µM) increased the permeability of the inner membrane of heart mitochondria to monovalent cations and at higher concentrations induced a more general permeability[178]. At higher duramycin concentrations the effect could not be inhibited by blocking the mitochondria's ATP/ADP transporter, as was seen at the lower concentrations, which suggested that a more destructive effect on the mitochondrial membranes had occurred.

To the best of the author's knowledge no report could be found in the literature of the effect that duramycin has on the intracellular ion concentration or influx/efflux of ions in tumour cells. Though, duramycin was shown to inhibit the Na^+-K^+ ATPase and an Mg^{2+}-dependent ATPase in Ehrlich ascites tumour cells and also permeabilise these cells to Pi and nucleotides[179]. As was shown in this study necrotic cell death can occur in cancer cell lines when treated with duramycin concentrations ≥10 µM (Chapter 3). Therefore the effect of duramycin on the 4 cancer cell lines A2780, AsPC-1, MIA PaCa-2 and SK-OV-3 was investigated with focus on $[Ca^{2+}]_i$ as Ca^{2+} overload can be an initiator of necrosis. Duramycin caused immediate increase in $[Ca^{2+}]_i$ in all 4 of the cancer cell lines in a duramycin concentration dependent manner. Concentrations <5 µM had very little effect on $[Ca^{2+}]_i$ which is in concurrence with previous results reported in this study (Chapters 3 and 4). At 50 µM a difference in the amount of increase in $[Ca^{2+}]_i$ was observed between the cell lines with a general trend that the ovarian cancer cell lines (A2780 and SK-OV-3) had a lower increase in $[Ca^{2+}]_i$ than the pancreatic cancer cell lines (AsPC-1 and MIA PaCa-2). The ovarian cancer cell lines A2780 and SK-OV-3 have been reported to have an upregulated expression of the mitochondrial Ca^{2+} transporter regulator MICU1[239]. This resulted in an enhanced ability of their mitochondria to buffer cytosolic Ca^{2+} compared to normal ovarian surface epithelium cells. This could explain why A2780 and SK-OV-3 had a lower increase in $[Ca^{2+}]_i$ than the pancreatic cancer cell lines as the mitochondria may have buffered some of the Ca^{2+}. However, loss of heterozygosity of the gene for MICU1 has also been shown to occur in human pancreatic samples[242] so it is possible that it is also expressed in AsPC-1 and MIA PaCa-2. This observation is perhaps unimportant as the difference between the cell lines was not found to be statistically significant ($p = 0.16$) (Student's T Test, significance $p < 0.05$). The presence of Ca_{ext} had no statistically significant effect on the percentage increase in $[Ca^{2+}]_i$ compared to the absence of Ca_{ext} for all 4 cancer cell lines ($p > 0.05$). However, there was a trend of a higher increase in $[Ca^{2+}]_i$ in A2780, MIA PaCa-2 and SK-OV-3 in the presence of Ca_{ext} when treated with duramycin ≥10 µM. Inhibition of Ca^{2+} entry in MIA PaCa-2 cells was shown to result in a smaller peak in $[Ca^{2+}]_i$ compared to when Ca^{2+} entry was allowed[117]. Thus a larger increase in $[Ca^{2+}]_i$ observed in this study when cells were in the presence of Ca_{ext} possibly indicated that Ca^{2+} influxed into the cancer cells upon duramycin treatment. The time taken to reach the maximal increase in $[Ca^{2+}]_i$ was increased in a duramycin concentration dependent manner in all 4 cancer cell lines. The presence of Ca_{ext}, which provided a Ca^{2+} gradient similar to *in vivo* cellular conditions, resulted in a longer time to reach the maximal increase in $[Ca^{2+}]_i$ (at concentrations ≥5 µM)

compared to the absent Ca_{ext} condition. The extent in the lengthened time between the absent and present Ca_{ext} conditions differed between the cell lines where the order, from smallest difference to largest difference, was AsPC-1, SK-OV-3, MIA PaCa-2 and A2780. This corresponded to the order in which it took to reach maximal $[Ca^{2+}]_i$, from shortest time to longest time. This also corresponded to the extent of which the cancer cell lines underwent a larger increase in $[Ca^{2+}]_i$ in the presence of Ca_{ext} (as discussed above). Therefore, the longer time to reach maximal increase in $[Ca^{2+}]_i$ was due to the higher rise in intracellular Ca^{2+} concentration. Again, this would suggest that the presence of Ca_{ext} resulted in an influx of Ca^{2+} into the cancer cell lines.

When the cancer cell lines A2780, AsPC-1, MIA PaCa-2 and SK-OV-3 were treated with the calcium ionophore control A23187 a rapid increase in $[Ca^{2+}]_i$ occurred followed by a declining phase, which is an indicator of intracellular Ca^{2+} clearance. A study showed that the return to basal levels of Ca^{2+} signal in MIA PaCa-2 cells corresponded to a recovery to low resting $[Ca^{2+}]_i$[117]. In this study, duramycin treatment did not elicit the same response as A23187, and a plateau in the Ca^{2+} fluorescence signal was observed for all 4 cell lines in both Ca_{ext} conditions. When investigated further, using MIA PaCa-2, the plateau was found to be maintained over a 60 minute time course. This indicated that duramycin caused a sustained increase in Fluo-3, AM fluorescence which potentially signified a prolonged increase in $[Ca^{2+}]_i$. Duramycin increased the $[Ca^{2+}]_i$ of epithelium cells in a concentration dependent manner (0.1-5 µM), detected by fluorescence of the calcium indicator Indo-1, AM and spectrofluorometry[87]. Indo-1, AM fluorescence was shown to plateau which was suggested to be a result of a sustained increase in $[Ca^{2+}]_i$ due to passive permeability of Ca^{2+}. Additionally, duramycin has been shown to have a sustained effect on the increased short circuit current, due to Cl^- secretion, in canine tracheal epithelium over a 75 minute period[86].

Confocal microscopy was also used to assess the effect of duramycin on the $[Ca^{2+}]_i$ of cancer cells. An increase in the fluorescence of Fluo-3, AM in AsPC-1 cells was imaged 1 minute post-duramycin addition. The fluorescence of Fluo-3, AM was then decreased 2 minutes post-duramycin addition, this decreased further until approximately 4 minutes post-duramycin addition after which there was no substantial change over the 30 minute time course. There was also a reduction in the fluorescence of the plasma membrane dye CellMask™ Orange which suggested that there was a loss in membrane integrity possibly due to duramycin-induced disruption to the cell membranes. Previous results had shown

that duramycin at this concentration (50 µM) over a 30 minute period would result in necrosis of approximately 60% of AsPC-1 cells (section 3.2.2). Thus a loss in cell membrane dye may have been because these cells were currently undergoing or had undergone cell death. Additionally, confocal microscopy experiments saw a reduction in the number of AsPC-1 cells retaining the cell membrane dye CellVue® Jade over a 20 minute time course. CellVue® Jade works through insertion into plasma membranes and thus disruption of the membrane by duramycin could potentially have displaced the dye. An increase in cells with PI cell nucleus staining was also observed over the 20 minutes, an indicator of a reduction in cell viability and of compromised cell membrane integrity.

It was observed that those AsPC-1 cells which remained relatively high in fluorescence of CellMask™ Orange cell membrane dye at the end of the 30 minute time course suffered significant interaction between the Fluo-3, AM and plasma membrane dye fluorophores at the beginning of the time course, this was visualised as areas of orange/yellow[243]. This interaction between the fluorophores was seen in the plasma membrane of all AsPC-1 cells upon addition of duramycin, something not seen with the untreated control cells in which the membrane dye appeared red (though was yellow in some areas of the plasma membrane indicating fluorophore interaction). Fluo-3, AM can become compartmentalised within the plasma membrane in membrane vacuoles after 1 hour of introduction to cells (dependent on cell type) or immediately if the AM ester is not completely esterified making it membrane impermeable[243, 244]. This artefact of membrane associated Fluo-3, AM likely occurred in those untreated cells that had areas of orange/yellow within the membrane. However the orange appearance of the cell membranes treated with duramycin, compared with the red of the control cells, showed that Fluo-3, AM became associated with the cell membrane upon duramycin addition. It is likely that this was due to the movement of Ca^{2+} from the cytosol towards the cell membrane, whether Fluo-3, AM bound to Ca^{2+} was then membrane associated (i.e. trapped within or at the plasma membrane) or whether it was Fluo-3, AM alone (unbound to Ca^{2+}) could not be determined from this study. Though, Fluo-3, AM has a relatively high affinity for Ca^{2+} and does not readily dissociate with a dissociation constant (K_d) for Ca^{2+} of 325 nM[244]. The membrane association of the Ca^{2+} dye could explain the apparent reduction in intracellular Fluo-3, AM fluorescence that occurred in the AsPC-1 cells during confocal microscopy which was contradictory to the results from the spectrofluorometry experiments in which Fluo-3, AM fluorescence was shown to remain elevated. It was possible that the detection of sustained Fluo-3, AM signal in spectrofluorometry was a result of Fluo-3, AM associated with plasma membranes.

However, faint intracellular Fluo-3, AM fluorescence was still observed within some of the AsPC-1 cells on confocal microscopy which may have also been detected by spectrofluorometry. It was improbable that an interaction between duramycin and Fluo-3, AM accounted for the membrane association as the slightly larger increase in $[Ca^{2+}]_i$ in the presence of Ca_{ext} could not have occurred had Fluo-3, AM been complexed to duramycin and if there was no free Fluo-3, AM in the cytosol. Fluo-3, AM fluorescence in microscopy can be due to a reduction in concentration due to leakage out of cells and so its fluorescence intensity decreases regardless of Ca^{2+} concentration[245]. However the interaction of the Fluo-3, AM and plasma membrane fluorophores (orange appearance of cell membranes) in the duramycin treated cells and the staining of Ca^{2+} in the cytosol up to 60 minutes in the untreated control cells would suggest that Fluo-3, AM had not leaked from the cells and had become, at least in part, membrane associated and remained within intact cells, respectively.

In summary, duramycin (>5 μM) treatment of cancer cell lines resulted in an immediate increase in $[Ca^{2+}]_i$ which showed a slight trend of rising higher when in the presence of Ca_{ext}. A longer time was taken to reach the maximal increase at higher duramycin concentrations due to a larger increase in $[Ca^{2+}]_i$ and was also longer in the presence of Ca_{ext} most probably due to an influx of Ca^{2+} into the cells. Unlike the A23187 control duramycin treatment resulted in a sustained high fluorescence of the Ca^{2+} indicator Fluo-3, AM which was most likely due to plasma membrane associated Fluo-3, AM as visualised by confocal microscopy. From these results two possible explanations for duramycin's mechanism of action on $[Ca^{2+}]_i$ emerged. Both of which suggested that the initial rise in $[Ca^{2+}]_i$ caused by duramycin treatment was due to a stimulation of Ca^{2+} release into the cytosol from internal stores such as the ER and the mitochondria. The release of Ca^{2+} through IP_3R channels or ryanodine receptors (RyRs) from the ER has been imaged as 'calcium sparks' by Ca^{2+} indicators and fluorescence microscopy[100, 246]. Calcium sparks are a result of locally released Ca^{2+} from the ER into the cytoplasm and, while the term has various meanings, it can be defined as 'the resultant local change in $[Ca^{2+}]_i$ in the presence of a Ca^{2+} indicator'[246]. The observed increase in Fluo-3, AM fluorescence in confocal microscopy upon addition of duramycin could therefore have been due to the release of Ca^{2+} from the ER. Regenerative Ca^{2+} release from channels such as IP_3R in the ER can be achieved when clusters of the channels release enough Ca^{2+} to propagate release from neighbouring IP_3R, this results in a 'calcium wave', a form of calcium-induced calcium release[100, 246]. A slow calcium signal in myotubes, observed as a rise in Fluo-3, AM fluorescence on fluorescence microscopy, was

found to be due to this form of Ca^{2+} release through IP_3R[101]. The increase in $[Ca^{2+}]_i$ upon duramycin treatment was also likely to have been due to an influx of Ca^{2+}, this is supported by the trend of a higher increase and a longer time to reach this increase in the presence of Ca_{ext}. It is possible that the concentration gradient (~20,000 fold gradient between intracellular and extracellular Ca^{2+}) produced by the Ca_{ext} in the buffer solution caused an influx of Ca^{2+} into the cells. It is also possible that duramycin had made the cancer cell membranes permeable to Ca^{2+} through the formation of pores. An increase in $[Ca^{2+}]_i$ in airway epithelial cells was attributed, at low duramycin concentrations, to release from internal stores and at higher concentrations to both release from internal stores and extracellular calcium influx[87]. A gradual rising phase in $[Ca^{2+}]_i$, as detected by the calcium indicator Indo-1, AM using photometry, in treated rat pituitary cells was attributed to open VGCC that allowed the influx of Ca^{2+} [247]. Store operated Ca^{2+} influx is a Ca^{2+} influx pathway in which a depletion in Ca^{2+} stored in the ER and loss of Ca^{2+} through PMCA results in the activation of Ca^{2+} influx. The stimulation of a loss in Ca^{2+} from the ER and successive addition of Ca_{ext} to MIA PaCa-2 cells was shown to result in a store operated influx of Ca^{2+} [117]. A2780 has been shown to express the principle components of store operated Ca^{2+} influx, the endoplasmic Ca^{2+} depletion sensor STIM1 and the pore forming calcium channel sub-unit ORAI1[106]. Thus it is possible that store operated Ca^{2+} influx was stimulated in the duramycin treated cancer cell lines due to the loss of Ca^{2+} from internal stores.

It is at this point that the two possible explanations for duramycin's mechanism of action on $[Ca^{2+}]_i$ diverge. This is due to the observation that in confocal microscopy there was an interaction between Fluo-3, AM and the plasma membrane dye fluorophores in duramycin treated AsPC-1 cells. Membrane association of Fluo-3, AM was suggested to account for the sustained fluorescence signal in the spectrofluorometry experiments. The first possible explanation arises from the theory that Fluo-3, AM remained bound to Ca^{2+} which was probable due to their relatively high affinity. After the rise in $[Ca^{2+}]_i$ Ca^{2+} would locate at the plasma cell membrane to be removed from the cell through Ca^{2+} homeostasis. Yet it is possible that the efflux of Ca^{2+} was inhibited in duramycin treated cells. Fluo-3, AM in complex with Ca^{2+} was shown to be able to efflux from the cancer cell lines in the A23187 treated control cells which experienced a clearance of Ca^{2+} shown by the reduction in Fluo-3, AM fluorescence. Thus the effect of membrane Fluo-3, AM association was duramycin treatment related. The membrane association of Fluo-3, AM and blocking of Ca^{2+} efflux by duramycin may have been due to a disruption of ATP-dependent plasma membrane Ca^{2+} pumps. Such disruption by duramycin has been reported for many different ATP-

dependent pumps in a variety of cell lines[70, 84, 85, 178, 179]. Duramycin has been shown to inhibit ATPase activity in plasma membranes by inhibiting the phosphorylation of ATP and inducing hydrolysis of ATP[84]. The major pathway for Ca^{2+} efflux in MIA PaCa-2 is the PMCA pump[100]. Removal of glycolytic ATP in MIA PaCa-2 was shown to result in PMCA inhibition which subsequently led to Ca^{2+} overload within minutes and cell death within 3-6 hours[117]. Thus duramycin may have inhibited PMCA-mediated Ca^{2+} efflux. Additionally, if Ca^{2+} clearance was blocked in the duramycin treated cells the prolonged increase in $[Ca^{2+}]_i$ may have resulted in protease cleavage of NCX exchangers in the plasma membrane[240]. As duramycin was bound to the cancer cell membranes and the exact position of the Fluo-3, AM could not be discerned it was possible that duramycin itself was a scavenger of the Ca^{2+} bound to Fluo-3, AM. Duramycin has the ability to disrupt the coagulation of cancer cell lines and prolong pro-thrombin clotting time (Appendix C, figure C.1)[58]. One requirement of coagulation and the pro-thrombin clotting time assay is Ca^{2+} [248] and thus it could be possible that Ca^{2+} scavenging by duramycin aids in its anti-coagulant action, though it is likely that the blocking of cell surface PE is the major route[58]. Duramycin disruption of Ca^{2+} efflux and the impairment of intracellular Ca^{2+} clearance is one explanation for duramycin's effect on $[Ca^{2+}]_i$ in cancer cell lines. The second possible explanation arises from the theory that Fluo-3, AM had dissociated from Ca^{2+}. If this were the case then unbound Fluo-3, AM could have been detected at the cell membrane though Ca^{2+} had been removed from the cell. The efflux of Ca^{2+} from the cancer cells may have occurred by transport through selective Ca^{2+} channels or through the formation of non-selective pores in the cell membranes, as has been documented for duramycin in the literature[88-91]. Relatively large conductance fluctuations for Na^+, Cl^-, Mg^{2+} and Ca^{2+} occurred in PE containing artificial membranes after duramycin treatment (>2 μM)[89]. Pores in the plasma membrane were concluded to be responsible for the leak currents observed for K^+, Na^+ and Ca^{2+} from duramycin treated HEK293, cardiomyocytes, neuroblastoma cells and skeletal muscle cells[90]. In this study, in the confocal experiments PI was shown to enter AsPC-1 cells after duramycin treatment which could have been the result of pores in the cell membranes. Yet, it is possible cell nuclei became stained due to membrane disruption during necrotic cell death as approximately 60% of the AsPC-1 cells would have been expected to be necrotic. Duramycin-induced formation of non-selective pores in the plasma membrane is the second explanation for duramycin's effect on $[Ca^{2+}]_i$ in cancer cell lines.

The mechanism of duramycin-induced cell death is yet to be fully elucidated though it is possible that the type of cell death that occurs is dependent on duramycin concentration.

In this study it has been shown that relatively high concentrations of duramycin (>500 µM) induced almost complete necrosis in cancer cell lines after 30 minutes treatment (Chapter 3). Relatively low concentrations (<5 µM) did not have an effect on apoptotic or necrotic cell death, cell proliferation or $[Ca^{2+}]_i$ (Chapters 3, 4 and 5). Whereas >5 µM duramycin treatment for >24 hours was shown to induce apoptosis in all cancer cell lines (Chapter 4). Depletion of Ca^{2+} from ER stores over a prolonged period of time can result in the activation of apoptosis[103]. Thus, it is possible that lower duramycin concentrations (5 µM) result in apoptotic cell death >24 hours due to slow release of Ca^{2+} from the ER. The amount of necrosis induced by duramycin after 30 minutes treatment was found to strongly correlate with the percentage increase in $[Ca^{2+}]_i$ in all of the cancer cell lines, A2780, AsPC-1, MIA PaCa-2 and SK-OV-3. An increase in $[Ca^{2+}]_i$ can result in Ca^{2+} overload and ultimately lead to cell death[117, 240]. This mechanism has been utilised in the treatment of cancer cells *in vitro* where the calcium electroporation, in which cell membranes are made permeable to Ca^{2+} transfer, of cancer cell lines was shown to induce cell death and acute ATP depletion[118]. Nude mice transfected with a human small cell lung cancer cell line were subjected to the electroporation and a reduction in tumour size with complete tumour necrosis was observed 6 days post treatment[118]. Though it was suggested in this study that an increase in $[Ca^{2+}]_i$ was related to duramycin-induced necrotic cell death a more definitive study would be required before a direct causal link could be concluded. However, it was established that duramycin treatment of cancer cell lines resulted in an increase in $[Ca^{2+}]_i$ likely due to release from internal stores and some influx of Ca^{2+}. Subsequently, through action on the plasma membrane, either duramycin inhibits the efflux of Ca^{2+} perhaps through the disruption of membrane ATPases or duramycin results in Ca^{2+} efflux through the formation of membrane pores. While both of these explanations are possible, based on current understanding, it is the former explanation that is favoured as Fluo-3, AM and Ca^{2+} do not easily dissociate.

Chapter 6 Photodynamic Therapy

Papers published in support of this chapter:

Broughton LJ, Giuntini F, Savoie H, Bryden F, Boyle RW, Maraveyas A, Madden LA. Duramycin-porphyrin conjugates for targeting of tumour cells using photodynamic therapy. *Journal of photochemistry and photobiology B, Biology*. 2016; 163:374-84.

6.1 Introduction

Photodynamic therapy (PDT) is a minimally invasive treatment which requires the introduction of a photosensitising drug which can be delivered either intravenously or topically and the application of light which can be guided to specific areas within the body using flexible optical fibres. PDT is also reliant on the availability of molecular oxygen and because of this its effectiveness as a treatment can be affected in areas of hypoxia[136]. Accumulation of the photosensitiser (PhtS) specifically in tumour tissue means that photodynamic treatment can have a selective cytotoxic effect towards cancer[119]. Activation of the PhtS with light at a specific wavelength excites the PhtS and leads to the production of cell damaging reactive oxygen species (ROS). This can occur via two mechanisms known as type I and type II reactions. Type I reactions involve the transfer of electrons from a substrate to the excited PhtS (oxidation) or transfer of a hydrogen atom to the PhtS (reduction) which subsequently causes the formation of free radicals that can react with molecular oxygen and produce ROS. Type II reactions, widely regarded as the predominate route employed in PDT, involve the direct transfer of energy from PhtS in its excited triplet state to ground state (triplet) molecular oxygen which is converted to a highly reactive excited singlet state[121, 122]. The generation of cell damaging ROS during PDT can ultimately cause apoptotic or necrotic cell death which occur through a variety of mechanisms[124].

As well as its direct cytotoxic effect on cancer, PDT can have anti-tumour effects via the induction of the inflammatory response[126] and damage to tumour vasculature[249]. Damage to tumours is detected by the body in a similar way to normal tissue so that PDT induced cell injury promotes an inflammatory response which, with input from the innate immune system, works to remove dead and irreparable cancer cells and thus can enhance the effects of PDT[126]. Preferential photodynamic damage to tumour vasculature or tumour tissue can be selected by manipulation of the drug-light interval. When relatively short intervals between the administration of PhtS and the application of light treatment are employed damage primarily occurs to the vasculature as the PhtS is localised to blood

vessels[127, 249]. This method has been used in the treatment of abundant vessel growth in age-related macular degeneration[120, 127] and could potentially be utilised in the targeting of tumour angiogenesis. In relation to this study, duramycin has been shown to bind phosphatidylethanolamine (PE) expressed on the tumour vasculature[59]. Thus a duramycin based PhtS could potentially be used to increase accumulation of PhtS in tumour vasculature and be used to target angiogenesis in the tumour vicinity.

PDT has been approved for the treatment of a variety of cancer types including premalignant and malignant skin cancers such as actinic keratosis, Bowen's disease and basal cell cancer[128, 129], head and neck cancers; early carcinomas of the oral cavity, pharynx, and larynx[130], Barrett's oesophagus and early oesophageal cancer[131], prostate cancer, bladder cancer, non-small cell lung cancer and brain tumours[119]. As well as being used as a direct anti-cancer therapy PDT has been used as a synergistic method combined with other major therapies e.g. chemotherapy, radiotherapy and surgery[15, 141, 142]. PDT does not compromise the outcome of these therapies and therefore can be used in conjunction with them without effecting future treatment options for residual or recurrent disease[119]. PDT has also been used to improve the quality of life in patients when other therapies have failed and as an alternative to major therapies in the treatment of highly localised head and neck tumours[11]. Advantages of PDT include good cosmetic outcome in skin cancers[143] and retained functional ability due to preserved normal tissue and minimal fibrosis[11, 130]. However, PDT is currently ineffective in the metastatic stages of cancer. Photodynamic treatment can also induce a substantial amount of pain in some patients. However, the main disadvantage of PDT, with regards to oncology, is the low selectivity that most PhtS have towards tumour tissue. This can result in damage to surrounding normal tissue and a prolonged sensitivity to light[119].

In this study, the class of PhtS selected was a porphyrin. Porphyrins are highly conjugated heterocyclic tetrapyrroles that were identified as having photodynamic properties over 45 years ago[147]. Due to their heterocyclic structure porphyrins have absorption in the visible light range and, existing in nature, give the red colour to haem in animals and the green colour to chlorophyll in plants[148]. Synthesised cyclic tetrapyrrolic derivatives are inherently similar to those found in nature and subsequently have little cytotoxicity in the absence of light[121]. The porphyrins TTP (5,10,15,20-tetra-p-tolyl porphyrin) and THNP (5,10,15,20-tetra-p-naphthyl-porphyrin) when incubated with the human melanoma cell line WM35 and treated with 4.5 J/cm^2 light irradiation induced cell death in a concentration dependent

manner[149]. The porphyrin 5-[Aminobutyl-N-oxycarbonyl)phenyl]phenyl]-10,15,20-tris(N-methyl-4-pyridinium) porphyrin trichloride plus light irradiation was able to reduce the cell survival and prevent colony forming of prostate epithelial cells at concentrations >8.75 μM[150]. The highest concentration (50 μM) reduced cell survival to ~20% and necrosis was identified as the main mechanism of cell death though autophagy was also induced. ROS (H_2O_2) production was detected only in cells that had been both drug treated and irradiated. Interestingly, PDT treatment of the prostrate epithelial cells was found to induce 10-fold more ROS than gamma irradiation[150].

The main disadvantage of PDT, the low selectivity of PhtS to their target tumour cells over non-tumour cells,[119] means that some PhtS require a long time to reach sufficient levels in the target tumour tissue and consequently a relatively large dose is needed[152]. Perhaps more importantly though this lack of selectivity has led to damage to non-tumour tissue. In an attempt to overcome this, research in PDT with regards to oncology has focused on the development of PhtS conjugated to tumour targeted biological molecules[120] which bind structural features overexpressed or enhanced in tumours. Porphyrins have been successfully conjugated to a variety of biological molecules including mAbs and their smaller fragments (Fab and scFv)[154], lipoproteins[155] and nanoparticles[156]. The scFv antibody fragment LAG3, which is specific towards colorectal cancer cell lines, was conjugated through its lysine residue to the porphyrin 5-(4-isothiocyanatophenyl)-10,15,20-tris(N-methyl-4-pyridinium) porphyrin trichloride[154]. Selective cytotoxic effect of the colorectal cancer cell line Caco-2 was observed after LAG3 plus 15 J/cm^2 light treatment where cell death was found to occur by apoptotic and necrotic pathways. The porphyrin derivative chlorin-e6 (Ce-6) was conjugated to low-density lipoproteins (LDL) the receptors for which were expressed on the retinoblastoma cell line Y79[155]. Photodynamic treatment reduced cell proliferation to 20% in the conjugate treated cells compared to a maximum of 90% in free and mixed (unconjugated) Ce-6 treated cells. Nanoparticles conjugated to porphyrin derivatives were able to significantly reduce the cell survival of the HeLa cancer cell line at relatively low concentrations (0.01 μM, IC_{50} was 0.1 μM) and showed no dark toxicity[156]. Thus the conjugation of these molecules allowed for a more targeted delivery of the PhtS.

Duramycin has been shown to bind to PE on the surface of cancer cell lines (Chapter 3) and have a cytotoxic and anti-proliferative effect (Chapters 3 and 4). However the detection of PE on the normal endothelial cell line HUVECs was also observed by duramycin as was an effect on their cell viability. Therefore an increase in duramycin's specificity to cancer cells

would be advantageous. Thus the aim of this chapter was to synthesise a duramycin conjugate that was bound to a porphyrin based PhtS. Then, after irradiation with visible (red) light, to assess its anti-proliferative effect on the ovarian cancer cell lines A2780 and SK-OV-3 and the pancreatic cancer cell lines AsPC-1 and MIA PaCa-2.

6.2 Results

6.2.1 Synthesis and analysis of the duramycin-porphyrin conjugate

The novel photosensitising agent duramycin-porphyrin conjugate was synthesised by conjugating duramycin to a porphyrin PhtS which was subsequently purified. This was then analysed to confirm its successful formation. Briefly, duramycin in solution with DMSO and TEA was treated with the porphyrin 5-[4-(N-succinimidyloxycarbonyl)phenyl]-10,15,20-tris(4-methylpyridinium) porphyrin trichloride and mixed on a rotating shaker at room temperature for 24 hours. The crude mixture was recovered using dichloromethane and filtration after which the solid was dissolved in TFA. The conjugate was then isolated out of the crude mixture, which also contained unreacted duramycin and porphyrin, and purified by semi-preparative HPLC. Analysis of the resultant purified compound was performed by various forms of mass spectrometry (MS) to confirm production of the duramycin-porphyrin conjugate (figure 6.1). All synthesis and analysis work on the conjugate was performed by Dr. F Giuntini. The mass of the conjugate recovered following the conjugation procedure was 4.8 mg which equated to a 34.4% yield (a 100% yield would have resulted in the recovery of 13.96 mg). The duramycin-porphyrin conjugate was synthesised twice in this study and the HPLC and MS analyses presented in this chapter were gained from the first batch of the conjugate though are representative of the results from both batches.

The purification of the crude conjugation mixture was performed by HPLC and the trace is presented in figure 6.2 (upper trace). The solvent was eluted first and is represented by the large peak at R_t = ~2.00 minutes. There was then 3 more elution's of interest with peaks at R_t = 6.20, 7.01 and 7.32 minutes. Previously, unconjugated porphyrin and unconjugated duramycin had been analysed by HPLC and their retention times found to be 7.01 and 7.32 minutes, respectively. Therefore as the compound began to be eluted at R_t = 6.20 minutes a small amount was taken and analysed by ESI-MS to identify its molecular weight (MW). The compound was confirmed as duramycin-porphyrin conjugate. Further analysis by HPLC plus liquid chromatography-mass spectrometry (LCMS) confirmed the peak at R_t = 6.20 minutes to be the duramycin-porphyrin conjugate. The purification of the compound isolated at R_t = 6.20 minutes was successful as only one peak at this retention time was shown in a subsequent HPLC trace of the conjugate (figure 6.2, lower trace).

The purified conjugate was analysed by ESI-MS (figure 6.3) and a peak with a mass of 675.66 was obtained. The porphyrin component of the conjugate is positively charged with a charge of 3 and the duramycin component is capable of attracting charge in the ionisation

chamber of the mass spectrometer. The conjugate therefore had an overall charge of 4 and so the obtained peak was a quarter of the mass of the conjugate (2702 g/mol) (minus a proton). This confirmed that the synthesis of duramycin-porphyrin conjugate had been successful and that the conjugation occurred at a 1:1 ratio of 1 duramycin molecule to 1 porphyrin molecule.

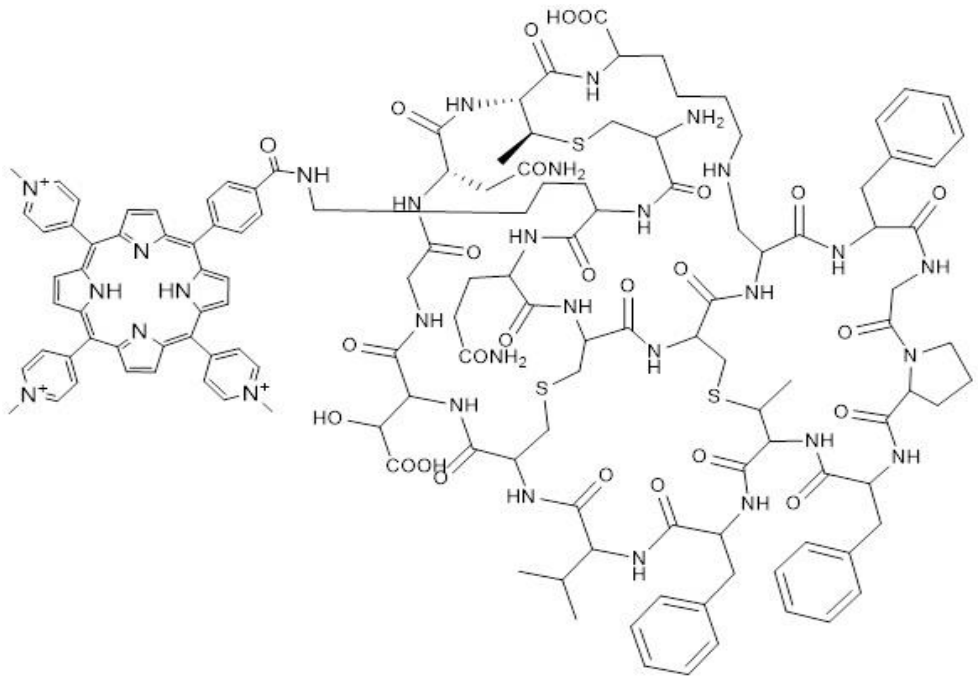

Figure 6.1: Structure of the duramycin-porphyrin conjugate.

A covalent amide bond was formed between the porphyrin and the duramycin through a reaction with the NHS ester of the porphyrin 5-[4-(N-succinimidyloxycarbonyl)phenyl]-10,15,20-tris(4-methylpyridinium) porphyrin trichloride and the ε-amino group of the lysine residue at duramycin's N-terminal. The solvent used was DMSO. MW = 2702 g/mol, molecular formula $C_{134}H_{159}N_{30}O_{26}S_3$.

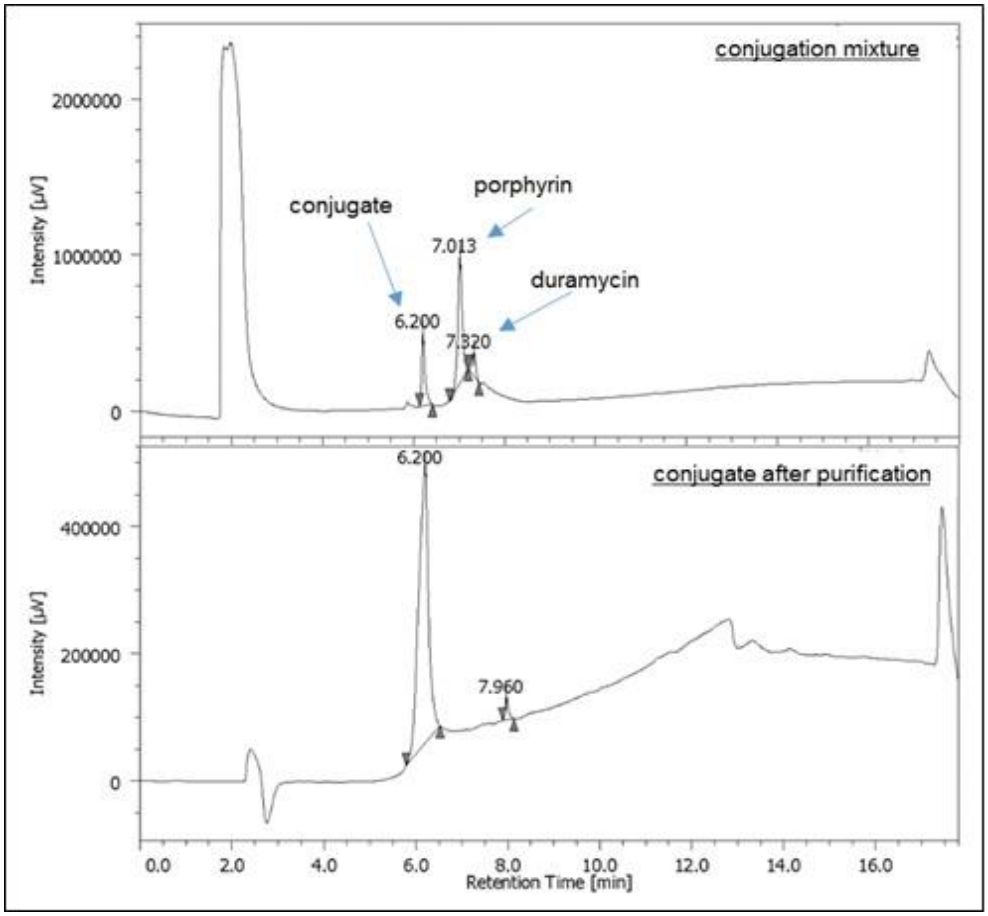

Figure 6.2: Purification of the duramycin-porphyrin conjugate by HPLC.

Duramycin-porphyrin conjugate was isolated by HPLC at R_t = 6.20 minutes with the additional collection of unreacted porphyrin at R_t = 7.01 and unreacted duramycin at R_t = 7.32 minutes (upper trace). The break in the trace line on the lower trace represents the void time in which the solvent front eluted. The small peak at R_t = 7.96 was due to a discrepancy within the instrument.

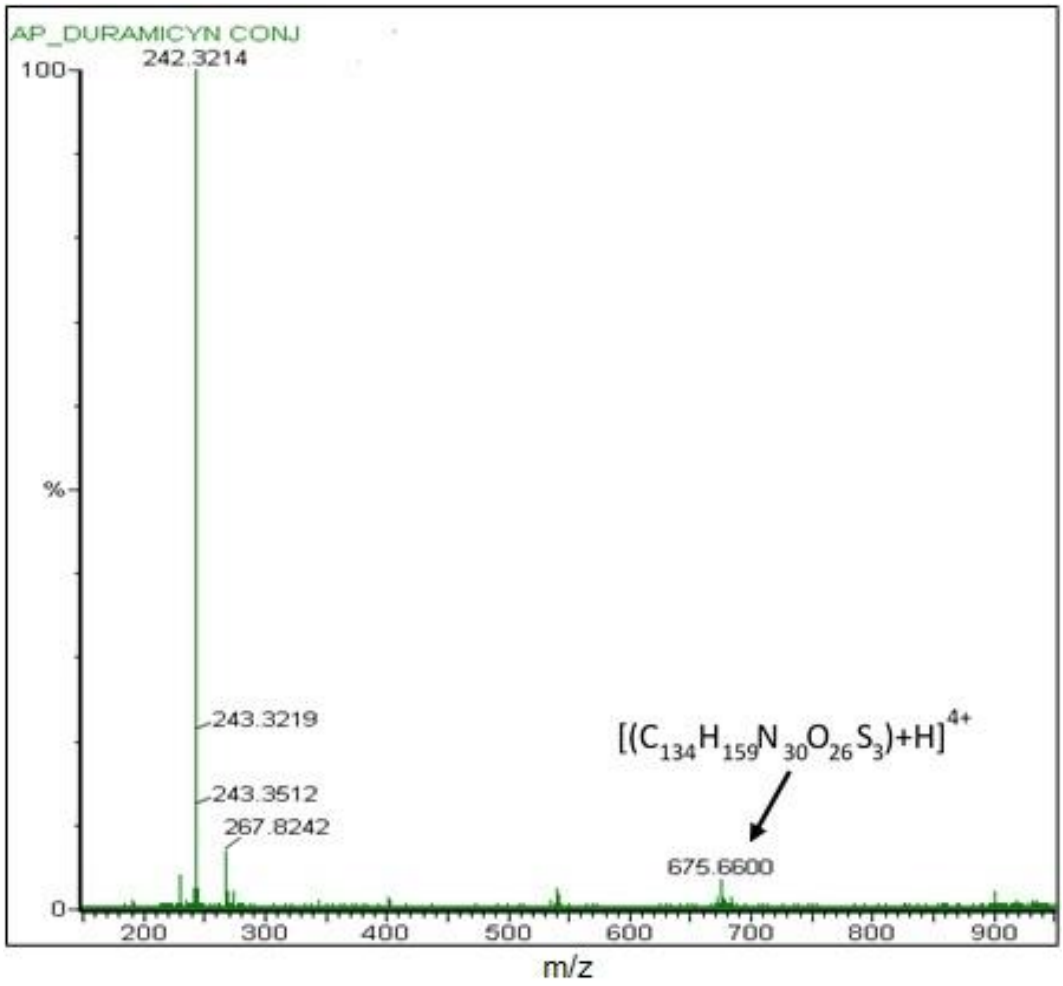

Figure 6.3: Mass spectrometry analysis of the duramycin-porphyrin conjugate. The peak for the conjugate was found to be ESI-MS (+): 675.66 $[(M+4H^{+})/4]^{4+}$ where the expected was 675.67. Conjugate retention time; R_t = 7.34 minutes. The peaks shown at <300.00 were unidentified though were most likely due to an impurity within the mass spectrometer.

6.2.2 Phosphatidylethanolamine detection on cancer cells

The duramycin-porphyrin conjugate was assessed for its ability to detect cell surface PE on the ovarian cancer cell lines A2780 and SK-OV-3 and the pancreatic cancer cell lines AsPC-1 and MIA PaCa-2 by flow cytometry. Briefly, cells ($2x10^5$) were suspended in PBS (50 µl) and incubated with the conjugate (1 µM-1 mM) in the dark at room temperature for 30 minutes. Cells were then washed, centrifuged and re-suspended in PBS (300 µl) and analysed using the flow cytometers 635 nm red diode laser. The level of PE expression was recorded as median fluorescence in the flow cytometers FL-4 channel. It had been shown that unconjugated duramycin could detect cell surface PE on the cancer cell lines in a concentration dependent relationship (Chapter 3). Therefore the aim of this experiment was to investigate whether the PE-binding ability of the duramycin component of the conjugate had been affected by the conjugation procedure. It was also assessed herein whether the porphyrin component of the conjugate had retained its fluorescent properties.

The duramycin-porphyrin conjugate detected PE on all of the cancer cell lines in a concentration dependent manner (figures 6.4 and 6.5). Both batches of the conjugate were shown to retain the ability to bind PE and have detectable fluorescence. Fewer concentrations were used in the assessment of the binding ability of the second batch because of a requirement for the conjugate in prospective experiments (Chapter 7) though figure 6.5 clearly shows the concentration dependent relationship. The duramycin-porphyrin conjugate detected similar levels of PE for all 4 cancer cell lines and optimal PE detection occurred at 1 mM (figure 6.4).

In addition to being detectable through the flow cytometers FL-4 channel the signal from the duramycin-porphyrin conjugate was also detectable through the FL-1 channel. This was most likely due to the fluorescence of the porphyrin component of the conjugate which has a wide absorption spectra from 422-635 nm.

a)

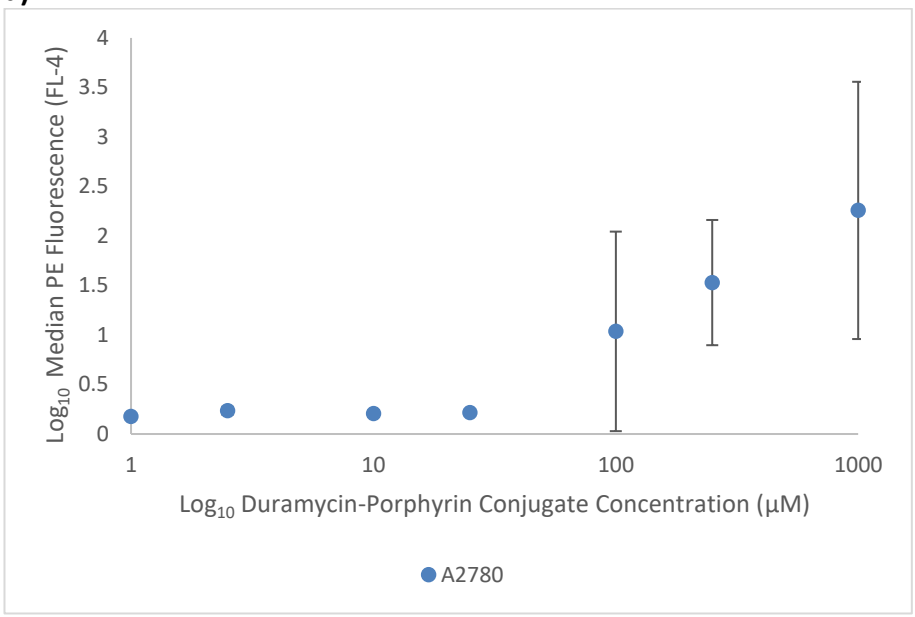
4
3.5
3
2.5
2
1.5
1
0.5
0
Log10 Median PE Fluorescence (FL-4)
1
10
100
1000
Log10 Duramycin-Porphyrin Conjugate Concentration (µM)
A2780

b)

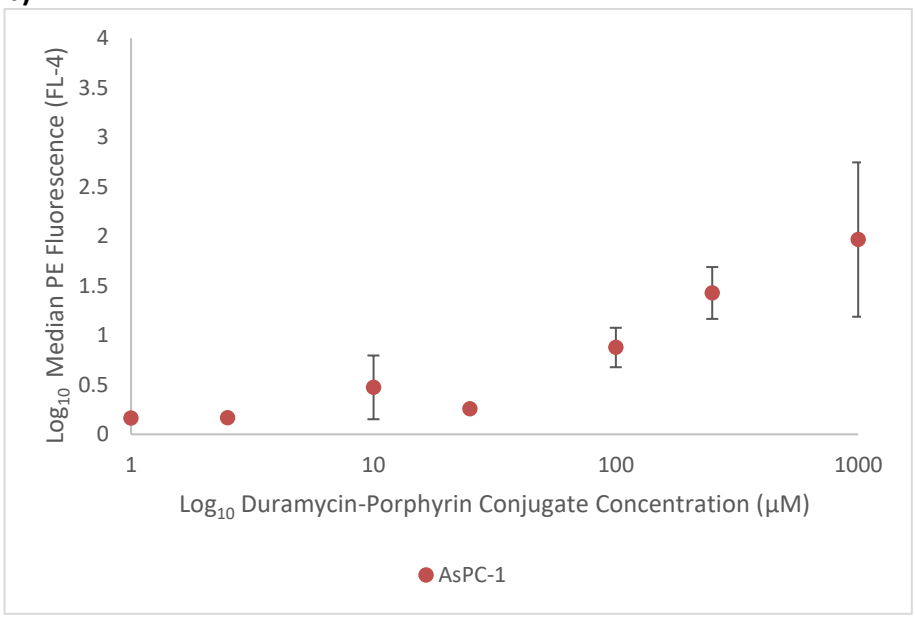
4
3.5
3
2.5
2
1.5
1
0.5
0
Log10 Median PE Fluorescence (FL-4)
1
10
100
1000
Log10 Duramycin-Porphyrin Conjugate Concentration (µM)
AsPC-1

c)

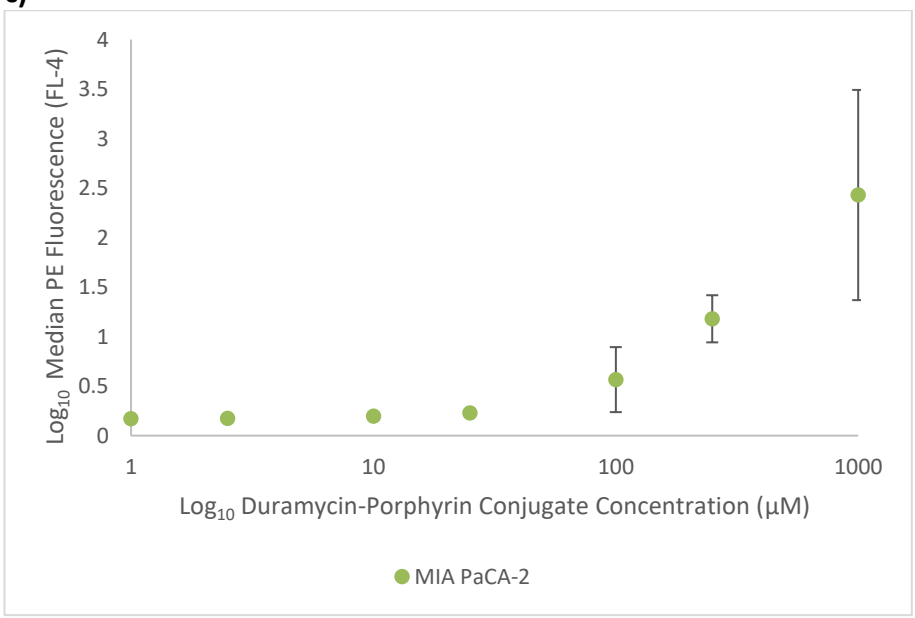
4
3.5
3
2.5
2
1.5
1
0.5
0
Log10 Median PE Fluorescence (FL-4)
1
10
100
1000
Log10 Duramycin-Porphyrin Conjugate Concentration (µM)
MIA PaCA-2

d)

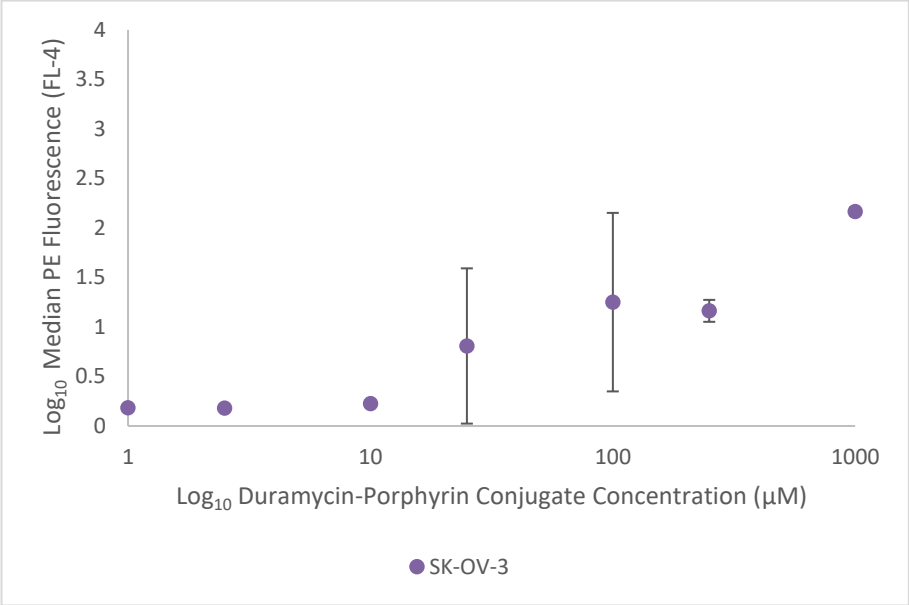

e)

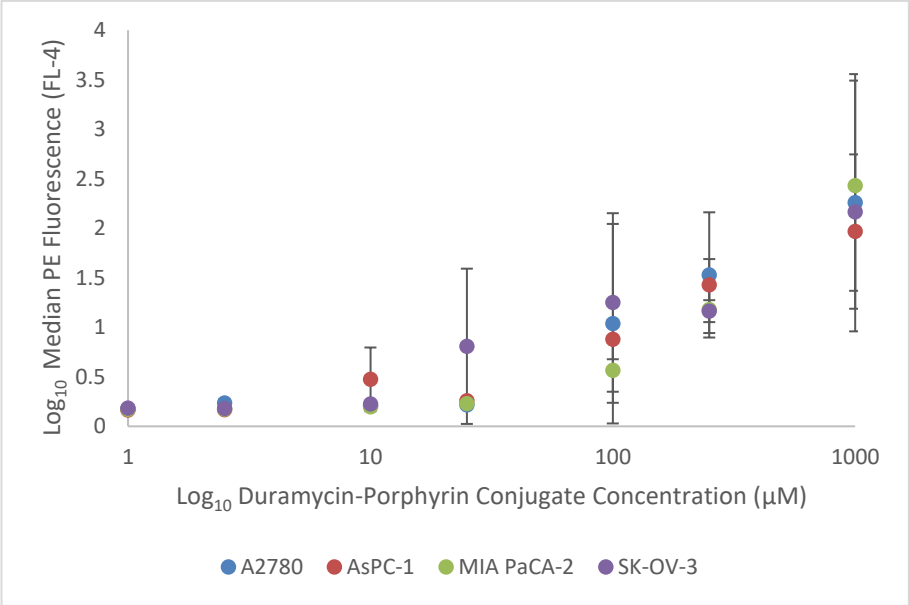

Figure 6.4: Detection of PE using the duramycin-porphyrin conjugate (first batch).

The duramycin-porphyrin conjugate was able to detect cell surface PE on the cancer cell lines a) A2780, b) AsPC-1, c) MIA PaCa-2 and d) SK-OV-3, in a concentration dependent manner. e) The level of PE detection was similar for all 4 cell lines. Log_{10} median PE fluorescence was used to state levels of PE expression. Error bars represent the SD of 2 replicates.

i)

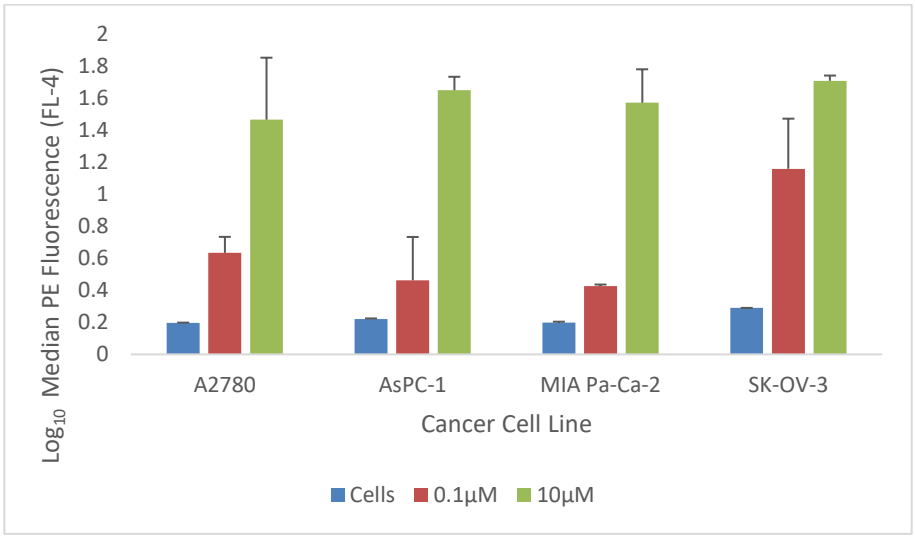

ii)

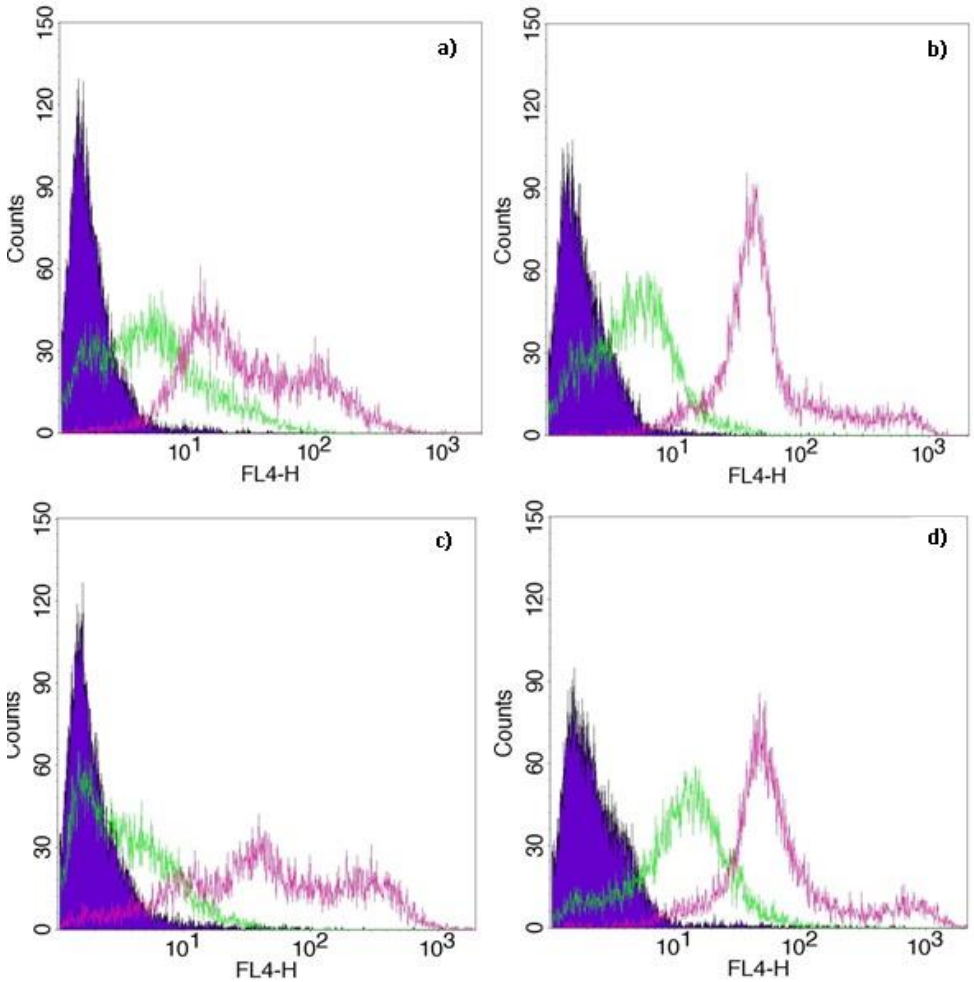

Figure 6.5: Detection of PE using the duramycin-porphyrin conjugate (second batch).

i) The duramycin-porphyrin conjugate was able to detect PE on the surface of the 4 cancer cell lines A2780, AsPC-1, MIA PaCa-2 and SK-OV-3 in a concentration dependent manner. Error bars represent the SD of 2 replicates. ii) Flow cytometry histograms showed a detectable shift in fluorescence on a) A2780, b) AsPC-1, c) MIA PaCa-2 and d) SK-OV-3 cells (purple) using 0.1 µM (green) and 10 µM (pink) duramycin-porphyrin conjugate.

6.2.3 Competitive binding for phosphatidylethanolamine

To further assess whether the ability off the duramycin-porphyrin conjugate to bind cell surface PE had been affected by the conjugation process a competition assay between the conjugate and unconjugated duramycin was performed. Briefly, cells ($2x10^5$) were suspended in PBS (50 µl) and incubated with duramycin-porphyrin conjugate (50 µM) at room temperature in the dark for 5 minutes. The cells were then washed, centrifuged and re-suspended in PBS. The '0 minute' sample was analysed by flow cytometry (635 nm red diode laser, FL-4 channel) and the median PE fluorescence taken. Cells were then incubated with unconjugated duramycin (50 µM) for 2, 5, 15 and 30 minutes to allow the unconjugated duramycin time to potentially displace the conjugate and competitively bind to PE. The median PE fluorescence reading was then taken.

The unconjugated duramycin was unable to compete with the pre-bound duramycin-porphyrin conjugate for the binding of PE on A2780 and MIA PaCa-2 cells (figure 6.6). The median PE fluorescence of A2780 and MIA PaCa-2 was determined, at 0 minutes, as 10.9±0.75 and 16.7±5.9, respectively. The median PE fluorescence of MIA PaCa-2 remained constant, within SD, at each interval along the 30 minute time course. The median PE fluorescence of A2780 however increased over time to a maximum of 12.8±0.16 at 30 minutes. Thus it was shown that the binding affinity of the conjugate was not affected by the conjugation procedure.

The competition assay was also performed where unconjugated duramycin was pre-bound to the cancer cells and the conjugate functioned as the competing species. The median PE fluorescence (488 nm argon laser, FL-1 channel) detected remained constant, within SD, at 8.3±1.8 for A2780 and 11.7±1.4 for MIA PaCa-2 over 30 minutes. However it could not be certain that the FL-1 signal originated from the unconjugated duramycin (labelled with a tertiary FITC antibody detected at 488 nm) as the duramycin-porphyrin conjugate signal was also detectable through this channel.

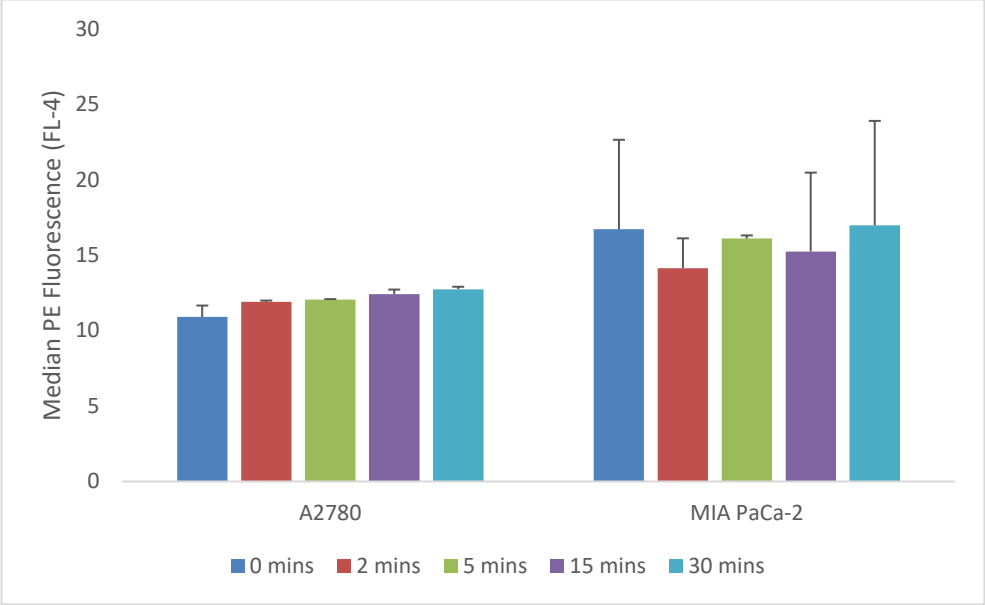

Figure 6.6: Competitive binding for PE between pre-bound duramycin-porphyrin conjugate and unconjugated duramycin.

The unconjugated duramycin was unable to compete with the conjugate for cell surface PE on the cancer cell lines A2780 and MIA PaCa-2. The median PE fluorescence of MIA PaCa-2 remained constant, within SD, at each interval during the 30 minute time course. However the median PE fluorescence of A2780 increased slightly over time. Error bars represent SD of 2 replicates.

6.2.4 Effect of duramycin-porphyrin conjugate on the light scattering properties of cancer cells

To assess if the duramycin-porphyrin conjugate had an effect on the forward scatter (FSC) and side scatter (SSC) of cancer cell lines, A2780, AsPC-1, MIA PaCa-2 and SK-OV-3 were treated with the conjugate (1 µM-1 mM) and analysed by flow cytometry. Briefly, cells ($2x10^5$) were incubated with the conjugate for 30 minutes in the dark at room temperature. They were then washed, centrifuged and re-suspended in PBS (300 µl) and were analysed by flow cytometry. Unconjugated duramycin had been shown to have an effect on the FSC and SSC of the cancer cell lines where concentrations >50 µM correlated with an increase in the FSC of AsPC-1 and SK-OV-3 and >200 µM correlated with an increase in SSC of A2780, AsPC-1, MIA PaCa-2 and SK-OV-3 (Chapter 3). It was the aim of this experiment to compare the effect that unconjugated duramycin had on the light scatter of cancer cell lines to the effect that the duramycin-porphyrin conjugate had on the cells.

The duramycin-porphyrin conjugate did not have an effect on the FSC of AsPC-1 and SK-OV-3 (figure 6.7). The FSC of A2780 and MIA PaCa-2 was increased when treated with the highest concentration of conjugate (1 mM). Conjugate treatment increased the SSC of all 4 of the cancer cell lines (figure 6.8). The SSC of the ovarian cancer cell lines A2780 and SK-OV-3 increased when treated with 1mM conjugate whereas for the pancreatic cancer cell lines AsPC-1 and MIA PaCa-2 this increase occurred at 250 µM.

Though the duramycin-porphyrin conjugate required higher concentrations to exert the same level of effect as the unconjugated duramycin both still increased the FSC (figure 6.9) and SSC (figure 6.10) in a concentration dependent manner. This further supported the finding that the duramycin component of the conjugate had maintained its functionality.

a)

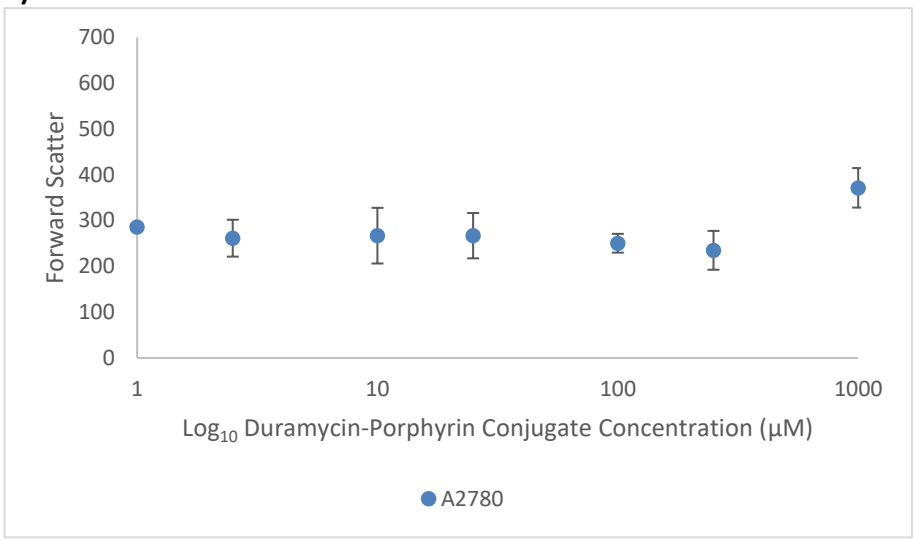

b)

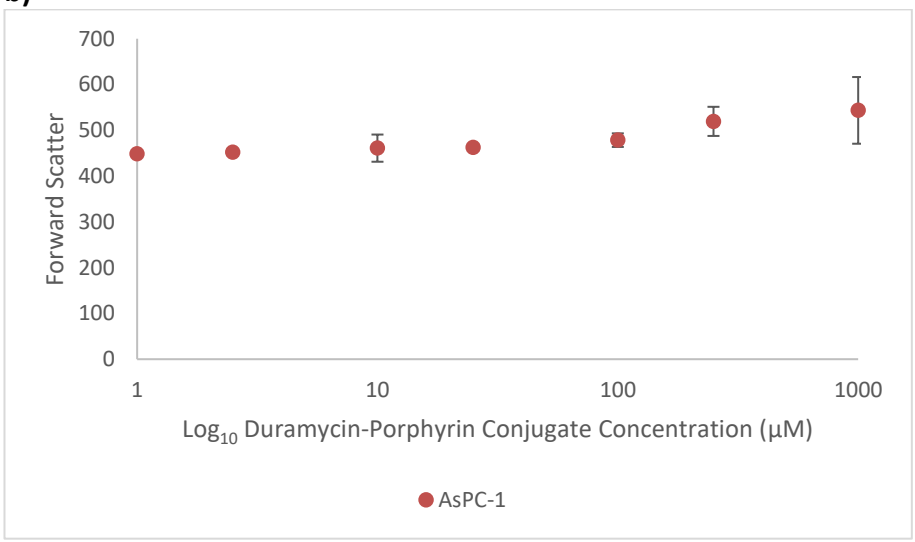

c)

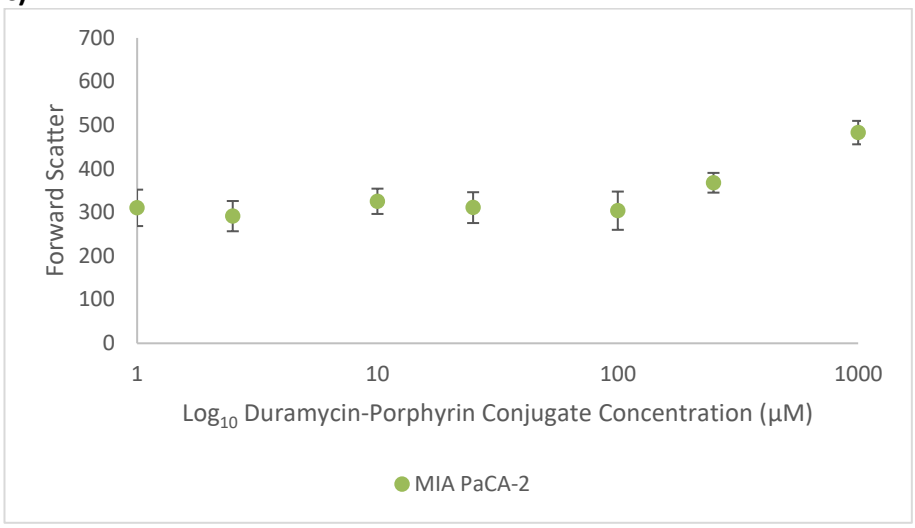

d)

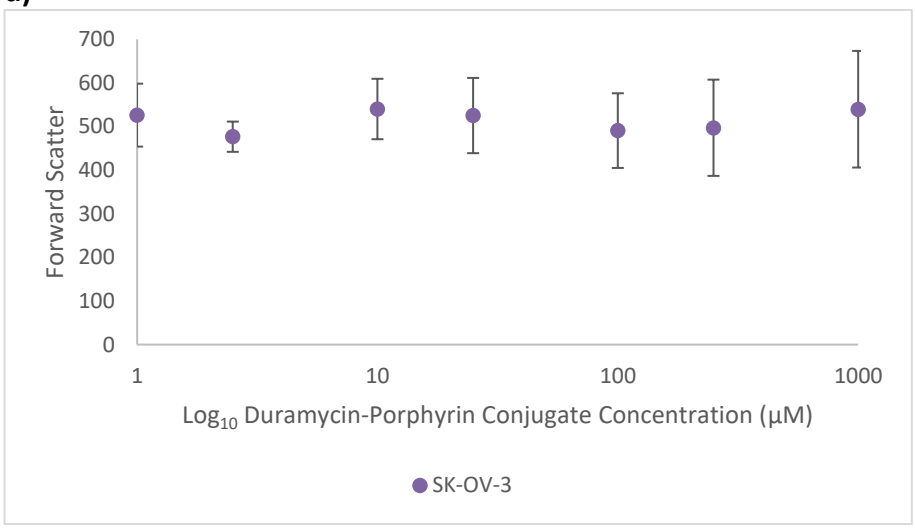

e)

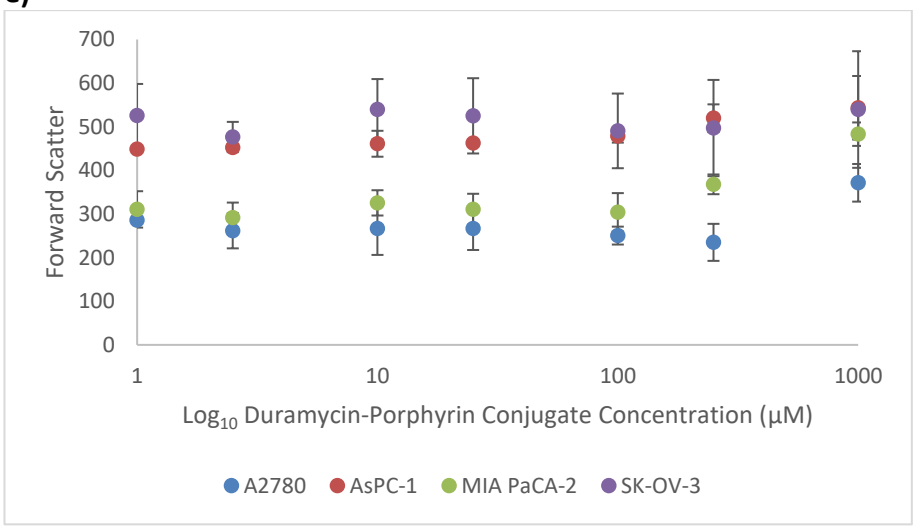

Figure 6.7: The effect of the duramycin-porphyrin conjugate on the FSC of cancer cell lines.

The FSC of the cancer cell lines b) AsPC-1 and d) SK-OV-3 were not affected by duramycin-porphyrin conjugate treatment. The FSC of a) A2780 and c) MIA PaCa-2 was increased when treated with 1mM conjugate. e) Comparison of all 4 cancer cell lines. Error bars represent SD of 2 replicates.

a)

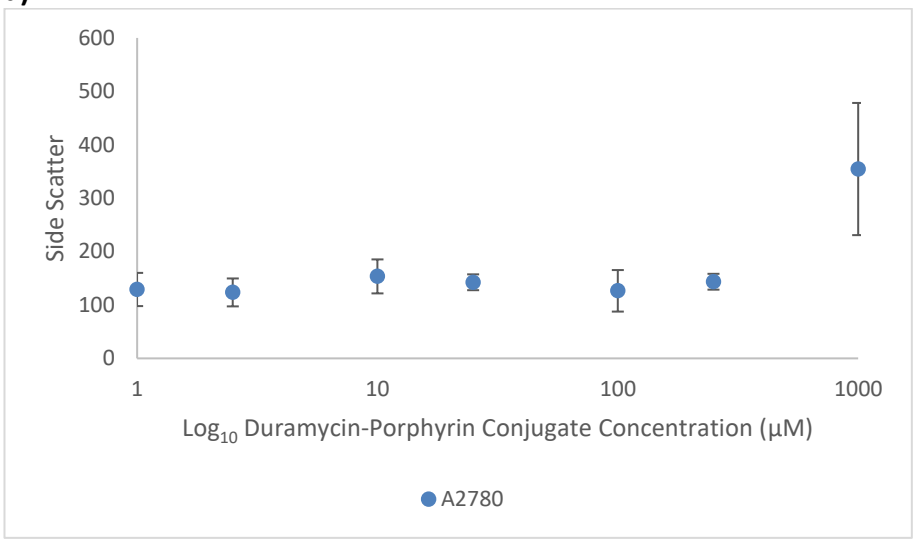
600
500
400
300
200
100
0
Side Scatter
1
10
100
1000
Log10 Duramycin-Porphyrin Conjugate Concentration (µM)
A2780

b)

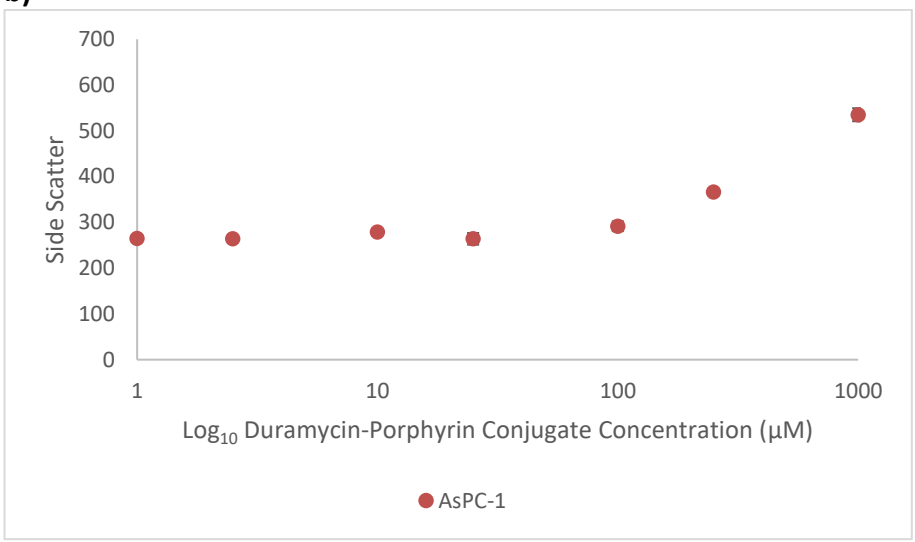
700
600
500
400
300
200
100
0
Side Scatter
1
10
100
1000
Log10 Duramycin-Porphyrin Conjugate Concentration (µM)
AsPC-1

c)

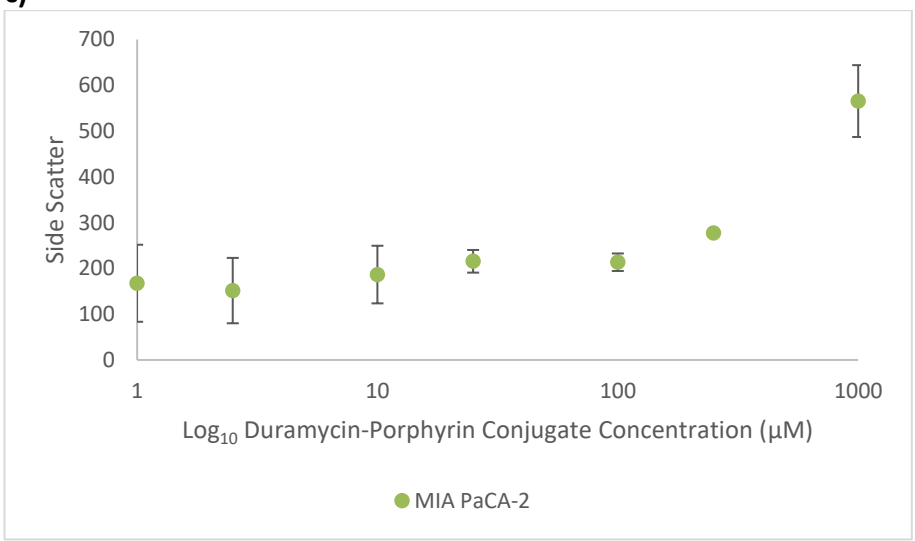
700
600
500
400
300
200
100
0
Side Scatter
1
10
100
1000
Log10 Duramycin-Porphyrin Conjugate Concentration (µM)
MIA PaCA-2

d)

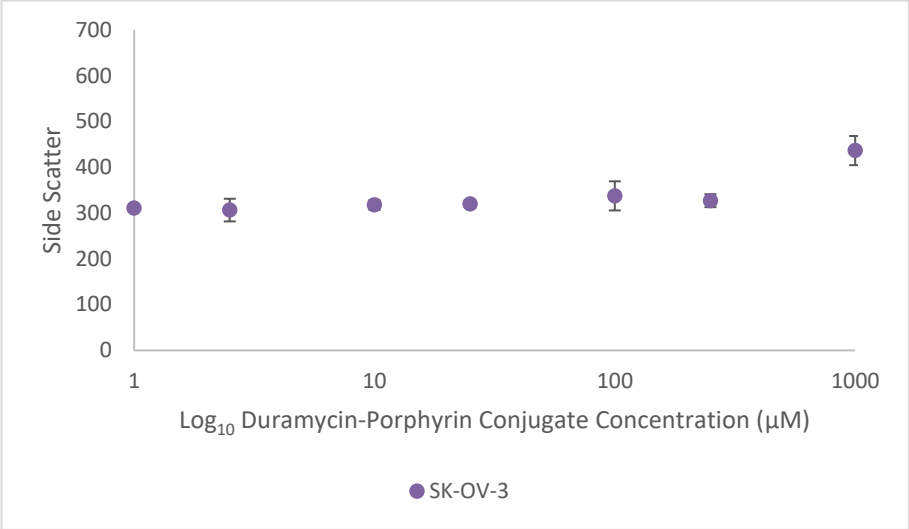

e)

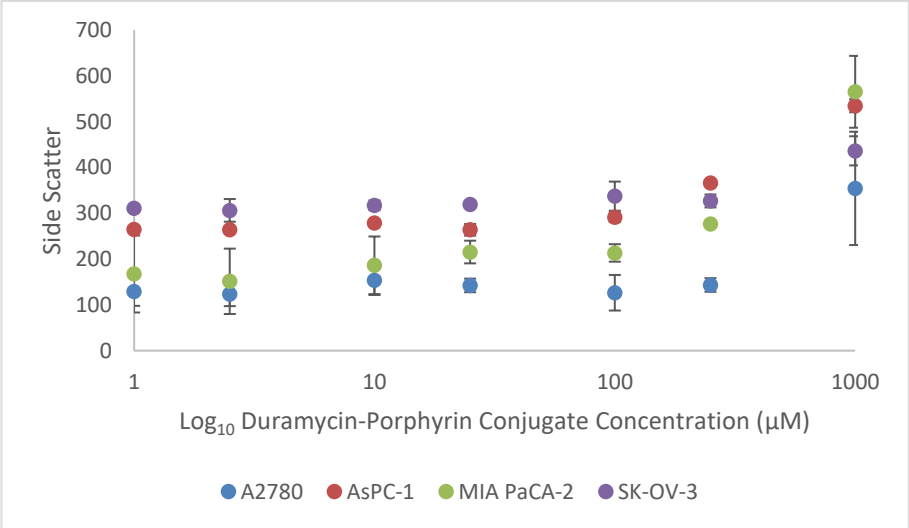

Figure 6.8: The effect of the duramycin-porphyrin conjugate on the SSC of cancer cell lines.

The SSC of a) A2780 and d) SK-OV-3 was increased when the cells were treated with 1mM duramycin-porphyrin conjugate and b) AsPC-1 and c) MIA PaCa-2 when treated with conjugate >250 µM. e) Comparison of all 4 cancer cell lines. Error bars represent SD of 2 replicates.

a)

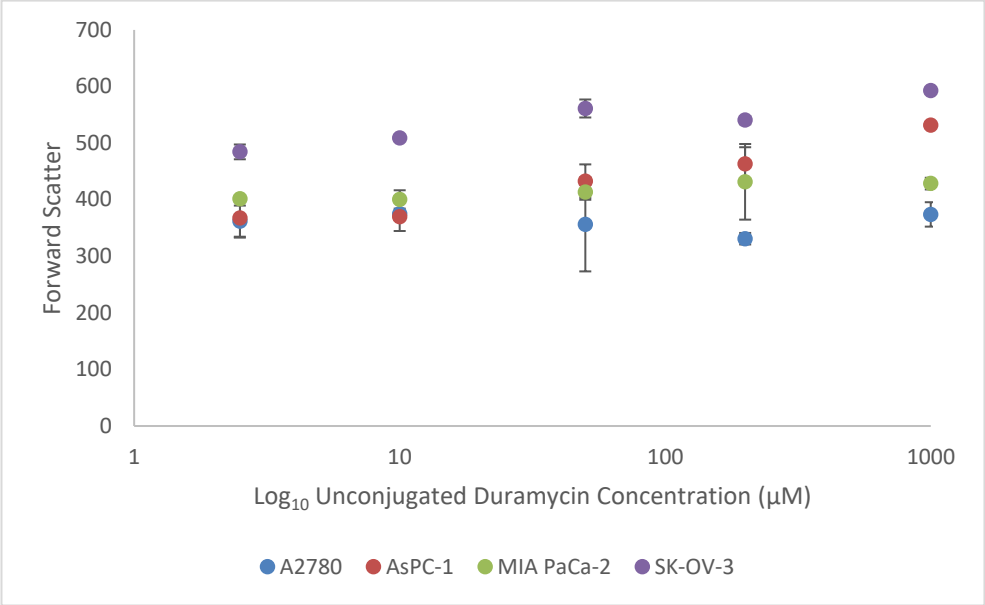

b)

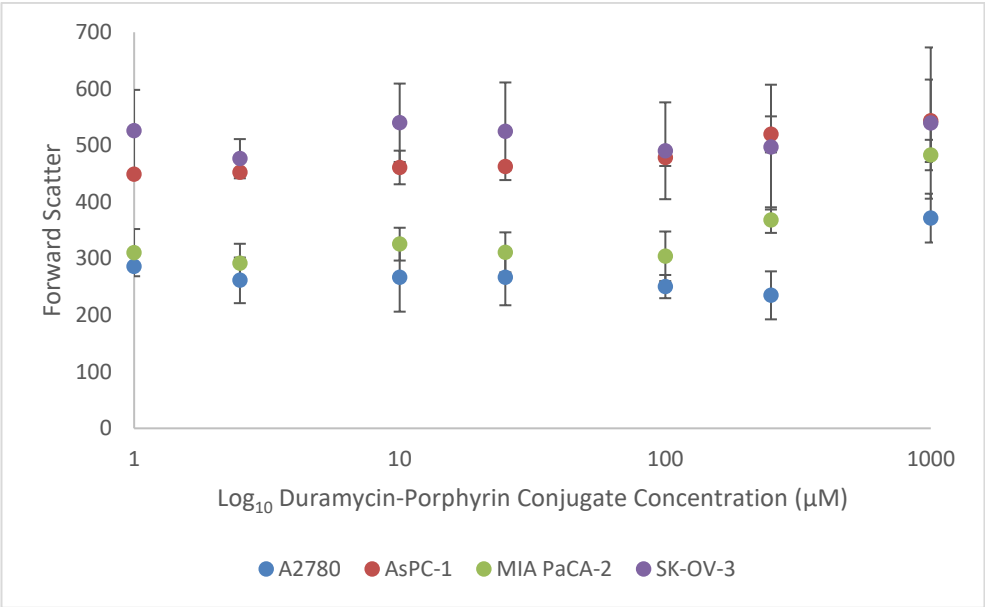

Figure 6.9: The effect of unconjugated duramycin and duramycin-porphyrin conjugate on the FSC of cancer cell lines.

a) Unconjugated duramycin increased the FSC of AsPC-1 and SK-OV-3 cells >50 µM. b) Duramycin-porphyrin conjugate had an effect on the FSC of A2780 and MIA PaCa-2 cells at 1mM. Error bars represent SD of 2 replicates.

a)

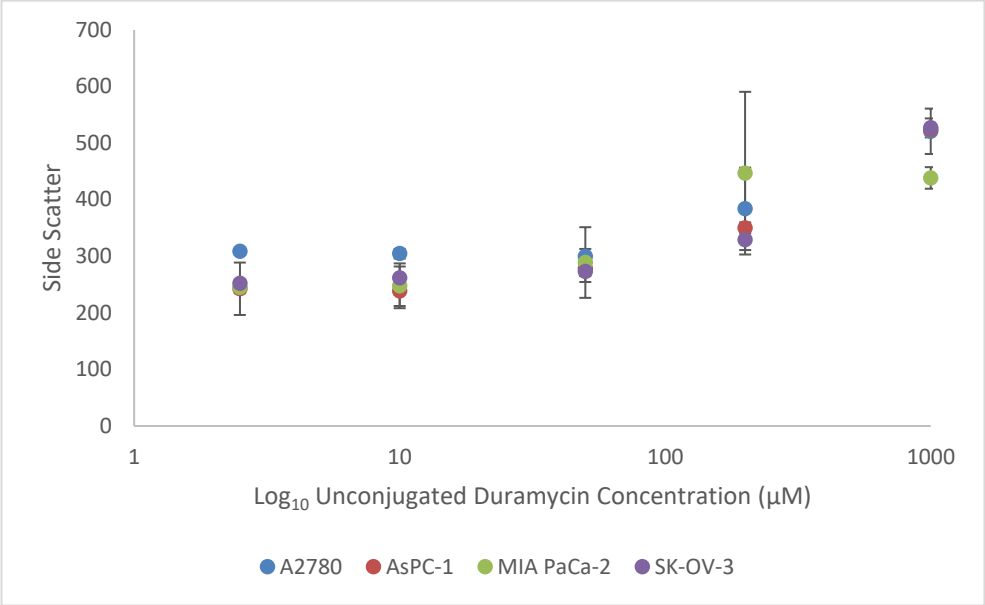

b)

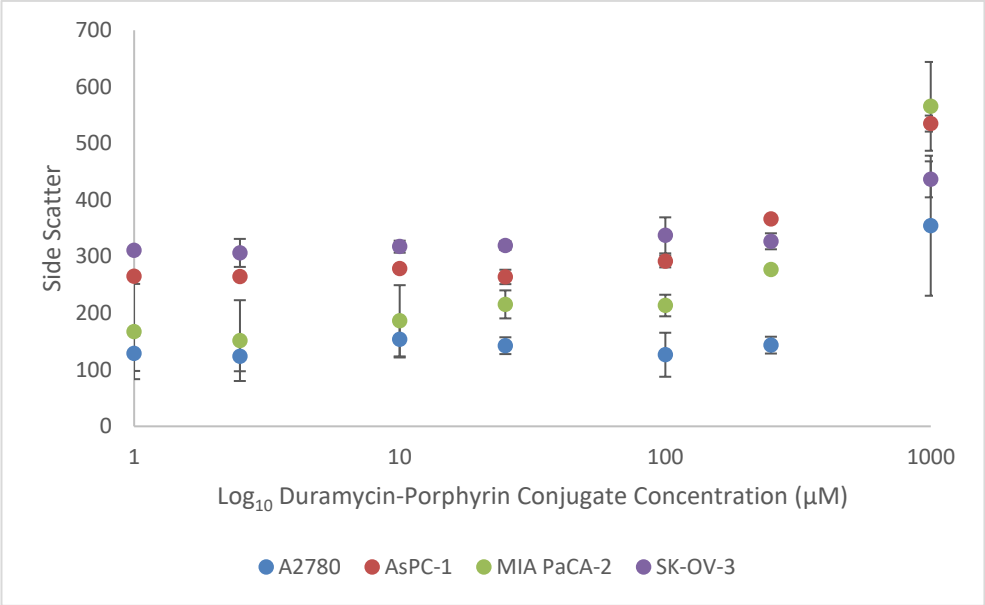

Figure 6.10: The effect of unconjugated duramycin and duramycin-porphyrin conjugate on the SSC of cancer cell lines.

a) Unconjugated duramycin increased the SSC of all 4 cancer cell lines >200 µM. b) Duramycin-porphyrin conjugate had an effect on the SSC of AsPC-1 and MIA PaCa-2 >250 µM and A2780 and SK-OV-3 cells at 1 mM. Error bars represent SD of 2 replicates.

6.2.5 Effect of photodynamic therapy on cancer cells

The duramycin-porphyrin conjugate was used in the photodynamic treatment of the ovarian cancer cell lines A2780 and SK-OV-3 and the pancreatic cancer cell lines AsPC-1 and MIA PaCa-2. Briefly, cells ($8x10^5$) were incubated with either capped porphyrin control, unconjugated duramycin or duramycin-porphyrin conjugate at concentrations 0.5 µM-10 µM in the dark for 5 minutes. Concentrations >10 µM had been previously demonstrated to induce necrotic cell death of the cancer cell lines mentioned above and the normal endothelial cell line HUVECs (Chapter 3). As targeted death of the tumour cells by light irradiation was the aim of this experiment concentrations above 10 µM were not used. Once cells were washed, centrifuged and re-suspended cells ($8x10^4$) were transferred to the wells of a 96 well sterile tissue culture plate and incubated for 5 minutes. The drug treated cancer cells were then irradiated with a light dose of 7.5 J/cm^2. A dark control (non-irradiated) plate was performed alongside each irradiated plate. After light treatment the plates were incubated for 24 hours before a MTT assay was performed to determine cell proliferation. Cell proliferation was calculated as a percentage of the untreated control cells. All drug dilutions were performed in quadruplicate as biological replicates and each assay in triplicate as technical replicates.

The duramycin-porphyrin conjugate, when irradiated, reduced the cell proliferation of all 4 cancer cell lines in a concentration dependent manner (figure 6.11). A significant difference in the effect on cell proliferation between the irradiated and non-irradiated conjugate conditions occurred at 0.5 µM for SK-OV-3 ($p = 0.04$), 2.5 µM for AsPC-1 ($p = 0.02$) and 5 µM for A2780 ($p = 0.03$) (Student's T Test, significance $p < 0.05$). At these concentrations the reduction in cell proliferation of the non-irradiated and irradiated conjugate treated cells was 65.9±2.4% and 17.7±26.9% for A2780, 86.4±4.9% and 6.3±2.4% for AsPC-1 and 95.5±3.9% and 86.9±3.8% for SK-OV-3, respectively. MIA PaCa-2 exhibited a lower sensitivity than the other cancer cell lines as the difference between the irradiated and non-irradiated conditions, which occurred at 5 µM, was not found to be statistically significant ($p = 0.32$). Additionally the highest concentration of conjugate (10 µM) reduced cell proliferation to only 36.3±13.4%. At the highest concentration (10 µM) cell proliferation was reduced to 3.2±3.7% in A2780, 1.8±1% in AsPC-1 and 2.7±2.2% in SK-OV-3. Thus, differences in the sensitivity to duramycin-porphyrin conjugate plus PDT light treatment were observed between the cancer cell lines. The duramycin-porphyrin conjugate showed dark toxicity (it had an effect on cell proliferation when non-irradiated) in A2780, AsPC-1 and SK-OV-3 at concentrations ≥5 µM.

No difference in the effect of unconjugated duramycin on cell proliferation was observed between the irradiated and non-irradiated conditions for all 4 cancer cell lines (figure 6.12). The unconjugated duramycin reduced cell proliferation in a concentration dependent manner >5 μM in all cancer cell lines as was observed previously (Chapters 3 and 4). The highest concentration of unconjugated duramycin (10 μM) reduced cell proliferation to 78.1±2.7% in A2780, 48.7±20.2% in AsPC-1, 40.3±16.3% in MIA PaCa-2 and 60.6±7.2% in SK-OV-3. The irradiated duramycin-porphyrin conjugate had a significantly enhanced cytotoxic effect over the unconjugated duramycin at 2.5 μM for A2780 ($p = 0.04$) and AsPC-1 ($p = 0.03$) and at all concentrations (0.5-10 μM) for SK-OV-3 ($p = 0.04$). The effect of the irradiated conjugate was not significantly different to the unconjugated duramycin for MIA PaCa-2 cells ($p = 0.91$).

The capped porphyrin control (unconjugated porphyrin) showed no dark toxicity in any of the 4 cancer cell lines (figure 6.13). However, when the cells were irradiated the capped porphyrin control at 10 μM reduced the cell proliferation of AsPC-1, MIA PaCa-2 and SK-OV-3. The cell proliferation of A2780 was significantly reduced when treated with irradiated capped porphyrin control at concentrations ≥5 μM ($p = 0.01$) compared to the non-irradiated control. At the highest concentration (10 μM) the irradiated capped porphyrin control reduced the cell proliferation of A2780 to 12.8±9.3%. This was not statistically significantly different to the effect of the irradiated duramycin-porphyrin conjugate ($p = 0.68$).

In summary, the cell proliferation of the ovarian cancer cell lines A2780 and SK-OV-3 and the pancreatic cancer cell line AsPC-1 was significantly affected by photodynamic treatment with duramycin-porphyrin conjugate (figure 6.14). The increased cytotoxic effect of duramycin-porphyrin conjugate plus irradiation over the other drug and irradiation conditions was most evident in AsPC-1 and SK-OV-3. While this effect was also shown in A2780 cells the irradiated capped porphyrin control showed similar levels of cytotoxicity as the irradiated conjugate at concentrations ≥5 μM. Reduction in cell proliferation of MIA PaCa-2 in conjugate treated cells was not statistically significantly different between the irradiated and non-irradiated conditions or compared to the unconjugated duramycin.

a)

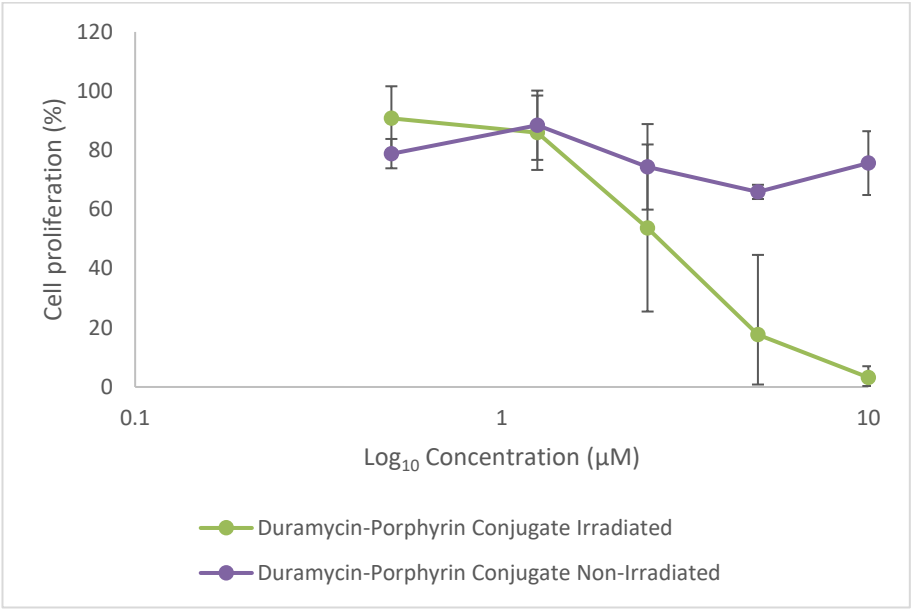
120
100
80
60
40
20
0
Cell proliferation (%)
0.1
1
10
Log10 Concentration (µM)
Duramycin-Porphyrin Conjugate Irradiated
Duramycin-Porphyrin Conjugate Non-Irradiated

b)

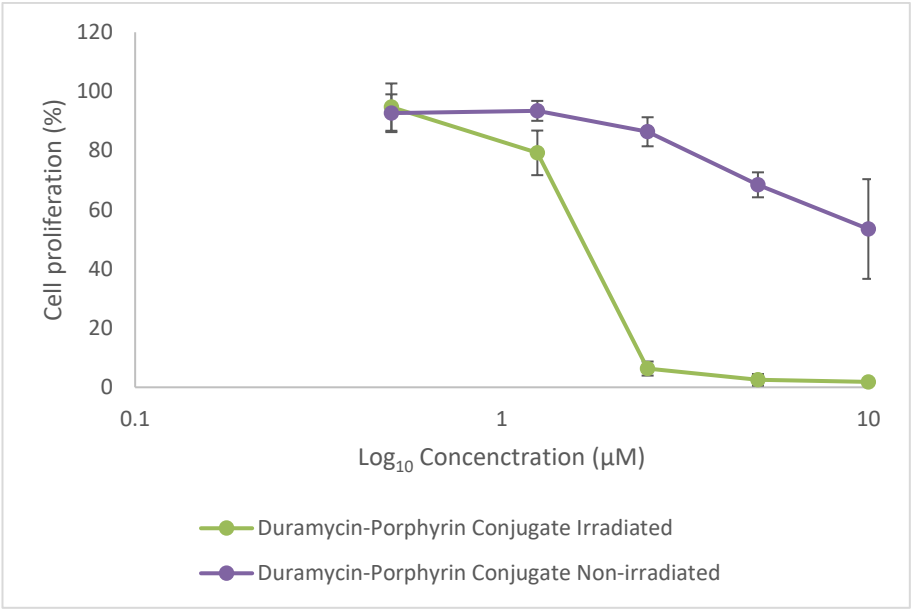
120
100
80
60
40
20
0
Cell proliferation (%)
0.1
1
10
Log10 Concenctration (µM)
Duramycin-Porphyrin Conjugate Irradiated
Duramycin-Porphyrin Conjugate Non-irradiated

c)

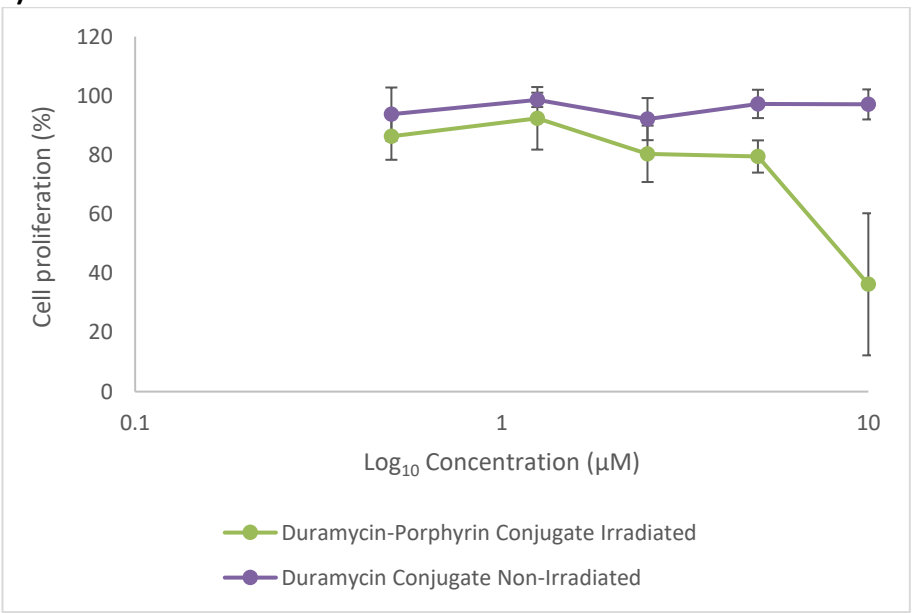
120
100
80
60
40
20
0
Cell proliferation (%)
0.1
1
10
Log10 Concentration (µM)
Duramycin-Porphyrin Conjugate Irradiated
Duramycin Conjugate Non-Irradiated

d)

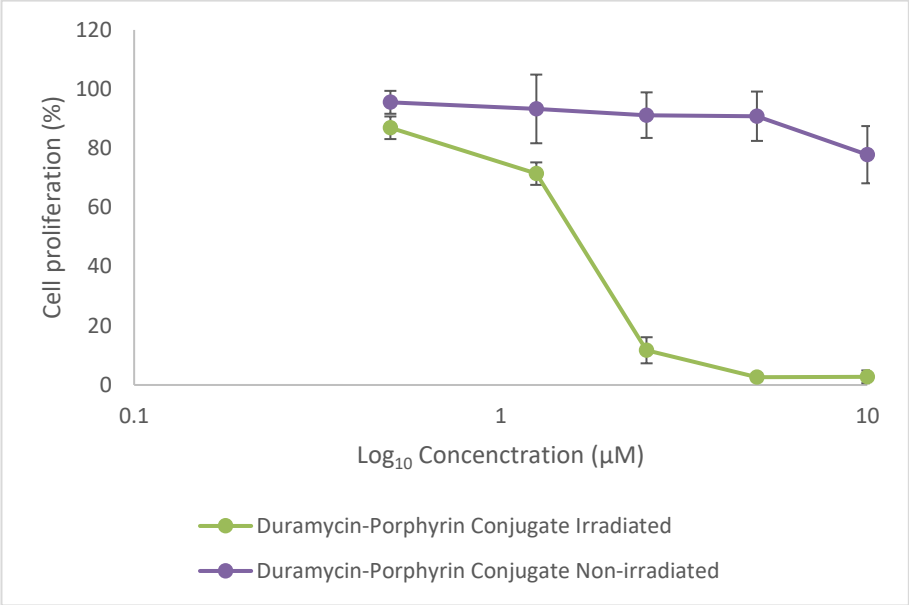

Figure 6.11: The effect of duramycin-porphyrin conjugate plus photodynamic light treatment on cancer cells.

A significant difference in reduction in cell proliferation between the irradiated and non-irradiated conjugate treated cells occurred at 0.5 µM for d) SK-OV-3, 2.5 µM for b) AsPC-1 and 5 µM for a) A2780. For c) MIA PaCa-2 this difference occurred at 5 µM though was not statistically significant. The highest concentration (10 µM) reduced cell proliferation to <3.2% in A2780, AsPC-1 and SK-OV-3 and 36.3% in MIA PaCa-2. Error bars represent SD of 3 independent experiments with 4 biological replicates.

a)

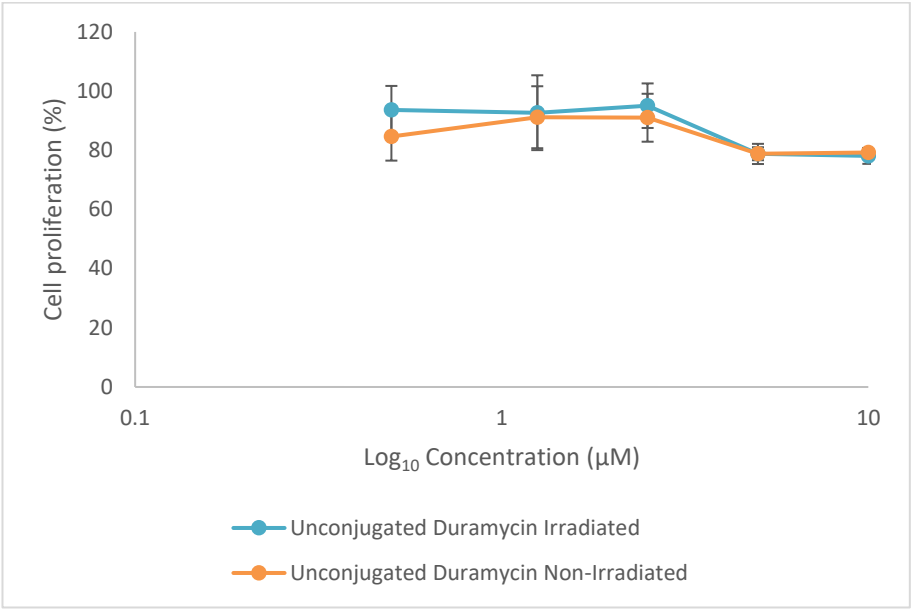
120
100
80
60
40
20
0
Cell proliferation (%)
0.1
1
10
Log10 Concentration (µM)
Unconjugated Duramycin Irradiated
Unconjugated Duramycin Non-Irradiated

b)

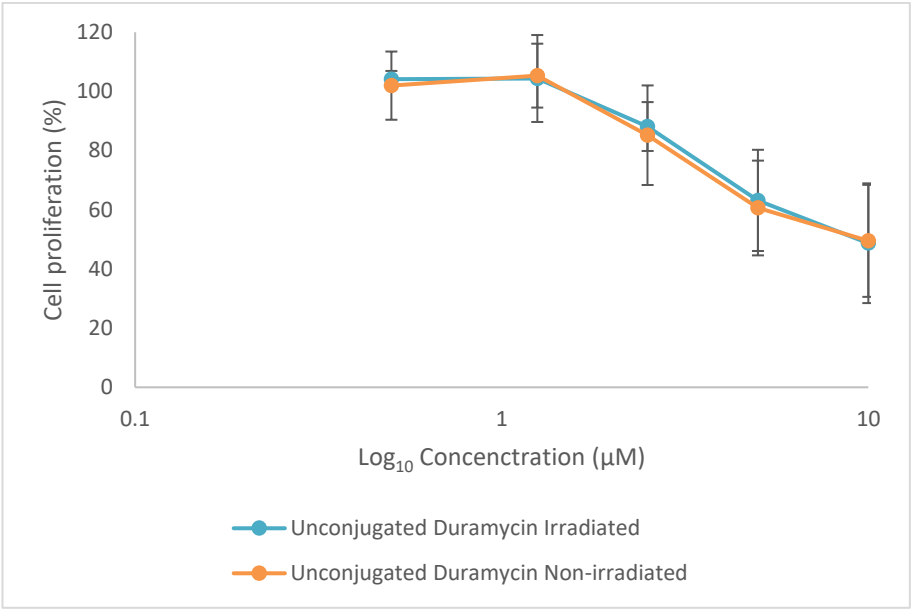
120
100
80
60
40
20
0
Cell proliferation (%)
0.1
1
10
Log10 Concenctration (µM)
Unconjugated Duramycin Irradiated
Unconjugated Duramycin Non-irradiated

c)

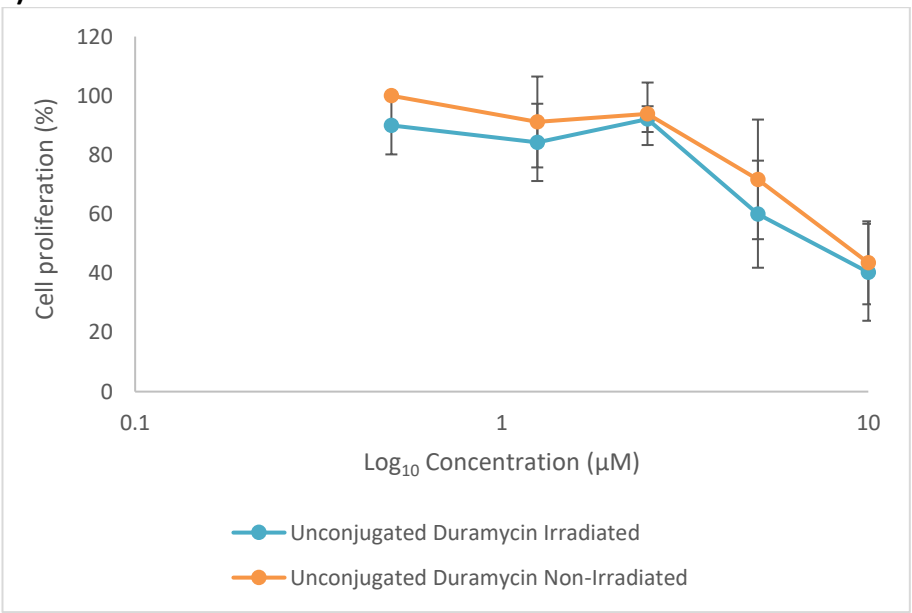
120
100
80
60
40
20
0
Cell proliferation (%)
0.1
1
10
Log10 Concentration (µM)
Unconjugated Duramycin Irradiated
Unconjugated Duramycin Non-Irradiated

d)

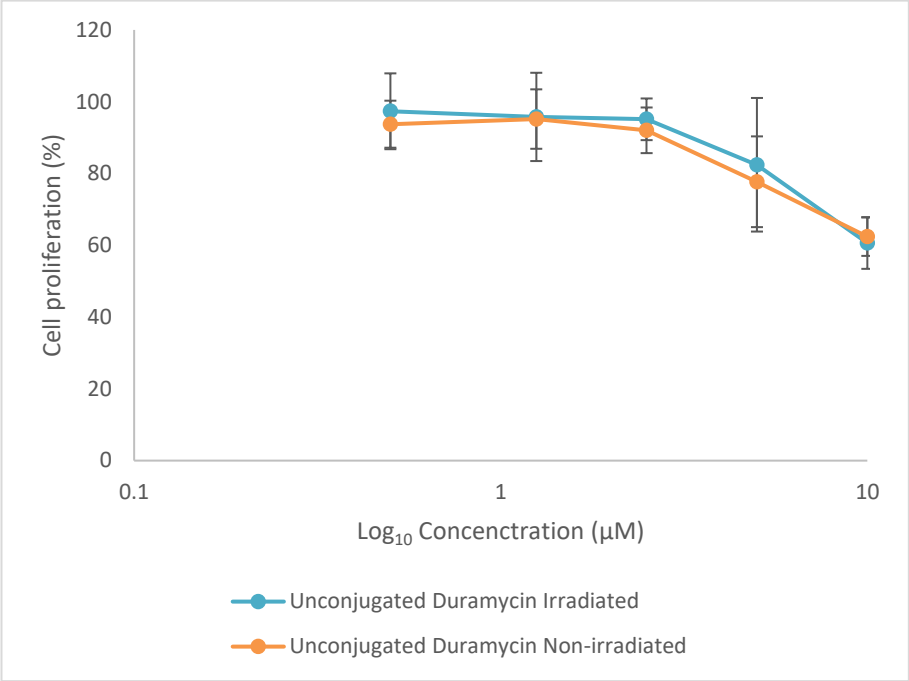

Figure 6.12: The effect of unconjugated duramycin plus photodynamic light treatment on cancer cells.

There was no difference in percentage cell proliferation between the irradiated and non-irradiated unconjugated duramycin treated cells. The unconjugated duramycin reduced cell proliferation in a concentration dependent manner in the cancer cell lines a) A2780, b) AsPC-1, c) MIA PaCa-2 and d) SK-OV-3. Error bars represent SD of 3 independent experiments with 4 biological replicates.

a)

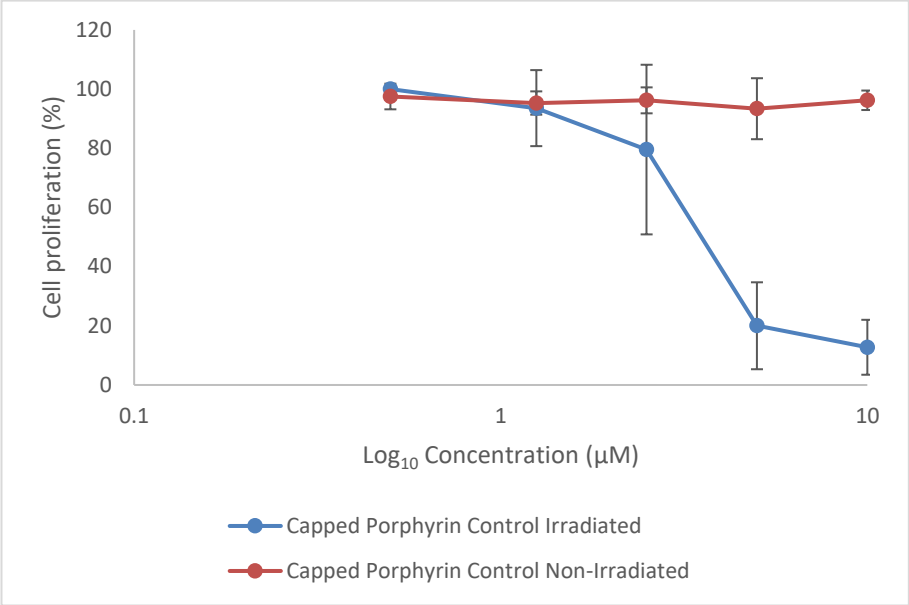
120
100
80
60
40
20
0
Cell proliferation (%)
0.1
1
10
Log10 Concentration (µM)
Capped Porphyrin Control Irradiated
Capped Porphyrin Control Non-Irradiated

b)

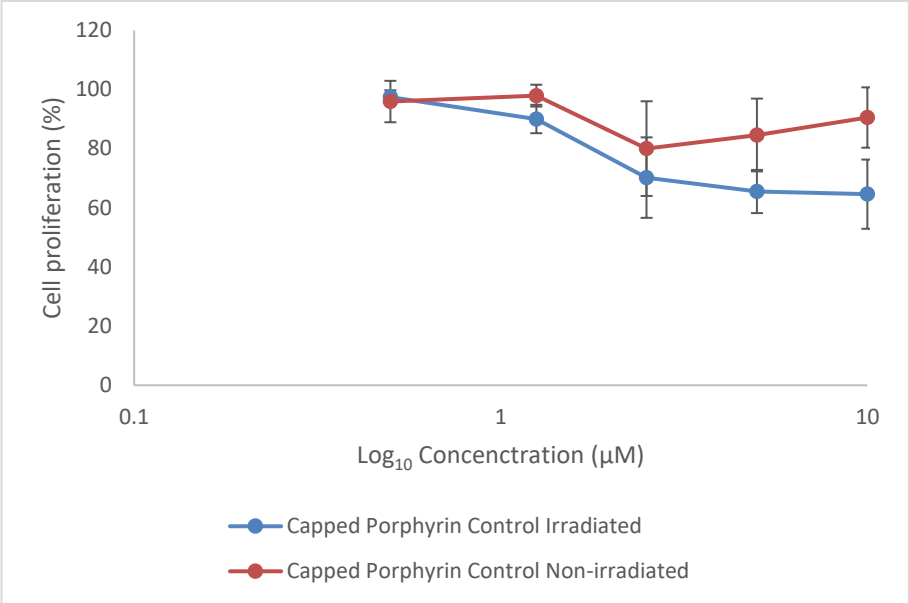
120
100
80
60
40
20
0
Cell proliferation (%)
0.1
1
10
Log10 Concenctration (µM)
Capped Porphyrin Control Irradiated
Capped Porphyrin Control Non-irradiated

c)

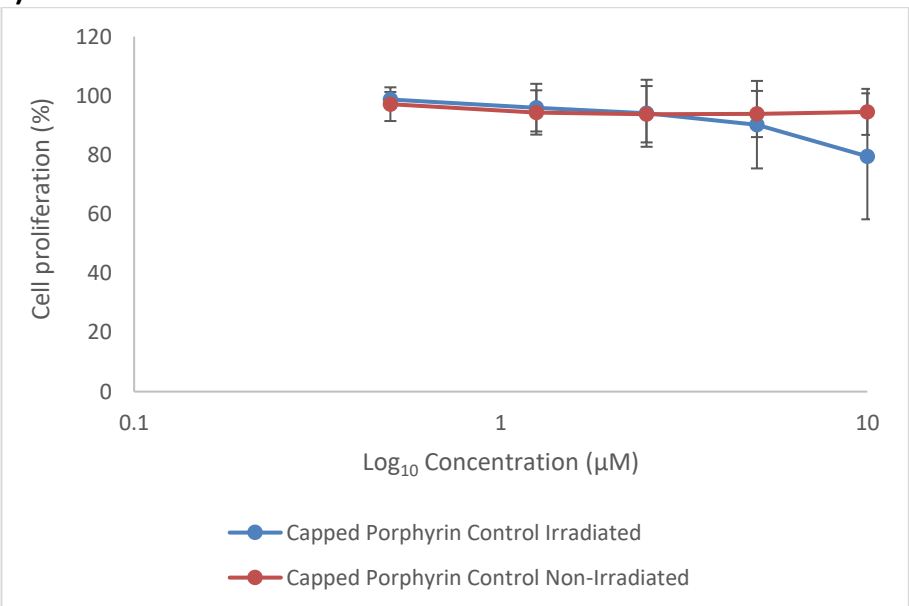
120
100
80
60
40
20
0
Cell proliferation (%)
0.1
1
10
Log10 Concentration (µM)
Capped Porphyrin Control Irradiated
Capped Porphyrin Control Non-Irradiated

d)

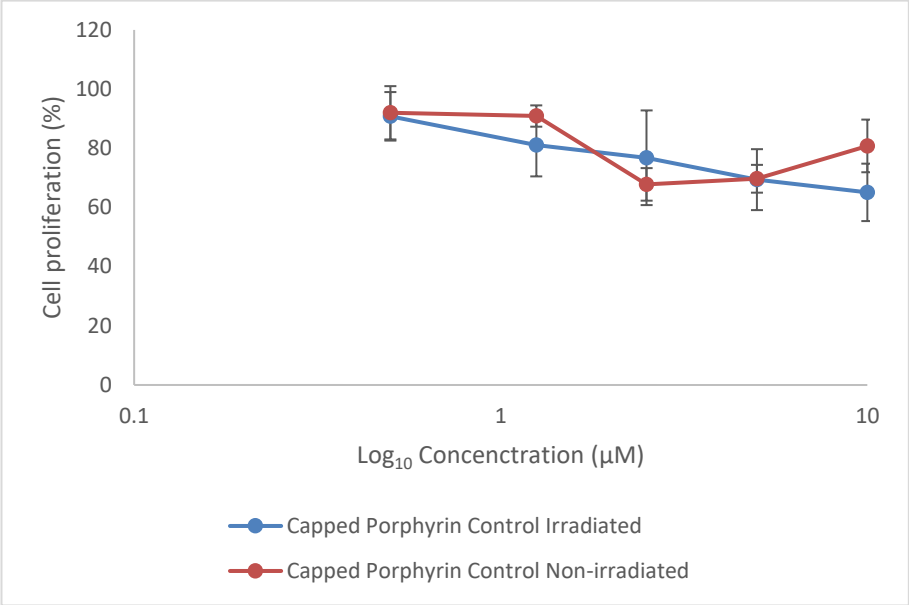

Figure 6.13: The effect of capped porphyrin control plus photodynamic light treatment on cancer cells.

a) Dark toxicity was not seen with the capped porphyrin control in A2780 however the irradiated capped porphyrin reduced cell proliferation at concentrations ≥5 µM. The irradiated capped porphyrin control reduced cell proliferation at 10 µM in b) AsPC-1, c) MIA PaCa-2 and d) SK-OV-3 cells. Error bars represent SD of 3 independent experiments with 4 biological replicates.

a)

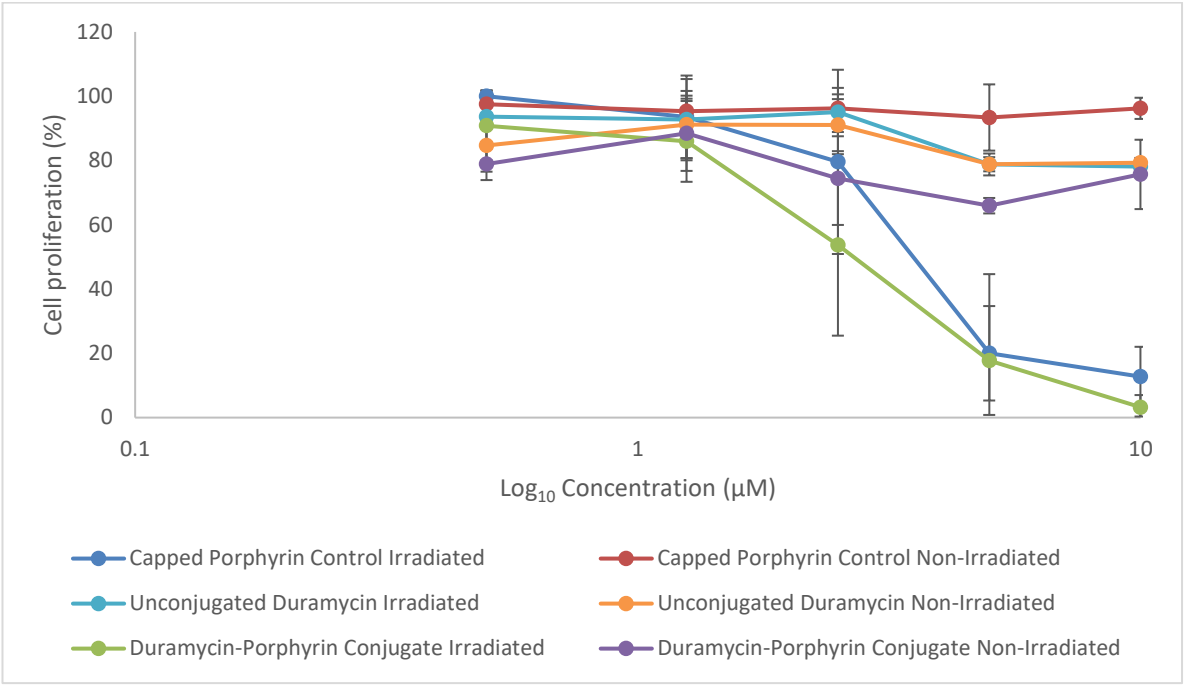
120
100
80
60
40
20
0
Cell proliferation (%)
0.1
1
10
Log10 Concentration (µM)
Capped Porphyrin Control Irradiated
Capped Porphyrin Control Non-Irradiated
Unconjugated Duramycin Irradiated
Unconjugated Duramycin Non-Irradiated
Duramycin-Porphyrin Conjugate Irradiated
Duramycin-Porphyrin Conjugate Non-Irradiated

b)

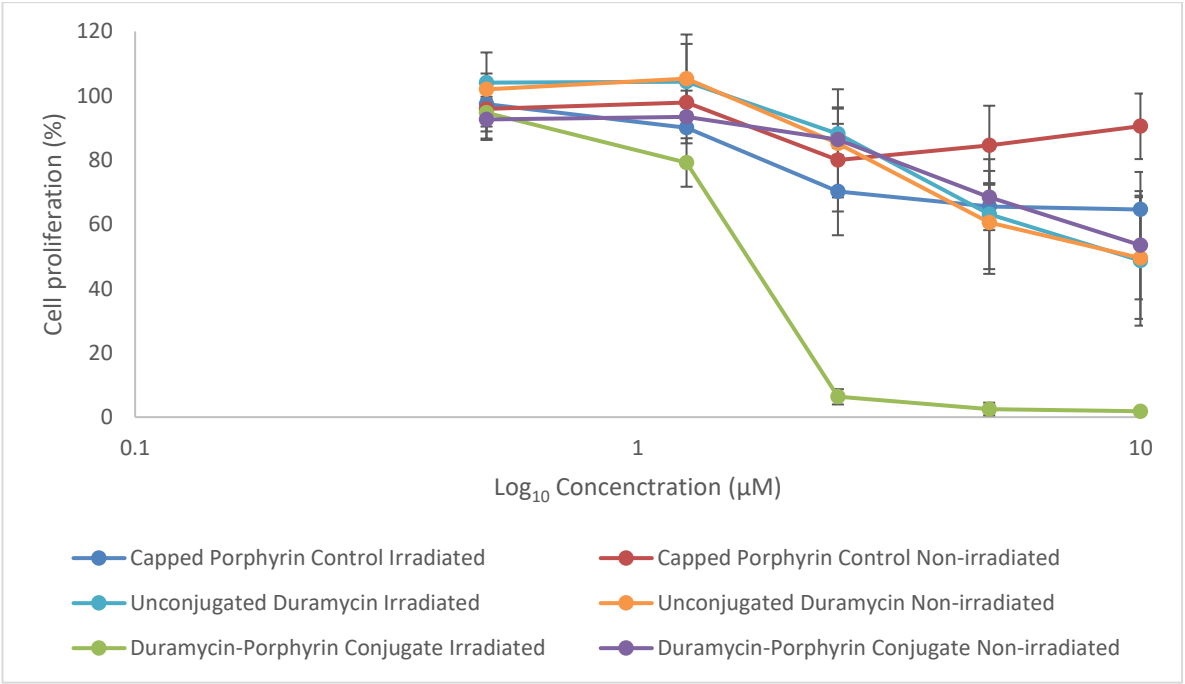
120
100
80
60
40
20
0
Cell proliferation (%)
0.1
1
10
Log10 Concenctration (µM)
Capped Porphyrin Control Irradiated
Capped Porphyrin Control Non-irradiated
Unconjugated Duramycin Irradiated
Unconjugated Duramycin Non-irradiated
Duramycin-Porphyrin Conjugate Irradiated
Duramycin-Porphyrin Conjugate Non-irradiated

c)

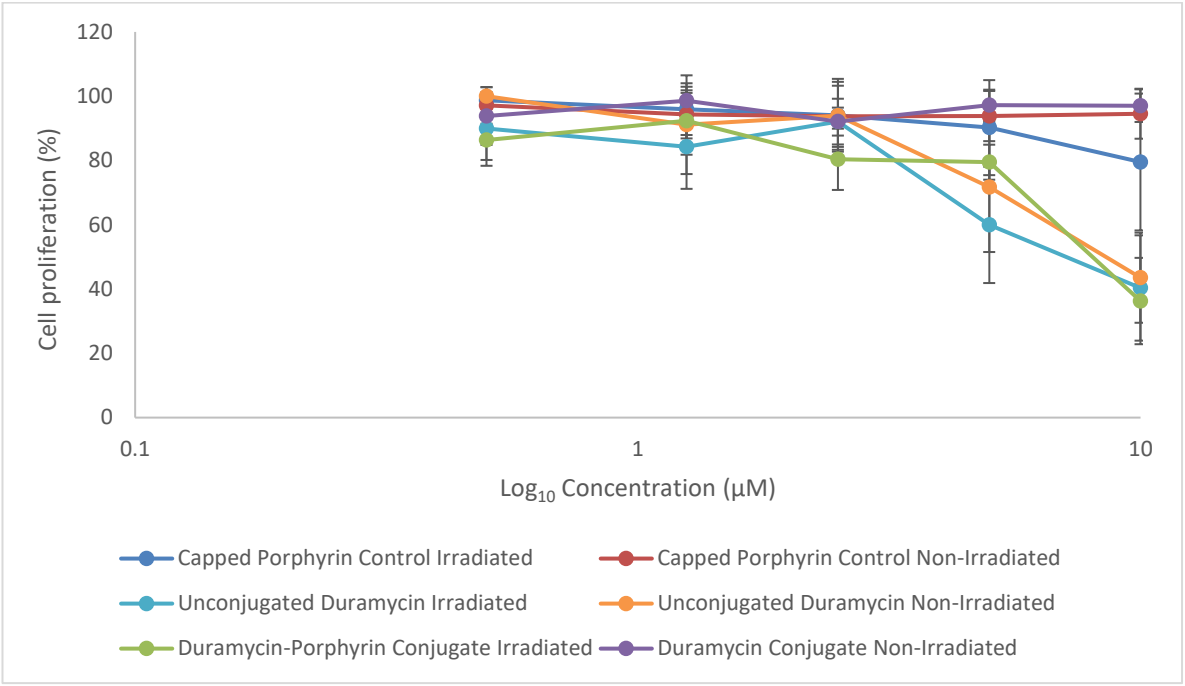

d)

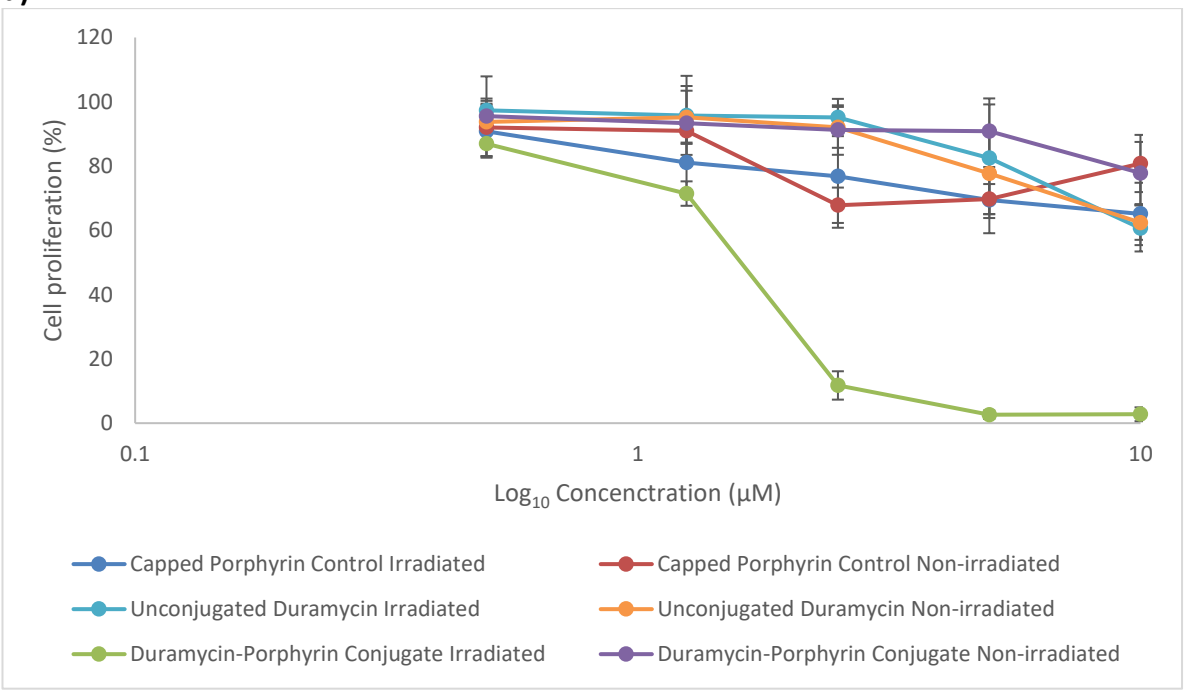

Figure 6.14: PDT Treatment of ovarian and pancreatic cancer cell lines.

The irradiated duramycin-porphyrin conjugate had an enhanced cytotoxic effect on the cell proliferation of a) A2780, b) AsPC-1 and d) SK-OV-3 compared to non-irradiated conjugate. No statistically significant difference was observed in c) MIA PaCa-2 between the irradiated and non-irradiated conjugate conditions or between the duramycin-porphyrin conjugate and unconjugated duramycin. The capped porphyrin control had a similar effect on cell proliferation as the irradiated conjugate for a) A2780. Error bars represent SD of 3 independent experiments with 4 biological replicates.

6.3 Discussion

The use of PDT as an anti-cancer therapy has been approved for a variety of cancer types[119, 128-131]. The aim of PDT is to bring about specific cytotoxic damage to tumours through the delivery of a photosensitising agent and light irradiation. However, the main drawback that has been faced in PDT with regards to oncology has been a low selectivity of PhtS to their target tumour tissue over surrounding normal tissue. This has resulted in phototoxic damage to the normal tissue and prolonged skin photosensitivity[119]. In an effort to overcome this research in PDT has focused on the development of PhtS conjugated to tumour targeted biological molecules[120]. The aim of this study was to produce a PhtS that could selectively bind to cancer cells through their cell surface PE expression and subsequently have an anti-cancer effect when irradiated. It had been demonstrated that duramycin concentrations ≤2.5 μM did not have an effect on cancer cell lines but could still reliably bind to PE and be detected by flow cytometry (Chapter 3). Therefore it was hypothesised that relatively low concentrations of duramycin (<2.5 μM) could possibly have an anti-cancer effect when light irradiated yet remain non-toxic to cancer cells when non-irradiated. It was also hypothesised that the duramycin-porphyrin conjugate could conceivably have an enhanced anti-cancer effect over unconjugated duramycin and the unconjugated capped porphyrin control.

A number of PhtS have been successfully developed through the conjugation of tetrapyrrole molecules such as porphyrins to biological molecules including mAbs[154, 250, 251], lipoproteins[155], nanoparticles[156] and polypeptides[15]. Tetrapyrroles are very efficient at undergoing intersystem crossing (ISC)[121]. A high ISC yield, a high possibility of conversion from the excited singlet state to the longer lived excited triplet state, from which energy transfers to ground state (triplet) oxygen, is an important property of any good PhtS[120]. An advantage of conjugating tetrapyrroles to peptides is that their relatively small size allows for good tissue penetration and usually renders them non-immunogenic[15]. The PhtS used in this study was the porphyrin 5-[4-(N-succinimidyloxycarbonyl)phenyl]-10,15,20-tris(4-methylpyridinium) porphyrin trichloride[151]. This porphyrin had previously been shown to exhibit antibacterial properties, be an efficient cytotoxic after 5 minutes of light treatment and be stable against photodegradation[151]. Furthermore, it had been shown that the conjugation procedure used with this porphyrin does not produce reactive intermediates or by-products[153, 154]. A number of biological molecules conjugated to porphyrin through lysine residues have been shown to retain their function. Poly(lysine) was reacted with a selection of porphyrins which were able to inactivate *Staphylococcus aureus* and

Escherichia coli after 30 minutes of light treatment and had no dark toxicity[151]. Porphycenes (electronic isomers of porphyrins) conjugated to poly(lysine) retained their phototoxic effect and were active against *E. coli*, methicillin resistant *S. aureus*, *Candida albicans* and *Acholeplasma laidlawii*[252]. The scFv antibody fragment LAG-3 when conjugated through its lysine residues to a porphyrin PhtS was shown to bind to the colorectal cancer cell line Caco-2 and effectively induce cell death following 15 J/cm^2 light treatment[154].

However, conjugation of porphyrins to peptides can be chemically challenging due to the requirement of bringing the two moieties together regioselectively whilst maintaining their separate functionalities[15]. Under the correct conditions many regions of a peptide may be nucleophilic including the N-terminal amino residue, cysteine's thiol group, lysine's ε-amino group and the hydroxyl group of serine, threonine and tyrosine[15]. Therefore, if reaction conditions are not controlled the conjugation can result in i) the joining of the porphyrin to an undesired residue, ii) multiple conjugations with other groups with comparable reactivity or iii) cross-linked structures due to possible multiple binding sites within the porphyrin[15]. In this study, to target the desired residue (the ε-amino group on the lysine residue positioned near to duramycin's N-terminal) a carboxylate group on the porphyrin molecule was activated with an *N*-hydroxysuccinimide (NHS) ester. NHS esters are highly amine-reactive and form stable amide bonds primarily with lysine's ε-amino group and the α-amino group of the N-terminal residue under physiological or slightly alkaline pH (pH 7.2-9)[253]. NHS esters can also cross-link with serine, threonine and tyrosine however this is unlikely to have occurred with the duramycin-porphyrin conjugate due to the much weaker nucleophilicity of these amino acids[254]. As the NHS ester was non-sulphonated, causing it to be water insoluble, the reaction was performed in the water miscible organic solvent DMSO. Trimethylamine (TEA) was added to the reaction to produce a pH of pH 9, provide a base in the non-aqueous DMSO solution and catalyse the reaction between the NHS and lysine[151]. In addition to the reaction conditions used the structure of duramycin meant it was reasonable to presume that the desired location for conjugation was achieved. The only exposed reactive functionality on duramycin is the ε-amino group of the N-terminal lysine residue as the α-amino group of the lysine and the amino terminus itself is folded inside the peptide's structure, thus hindering reaction with porphyrin. The amine groups of the other lysine present in duramycin are involved in bonds with other residues. This is supported by the structure of duramycin B, which differs from duramycin by one amino acid at residue 2, presented by Zimmerman *et al*.[66] which clearly showed that the peptide's terminals were hindered within its structure. Additionally, the

conjugation of the porphyrin to duramycin at this chosen location was likely to have minimised interference with the PE binding site[68]. HPLC analyses of the purified duramycin-porphyrin conjugate rendered a single peak at R_t = 6.20 minutes which was confirmed as the conjugate by both ESI:MS and LCMS. If a cross-linked structure, whereby 2 porphyrin molecules had bonded to duramycin, had occurred the HPLC and MS traces would most probably have shown 2 separate peaks corresponding to the single bound porphyrin and the cross-linked structure. The mass found for the isolated conjugate would have also been greater. Therefore it was highly likely that the duramycin-porphyrin conjugate had a 1:1 binding ratio of 1 duramycin: 1 porphyrin.

An essential part in the development of a targeted therapeutic is verifying the delivery of the drug to the desired target[120]. In this study, the duramycin-porphyrin conjugate was used to detect cell surface PE expression on ovarian cancer cell lines A2780 and SK-OV-3 and pancreatic cancer cell lines AsPC-1 and MIA PaCa-2 by flow cytometry. The conjugate was able to detect PE expression on all 4 of the cancer cell lines in a concentration dependent manner where optimal PE detection occurred at 1 mM. Optimal PE detection with unconjugated duramycin on the same cancer cell lines was similarly shown at the 1 mM concentration (Chapter 3). In addition to showing that the duramycin-porphyrin conjugate could bind to its target (PE on cancer cell surfaces) it was also shown herein that the fluorescence of the porphyrin component had not been affected by the conjugation procedure. This was supported when it was shown that the unconjugated duramycin could not displace pre-bound duramycin-porphyrin conjugate from PE expressing cancer cell lines. The median PE fluorescence detected by the duramycin-porphyrin conjugate was seen to remain constant for MIA PaCa-2 over a 30 minute time course and slightly increased for A2780. Additionally, both unconjugated duramycin and the duramycin-porphyrin conjugate had the ability to increase the FSC and SSC of the cancer cell lines A2780, AsPC-1, MIA PaCa-2 and SK-OV-3 albeit at slightly different concentrations. The higher concentration of conjugate required to exert effect on the cancer cell lines light scattering properties is potentially beneficial for PDT treatment as minimisation of non-targeted damage is a desired characteristic of PhtS[145].

The literature reports a number of studies that have investigated the effect of PDT on ovarian and pancreatic cancer in a variety of models including cell lines[132], 3D cell culture[133-135], transplanted mice[137, 138] and Phase I/II human trials[139, 140]. A panel consisting of the pancreatic cancer cell lines AsPC-1, BxPC-3, Capan-1, Capan-2 and PANC-1 was subjected

to photodynamic light treatment using the benzoporphyrin derivative (BPD) PhtS verteporfin[132]. Though cytotoxic response to the photodynamic treatment was cell line specific a dose of ~6 μM·J/cm^2 was effective enough to induce almost complete cell death in all of the cell lines. The high expression of the anti-apoptotic factor Bcl-XL in the AsPC-1 cells was shown to decrease in response to the treatment and a shift towards pro-apoptotic factors (Bax) occurred. Another BPD PhtS was used in the photodynamic treatment of OVCAR5 ovarian carcinoma 3D cell cultures[133, 134]. Reduction in the cell viability and volume of the 3D cell cultures occurred with 0.25 μM BPD at a light dose of 10 μM·J/cm^2. Fluorescent imaging showed that the PhtS penetrated the whole of the 3D cultures and uptake of the PhtS increased in a concentration dependent relationship. In a study where OVCAR5 cells were grown at high density in a culture film the PhtS pheophorbide-*a* and a supply of sensitised oxygen gas was delivered by a fibre optic system[135]. Irradiation of the *in vitro* cell cultures for 1 hour reduced their cell viability by 60±5%. This delivery of flowing oxygen along with PhtS and light treatment to the tumour environment was theorised to be a promising treatment for difficult to reach hypoxic tumours in the peritoneal cavity. An immunoconjugated PhtS (Ce-6-OC125), a mAb which recognised the antigen CA125 expressed on 80% of non-mucinous cancers, was used in the photodynamic treatment of OVCAR3 transplanted Balb C mice[137]. The median survival of control mice was lower (38.5 days) than mice which received 3 or 4 courses of PDT treatment (47.5 and 58 days, respectively). Necropsies of the mice showed that 89% of the control animals died with large ascites and tumour burden compared to only 27% of the PDT treated animals. A phase I trial involving 16 patients with adenocarcinoma was conducted with Foscan® and percutaneous delivery of light treatment. Extensive areas of necrosis in the pancreatic tumours were imaged in all patients. PDT treatment with verteporfin was used in 15 patients with locally advanced pancreatic cancer in a Phase I/II trial[140]. When treated with a light dose of 40 J/cm lesions, 12 mm in length, were consistently seen however the volume of necrosis within the tumours varied considerably between patients (range 0-23 cm^3, mean 3.5 cm^3). Therefore, the literature had extensively shown that PDT could be a promising anti-cancer therapy in the treatment of ovarian and pancreatic cancers.

In this study, the ovarian cancer cell lines A2780 and SK-OV-3 and the pancreatic cancer cell lines AsPC-1 and MIA PaCa-2 were treated with the newly developed PhtS, duramycin-porphyrin conjugate. Reduction in cell proliferation after duramycin-porphyrin conjugate treatment and irradiation with 7.5 J/cm^2 red light occurred in all 4 cancer cell lines in a concentration dependent manner. A statistically significant difference in the effect on cell

proliferation between the non-irradiated and irradiated conjugate occurred at 0.5 µM for SK-OV-3, 2.5 µM for AsPC-1 and 5 µM for A2780 (Student's T Test, significance $p < 0.05$). Though there was a trend that the irradiated conjugate >5 µM had a greater effect than the non-irradiated conjugate on MIA PaCa-2 no statistically significant difference was observed between the irradiated and non-irradiated conditions. Treatment with 10 µM conjugate plus irradiation was effective enough to reduce cell proliferation to <3.2% in A2780, AsPC-1 and SK-OV-3. However, cell proliferation in MIA PaCa-2 was only ever reduced to 36.3% at the highest concentration. Additionally, reduction in cell proliferation of MIA PaCa-2 by the duramycin-porphyrin conjugate was not statistically significantly different to the unconjugated duramycin. The lower sensitivity of MIA PaCa-2 may mean that this cancer cell line is not a candidate for PDT using the duramycin-porphyrin conjugate. Out of the 2 pancreatic cancer cell lines used in this study MIA PaCa-2 is the less aggressive form. Samkoe *et al.*[138] discovered that the aggressive, fast growing pancreatic cancer cell line AsPC-1 responded better to verteporfin PDT than the less aggressive cell line, PANC-1, in transplanted mice. A light dose of 40 J/cm induced complete vascular occlusion in the tumours of AsPC-1 transplanted mice but not so in PANC-1. It was concluded that this difference in reaction to light treatment between cell lines could depend on tumour aggressiveness and other inherent biophysical properties. It has been observed in human trials that differences in response to light treatment are of clinical importance where light dose can raise different reactions in patients even when the same type of malignancy is being treated[139, 144]. Foscan®-PDT successfully induced tumour necrosis in patients with pancreatic adenocarcinoma however response to treatment varied between patients with areas of necrotic tumour tissue ranging from 9 to 60 cm^3 (median 36 cm^3)[139]. In a Phase II trial involving PDT isotropic light detectors were placed into subjects peritoneal cavity to measure the real-time light dose that tumours received to ensure a uniform dose was delivered[144]. Differences in the measured dose were seen between the 2 forms of detector used. It was concluded that the main reason for this was variability in the optical properties of tissues which can be affected by PhtS and oxygen concentration present in a specific part of tissue at a specific time point. Therefore the optical properties of tissues can vary within the tissue and at different time-points along the course of PDT treatment making uniform reaction to treatment difficult to achieve[120]. Thus, differences in sensitivity to PDT treatment observed between cell lines *in vitro* could potentially be important when transferring future work to *in vivo* study.

The capped porphyrin control when irradiated slightly reduced the cell proliferation of AsPC-1, SK-OV-3 and MIA PaCa-2 at 10 µM. This capped porphyrin control was also used in PDT experiments with prostate epithelial cells taken from patients with benign prostatic hyperplasia and prostate cancer[150]. Concentrations of the capped porphyrin >8.75 µM induced necrosis and prevented colony forming in the irradiated prostate cells. In this study, it was seen in A2780 that the capped porphyrin control produced statistically similar levels of reduced cell proliferation to the irradiated conjugate. An explanation for this could be that there was an increased uptake and localisation of the capped porphyrin control in this cancer cell line. However, DNA damage in the prostate cells in the above study, which suggested localisation occurred in the nucleus, was induced after 1 hour incubation with the porphyrin[150]. This movement into the cell and localisation of the capped porphyrin is unlikely to have occurred in the A2780 cells in the relatively short 5 minute incubation period used in this study. Free (unconjugated) PhtS tend to reduce cell proliferation to some extent as all current clinical PDT agents are non-targeted[149]. Reported studies have shown a reduction in cell viability when treated with free PhtS however phototoxic potential is often not equal to the conjugated version. For example, the Ce-6-17.1a immunoconjugate when irradiated reduced the cell survival of HT29 colorectal cancer cells by 90% whereas the equivalent free Ce-6 reduced it by only 35%[251]. Similarly this was seen when a Ce-6-LDL conjugate reduced cell proliferation of Y79 cells by 80% compared to the 10% seen by free Ce-6[155]. However, due to the lack of selectivity, large doses of unconjugated PhtS are often required to exert effect in tissue[152]. Therefore when translated to the *in vivo* environment relatively small doses of free PhtS may become diluted. Biodistribution of free Foscan® in nude mice bearing head and neck xenografts (HNX-OE) showed a random distribution in organs and no specific tumour uptake[250]. Thus irradiated A2780 tumours *in vivo* may not experience an anti-cancer effect from the capped porphyrin control and an enhanced effect of the duramycin-porphyrin conjugate over the capped control could potentially be observed.

The differences in sensitivities to photodynamic treatment between the cancer cell lines could potentially be explained by the various cytoprotective mechanisms that cancer cells can employ to evade PDT induced cell death. Detoxifying enzymes involved in ROS metabolism such as superoxide dismutase (SOD) present in cancer cells have been implicated in the protection against PDT effects[119, 255]. For example, SOD2 is an antioxidant enzyme located in the mitochondrial matrix where it catalyses the dismutation of superoxide radicals into H_2O_2 and O_2[256] and thus can remove some of the more cell

damaging ROS produced by photodynamic treatment. Inhibition of SOD2 resulted in a synergistic effect on the reduction in cell viability in PDT treated pancreatic cancer cells (HPAC, HPAF-II, PANC-1)[255]. Other cytoprotective mechanisms have been demonstrated to be induced by PDT itself including; i) initiation of stress-related transcription factors e.g. hypoxia-inducible transcription factor-1 (HIF-1) and nuclear factor erythroid 2-related factor 2 (NRF2), ii) increased heat shock protein (HSP) levels e.g. elevated HSP60 and HSP70 have been seen to be inversely correlated with PDT sensitivity and iii) activation of NF-κB which can lead to apoptosis supression[119]. There are many other mechanisms for evading cell death that PDT or ROS production can induce, the above have been highlighted as the literature has reported that some of these protective mechanisms are active in the ovarian and pancreatic cancer cell lines used in this study.

The theory of using PDT as an anti-cancer therapy is to increase the amount of ROS to above the cells tolerance threshold so that cell death is induced[124]. However, if PDT produces sub-lethal doses of ROS cells can suffer from prolonged oxidative stress. In order to restore intracellular redox a number of antioxidant genes and detoxification enzymes can be activated[257]. NRF2 is the principal transcription factor involved in this antioxidant response and many downstream genes are its target including i) antioxidant genes such as SOD1, NAD(P)H dehydrogenase [quinone] 1 (NQO1), heme oxygenase (decycling) 1 (HMOX1) and glutamate-cysteine ligase catalytic subunit (GCLC) and ii) detoxification enzymes such as glutathione S-transferase A3 (GSTA3) and thioredoxin reductase 1 cytoplasmic (TXNRD1)[258]. NRF2 and some of its downstream target genes were found to be overexpressed in cisplatin resistant A2780[259] and SK-OV-3[260]. NRF2 was also found to be overexpressed and transcriptionally active in the AsPC-1 cell line and was associated with its chemotherapeutic drug resistance[261]. Reduction of NRF2 levels resulted in a sensitisation of the AsPC-1 cells to cisplatin and camptothecin treatment. Additionally, siRNA knockdown of NRF2 resulted in the reduced expression of oxidative stress genes in AsPC-1[258]. Thus, while the effect of NRF2 in the cancer cell lines used in this study has not been directly correlated to PDT effect it has been shown to be present in the cell lines. HIF-1, an important transcriptional regulator in the cellular response to oxygen, can accumulate in cells as a response to short term hypoxic conditions produced by PDT-induced ROS. HIF-1-α accumulation can ultimately lead to the activation of genes important in tumour metastasis, progression, angiogenesis, adaptive survival and apoptosis[257, 262]. Induction of hypoxia by exposure to 4% O_2 for 24 hours stimulated production of HIF-1-α in MIA PaCa-2 cells[263]. Introduction of extracellular SOD resulted in the inhibition of the MIA PaCa-2 cells

due to scavenging of ROS and therefore a reversal in hypoxia. Upregulation of HIF-1-α was observed after oxidative stress induced ROS production in SK-OV-3 cells[262]. Also, higher levels of HIF-1-α were seen to accompany the hypoxic state of A2780 cells compared to cells grown in normoxic conditions[264]. NF-κB is a transcription factor family which plays a role in apoptosis suppression, proliferation and HIF-1 activation. It is activated when its inhibitor is degraded by the IκB kinase (IKK) complex. ROS and hypoxia produced by PDT can activate NF-κB through oxidation and hydroxylation of the IKK complex, respectively[257]. Treatment of SK-OV-3 cells with an inhibitor of NADPH oxidase (a source of ROS) and various antioxidants lead to reduced NF-κB activity and subsequently a reduction in cell proliferation[265]. HSPs play a role in pro-survival pathways and can also bind proteins that have been oxidatively damaged[119]. For example, expression of HSP70 in heat treated HL60 leukaemia cells was correlated with reduced PDT-induced apoptosis[266]. HSP70 was found to be overexpressed in a highly invasive population of MIA PaCa-2 cells[267]. Additionally, SK-OV-3 has been shown to have an upregulation of the gene *SOD2* which encodes the antioxidant SOD2 enzyme[256]. It is possible that these mechanisms could be employed by the cancer cell lines used in this study to promote varying degrees of resistance to photodynamic treatment. Importantly however, photodynamic effect usually occurs very close to the localisation of the PhtS[119] and when the PhtS binding site is the plasma membrane necrotic cell death can rapidly follow irradiation. This rapid cell death is theorised to be due to a loss in cell membrane integrity and a consequent depletion of intracellular ATP[268]. The duramycin-porphyrin conjugate binds to cancer cell membranes and thus it is possible that cell death after light irradiation occurs by rapid necrosis. This could potentially reduce the risk of PDT-induced cytoprotective mechanisms.

In conclusion, the duramycin-porphyrin conjugate plus PDT treatment was shown to effectively reduce the cell proliferation of ovarian and pancreatic cancer cell lines. With a relatively low effective concentration (0.5-5 μM) the conjugate offered an enhanced anti-cancer effect over unconjugated duramycin. Duramycin has been shown to effect non-tumour cells such as erythrocytes[59] and HUVECs (Chapter 3). The duramycin-porphyrin conjugate could potentially be used in the targeted delivery of PhtS and duramycin so that cell death occurs in cancer cells and damage to normal cells is limited. This theory would need to be assessed in future work on this project in a suitably statistically balanced study of the effect of the duramycin-porphyrin conjugate on normal cells versus cancer cells.

Chapter 7 Chorioallantoic Membrane Assays

7.1 Introduction

Chick embryo development lasts 21 days before hatching[157]. During this development three extraembryonic membranes are formed which enclose and support the developing embryo. These are the yolk sac, the amnion and the chorioallantoic membrane (CAM) which is formed from the fusing of the chorion and the allantois on the 3rd/ 4th day of incubation[157]. The CAM consists of three layers, the ectoderm, the most exterior layer, is an epithelial layer formed from the chorion. The mesodermal layer is a highly vascularised mesenchyme formed from the allantois. Likewise the endodermal layer is formed from the allantois and is comprised of allantoic epithelium[157]. The CAM is connected to the chick embryo's blood circulation through allantoic arteries and veins which are associated with lymph vessels[158]. The CAM mediates the movement of calcium from the egg shell so that it can be deposited into the chick embryo and yolk[159]. The CAM is also involved in the storage of excretions and in the transport of sodium and chloride from the allantoic sac[158]. By the 16th day of incubation the CAM covers the majority of the yolk sac and becomes tightly pressed against the egg shell membrane where it functions as a gas exchange membrane receiving oxygen and eliminating carbon dioxide.

It has long been established that the CAM of chicken eggs can be used to study transplanted tumours[162, 163, 269] and was first described in the literature over 100 years ago. The CAM provides an excellent model to study tumours as the chick embryos are naturally immunodeficient in the earlier periods of incubation. Chick embryos do not develop an immune system until the 2nd week of incubation when T and B cells are initially detected at the 11th and 12th day of growth, respectively. The chick embryo is not fully immunocompetent until the 18th day of incubation[161]. As the conditions for rejection are not yet developed chick embryos accept the implantation of various tissues from numerous species. The CAM also contains extracellular matrix proteins such as laminin, fibronectin, collagen and integrin $\alpha_v\beta_3$ and so can mimic the physiological tumour environment[22]. When tumour cells are grown on CAM assays they display many *in vivo* characteristics such as angiogenesis, mass development and metastasis[158]. Typically 2-5 days after tumour cells are implanted on the CAM the tumour xenografts form a visible mass and are penetrated by blood vessels that originated from the CAM[157]. The CAM model has been used in oncological studies to investigate the angiogenic and metastatic potential of cancer[22, 164], evaluate novel drug delivery systems[158] and assess anti-cancer agents[165, 270]. Tumour cells

grafted onto the CAM surface can be used as a model for spontaneous metastasis whereby the tumour cells migrate from the original tumour site on the CAM epithelial surface into the mesenchyme where they can actively enter the vasculature and migrate to secondary tissues and organs[157]. Squamous cell carcinoma transplanted onto the CAM surface was shown to form multiple nodules at the site of implantation. The cancer cells were then shown to have metastasised from the implantation site to the chick embryo's eyes, brain, liver and myocardium[164]. Anti-cancer agents can be assessed on the CAM through a number of physiologically relevant delivery routes. Drugs can be applied topically to the CAM, intravenously injected into the CAM blood supply, amnion or yolk sac and intraperitoneally injected within the body of the embryo. Thus drug biodistribution, toxicity, activity and pharmacokinetics can be evaluated[158]. Paclitaxel, an anticancer drug with antiangiogenic properties, loaded into polymer microspheres was applied topically to the CAM and was shown to induce vascular occlusion and inhibit angiogenesis[165].

In studies of photodynamic therapy (PDT) the CAM model has been used to assess the antiangiogenic and anti-cancer potential of photosensitisers (PhtS)[171, 172, 271]. The topical application of a number of different PhtS (5-aminolevulinic acid (ALA), sulfonated chloro-aluminium phthalocyanine ($AlPcS_n$) and lutetium texaphyrin (Lutex)) on the CAM highlighted that a higher percentage of vessel damage occurred in arteries than in venules[173]. A number of different porphycene PhtS, derivatives of porphyrin, were assessed using the CAM[171]. The porphycenes were incorporated into liposomes, used as delivery vehicles, which were then either topically applied to the CAM or injected into the yolk sac. Both topical and systemic application of the porphycene PhtS resulted in penetration into the CAM and, after light irradiation, in blood vessel damage. Non-cancerous tumours were treated with porphycene at 5 μg/G chick embryo body weight and irradiated for 30 minutes. Irradiated tumours were reduced in volume compared to non-irradiated tumours and complete tumour regression occurred at the point of irradiation[171]. Another study that incorporated porphycenes into liposomes showed differences in toxicity *in vitro* and *in vivo*. The proximity to the outer surface of the liposome bilayer determined the toxic effect against PDT treated epithelial cells[172]. However this was not an influential parameter in the effect on blood vessel damage in PDT treated CAM models. Thus the CAM model can be employed to perform cheap and fast evaluation of differences in drug delivery mechanisms and PDT effect between *in vitro* and *in vivo* models.

The CAM model has also been used as a tool to assess the diagnostic abilities of fluorescent agents against tumour cells[272, 273]. Chlorin e6 (Ce-6) encapsulated in a polyvinylpyrrolidone (PVP) carrier was applied topically to the entire CAM surface area transplanted with the human bladder cancer cell line MGH[272]. No irritation (hyperaemia, lysis, haemorrhage or coagulation of blood vessels) of the CAM tissue was observed after 30 minutes of topical treatment. Higher fluorescence intensity of Ce-6-PVP was observed in the tumour tissue than on the CAM tissue 30 minutes post-treatment. Thus Ce-6-PVP was found to be a potential *in vivo* diagnostic agent. Similarly this result was found in the same bladder cancer xenograft type using the PhtS hypericin[273]. The Ce-6-PVP PhtS was shown to accumulate quickly in the tumour tissue (30 minutes) and have a rapid clearance (4 hours) thus this CAM model also provided preliminary pharmacokinetic information[272].

The CAM model is ideal for an *in vivo* evaluation of PDT effect as its transparency means that changes to the vasculature during PDT treatment can be monitored in real time. Additionally tumour development, regression and necrosis can be imaged at time points during the course of the PDT. This eliminates the need to sacrifice the chick embryos after each treatment. A further advantage of using chicken eggs is their low cost, fast growth and simplicity compared to mammalian models. Owing to their short incubation time (21 days) longer term evaluation of drug effects is not possible[158] such as a sustained effect on CAM irritation or prolonged light sensitivity. However the CAM model provides an excellent bridge between *in vitro* cell culture experiments and *in vivo* mammalian studies. Therefore the aim of this chapter was to undertake a preliminary *in vivo* investigation into the effect of unconjugated duramycin and duramycin-porphyrin conjugate, with and without light irradiation, on CAM tumour xenografts.

7.2 Results

7.2.1 Effect of duramycin treatment on chorioallantoic membrane tumour xenografts

It was investigated whether duramycin treatment had an effect on tumour xenografts formed from the human ovarian cancer cell line SK-OV-3 and established on the CAM of chicken eggs. Briefly, fertilized White Leghorn chicken eggs were placed in an incubator (37°C, 70% humidity) and the embryo was allowed to incubate for 5 days before the shell over the air sac and the shell membrane was removed to expose the CAM. On the 8th day of incubation SK-OV-3 cells (1x10^{6}) were suspended in Matrigel (10 µl) to form a gel and grafted onto the surface of the CAM. The SK-OV-3 cells were established on the CAM for 3 days so that sufficient growth of the tumour occurred and that penetration of allantoic blood vessels into the tumour was stimulated. On the 11th day the eggs were removed from the incubator, for a maximum of 5 minutes at a time so that dehydration of the membrane was avoided, and either 50 µM or 4.97 mM duramycin (10 µl) was applied topically to the tumours. The tumours were treated with duramycin at 0, 24 and 48 hours and subsequently imaged at 0 hours (pre-treatment) and at 24, 48 and 72 hours. The re-application of duramycin every 24 hours was required as the tumour xenografts were penetrated by the CAM vasculature and removal of duramycin via the blood circulation could have reduced its concentration in the vicinity of the tumour. Duramycin at 50 µM was chosen as this concentration had been shown to induce ~50% necrosis, increase intracellular Ca^{2+} concentration, reduce cell proliferation by ~60-80% after 30 minutes treatment and ~65-90% after ≥24 hours treatment in the cancer cell lines A2780, AsPC-1, MIA PaCa-2 and SK-OV-3 (Chapters 3, 4 and 5). Thus it was theorised that an effect would be seen on the SK-OV-3 tumour xenografts using 50 µM duramycin. As it was uncertain what the impact of a vasculature system would have on duramycin concentration neat duramycin (4.97 mM) was used as a high concentration positive control on the tumours.

SK-OV-3 tumours successfully grew on all 7 eggs grafted with the cancer cells and a visible tumour mass and angiogenesis of the CAM blood vessels surrounding the tumour could be seen on the 3rd day of tumour growth. The tumours were associated with irritation of the CAM which lead to coagulation and haemorrhage, though the extent varied between the tumours (figure 7.1 and figure 7.2). A large amount of coagulation occurred around the margins of the tumour on Egg 3 (figure 7.1). Moderate coagulation was seen around the tumours on Eggs 2 and 5 at all time-points and on Egg 1 at 72 hours post-treatment. A small

amount of coagulation occurred around the edges of the tumour on Egg 4. An area of haemorrhagic bleeding was observed around the tumour on Egg 1 after 24 hours of duramycin treatment. A relatively large amount of coagulation occurred on Egg 2 of the 4.97 mM treated tumours (figure 7.2). A small amount of coagulation was seen around the pre-treated tumour of Egg 1 and a large area of coagulation surrounded the tumour at 24 hours post-treatment accompanied by a complete loss of blood circulation in the CAM.

Duramycin at 50 μM was used to treat the tumours on 5 out of 7 of the eggs. The duramycin treatment had little effect on the tumours after 24 hours and they appeared 'healthy' which was shown by a preserved white colouration (figure 7.1). However there was a slight reduction in tumour volume (i.e. the tumour was thinner) for the xenografts on Eggs 2, 4 and 5. At 48 hours post-treatment the tumours on all 5 eggs had a slight discolouration in which the tumours had become a yellow colour. Viable implants of endometrium onto the CAM appeared white or pink in colour[274] and so it is possible that the discolouration from white tumours to yellow was an indicator of a reduction in the health of the tumours. At 72 hour post-treatment all 5 tumours had a yellow-discolouration and were reduced in volume. The reduction in volume was not so evident for the tumour on Egg 1 but was more pronounced on Eggs 3 and 5 in which the tumour appeared to be thinner. The most obvious effect of the duramycin treatment was seen on the tumours on Eggs 2 and 4 which appeared both thinner and smaller in size.

Interestingly, the presence of a SK-OV-3 tumour micro-nodule was observed in close proximity to the original SK-OV-3 tumour on Egg 5 (figure 7.1). There was a patch of white-grey close to the tumour on Egg 3 at 72 hours however it could not be positively identified as a micro-nodule from the observations made.

The blood vessels of the CAM became darker in colour over the treatment period in Eggs 2, 4 and 5 (figure 7.1). The background of the CAM also became darker in these images which was likely because the chick embryo had moved to underneath the opening in the shell.

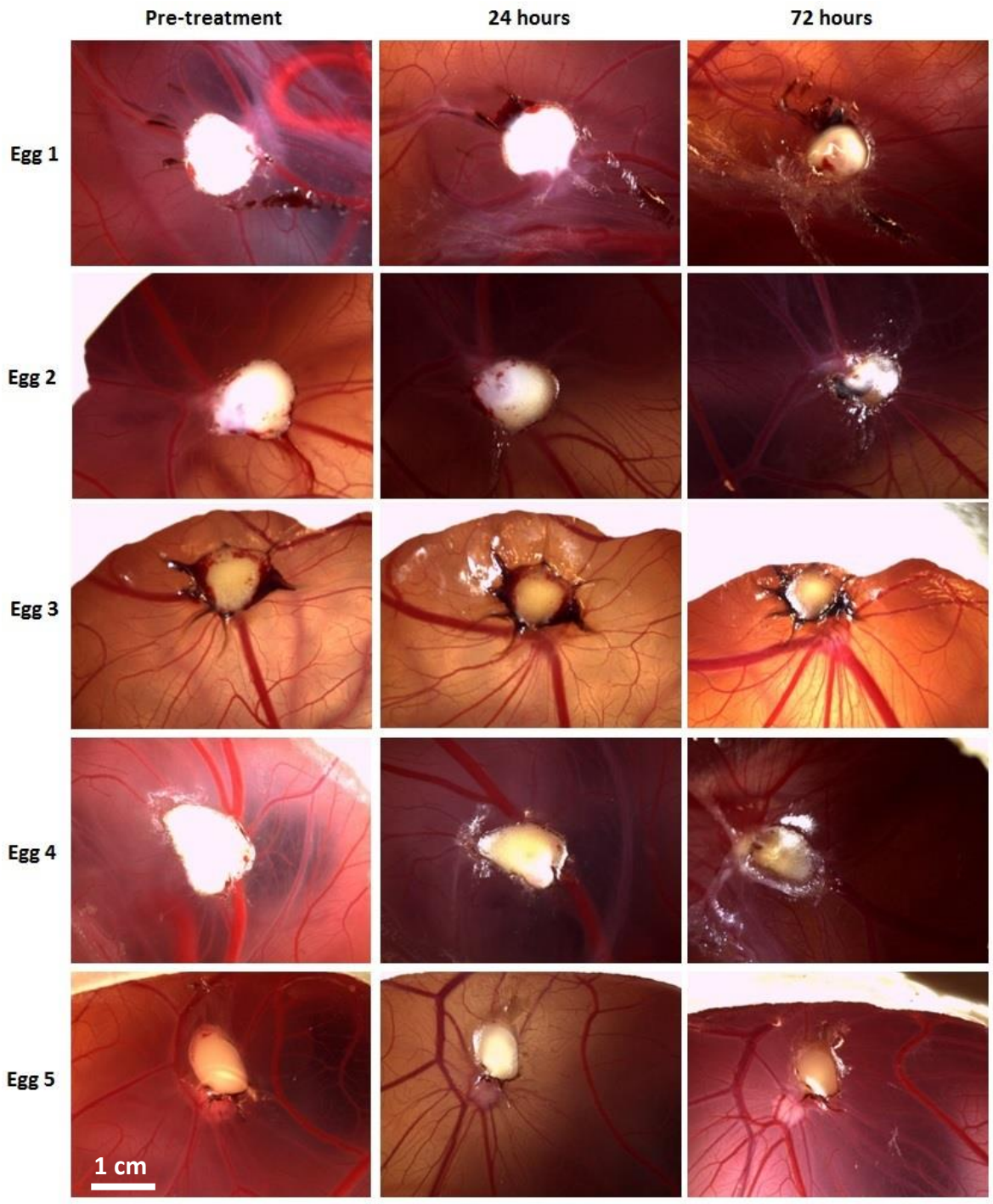

Figure 7.1: Duramycin (50 µM) treated tumour xenografts on the CAM.
Ovarian (SK-OV-3) tumour xenografts were treated with 50 µM duramycin over a 72 hour period. There was little effect on the tumours after 24 hours treatment with duramycin and the tumours appeared healthy. After 72 hours treatment the tumours were reduced in volume and had a yellow-discolouration. Magnification x1.

It was intended that 2 of the 7 SK-OV-3 xenografts would be treated with 4.97 mM duramycin over a 72 hour period. However after 24 hours treatment the chick embryo in Egg 1 (figure 7.2) had died. The embryos were considered dead if they were motionless and the contents of the egg were cloudy[168]. Thus the egg was removed from the study. It was not known if the death was a result of the duramycin treatment or from natural causes as chick embryo mortality can occur spontaneously or due to a number of factors[275]. The tumour on Egg 2 appeared healthy in colour (white) after 24 hours treatment though was reduced in volume. Observation of the egg at 48 hours post-treatment showed that the tumour had completely disintegrated. Therefore the experiment was ended at 48 hours.

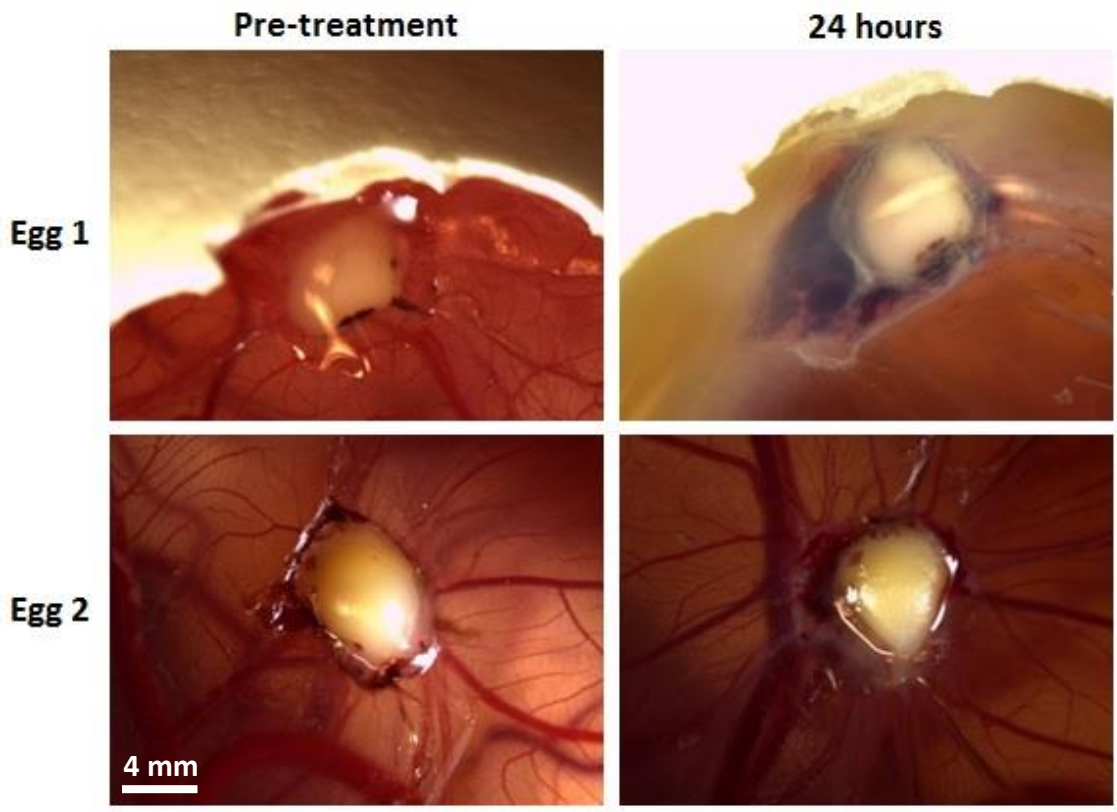

Figure 7.2: Duramycin (4.97 mM) treated tumour xenografts on the CAM.
SK-OV-3 tumour xenografts were treated with 4.97 mM duramycin with an intended treatment period of 72 hours. However after 24 hours treatment the chick embryo in Egg 1 had died thus this egg was removed from the experiment. The tumour on Egg 2 after 24 hours treatment appeared healthy though with a marked reduction in volume. At 48 hours post-treatment the tumour had completely disintegrated and so the experiment was ended. Magnification x2.5.

7.2.2 Effect of photodynamic therapy on chorioallantoic membrane tumour xenografts

Once it had been established that duramycin had an effect on the health and volume of SK-OV-3 tumours on the CAM it was investigated whether the duramycin-porphyrin conjugate and PDT light treatment had an effect on the tumours. SK-OV-3 tumours were grafted and allowed to establish as described above and then treated with either duramycin-porphyrin conjugate or unconjugated duramycin. A total of 4 eggs were available for the experiment and so 1 egg was treated with unconjugated duramycin plus light irradiation, 2 eggs were treated with duramycin-porphyrin conjugate plus light irradiation and 1 egg was treated with the conjugate but not irradiated which served as the dark control. Briefly, 50 µM duramycin-porphyrin conjugate (10 µl) or unconjugated duramycin (10 µl) was applied topically to the SK-OV-3 tumours and the eggs were incubated in the dark for 5 minutes in an incubator (37°C, 70% humidity). After incubation the eggs were irradiated with 7.5 J/cm^2 red light (an irradiation time of 4 minutes and 41 seconds) and then imaged and returned to the incubator. The eggs were treated at 0, 24, 48 and 72 hours and imaged before and after each treatment except for the dark control egg which was kept in the dark in the incubator for the duration of the experiment.

The tumours grew successfully on all 4 eggs. There was a very small amount of coagulation present around the edges of all of the tumour xenografts which was observed before and during the treatment period. Representative images of the 2 tumours that were treated with duramycin-porphyrin conjugate and PDT light treatment are presented in figure 7.3. A similar effect of the treatment was observed for both SK-OV-3 tumours. At 24 hours post-treatment the tumours appeared healthy with no apparent effect on tumour volume. At 48 hours the tumours appeared thinner and had a yellow-discolouration which then became more prominent at 72 hours.

The duramycin-porphyrin conjugate treated dark control tumour at 24 hours post-treatment appeared healthy and had increased in size. There was a very slight discolouration to the tumour xenograft at 48 and 72 hours post-treatment with no other observable changes.

The SK-OV-3 tumour xenograft treated with unconjugated duramycin plus light irradiation appeared healthy with no discolouration at 24 hours post-treatment (figure 7.4). However at 48 hours yellow-discolouration was evident and this was enhanced at 72 hours. The tumour at 72 hours post-treatment had become thinner yet had increased in width.

All chick embryos survived the 72 hour treatment period and no embryotoxicity was observed. All of the observable CAM vasculature remained healthy over the PDT treatment period with the exception of the relatively low level of coagulation present at the edges of the tumours.

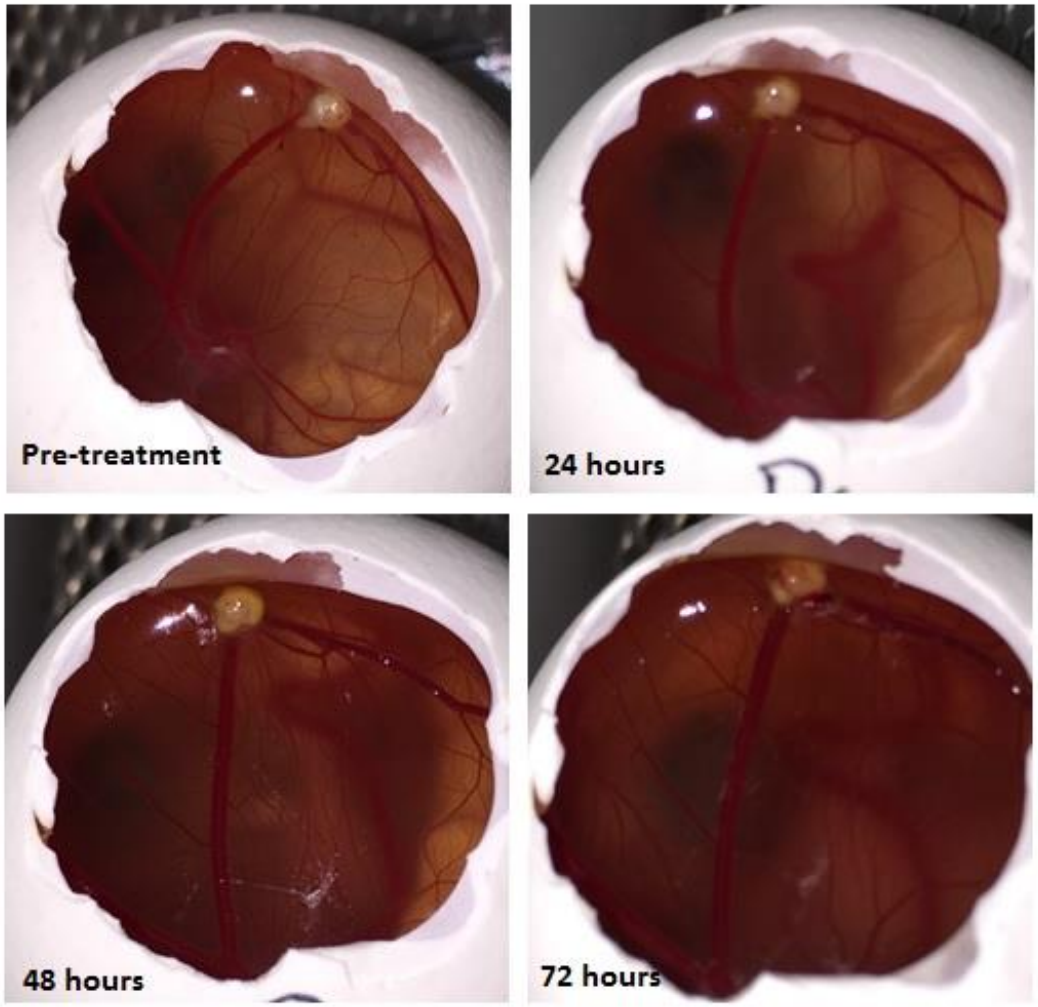

Figure 7.3: Photodynamic light therapy of CAM tumour xenografts with duramycin-porphyrin conjugate.

SK-OV-3 tumour xenografts were subjected to PDT light treatment with 50 µM duramycin-porphyrin conjugate over a 72 hour period. At 24 hours post-treatment the tumours appeared healthy. At 48 and 72 hours post-treatment the tumours were reduced in volume and had become discoloured. The above image is representative of the 2 eggs treated with duramycin-porphyrin conjugate plus PDT and corresponds to the histological sections in figure 7.6. Magnification x1.

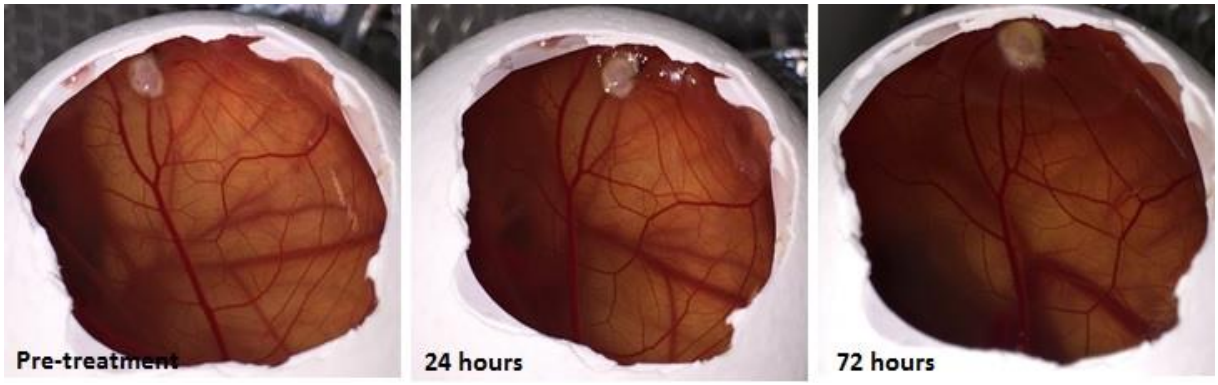

Figure 7.4: Photodynamic light therapy of CAM tumour xenografts with unconjugated duramycin.

As a control a SK-OV-3 tumour xenograft was treated with 50 µM unconjugated duramycin and subjected to PDT light treatment. At 24 hours post-treatment the tumour appeared healthy. At 72 hours post-treatment the tumour appeared to be thinner yet had increased in width and had become slightly discoloured. Magnification x1.

7.2.2.1 Histological staining of tumour xenografts

To provide a more in depth analysis to support the qualitative observations described above the PDT treated SK-OV-3 tumour xenografts were histologically stained with a Haematoxylin and Eosin (H&E) stain. The active staining ingredient of haematoxylin, haemalum, binds to basophilic structures and so stains the nucleus and the endoplasmic reticulum a blue or violet colour, due to their RNA and DNA content. The counterstain eosin binds to acidophilic structures such as the cytoplasm and cellular membranes which appear pink or red in colour. After the treatment at 72 hours the SK-OV-3 tumours were dissected from the CAM, snap-frozen and sectioned into 12 µM sections and placed onto microscope slides using the methods described in section 2.10.4 and section 2.10.5. As much of the tumour was sectioned as possible, horizontally, in the orientation presumed to be the site of topical application of duramycin towards the part of the tumour that protruded into the CAM deeper layers. This presumed orientation of the tumours was supported by a section taken after the last section of the dark control tumour. This end section consisted only of the CAM mesoderm and neovascularisation was observed which suggested that the lowest part of the tumour had protruded into the mesoderm. The sections were stained with H&E stain (section 2.10.6) and imaged by microscopy at 10x magnification. The interpretation of the slides was performed by a trained consultant pathologist (Dr J. Cooke) in a blinded fashion.

The sections shown in figure 7.5 were taken from both of the duramycin-porphyrin conjugate plus light irradiation treated chick eggs and are taken from, approximately, the midsection of the tumours. The margin between the SK-OV-3 tumour and the CAM could be clearly seen and the tumour appeared to be completely enveloped by CAM. Destruction of the ectodermal CAM layer occurred where the tumour came into contact with the CAM (figure 7.5a) though parts remained intact (figure 7.5b). The tumour was in direct contact with the mesodermal layer in the majority of the sections taken from both of the conjugate plus irradiation treated tumours.

Representative sections of the SK-OV-3 tumour treated with duramycin-porphyrin conjugate and light irradiation are shown in figure 7.6. A relatively small amount of necrosis was shown around the edges of the tumour on all of the sections. The majority of the sections showed that the tumour core remained viable however oedema was observed in the core of the tumour in some of the sections. The tumour in figure 7.7 was also treated with duramycin-porphyrin conjugate and light irradiation. Areas of necrosis were observed around the edges of the tumour but the core remained viable with no observable oedema. An area in one section that had been taken from the site close to the topical application of duramycin-porphyrin conjugate showed a complete loss of cellular structure (figure 7.7, top left). The section of tumour taken from directly below this site showed extensive necrosis (figure 7.7, top right).

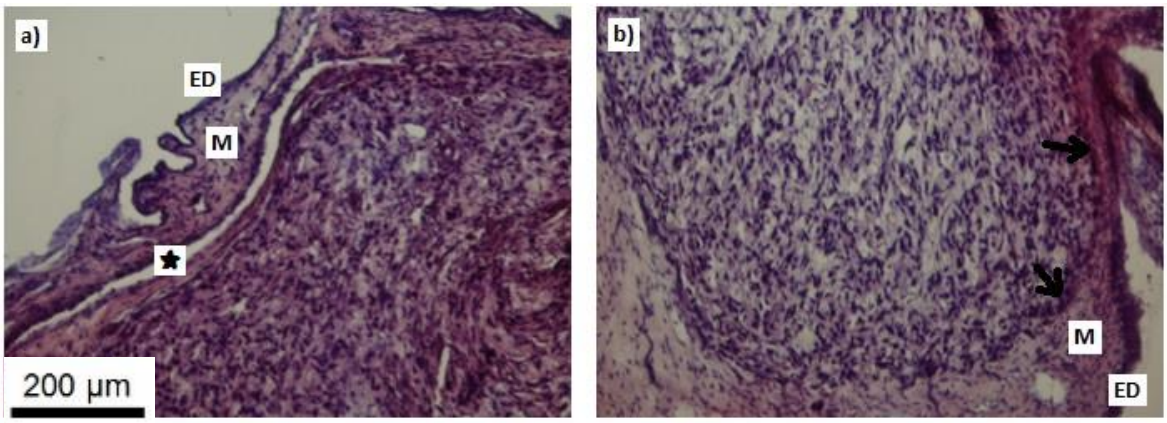

Figure 7.5: The interaction between the SK-OV-3 xenograft tumour and the CAM.

Destruction of the ectodermal layer of the CAM occurred where the tumour met the CAM though some parts remained intact (intact areas indicated by black arrow on b). The tumour came into contact with the CAM mesoderm. The black star in a) depicts a blood vessel within the mesodermal layer. ED – endoderm and M – mesoderm. Magnification x10.

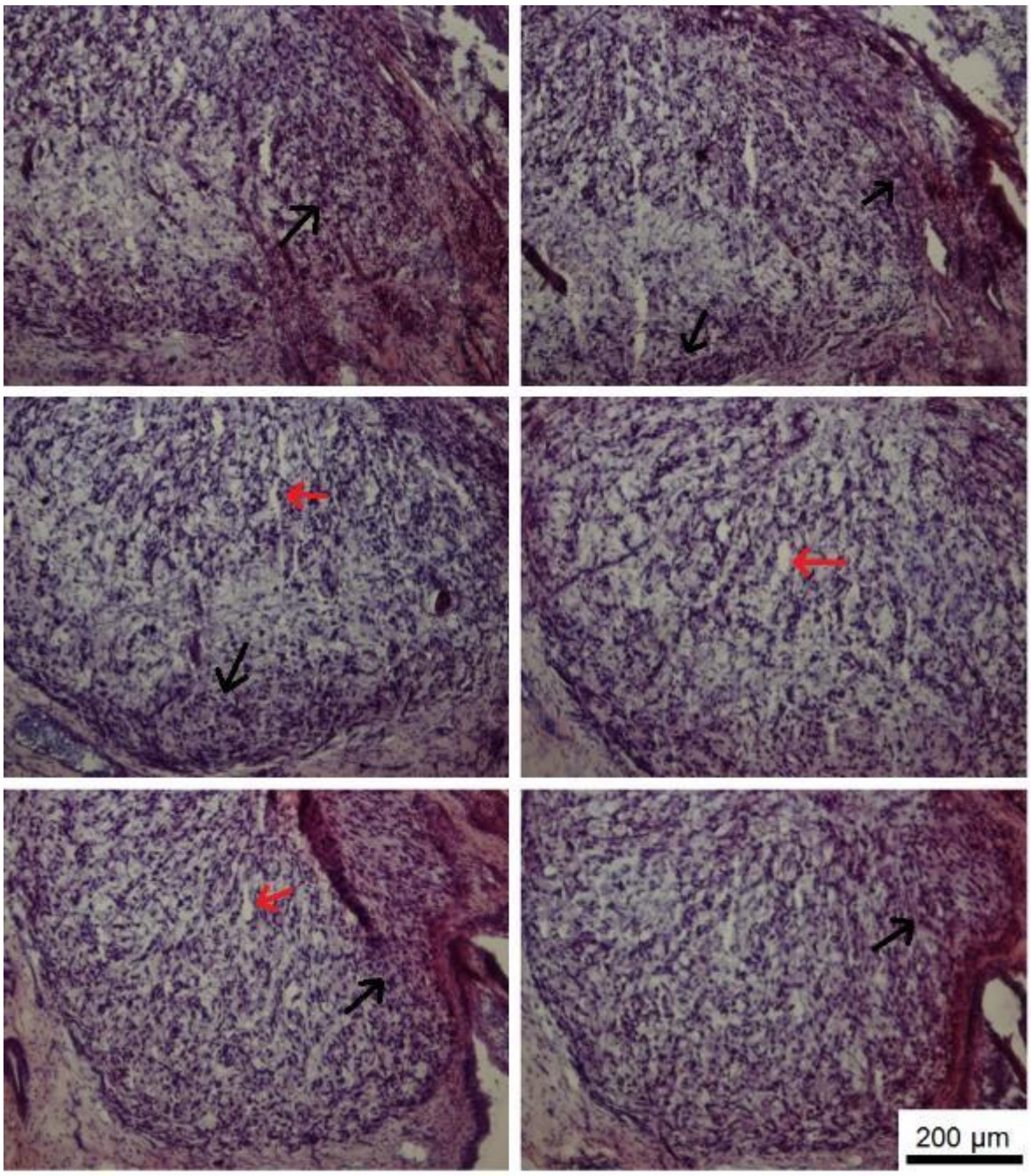

Figure 7.6: H & E stained sections of CAM tumour xenografts treated with duramycin-porphyrin conjugate and photodynamic light treatment.

Areas of necrosis, indicated by black arrows, were observed around the edges of the duramycin-porphyrin conjugate (50 µM) + PDT light treated tumour. Necrotic areas were not seen in the core of the tumours though some oedema was observed, indicated by red arrows. Magnification x10.

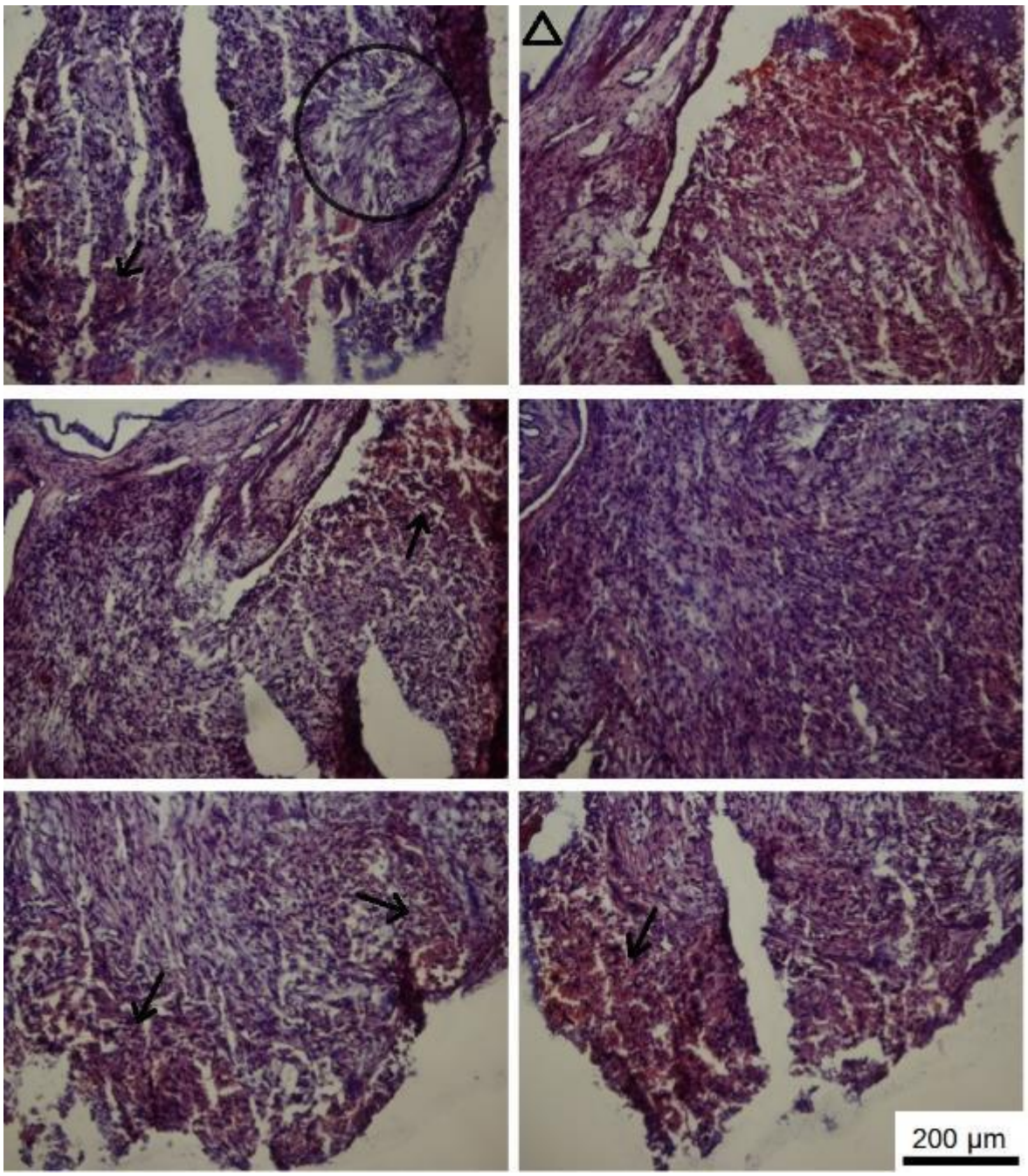

Figure 7.7: H & E stained sections of CAM tumour xenografts treated with duramycin-porphyrin conjugate and photodynamic light treatment.

Areas of necrosis, indicated by black arrows, were observed around the edges of the duramycin-porphyrin conjugate (50 µM) + PDT light treated tumour. Extensive necrosis was seen in a section (black triangle) taken from an area close to the topical site of duramycin-porphyrin conjugate treatment. The black circle represents an area which had experienced a complete loss in cellular structure. The core of the tumour remained viable. Magnification x10.

The dark control SK-OV-3 tumour xenograft, treated with duramycin-porphyrin conjugate but was not irradiated, showed areas of necrosis around the edges of the tumour in the majority of sections (figure 7.8). However the core of the tumour appeared viable. Extensive necrosis was observed in a section taken from the lowest part of the tumour and the tumour had detached from the CAM (figure 7.8, bottom right).

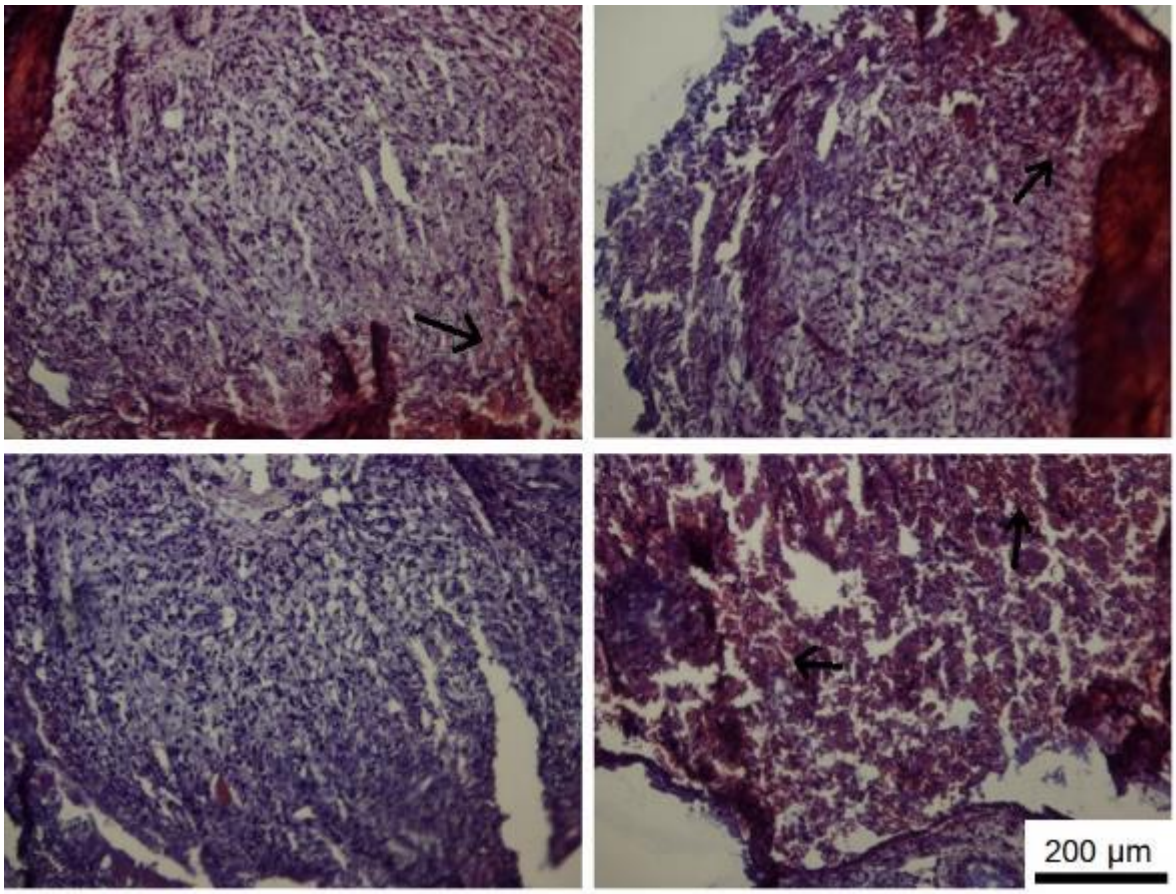

Figure 7.8: H & E stained sections of CAM tumour xenografts treated with duramycin-porphyrin conjugate (dark control).

Areas of necrosis, indicated by black arrows, were observed at the edges of the duramycin-porphyrin conjugate treated dark control tumour. The majority of the sections from this tumour showed a viable centre. However an area of extensive necrosis was observed in the lowest part of the tumour (bottom right). Magnification x10.

Unfortunately, the SK-OV-3 tumour that had been treated with unconjugated duramycin and light irradiation suffered damage when sectioning. A number of the sections that were taken smeared as the CAM tissue that surrounded the tumour was not adequately frozen at the initial cryostat temperature of -20°C for the sample block and -20°C for the chamber. Thus the temperature was adjusted to -30°C for the sample block and -25°C for the chamber which provided some successful sections for this tumour. Extensive necrosis of tissue with complete loss of cellular and nuclear structure was observed (figure 7.9). However as the tumour had become completely detached from the CAM, perhaps after dissection or during sectioning, it was not possible to distinguish if the sectioned tissue was the SK-OV-3 tumour or CAM. Thus no conclusive results could be gained from the sections.

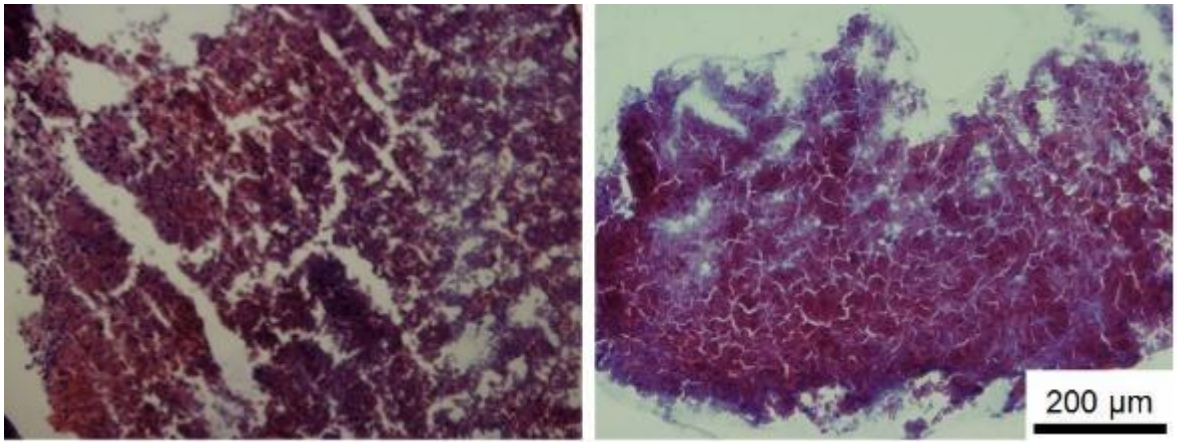

Figure 7.9: H & E stained sections of CAM tumour xenografts treated with unconjugated duramycin and photodynamic light treatment.

The majority of the sections obtained from the unconjugated duramycin + PDT light treatment tumour suffered a large amount of smearing due to insufficient freezing of the surrounding CAM tissue. The successful sections showed extensive necrosis and a complete loss in nuclear and cellular outline. It could not be distinguished whether the stained tissue in these sections was CAM or tumour. Magnification x10.

7.3 Discussion

The CAM model has been used in oncological studies for the assessment of anti-cancer agents primarily with a focus on their antiangiogenic effects. Paclitaxel, an anti-cancer drug with antiangiogenic properties, was loaded into microspheres made up of poly(D,L-lactic acid) (PLA) and ethylene-vinyl acetate (EVA) polymers and applied topically to the CAM. The paclitaxel treatment was shown to induce vascular occlusion and inhibit angiogenesis[165]. A toxicological study compared the LD_{50} of 10 anti-cancer agents (paclitaxel, carmustine, camptothecin, cyclophosphamide, vincristine, cisplatin, aloin, mitomycin C, actinomycin-D and melphalan) that were intravenously injected into the CAM vasculature to the LD_{50} values reported for mice and rat models[168]. Moderate correlations were found between intravenously injected CAM and intravenously and intraperitoneally injected rodents. However, all of the anti-cancer drugs had a concentration dependent effect on chick embryo mortality. This study showed that the CAM is a viable model for acute toxicity screening of anti-cancer agents before full toxicological studies are undertaken in rodents or other animal models.

In this study, the CAM model was utilised to evaluate the effect of topical duramycin treatment of ovarian (SK-OV-3) tumour xenografts. Duramycin at 50 µM was used to treat the tumours grafted onto 5 chicken eggs. After 24 hours of treatment all of the tumours appeared healthy however a slight reduction in tumour volume was observed in 3 of the 5 tumours. At 48 hours all 5 of the tumours had become slightly discoloured, having a yellow appearance. When the tumours were observed at 72 hours all 5 tumours were further discoloured and were reduced in volume. The reduction in tumour size varied between the tumours with 2 of the tumours having a more enhanced reduction in volume. The reduction in tumour size was most likely due to both necrotic cell death, seen previously with *in vitro* duramycin treatment (Chapter 3) and supported by the histological analysis in this chapter, and reduced cell proliferation (Chapters 3 and 4). This is in support of the literature which reported that graphene oxide treated glioblastoma tumours on CAM were reduced in tumour volume and weight, compared to untreated control tumours[167]. It was proposed that this was most likely a result of graphene oxide induced cell death, through apoptosis, and a reduction in cell proliferation which was verified by histological staining and *in vitro* cell culture experiments.

Duramycin in its ‘neat’ form of 4.97 mM was used to treat the tumours on 2 of the chicken eggs. The experimental plan was to treat the tumours over a 72 hour period as with the

above tumours. However, although at 24 hours the tumour on 1 of the eggs appeared healthy, at 48 hours the tumour had completely disintegrated. It could not be certain whether this was a result of the duramycin treatment although it is possible that the relatively high concentration of duramycin caused extensive tumour cell death. If the tumour had broken apart then the dead cancer cells would be free to circulate through the CAM circulatory system and would have been removed from the graft site. The other egg was lost from the experiment at 24 hours due to chick embryo mortality. One possibility for this was that the duramycin was at a high enough concentration to cause toxicity. Another possibility was that the tumour graft itself had an effect on the embryo. Embryo mortality was increased in osteosarcoma grafted chick eggs compared to non-grafted eggs[169]. It was speculated that this could have been due to dissemination of tumour cells into the embryo or a secretion of factors which caused blood coagulation, a possibility in this study due to the large area of coagulation seen around the tumour on the CAM of the dead embryo. However there are a number of technical errors or inherent biological reasons that can result in chick embryo death including incubation problems such as changes in heat and humidity, bacterial contamination, dehydration and vibration or nutritional deficiencies, hypercalcemia and genetic or developmental defects[275, 276]. The disintegration of the tumour and the embryotoxicity observed when using 4.97 mM duramycin may indicate that the tumour and/or the chick embryo had a concentration dependent reaction to duramycin treatment.

The CAM model has been used as a model for metastasis[164] as transplanted tumour cells can migrate through the CAM mesodermal layer, enter the vasculature and establish at secondary sites[22]. A SK-OV-3 tumour micro-nodule was observed in close proximity to the original tumour on one of the duramycin treated eggs. Tumour micro-nodules around osteosarcoma tumour xenografts were not seen on the CAM until it was turned upside down[169]. It is therefore possible that tumour micro-nodules were present on more than one of the SK-OV-3 tumours in this study but were not visible from the top of the CAM. On another of the eggs there was a discoloured grey area near the original tumour that could have been a micro-nodule. To positively identify the grey area as a micro-nodule it may have been beneficial to look at the underside of the CAM. However it is possible that this discoloured area was representative of blood vessel damage as the emptying of blood vessels, specifically venules, can lead to blanching[171].

In this study, the blood vessels in some of the chick eggs treated with duramycin appeared to darken in colour along with the CAM background. PDT treatment of the CAM with porphycene PhtS resulted in a darkening of small arterioles and a reduction in the optical density (OD) of the blood vessels, measured as a comparison to the CAM background[171]. The change in colour was associated with the occlusion of small arterioles but the true OD of some of the blood vessels could not be measured as the embryo had moved to under the opening in the shell which darkened the CAM background. It is likely that the darkening of the images observed in this study was due to chick embryo movement and so an effect of duramycin on CAM blood vessels could not be gained from this observation.

The SK-OV-3 xenografts were associated with irritation of the CAM in the form of coagulation which was observed around the edges of all tumours in both the unconjugated and conjugated duramycin experiments. This was more evident in the unconjugated duramycin treated tumours. The coagulation was observed prior to the addition of duramycin and so it was most likely stimulated by the SK-OV-3 tumour rather than by the duramycin treatment. SK-OV-3 cancer cells promote relatively fast coagulation in prothrombin time clotting time assays as observed in the author's own investigations (data not shown in this study) and reported in the literature[227]. There was one incident of haemorrhagic bleeding of the CAM close to the tumour site after 24 hours duramycin treatment which had coagulated when the egg was observed at 48 hours. It is possible that the bleeding was due to already established blood vessel damage rather than the duramycin treatment. Indeed duramycin has been shown to disrupt cancer cell coagulation[58] and so may be expected to prevent rather than cause it on the CAM. Perhaps the lack of reduction in coagulation after duramycin addition shows that its anti-coagulant effect does not negate the pro-coagulant factors in an *in vivo* model. This speculation could warrant investigation into duramycin's anti-coagulant properties in future CAM work in this project.

PDT on CAM in oncological studies has largely been used to assess the antiangiogenic and anti-cancer potential of PhtS. A number of light irradiated porphycene PhtS applied topically and systemically on the CAM showed an antiangiogenic effect[171]. Small arterioles became constricted, occluded and darkened in colour over the PDT treatment (4-16 minutes) whereas venules emptied which lead to vessel blanching. Larger arterioles also became occluded post-irradiation (3-4 hours). PDT is often used in the treatment of surface-exposed malignancies[128-131] and the CAM model provides a quick and simple means

of assessment for the topical application of PhtS. However this limits the application of the PhtS. To better represent mammalian models the photosensitising drug can be injected intraperitoneally into the chick embryo where it is delivered to the tumour via the CAM blood circulation. The intraperitoneal injection of a number of PhtS; ALA, $AlPcS_n$, BPD-MA and Lutex, was found to produce higher vascular damage to the CAM than the topical application[173, 175]. The light irradiation of ALA 90 minutes post-injection into chick embryos induced vascular damage in the CAM and showed fluorescence in transplanted ovarian tumours (formed from the NuTu-19 cancer cell line)[176]. This study also showed that the chick embryo was able to metabolically convert the intraperitoneally injected ALA into its photoactive form protophorphyrin IX (PpIX). The CAM model has also been used to evaluate nanoparticles as PhtS drug delivery systems. A hydrophobic porphyrin, meso-tetra(*p*-hydroxyphenyl)porphyrin (*p*-THPP), was evaluated on CAM in both its free and nanoparticle encapsulated forms[177]. Intravenous injection of both *p*-THPP formulations resulted in distribution through the entire CAM circulatory system in just 5 seconds however only nanoparticle-*p*-THPP remained in the vasculature up to 25 minute post-injection. The effect of PDT light irradiation on the vasculature, namely vascular occlusion, was significantly enhanced for the *p*-THPP with nanoparticle carriers.

In this study the duramycin-porphyrin conjugate was topically applied to SK-OV-3 tumour xenografts on the CAM and light irradiated to assess the treatment's anti-tumour effect. There was no embryotoxicity observed during the PDT experiments and the observable CAM vasculature remained healthy throughout the course of the treatment except for a small amount of coagulation associated with the tumours. The tumours were imaged at specific time points throughout the course of the PDT treatment so that observations could be made on the appearance of the tumours. A similar effect was seen on both of the tumours that were treated with the duramycin-porphyrin conjugate plus light irradiation. The tumours appeared healthy with no change in tumour volume or colour at 24 hours post-treatment. At 48 hours the tumours were reduced in thickness and had a yellow-discolouration. This effect was more prominent at 72 hours. The dark control tumour, treated with the conjugate and not irradiated, had increased in volume at 24 hours post-treatment and became discoloured at 48 hours with no further observable change. The unconjugated duramycin control tumour (treated with unconjugated duramycin and light irradiation) showed no observable change at 24 hours post-treatment, became discoloured at 48 hours and was reduced in thickness yet increased in width at 72 hours. The ability to observe PDT effect on tumour grafts as treatment progresses is a major benefit of using

the CAM model and avoids the use of more expensive, time-consuming and technically difficult techniques (MRI and full body fluorescence imaging) required with mammalian models.

However, the observations made when imaging tumour xenografts on CAM, although valuable, are qualitative and thus subjective. Therefore the SK-OV-3 tumours were sectioned and stained for histological analysis. The margin between the tumours and the CAM could be clearly seen and the CAM was shown to have completely encapsulated the tumour. Where the tumour met the CAM the ectoderm, the most exterior layer, had been destroyed and the tumour was seen to be in direct contact with the CAM mesoderm. This supports findings in the literature in which destruction of the CAM ectoderm was seen in immunohistochemical stains of SK-OV-3 tumour xenografts that had been applied to the CAM through Matrigel-cell mixtures similar to the method used in this study[22].

The H&E stained sections from both of the duramycin-porphyrin conjugate plus PDT light treated tumours showed necrosis around the edge of the tumour in the majority of the sections. The core of the tumours appeared to have 'normal' structure and thus were most likely viable, though oedema was observed throughout the core of one of the tumours. In one of the tumours the section from the most exterior site of the tumour, which received the topical application of duramycin-porphyrin conjugate and inherently was most in contact with the PDT light beam, showed an area of complete loss in cellular structure. The section of the tumour taken from directly beneath this showed extensive necrosis. The dark control (conjugate treated, non-irradiated) tumour xenograft showed areas of necrotic cell death around the edges of the tumour yet the core showed a high level of viability. It is therefore possible that the duramycin-porphyrin conjugate did not penetrate beyond the superficial layers of the tumours. It is also possible that the PDT irradiance dose was not strong enough to penetrate into the core of the tumour, provide a sufficient cytotoxic dose and/or produce an effect significantly greater than the non-irradiated conjugate. This is in contrast to the *in vitro* PDT experiments in which 10 µM irradiated duramycin-porphyrin conjugate at the same light dose (7.5 J/cm^2) reduced the cell viability of SK-OV-3 by 97.2% (Chapter 6). There are a number of experimental variables that could have led to the production of only superficial damage to the tumour xenografts including too low conjugate concentration (50 µM) for the *in vivo* tumour, too low conjugate volume (10 µl), too low irradiance dose (7.5 J/cm^2) and a too short incubation time for the duramycin-porphyrin conjugate (5 minutes). Gottfried *et al*.[171] employed 3 increasing irradiance doses

to PDT treated CAM which showed increasing damage to the CAM vasculature. An increase in irradiance dose may be difficult in this study as a longer irradiation time would be required which may exceed the maximum period (5 minutes) that the chicken eggs could be outside the incubator. Toledano *et al.*[172] used a fluorimeter to measure the uptake time of porphycenes into the CAM. Future work involving the CAM SK-OV-3 tumour model could employ a similar method for duramycin-porphyrin conjugate uptake to optimise the length of incubation time. Of the few sections taken from the unconjugated duramycin control tumour the tissue showed extensive necrosis and complete loss of cellular and nuclear structure. Though, as it could not be distinguished whether the tissue was of tumour or CAM origin, no usable data could be taken from this control.

A number of porphycene PhtS were shown to be insoluble in water, alike to the duramycin-porphyrin conjugate, and so a suspension of 10% v/v DMSO was required to form a solution[171]. However the DMSO was found to be toxic in the CAM. No toxicity to the CAM itself or to the chick embryo was seen using the duramycin-porphyrin conjugate in this study. Thus it is possible that the DMSO in the conjugate (~1% v/v at 50 µM) was not present at concentrations toxic to the CAM. Vargas *et al*.[177] found that while 20 µl of 20% v/v DMSO injected into the CAM circulatory system had no effect on embryo survival, higher volumes (50-100 µl) reduced survival to ~50%. It is possible that the smaller volumes of duramycin-porphyrin conjugate used in this study also contributed to the lack of DMSO toxicity.

Clearly the work presented in this chapter can only be seen to have provided a preliminary investigation into the effect of duramycin on CAM tumour xenografts. A number of optimisation questions have been generated that would need to be addressed before a suitably statistically powered study can be designed to quantify the existence of duramycin and PDT effects. Further work with this model is needed and a number of directions can be gained from recent literature. For example Lokman *et al.*[22] found that SK-OV-3 tumours showed a moderate degree (as compared to 2 other ovarian cancer cell lines) of cell invasion into the CAM mesoderm. Future CAM experiments could involve staining sections to assess the degree of tumour cell invasion into the CAM. This could then lead to the evaluation of the anti-metastatic potential of duramycin. Chin *et al.*[272] measured the distribution of a PhtS between the CAM tissue and a tumour xenograft via a fluorescence endoscopy system coupled to a colour detecting video camera. The same method was used by Saw *et al.*[273] in which the PhtS when excited by blue light fluoresced red in tumour tissue.

The red/ blue fluorescence intensity ratio was calculated for the tumour tissue vs. CAM tissue. A similar technique could be applied to future CAM studies using the duramycin-porphyrin conjugate to distinguish if selective uptake occurs in the tumour over the CAM tissue. Further a number of experimental conditions could be employed such as different light irradiation doses, conjugate concentrations and volumes and conjugate incubation times to optimise the conditions for PDT in this model. Given the degree of tumour edge necrosis observed in SK-OV-3 the CAM should be used to assess the effect on the other cancer cell lines used in this study. The literature has reported the use of A2780 and MIA PaCa-2 in CAM tumour xenografts. A2780 cancer cells were grafted onto the CAM and intravenously injected with anti-cancer agents to assess the inhibition of tumour growth and antiangiogenesis[166]. Sunitinib was used as a PhtS in the light irradiation of A2780 xenografts in which it produced blood vessel occlusion and resulted in necrotic masses in the tumours 24 hours after treatment[277]. MIA PaCa-2 xenografts on CAM showed that RNA-silencing of CD147 (a glycoprotein associated with poor prognosis in malignancy) reduced the invasiveness of MIA PaCa-2 cells through the CAM[170]. Therefore future work on CAM could involve a comparison of all 4 of the cancer cell lines, A2780, AsPC-1, MIA PaCa-2 and SK-OV-3, to assess if duramycin and duramycin-porphyrin conjugate treatment has any tumour specific effects on CAM xenografts.

This study provides some preliminary evidence that duramycin treatment and duramycin-porphyrin conjugate treatment, plus PDT light irradiation, may have an effect on the tumour viability and tumour volume of SK-OV-3 CAM xenografts. Optimisation of the technique, tumour model and endpoints should precede a more definitive study. This work and the existing increasing literature suggest that experiments involving the CAM model could offer an easy, fast and cost-effective bridge between cell culture work and future whole-animal experiments. Further work with the CAM should be undertaken with the ambition of using duramycin as a novel anti-cancer agent and the duramycin-porphyrin conjugate in the PDT treatment of cancer.

Chapter 8 Discussion

The development of novel, effective anti-cancer agents is a constant process in the treatment of malignant disease and in the field of oncological research. There is a current trend in the treatment of malignancy of personalised medicine and thus an emphasis on the development of targeted anti-cancer therapy (TAT)[14]. The aim of TAT is to produce anti-cancer drugs that specifically act on well-defined biological receptors or pathways so that tumour tissue is selectively injured while damage to surrounding normal tissue is minimised. The current study has shown that duramycin is a potential novel anti-cancer agent and has established a number of findings that contribute to its effectiveness against cancer cell lines. Through the selective binding of phosphatidylethanolamine (PE), expressed on cancer cell surfaces, duramycin has been shown to induce apoptotic and necrotic cell death, reduce cancer cell proliferation, effect cancer cell membranes, effect intracellular calcium ion concentration ($[Ca^{2+}]_i$) and be applicable to the development of a photosensitising agent for use in photodynamic therapy (PDT).

The expression of PE has been shown to occur on the surface of cancer cell lines[49], tumours[61], tumour vascular endothelium[59] and tumour-derived microparticles[60]. The expression of PE on pancreatic cancer cell lines was found to be increased when the cells were apoptotic and further so when the cells were necrotic[49]. PE was found in much higher abundance in xenografts formed from a number of different tumour types (lung, colon, pancreatic and glioblastoma) than in their normal tissue counterparts[61]. The expression of PE on the cell surface has also been recently observed in response to chemotherapeutic treatment[62, 63]. Thus PE could potentially be a useful biomarker for cancer both *in vitro* and *in vivo*. In this study duramycin was used to screen for cell surface PE expression on a number of cancer cell lines. PE was found to be expressed on all seventeen cancer cell lines screened which represented seven different cancer types; ovarian, pancreatic, breast, colon, lymphoma, multiple myeloma and leukaemia. It was therefore established that PE could be used as a biomarker for a wide variety of cancer types and that duramycin could be used as a detection method. Further analysis of duramycin's ability to detect PE was performed using the ovarian cancer cell lines A2780 and SK-OV-3 and the pancreatic cancer cell lines AsPC-1 and MIA PaCa-2, which were the cancer cell lines focused on for the remainder of the study. The detection of PE expression on these cell lines was shown to be both cell line specific and dependent on duramycin concentration.

Duramycin had previously been shown to induce lysis of erythrocytes[59] and cinnamycin had been seen to induce lysis of erythrocytes[180] and the HeLa cancer cell line[39]. In this study, duramycin treatment of ovarian and pancreatic cancer cell lines was shown to reduce cell viability and induce cell death in a duramycin concentration dependent manner. The principle mechanism of cell death induced by 30 minute duramycin treatment was necrosis of which there appeared to be a threshold concentration (>10 μM for AsPC-1, MIA PaCa-2 and SK-OV-3 and >25 μM for A2780). At relatively high concentrations (>500 μM) duramycin treatment resulted in necrosis of the majority of cancer cells. Within a narrow concentration range (5-10 μM) duramycin induced apoptotic cell death in the SK-OV-3 cell line. When this was investigated further it was shown that apoptosis occurred in all four cancer cell lines within the 5-10 μM concentration range when treated with duramycin for 24 hours. In addition to its cytotoxic effect on cancer cells duramycin was investigated for its anti-proliferative effect. It had been previously shown that duramycin treatment reduced the cell proliferation of three pancreatic cancer cell lines when treated for 48 hours[49]. In this study, duramycin was shown to reduce the cell proliferation of the cancer cell lines A2780, AsPC-1, MIA PaCa-2 and SK-OV-3 in a duramycin concentration dependent manner. Here it was shown that the IC_{50} values for 30 minute duramycin treatment were 3.4 μM, 7.1 μM, 10.0 μM and 18.5 μM for SK-OV-3, AsPC-1, A2780 and MIA PaCa-2, respectively and for 24 hour treatment 7.6 μM, 7.1 μM, 3.6 μM and 18.4 μM, respectively. Thus it was shown that differences in sensitivity to duramycin treatment existed between the cancer cell lines. The amount of reduction in cell proliferation by duramycin was found to have a strong correlation with the extent of duramycin-induced necrotic cell death. The majority of the literature that has been published on duramycin has used it as an imaging agent for either cancer[59, 63, 82] or acute cell death in other disease[64, 74, 76-79]. An important finding of this study, which was a development upon the preliminary study by Yates *et al*.[49], was that in addition to its value as an imaging agent duramycin could potentially be used as a direct anti-cancer agent due to its cytotoxic and anti-proliferative properties.

A novel finding in this study was that duramycin had an effect on the $[Ca^{2+}]_i$ of cancer cell lines. There were numerous reports in the literature[70, 85-91, 178, 179] of the effect that duramycin had on a wide variety of ion transporters and channels, including Cl^- channels, Ca^{2+} channels, Na^+/K^+ pumps and other ATP-dependent transporters. A number of these studies concluded that duramycin's effect on ion movement and concentration was most likely a result of the formation of non-selective pores in the plasma membrane[88-91, 178]. Duramycin-induced plasma membrane pores had been shown in artificial black lipid

membranes and epithelial cell membranes[88, 89]. It had also been shown that duramycin was able to inhibit the action of plasma membrane ATPases[70, 84, 85, 178, 179]. Despite this wide knowledge base in the literature, to the best of the Author's knowledge, there had been no investigation into the effect that duramycin had on the influx and efflux of ions in tumour cells. The calcium ion was chosen as focus in this study as an increase in $[Ca^{2+}]_i$ and a subsequent Ca^{2+} overload can be an initiator of apoptotic[103, 113] and necrotic[118, 240] cell death. Permeabilisation of cancer cell lines *in vitro* and tumours *in vivo* with calcium resulted in an immediate drop in ATP levels, reduction in cell survival, reduction in tumour volume and complete tumour necrosis[117]. Thus it was hypothesised that the apoptotic and necrotic cell death induced by duramycin in the cancer cell lines in this study may have been correlated with Ca^{2+}. Duramycin (>5 µM) caused an immediate increase in $[Ca^{2+}]_i$ in the cancer cell lines A2780, AsPC-1, MIA PaCa-2 and SK-OV-3. In addition to spectrofluorometry this initial increase in $[Ca^{2+}]_i$ was visualised using confocal microscopy of AsPC-1 cells treated in real time with 50 µM duramycin. Duramycin concentrations <5 µM had very little effect on $[Ca^{2+}]_i$ which was in agreement with the results from the cell death and proliferation experiments. The increase in $[Ca^{2+}]_i$ was suggested to be due to release of Ca^{2+} from internal stores such as the ER and also from extracellular influx. An interesting finding was that duramycin treatment of the cancer cell lines resulted in a sustained high fluorescence of the Ca^{2+} indicator Fluo-3, AM. It was theorised that this was due to membrane associated Fluo-3, AM likely bound to Ca^{2+}. The potential inhibition of Ca^{2+} efflux by duramycin could have been due to disruption to plasma membrane ATPase pumps which would have resulted in impaired intracellular Ca^{2+} clearance. Alternatively, if the Fluo-3, AM had dissociated from the Ca^{2+} and they had been free to efflux from the cell then it was possible that duramycin treatment resulted in the formation of non-selective pores in the plasma membrane. Both ATPase disruption and pore formation have been observed in the literature[70, 84, 85, 88-91, 178, 179] and both rely upon duramycin's disruptive effect on plasma membranes. The effect of duramycin on cancer cell membrane integrity was, briefly, investigated in this study. Confocal microscopy revealed that duramycin treated AsPC-1 cells suffered a loss in cell membrane stain, confirmed by two different membrane stains, and that there was an increase in cell numbers with PI stained nuclei. This indicated that permeabilisation of the cell membrane had occurred, probably due to a reduction in cell viability, and thus membrane integrity had been compromised. This membrane disruption was concluded to be the most likely explanation for duramycin-induced cell death rather than a specific Ca^{2+} signalling mechanism. Direct causation

between Ca^{2+} overload and necrosis was not proven in this study though the extent of necrotic cell death following duramycin treatment had a strong positive correlation (r = 0.79-0.98) with the amount of increase in $[Ca^{2+}]_i$ for all of the cancer cell lines A2780, AsPC-1, MIA PaCa-2 and SK-OV-3.

A desirable property for an anti-cancer agent is a selective effect towards tumour cells over non-tumour cells. In this study, duramycin was shown to reduce the cell viability of the normal endothelial cell line HUVECs in a concentration dependent manner, in a much similar way to the ovarian cancer cell line A2780. The results supported the findings from studies which had reported the cytotoxic effect of duramycin and cinnamycin on erythrocytes[59, 180]. Duramycin had the potential to be an effective anti-cancer agent but had a narrow therapeutic window; to be successfully applied to the clinical setting some form of enhancement to its cytotoxic effect towards tumour cells that would limit its effect on non-tumour cells was required. Therefore one aim in this current study was to develop a duramycin conjugate that was bound to a photosensitising agent. This study had shown that duramycin at a concentration of 2.5 µM had no anti-cancer effect on the cancer cell lines A2780, AsPC-1, MIA PaCa-2 and SK-OV-3. It was hypothesised that if the irradiated duramycin conjugate could produce an enhanced anti-cancer effect over the non-irradiated conjugate then duramycin could potentially be employed in the PDT treatment of cancer. The main disadvantage of PDT is the lack of selectivity that photosensitisers (PhtS) have for their target tumour tissue which can result in damage to surrounding normal tissue and a prolonged skin photosensitivity[119]. To overcome this a number of PhtS have been conjugated to biological molecules which selectively target cancer through their binding to structural features overexpressed or enhanced in tumours[120, 154-156]. Duramycin selectively binds to PE and thus was an attractive candidate for PDT, it had the potential to offer the advantage of a more direct PhtS application to tumour tissue.

An important result of this study was that duramycin was successfully conjugated to a porphyrin PhtS which was confirmed through multiple mass spectrometry analyses and was purified by HPLC. The reaction conditions for this conjugation were determined (by Dr F. Giuntini) so that a covalent amide bond was specifically formed through the reaction with the NHS ester of the porphyrin and the ε-amino group on the lysine residue at duramycin's N-terminal (refer to figure 6.1). The conjugation of the porphyrin to duramycin at this chosen location was hypothesised to minimise interference with the PE binding site[66, 68]. The duramycin component of the duramycin-porphyrin conjugate was shown to

retain its ability to detect PE expression on the cancer cell lines A2780, AsPC-1, MIA PaCa-2 and SK-OV-3 and the porphyrin component preserved its fluorescent properties. While the intrinsic nature of PDT, which requires that a light source come into close contact with the tumour, lends itself more readily to surface exposed or easily reached cancers such as skin cancers[128, 129], head and neck cancers[130], oesophageal cancers[131] and non-small cell lung cancer[119] it has been applied to ovarian and pancreatic cancer in cell line studies through to phase I/II human trials[132-135, 137-140]. In this proof of concept study the newly developed duramycin-porphyrin conjugate plus 7.5 J/cm^2 red light irradiation was shown to reduce the cell proliferation of the ovarian cancer cell lines A2780 and SK-OV-3 and the pancreatic cancer cell lines AsPC-1 and MIA PaCa-2 in a concentration dependent manner. Differences in the sensitivity to duramycin PDT treatment were observed between the cancer cell lines. The larger effect of the irradiated duramycin-porphyrin conjugate on cell proliferation compared to the effect of the non-irradiated conjugate was statistically significant at 0.5 µM for SK-OV-3, 2.5 µM for AsPC-1 and 5 µM for A2780. Therefore the irradiated conjugate had an enhanced anti-proliferative effect over the non-irradiated conjugate and, for AsPC-1 and SK-OV-3, this occurred at concentrations that did not have a cytotoxic effect when not irradiated. Importantly, for A2780, AsPC-1 and SK-OV-3, there was an enhanced effect of the duramycin-porphyrin conjugate plus light irradiation on cell proliferation over unconjugated duramycin. Thus this study showed that relatively low concentrations of duramycin could be safely applied to cancer cells without causing a cytotoxic effect which is initiated only when light irradiation at a specific wavelength is applied. There was no statistically significant difference between the effect of the duramycin-porphyrin conjugate and unconjugated duramycin on the cell proliferation of MIA PaCa-2. This study therefore highlighted that the efficacy of duramycin plus PDT light treatment may be dependent on cancer cell line which may have potentially important implications in any future *in vivo* studies. It has been observed in human clinical trials that patient response to PDT treatment can vary widely, even when the same type of malignancy is being treated[139, 144] which has been attributed to tumour aggressiveness[138] and the optical properties of tumours which can vary along the course of PDT treatment[120]. Additionally, the effect of the duramycin-porphyrin conjugate on cell proliferation was shown to be greater than the capped porphyrin control in all the cancer cell lines besides A2780 in which a similar trend in reduction in cell proliferation was observed. This study showed that the phototoxic action of the porphyrin PhtS against the cancer cells was enhanced when conjugated to duramycin, most likely due to duramycin's selectivity for PE.

Further studies involving the investigation of the selectivity of the duramycin-porphyrin conjugate towards tumour cells over non-tumour cells compared to the capped porphyrin control and unconjugated duramycin are advised.

In providing context to the findings that duramycin binds to cell surface exposed PE, has an effect on cancer cell membranes, increases $[Ca^{2+}]_i$ and can be used as an effective PDT agent it is important to bring attention to the effect that reactive oxygen species (ROS) can have on membrane lipids. ROS formed in tissue during PDT light treatment can cause peroxidation of membrane phospholipids and cause local phase transitions[278]. This allows the influx of Ca^{2+} and the release of Ca^{2+} from intracellular stores[278]. Increased $[Ca^{2+}]_i$ from lipid peroxidation can lead to the inhibition of the phospholipid transporters APTLs and the activation of ABC transporters and scramblases which subsequently can result in the cell surface exposure of PE and PS[41, 200]. The general scrambling of membrane phospholipids and the resultant loss of asymmetry can lead to loss of membrane integrity. Thus ROS produced during PDT with the duramycin-porphyrin conjugate could potentially be synergistic to duramycin's effect on cancer cell membranes and also its effect on $[Ca^{2+}]_i$, both of which have been suggested in this study to be linked with increased risk of cancer cell death.

The traditional form of *in vitro* cell culture, the 2D monolayer, provides many advantages for the initial stages of anti-cancer drug testing as it is relatively inexpensive and reliable due to its high degree of reproducibility. However the intrinsic differences between 2D monolayer culture of cancer cells and the 3D tumour environment mean that 2D culture does not accurately mimic the *in vivo* tumour[209, 210]. Thus some anti-cancer agents that have been screened thoroughly *in vitro* fail to produce an adequate effect *in vivo*[216] and a small proportion of drugs successfully enter into clinical trials[217]. Therefore, to provide some evidence that duramycin treatment would be transferable to the clinical setting, its effect on the cell proliferation of 2D monolayer cultures and 3D tumour spheroids was investigated. Duramycin reduced the cell proliferation of both the 2D and 3D cultures of A2780, AsPC-1, MIA PaCa-2 and SK-OV-3 in a concentration dependent manner. A relatively high resistance to duramycin treatment was observed in the SK-OV-3 spheroids. This was theorised to be a result of i) low permeability[237] of the spheroids, perhaps, due to a high level of aggregation of the cells in the spheroids[221], ii) an initial low viability due to a high level of necrotic cells[233] and/ or iii) a high level of quiescent cells[210, 215, 236]. The most important finding from the 2D vs 3D culture experiments was that no statistically significant

difference in the effect of duramycin on cell proliferation was found between the culture types. Although, it should be acknowledged that there were some cell line specific differences found between the two culture types, such as differences in sensitivity to duramycin treatment and differences in the concentration of duramycin required to reduce cell proliferation compared to the untreated controls. It is often found that 3D tumour spheroids are more resistant to anti-cancer drug treatment than 2D monolayers[210, 221, 226]. This has been attributed to spheroids (impermeable) necrotic cores, relatively low proliferative rate and the expression of genes that confer drug resistance and promote pro-survival pathways. However, there are some anti-cancer agents that have been reported to have a similar effect on 2D and 3D cancer cell culture[210, 234, 235]. It was possible that the similar effect of duramycin on the 2D and 3D cultures seen in this study was a result of duramycin's relatively small size (19 amino acids, ~2 kDa), which allowed it to efficiently permeate the spheroids, and duramycin's anti-cancer mechanism. It was hypothesised that duramycin could possibly have an advantage over other 'small' anti-cancer agents as its anti-cancer effect is not dependent on uptake into the active cancer cell (such as 5-FU) but rather through binding to and affecting cancer cell membranes.

To further the work with more realistic models of the *in vivo* tumour environment[22, 158] SK-OV-3 tumour xenografts were formed on the chorioallantoic membrane (CAM) of fertilised chicken eggs. The CAM model had been used in oncological studies to investigate properties of tumours (e.g. metastasis, angiogenesis)[22, 164], novel anti-cancer agents[158, 165, 270] and in the assessment of PDT effect[171-173, 271]. In this study, duramycin (50 µM) treatment of five SK-OV-3 tumour xenografts on the CAM resulted in the reduction of tumour size over a 72 hour treatment period. A reduction in the size of glioblastoma tumours on the CAM had been shown to be a result of apoptotic cell death as confirmed by histological analysis[167]. Thus it was suggested that the reduction in tumour size seen in this study was a result of necrosis, as seen in the cell culture experiments and supported by later findings from the histological analysis of duramycin-porphyrin conjugate treated tumour xenografts. The CAM model was then used to assess the effect of duramycin-porphyrin conjugate and PDT light treatment (7.5 J/cm^2). The appearance of the SK-OV-3 tumours was monitored at regular time points over the PDT treatment period. Here it was seen that the duramycin-porphyrin conjugate plus light irradiation reduced tumour thickness after 48 hours of treatment. The dark control tumour (conjugate treated, not irradiated) increased in size up to 24 hours and became discoloured at 48 hours. The unconjugated duramycin control tumour (unconjugated duramycin treated, light irradiated) was

discoloured at 48 hours and reduced in thickness at 72 hours. The CAM and its vasculature which could be observed from the opening in the egg shell appeared to be healthy throughout the course of the treatment. It is also important to note that no embryotoxicity was observed. Histological analysis of the tumours showed that the conjugate plus light irradiation produced areas of necrosis around the edges of the tumours, which was extensive and accompanied by a loss in cellular structure at the site of topical application of the conjugate, but the core of the tumours remained viable (though oedema was observed in one tumour). The dark control tumour also stained for necrosis around its edges and remained viable at its core. Unfortunately no useful information was gained from the unconjugated duramycin treated tumour in the histological stains. The superficial effect of the duramycin-porphyrin conjugate on the SK-OV-3 tumours may have indicated that the conjugate was unable to penetrate into the core of the tumours, perhaps due to biophysical properties of the tumours rather than the conjugate which was relatively small in size (2.7 kDa). Though a number of other experimental variables could have produced this superficial effect (discussed below in Future Work). Further work using the CAM model is undoubtedly required in the assessment of duramycin plus PDT treatment. However, this preliminary study showed that both unconjugated duramycin and the duramycin-porphyrin conjugate had the ability to effect the tumour size and tumour viability of CAM tumour xenografts.

In conclusion, this study has provided evidence that duramycin can be used to target cancer cells through its selective binding to PE expressed on their cell surfaces. The results presented have strengthened the knowledge that duramycin is an effective cytotoxic and an anti-proliferative agent. This study is the first to show that duramycin has an effect on intracellular ion concentration in cancer cells and, in agreement with the literature, suggests that this is a result of the formation of non-selective pores in the plasma membrane. Furthermore, development of the duramycin-porphyrin conjugate has provided a novel PhtS for use in PDT treatment against cancer. Duramycin has therefore been characterised as a promising anti-cancer agent. However, this hypothesis must be evaluated with further studies *in vitro* and subsequently with *in vivo* models of tumours before it could be expressed as applicable to the clinical setting.

Future work

In this study the detection of duramycin by flow cytometry was achieved using a secondary antibody to duramycin and subsequently a tertiary antibody fluorescently labelled with fluorescein isothiocyanate (FITC). A number of studies in the literature have biotinylated duramycin via an *N*-hydroxysuccinimide (NHS) ester which was then labelled with a fluorescent streptavidin molecule[59, 60, 74]. Further work on this project could employ this method so that duramycin could be labelled with FITC in a one-step procedure. Whether this would offer any benefits in the detection of duramycin bound to PE over the method used in this study would need to be determined. It is recommended that future work on this project involve the elucidation of the specific mechanism of duramycin-induced cell death. Perhaps, to confirm which of the two theories presented in this study in regards to whether Ca^{2+} efflux occurs in duramycin treated cells, in depth imaging studies could be performed in an attempt to visualise the presence of plasma membrane pores or the localisation of Ca^{2+} at or within the membrane. The movement and concentrations of ions other than Ca^{2+}, such as Na^{+}, K^{+} or Cl^{-}, could be investigated to see if there is an effect on these ions in duramycin-treated cancer cells and also to test whether non-selective pores that grant membrane permeability are formed. Additionally, lipidomics research may be able to show whether duramycin does indeed cause the translocation of PE in the plasma membranes of cancer cells, as seen with cinnamycin[39] and inferred with duramycin using PE-containing liposomes[73]. This could add to the understanding of how duramycin effects cell membranes and also whether it promotes its own binding. Investigation into whether duramycin promotes outward translocation of PE is warranted as the maintenance of membrane phospholipid asymmetry is performed by a group of P4-type ATPases. The P-type ATPases are a large family of transporters which also include the P2-type ATPases that transport Ca^{2+} and Mg^{2+} (SERCA, PMCA) and monovalent ions such as the Na^{+}/K^{+}-ATPases and the H^{+}/K^{+}-ATPases[43]. The literature has reported an effect of duramycin on all of these metal ion transporters/ pumps. The P2- and P4-type ATPases are thought to contain three analogous cytoplasmic domains that are involved in the ATPase catalytic cycle[43]. If duramycin can so readily effect the P2-type ATPases perhaps it can also effect the P4-type ATPases responsible for the membrane distribution of PE. The similarities recently observed between these two subfamilies of P-type ATPases[43], specifically the link between Ca^{2+} and phospholipid transport[47], are intriguing yet were beyond the scope of investigation in this current study.

Recommendations are made for the continuation of PDT experiments on additional cancer cell lines to identify any further cell line specific reactions (such as the relatively low sensitivity of MIA PaCa-2 shown in this study) and also on non-tumour cell lines. It was shown in this study that duramycin could detect PE on and reduce the cell viability of HUVECs. The duramycin-porphyrin conjugate PDT experiments could be repeated using HUVECs and other normal cell lines to assess treatment effect. If the PDT treatment had a similar effect on the non-tumour cells as on the tumour cells then this may provide parameters for any future *in vivo* studies. For example, the requirement for precise application of the PDT light to the tumour tissue so as to limit damage to surrounding normal tissue. PDT has been shown to be applicable to TAT and to have valuable synergistic effect when in combination with other major cancer therapies[15, 141, 142]. However only a limited number of PhtS have been approved by the FDA and EU for use in the clinical setting[120, 149]. Thus work towards future *in vivo* PDT studies is encouraged as duramycin has the potential to be an effective PDT agent.

This study presented a preliminary investigation into the effect that duramycin-porphyrin conjugate and PDT light treatment has on CAM tumour xenografts. However due to time and material constraints only four chicken eggs were available to the study. Prospective experiments using the CAM model could include additional/ a higher number of controls such as untreated controls (no drug, no light), dark toxicity controls (drug only) and light sensitivity controls (light irradiation only). These could be performed using the duramycin-porphyrin conjugate, unconjugated duramycin and the capped porphyrin control. This could show whether the duramycin-porphyrin conjugate has an enhanced anti-cancer effect over its unconjugated substituents. In this study the PDT treatment caused superficial cell death damage to the SK-OV-3 tumour xenografts. This potentially meant that the conjugate did not permeate through the tumours, as was suggested for unconjugated duramycin in the SK-OV-3 tumour spheroids. The reason for this potential lack of permeability in the tumour spheroids was thought to be due to a necrotic core however the histological analysis of the CAM tumours revealed a viable core. Thus future work could involve the comparison of histological stains of tumours grown on the CAM and as 3D spheroids. To evaluate the permeability of the duramycin-porphyrin conjugate the distribution of the conjugate could potentially be detected in the two tumour types using some form of fluorescence microscopy[272, 273]. The superficial effects of tumour damage, however, may have been a result of a number of experimental variables other than drug permeability such as conjugate concentration, conjugate volume, irradiance dose and the

incubation time with the duramycin-porphyrin conjugate. Future experiments could focus on adjusting these variables to optimise the conditions for PDT in this model. For example Gottfried *et al*.[171] and Toledano *et al*.[172] measured the CAM uptake time of their PhtS using a fluorimeter. This method could potentially be applied to the tumours grafted onto the CAM to establish a more appropriate incubation time for the duramycin-porphyrin conjugate. Additionally, if the tumour xenografts on the CAM could be characterised so that they were uniform in size then, after dissection, the tumours could be weighed to compare the reduction in mass between the control and treated tumours[167]. Finally, SK-OV-3 was chosen for the CAM experiments due to time constraints and a method for this cancer cell line had already been established within this research group (by Dr Y. Xiao). Therefore it is recommended that future CAM experiments involve tumour xenografts formed from a variety of cancer cell lines.

References

1. Mathers CD, Loncar D. Projections of global mortality and burden of disease from 2002 to 2030. *PLoS medicine*. 2006;3(11):e442.
2. WHO. Projections of mortality and causes of death, 2015 and 2030. *World Health Organization*. 2013.
3. OFNS. Cancer Registration Statistics, England: 2014. *Office for National Statistics*. 2016:1-17.
4. OFNS. Deaths registered in England and Wales: 2015. *Office for National Statistics*. 2016:1-8.
5. WHO. International Statistical Classification of Diseases and Related Health Problems 10th Revision (ICD-10). *World Health Organization*. 2016:C00-D48.
6. Hanahan D, Weinberg RA. The hallmarks of cancer. *Cell*. 2000;100(1):57-70.
7. Hanahan D, Weinberg Robert A. Hallmarks of Cancer: The Next Generation. *Cell*. 2011;144(5):646-74.
8. Chowanadisai W, Messerli SM, Miller DH, Medina JE, Hamilton JW, Messerli MA, et al. Cisplatin Resistant Spheroids Model Clinically Relevant Survival Mechanisms in Ovarian Tumors. *PLoS One*. 2016;11(3):e0151089.
9. Sheikh R, Walsh N, Clynes M, O'Connor R, McDermott R. Challenges of drug resistance in the management of pancreatic cancer. *Expert review of anticancer therapy*. 2010;10(10):1647-61.
10. Schniewind B, Christgen M, Kurdow R, Haye S, Kremer B, Kalthoff H, et al. Resistance of pancreatic cancer to gemcitabine treatment is dependent on mitochondria-mediated apoptosis. *Int J Cancer*. 2004;109(2):182-8.
11. Nyst HJ, Tan IB, Stewart FA, Balm AJ. Is photodynamic therapy a good alternative to surgery and radiotherapy in the treatment of head and neck cancer? *Photodiagnosis Photodyn Ther*. 2009;6(1):3-11.
12. Sorensen HT, Mellemkjaer L, Olsen JH, Baron JA. Prognosis of cancers associated with venous thromboembolism. *The New England journal of medicine*. 2000;343(25):1846-50.
13. Khorana AA, Francis CW, Culakova E, Lyman GH. Risk factors for chemotherapy-associated venous thromboembolism in a prospective observational study. *Cancer*. 2005;104(12):2822-9.
14. Li J, Chen F, Cona MM, Feng Y, Himmelreich U, Oyen R, et al. A review on various targeted anticancer therapies. *Targeted oncology*. 2012;7(1):69-85.
15. Giuntini F, Alonso CM, Boyle RW. Synthetic approaches for the conjugation of porphyrins and related macrocycles to peptides and proteins. *Photochem Photobiol Sci*. 2011;10(5):759-91.
16. Kwekkeboom DJ, Bakker WH, Kam BL, Teunissen JJM, Kooij PPM, de Herder WW, et al. Treatment of patients with gastro-entero-pancreatic (GEP) tumours with the novel radiolabelled somatostatin analogue [(177)Lu-DOTA(0),Tyr(3)]octreotate. *European Journal of Nuclear Medicine and Molecular Imaging*. 2003;30(3):417-22.
17. Sodek KL, Ringuette MJ, Brown TJ. Compact spheroid formation by ovarian cancer cells is associated with contractile behavior and an invasive phenotype. *Int J Cancer*. 2009;124(9):2060-70.
18. Desjardins M, Xie J, Gurler H, Muralidhar GG, Sacks JD, Burdette JE, et al. Versican regulates metastasis of epithelial ovarian carcinoma cells and spheroids. *Journal of ovarian research*. 2014;7:70.
19. Desai A, Xu J, Aysola K, Qin Y, Okoli C, Hariprasad R, et al. Epithelial ovarian cancer: An overview. *World journal of translational medicine*. 2014;3(1):1-8.

20. CGARN. Integrated genomic analyses of ovarian carcinoma. *Nature*. 2011;474(7353):609-15.
21. OFNS. Cancer survival in England: Patients diagnosed between 2010 and 2014 and followed up to 2015. *Office for National Statistics*. 2016:1-15.
22. Lokman NA, Elder ASF, Ricciardelli C, Oehler MK. Chick Chorioallantoic Membrane (CAM) Assay as an In Vivo Model to Study the Effect of Newly Identified Molecules on Ovarian Cancer Invasion and Metastasis. *International Journal of Molecular Sciences*. 2012;13(8):9959-70.
23. Zhong ZF, Tan W, Wang SP, Qiang WA, Wang YT. Anti-proliferative activity and cell cycle arrest induced by evodiamine on paclitaxel-sensitive and -resistant human ovarian cancer cells. *Sci Rep*. 2015;5:16415.
24. Zhou J, O'Brate A, Zelnak A, Giannakakou P. Survivin Deregulation in β-Tubulin Mutant Ovarian Cancer Cells Underlies Their Compromised Mitotic Response to Taxol. *Cancer research*. 2004;64(23):8708-14.
25. Li J, Wientjes MG, Au JL. Pancreatic cancer: pathobiology, treatment options, and drug delivery. *The AAPS journal*. 2010;12(2):223-32.
26. Haugk B. Pancreatic intraepithelial neoplasia-can we detect early pancreatic cancer? *Histopathology*. 2010;57(4):503-14.
27. Ying H, Dey P, Yao W, Kimmelman AC, Draetta GF, Maitra A, et al. Genetics and biology of pancreatic ductal adenocarcinoma. *Genes & development*. 2016;30(4):355-85.
28. Kleeff J, Beckhove P, Esposito I, Herzig S, Huber PE, Lohr JM, et al. Pancreatic cancer microenvironment. *Int J Cancer*. 2007;121(4):699-705.
29. Visser BC, Muthusamy VR, Yeh BM, Coakley FV, Way LW. Diagnostic evaluation of cystic pancreatic lesions. *HPB : The Official Journal of the International Hepato Pancreato Biliary Association*. 2008;10(1):63-9.
30. Vera R, Dotor E, Feliu J, Gonzalez E, Laquente B, Macarulla T, et al. SEOM Clinical Guideline for the treatment of pancreatic cancer (2016). *Clinical & translational oncology : official publication of the Federation of Spanish Oncology Societies and of the National Cancer Institute of Mexico*. 2016;18(12):1172-8.
31. Vaccaro V, Sperduti I, Vari S, Bria E, Melisi D, Garufi C, et al. Metastatic pancreatic cancer: Is there a light at the end of the tunnel? *World Journal of Gastroenterology : WJG*. 2015;21(16):4788-801.
32. Belhocine TZ, Prato FS. Transbilayer phospholipids molecular imaging. *EJNMMI research*. 2011;1(1):17.
33. Vance JE. Phosphatidylserine and phosphatidylethanolamine in mammalian cells: two metabolically related aminophospholipids. *Journal of lipid research*. 2008;49(7):1377-87.
34. Jain SK. In vivo externalization of phosphatidylserine and phosphatidylethanolamine in the membrane bilayer and hypercoagulability by the lipid peroxidation of erythrocytes in rats. *Journal of Clinical Investigation*. 1985;76(1):281-6.
35. Fadeel B, Xue D. The ins and outs of phospholipid asymmetry in the plasma membrane: roles in health and disease. *Crit Rev Biochem Mol Biol*. 2009;44(5):264-77.
36. van Deenen LL. Topology and dynamics of phospholipids in membranes. *FEBS letters*. 1981;123(1):3-15.
37. Rockenfeller P, Koska M, Pietrocola F, Minois N, Knittelfelder O, Sica V, et al. Phosphatidylethanolamine positively regulates autophagy and longevity. *Cell death and differentiation*. 2015;22(3):499-508.
38. Daleke DL. Regulation of transbilayer plasma membrane phospholipid asymmetry. *Journal of lipid research*. 2003;44(2):233-42.

39. Makino A, Baba T, Fujimoto K, Iwamoto K, Yano Y, Terada N, et al. Cinnamycin (Ro 09-0198) promotes cell binding and toxicity by inducing transbilayer lipid movement. *The Journal of biological chemistry*. 2003;278(5):3204-9.
40. Aoki Y, Uenaka T, Aoki J, Umeda M, Inoue K. A novel peptide probe for studying the transbilayer movement of phosphatidylethanolamine. *Journal of biochemistry*. 1994;116(2):291-7.
41. Marconescu A, Thorpe PE. Coincident exposure of phosphatidylethanolamine and anionic phospholipids on the surface of irradiated cells. *Biochimica et biophysica acta*. 2008;1778(10):2217-24.
42. van Meer G, Voelker DR, Feigenson GW. Membrane lipids: where they are and how they behave. *Nat Rev Mol Cell Biol*. 2008;9(2):112-24.
43. Andersen JP, Vestergaard AL, Mikkelsen SA, Mogensen LS, Chalat M, Molday RS. P4-ATPases as Phospholipid Flippases-Structure, Function, and Enigmas. *Frontiers in physiology*. 2016;7:275.
44. Maulik N, Kagan VE, Tyurin VA, Das DK. Redistribution of phosphatidylethanolamine and phosphatidylserine precedes reperfusion-induced apoptosis. *The American journal of physiology*. 1998;274(1 Pt 2):H242-8.
45. Daleke DL. Phospholipid flippases. *The Journal of biological chemistry*. 2007;282(2):821-5.
46. Yamaji-Hasegawa A, Tsujimoto M. Asymmetric distribution of phospholipids in biomembranes. *Biological & pharmaceutical bulletin*. 2006;29(8):1547-53.
47. Montigny C, Lyons J, Champeil P, Nissen P, Lenoir G. On the molecular mechanism of flippase- and scramblase-mediated phospholipid transport. *Biochimica et biophysica acta*. 2016;1861(8 Pt B):767-83.
48. Emoto K, Toyama-Sorimachi N, Karasuyama H, Inoue K, Umeda M. Exposure of Phosphatidylethanolamine on the Surface of Apoptotic Cells. *Experimental cell research*. 1997;232(2):430-4.
49. Yates KR, Welsh J, Udegbunam NO, Greenman J, Maraveyas A, Madden LA. Duramycin exhibits antiproliferative properties and induces apoptosis in tumour cells. *Blood Coagul Fibrinolysis*. 2012;23(5):396-401.
50. Emoto K, Kobayashi T, Yamaji A, Aizawa H, Yahara I, Inoue K, et al. Redistribution of phosphatidylethanolamine at the cleavage furrow of dividing cells during cytokinesis. *Proceedings of the National Academy of Sciences of the United States of America*. 1996;93(23):12867-72.
51. Iwamoto K, Kobayashi S, Fukuda R, Umeda M, Kobayashi T, Ohta A. Local exposure of phosphatidylethanolamine on the yeast plasma membrane is implicated in cell polarity. *Genes Cells*. 2004;9(10):891-903.
52. Tavoosi N, Davis-Harrison RL, Pogorelov TV, Ohkubo YZ, Arcario MJ, Clay MC, et al. Molecular Determinants of Phospholipid Synergy in Blood Clotting. *Journal of Biological Chemistry*. 2011;286:23247-53.
53. Falls LA, Furie B, Furie BC. Role of Phosphatidylethanolamine in Assembly and Function of the Factor IXa-Factor VIIIa Complex on Membrane Surfaces. *Biochemistry*. 2000;39:13216-22.
54. Beals JM, Castellino FJ. The interaction of bovine Factor IX, its activation intermediate, Factor IXα, and its activation products, Factor IXaα and Factor IXaβ, with acidic phospholipid vesicles of various compositions. *Biochem J*. 1986;236:861-9.
55. Smeets EF, Comfurius P, Bevers EM, Zwaal RFA. Contribution Of Different Phospholipid Classes To The Prothrombin Converting Capacity Of Sonicated Lipid Vesicles. *Thrombosis Research*. 1996;81:419-26.
56. Smirnov MD, Ford DA, Esmon CT, Esmon NL. The effect of membrane composition on the hemostatic balance. *Biochemistry*. 1999;38(12):3591-8.

57. Neuenschwander PF, Bianco-Fisher E, Rezaie AR, Morrisey J. Phosphatidylethanolamine Augments Factor VIIa-Tissue Factor Activity: Enhancement of Sensitivity to Phosphatidylserine. *Biochemistry*. 1995;34:13988-93.
58. Yates KR, Welsh J, Echrish HH, Greenman J, Maraveyas A, Madden LA. Pancreatic cancer cell and microparticle procoagulant surface characterization: involvement of membrane-expressed tissue factor, phosphatidylserine and phosphatidylethanolamine. *Blood Coagul Fibrinolysis*. 2011;22(8):680-7.
59. Stafford JH, Thorpe PE. Increased Exposure of Phosphatidylethanolamine on the Surface of Tumor Vascular Endothelium. *Neoplasia*. 2011;13(4):299-IN2.
60. Larson MC, Woodliff JE, Hillery CA, Kearl TJ, Zhao M. Phosphatidylethanolamine is externalized at the surface of microparticles. *Biochimica et Biophysica Acta (BBA) - Molecular and Cell Biology of Lipids*. 2012;1821(12):1501-7.
61. Fernandez R, Garate J, Lage S, Teres S, Higuera M, Bestard-Escalas J, et al. Identification of Biomarkers of Necrosis in Xenografts Using Imaging Mass Spectrometry. *Journal of the American Society for Mass Spectrometry*. 2016;27(2):244-54.
62. Elvas F, Vangestel C, Pak K, Vermeulen P, Gray B, Stroobants S, et al. Early Prediction of Tumor Response to Treatment: Preclinical Validation of 99mTc-Duramycin. *Journal of nuclear medicine : official publication, Society of Nuclear Medicine*. 2016;57(5):805-11.
63. Luo R, Niu L, Qiu F, Fang W, Fu T, Zhao M, et al. Monitoring Apoptosis of Breast Cancer Xenograft After Paclitaxel Treatment With 99mTc-Labeled Duramycin SPECT/CT. *Molecular imaging*. 2016;15.
64. Zhao M, Li Z, Bugenhagen S. 99mTc-labeled duramycin as a novel phosphatidylethanolamine-binding molecular probe. *Journal of nuclear medicine : official publication, Society of Nuclear Medicine*. 2008;49(8):1345-52.
65. Hayashi F, Nagashima K, Terui Y, Kawamura Y, Matsumoto K, Itazaki H. The Structure Of PA48009: The Revised Structure. *The Journal of antibiotics*. 1990;43(11):1421-30.
66. Zimmermann N, Freund S, Fredenhagen A, Jung G. Solution structures of the lantibiotics duramycin B and C. *European Journal of Biochemistry*. 1993;216(2):419-28.
67. Sahl HG, Bierbaum G. Lantibiotics: biosynthesis and biological activities of uniquely modified peptides from gram-positive bacteria. *Annual review of microbiology*. 1998;52:41-79.
68. Zhao M. Lantibiotics as probes for phosphatidylethanolamine. *Amino Acids*. 2011;41(5):1071-9.
69. Hosoda K, Ohya M, Kohno T, Maeda T, Endo S, Wakamatsu K. Structure determination of an immunopotentiator peptide, cinnamycin, complexed with lysophosphatidylethanolamine by 1H-NMR1. *Journal of biochemistry*. 1996;119(2):226-30.
70. Navarro J, Chabot J, Sherrill K, Aneja R, Zahler SA, Racker E. Interaction of duramycin with artificial and natural membranes. *Biochemistry*. 1985;24(17):4645-50.
71. Clejan S, Guffanti AA, Cohen MA, Krulwich TA. Mutation of Bacillus firmus OF4 to duramycin resistance results in substantial replacement of membrane lipid phosphatidylethanolamine by its plasmalogen form. *Journal of bacteriology*. 1989;171(3):1744-6.
72. Machaidze G, Seelig J. Specific binding of cinnamycin (Ro 09-0198) to phosphatidylethanolamine. Comparison between micellar and membrane environments. *Biochemistry*. 2003;42(43):12570-6.
73. Iwamoto K, Hayakawa T, Murate M, Makino A, Ito K, Fujisawa T, et al. Curvature-Dependent Recognition of Ethanolamine Phospholipids by Duramycin and Cinnamycin. *Biophysical journal*. 2007;93(5):1608-19.

74. Li Z, Wells CW, North PE, Kumar S, Duris CB, McIntyre JA, et al. Phosphatidylethanolamine at the luminal endothelial surface--implications for hemostasis and thrombotic autoimmunity. *Clin Appl Thromb Hemost*. 2011;17(2):158-63.
75. Zhao M, Li Z. A single-step kit formulation for the (99m)Tc-labeling of HYNIC-Duramycin. *Nuclear medicine and biology*. 2012;39(7):1006-11.
76. Audi S, Li Z, Capacete J, Liu Y, Fang W, Shu LG, et al. Understanding the in vivo uptake kinetics of a phosphatidylethanolamine-binding agent (99m)Tc-Duramycin. *Nuclear medicine and biology*. 2012;39(6):821-5.
77. Zhang Y, Stevenson GD, Barber C, Furenlid LR, Barrett HH, Woolfenden JM, et al. Imaging of rat cerebral ischemia-reperfusion injury using(99m)Tc-labeled duramycin. *Nuclear medicine and biology*. 2013;40(1):80-8.
78. Johnson SE, Li Z, Liu Y, Moulder JE, Zhao M. Whole-body imaging of high-dose ionizing irradiation-induced tissue injuries using 99mTc-duramycin. *Journal of nuclear medicine : official publication, Society of Nuclear Medicine*. 2013;54(8):1397-403.
79. Audi SH, Jacobs ER, Zhao M, Roerig DL, Haworth ST, Clough AV. In vivo detection of hyperoxia-induced pulmonary endothelial cell death using (99m)Tc-duramycin. *Nuclear medicine and biology*. 2015;42(1):46-52.
80. Wang L, Wang F, Fang W, Johnson SE, Audi S, Zimmer M, et al. The feasibility of imaging myocardial ischemic/reperfusion injury using (99m)Tc-labeled duramycin in a porcine model. *Nuclear medicine and biology*. 2015;42(2):198-204.
81. Liu Z, Larsen BT, Lerman LO, Gray BD, Barber C, Hedayat AF, et al. Detection of atherosclerotic plaques in ApoE-deficient mice using (99m)Tc-duramycin. *Nuclear medicine and biology*. 2016;43(8):496-505.
82. Elvas F, Vangestel C, Rapic S, Verhaeghe J, Gray B, Pak K, et al. Characterization of [(99m)Tc]Duramycin as a SPECT Imaging Agent for Early Assessment of Tumor Apoptosis. *Molecular imaging and biology : MIB : the official publication of the Academy of Molecular Imaging*. 2015;17(6):838-47.
83. Yao S, Hu K, Tang G, Liang X, Du K, Nie D, et al. Positron emission tomography imaging of cell death with [(18)F]FPDuramycin. *Apoptosis : an international journal on programmed cell death*. 2014;19(5):841-50.
84. Nakamura S, Racker E. Inhibitory effect of duramycin on partial reactions catalyzed by sodium-potassium adenosinetriphosphatase from dog kidney. *Biochemistry*. 1984;23(2):385-9.
85. Stone D, Xie X, Racker E. Inhibition of clathrin-coated vesicle acidification by duramycin. *Journal of Biological Chemistry*. 1984;259(5):2701-3.
86. Cloutier MM, Guernsey L, Mattes P, Koeppen B. Duramycin enhances chloride secretion in airway epithelium. *American Journal of Physiology-Cell Physiology*. 1990;259(3):C450-C4.
87. Cloutier MM, Guernsey L, Sha'afi RI. Duramycin increases intracellular calcium in airway epithelium. *Molecular Membrane Biology*. 1993;10(2):107-18.
88. Roberts M, Hladky S, Pickles R, Cuthbert A. Stimulation of sodium transport by duramycin in cultured human colonic epithelia. *Journal of Pharmacology and Experimental Therapeutics*. 1991;259(3):1050-8.
89. Sheth TR, Henderson RM, Hladky SB, Cuthbert AW. Ion channel formation by duramycin. *Biochimica et Biophysica Acta (BBA) - Biomembranes*. 1992;1107(1):179-85.
90. Zebedin E, Koenig X, Radenkovic M, Pankevych H, Todt H, Freissmuth M, et al. Effects of duramycin on cardiac voltage-gated ion channels. *Naunyn-Schmiedeberg's archives of pharmacology*. 2008;377(1):87-100.
91. Oliynyk I, Varelogianni G, Roomans GM, Johannesson M. Effect of duramycin on chloride transport and intracellular calcium concentration in cystic fibrosis and non-cystic fibrosis epithelia. *APMIS*. 2010;118(12):982-90.

92. Rzeźnicka II, Sovago M, Backus EHG, Bonn M, Yamada T, Kobayashi T, et al. Duramycin-Induced Destabilization of a Phosphatidylethanolamine Monolayer at the Air−Water Interface Observed by Vibrational Sum-Frequency Generation Spectroscopy. *Langmuir*. 2010;26(20):16055-62.
93. Berg J, Yang H, Jan LY. Ca2+-activated Cl- channels at a glance. *Journal of cell science*. 2012;125(Pt 6):1367-71.
94. Zeitlin PL, Boyle MP, Guggino WB, Molina L. A phase I trial of intranasal Moli1901 for cystic fibrosis. *Chest*. 2004;125(1):143-9.
95. Grasemann H, Stehling F, Brunar H, Widmann R, Laliberte TW, Molina L, et al. INhalation of moli1901 in patients with cystic fibrosis*. *Chest*. 2007;131(5):1461-6.
96. McNulty MJ, Hutabarat RH, Findlay JW, Devereux K, Knick VC, Harvey RJ, et al. Pharmacokinetics and tissue distribution of the nonadecapeptide Moli1901 in rats and mice. *Xenobiotica; the fate of foreign compounds in biological systems*. 2003;33(2):197-210.
97. Rickert DE, Dingley K, Ubick E, Dix KJ, Molina L. Determination of the tissue distribution and excretion by accelerator mass spectrometry of the nonadecapeptide 14C-Moli1901 in beagle dogs after intratracheal instillation. *Chemico-Biological Interactions*. 2005;155(1–2):55-61.
98. Flume PA, Van Devanter DR. State of progress in treating cystic fibrosis respiratory disease. *BMC medicine*. 2012;10:88.
99. MacVinish LJ, Cope G, Ropenga A, Cuthbert AW. Chloride transporting capability of Calu-3 epithelia following persistent knockdown of the cystic fibrosis transmembrane conductance regulator, CFTR. *British Journal of Pharmacology*. 2007;150(8):1055-65.
100. Parkash J, Asotra K. Calcium wave signaling in cancer cells. *Life sciences*. 2010;87(19-22):587-95.
101. Eltit JM, Hidalgo J, Liberona JL, Jaimovich E. Slow calcium signals after tetanic electrical stimulation in skeletal myotubes. *Biophysical journal*. 2004;86(5):3042-51.
102. Clapham DE. Calcium signaling. *Cell*. 2007;131(6):1047-58.
103. Parekh AB, Putney JW, Jr. Store-operated calcium channels. *Physiological reviews*. 2005;85(2):757-810.
104. Lehen'kyi V, Raphael M, Prevarskaya N. The role of the TRPV6 channel in cancer. *The Journal of physiology*. 2012;590(6):1369-76.
105. Monteith GR, Davis FM, Roberts-Thomson SJ. Calcium channels and pumps in cancer: changes and consequences. *The Journal of biological chemistry*. 2012;287(38):31666-73.
106. Schmidt S, Liu G, Liu G, Yang W, Honisch S, Pantelakos S, et al. Enhanced Orai1 and STIM1 expression as well as store operated Ca(2+) entry in therapy resistant ovary carcinoma cells. *Oncotarget*. 2014;5(13):4799-810.
107. Heighway J, Betticher DC, Hoban PR, Altermatt HJ, Cowen R. Coamplification in tumors of KRAS2, type 2 inositol 1,4,5 triphosphate receptor gene, and a novel human gene, KRAG. *Genomics*. 1996;35(1):207-14.
108. Sakakura C, Hagiwara A, Fukuda K, Shimomura K, Takagi T, Kin S, et al. Possible involvement of inositol 1,4,5-trisphosphate receptor type 3 (IP3R3) in the peritoneal dissemination of gastric cancers. *Anticancer Res*. 2003;23(5a):3691-7.
109. Kusner LL, Mygland A, Kaminski HJ. Ryanodine receptor gene expression thymomas. *Muscle & nerve*. 1998;21(10):1299-303.
110. Yee NS. Roles of TRPM8 Ion Channels in Cancer: Proliferation, Survival, and Invasion. *Cancers (Basel)*. 2015;7(4):2134-46.
111. Yee NS, Zhou W, Lee M. Transient receptor potential channel TRPM8 is over-expressed and required for cellular proliferation in pancreatic adenocarcinoma. *Cancer Lett*. 2010;297(1):49-55.

112. Wang CY, Lai MD, Phan NN, Sun Z, Lin YC. Meta-Analysis of Public Microarray Datasets Reveals Voltage-Gated Calcium Gene Signatures in Clinical Cancer Patients. *PLoS One*. 2015;10(7).
113. Roderick HL, Cook SJ. Ca2+ signalling checkpoints in cancer: remodelling Ca2+ for cancer cell proliferation and survival. *Nat Rev Cancer*. 2008;8(5):361-75.
114. Chen R, Valencia I, Zhong F, McColl KS, Roderick HL, Bootman MD, et al. Bcl-2 functionally interacts with inositol 1,4,5-trisphosphate receptors to regulate calcium release from the ER in response to inositol 1,4,5-trisphosphate. *The Journal of cell biology*. 2004;166(2):193-203.
115. Danial NN, Korsmeyer SJ. Cell death: critical control points. *Cell*. 2004;116(2):205-19.
116. Li DM, Sun H. PTEN/MMAC1/TEP1 suppresses the tumorigenicity and induces G1 cell cycle arrest in human glioblastoma cells. *Proceedings of the National Academy of Sciences of the United States of America*. 1998;95(26):15406-11.
117. James AD, Chan A, Erice O, Siriwardena AK, Bruce JIE. Glycolytic ATP Fuels the Plasma Membrane Calcium Pump Critical for Pancreatic Cancer Cell Survival. *The Journal of biological chemistry*. 2013;288(50):36007-19.
118. Frandsen SK, Gissel H, Hojman P, Tramm T, Eriksen J, Gehl J. Direct therapeutic applications of calcium electroporation to effectively induce tumor necrosis. *Cancer research*. 2012;72(6):1336-41.
119. Agostinis P, Berg K, Cengel KA, Foster TH, Girotti AW, Gollnick SO, et al. Photodynamic therapy of cancer: an update. *CA Cancer J Clin*. 2011;61(4):250-81.
120. Zhu TC, Finlay JC. The role of photodynamic therapy (PDT) physics. *Medical Physics*. 2008;35(7):3127.
121. Josefsen LB, Boyle RW. Photodynamic therapy and the development of metal-based photosensitisers. *Metal-based drugs*. 2008;2008:276109.
122. Sharman WM, Allen CM, van Lier JE. Photodynamic therapeutics: basic principles and clinical applications. *Drug discovery today*. 1999;4(11):507-17.
123. Rajendran M. Quinones as photosensitizer for photodynamic therapy: ROS generation, mechanism and detection methods. *Photodiagnosis Photodyn Ther*. 2016;13:175-87.
124. Wang J, Yi J. Cancer cell killing via ROS: to increase or decrease, that is the question. *Cancer biology & therapy*. 2008;7(12):1875-84.
125. Korbelik M. Induction of tumor immunity by photodynamic therapy. *Journal of clinical laser medicine & surgery*. 1996;14(5):329-34.
126. Korbelik M. PDT-associated host response and its role in the therapy outcome. *Lasers Surg Med*. 2006;38(5):500-8.
127. Chen B, Pogue BW, Hoopes PJ, Hasan T. Vascular and cellular targeting for photodynamic therapy. *Critical reviews in eukaryotic gene expression*. 2006;16(4):279-305.
128. Nestor MS, Gold MH, Kauvar AN, Taub AF, Geronemus RG, Ritvo EC, et al. The use of photodynamic therapy in dermatology: results of a consensus conference. *Journal of drugs in dermatology : JDD*. 2006;5(2):140-54.
129. Braathen LR, Szeimies RM, Basset-Seguin N, Bissonnette R, Foley P, Pariser D, et al. Guidelines on the use of photodynamic therapy for nonmelanoma skin cancer: an international consensus. International Society for Photodynamic Therapy in Dermatology, 2005. *J Am Acad Dermatol*. 2007;56(1):125-43.
130. Jerjes W, Upile T, Akram S, Hopper C. The surgical palliation of advanced head and neck cancer using photodynamic therapy. *Clin Oncol (R Coll Radiol)*. 2010;22(9):785-91.
131. Wolfsen HC. Carpe luz--seize the light: endoprevention of esophageal adenocarcinoma when using photodynamic therapy with porfimer sodium. *Gastrointest Endosc*. 2005;62(4):499-503.

132. Celli JP, Solban N, Liang A, Pereira SP, Hasan T. Verteporfin-based photodynamic therapy overcomes gemcitabine insensitivity in a panel of pancreatic cancer cell lines. *Lasers Surg Med*. 2011;43(7):565-74.
133. Anbil S, Rizvi I, Celli JP, Alagic N, Pogue BW, Hasan T. Impact of treatment response metrics on photodynamic therapy planning and outcomes in a three-dimensional model of ovarian cancer. *J Biomed Opt*. 2013;18(9):098004.
134. Rizvi I, Anbil S, Alagic N, Celli J, Zheng LZ, Palanisami A, et al. PDT dose parameters impact tumoricidal durability and cell death pathways in a 3D ovarian cancer model. *Photochem Photobiol*. 2013;89(4):942-52.
135. Bartusik D, Aebisher D, Ghogare A, Ghosh G, Abramova I, Hasan T, et al. A fiberoptic (photodynamic therapy type) device with a photosensitizer and singlet oxygen delivery probe tip for ovarian cancer cell killing. *Photochem Photobiol*. 2013;89(4):936-41.
136. Golab J, Olszewska D, Mroz P, Kozar K, Kaminski R, Jalili A, et al. Erythropoietin restores the antitumor effectiveness of photodynamic therapy in mice with chemotherapy-induced anemia. *Clinical cancer research : an official journal of the American Association for Cancer Research*. 2002;8(5):1265-70.
137. Goff BA, Blake J, Bamberg MP, Hasan T. Treatment of ovarian cancer with photodynamic therapy and immunoconjugates in a murine ovarian cancer model. *British Journal of Cancer*. 1996;74(8):1194-8.
138. Samkoe KS, Chen A, Rizvi I, O'Hara JA, Hoopes PJ, Pereira SP, et al. Imaging tumor variation in response to photodynamic therapy in pancreatic cancer xenograft models. *Int J Radiat Oncol Biol Phys*. 2010;76(1):251-9.
139. Bown SG, Rogowska AZ, Whitelaw DE, Lees WR, Lovat LB, Ripley P, et al. Photodynamic therapy for cancer of the pancreas. *Gut*. 2002;50(4):549-57.
140. Huggett MT, Jermyn M, Gillams A, Illing R, Mosse S, Novelli M, et al. Phase I/II study of verteporfin photodynamic therapy in locally advanced pancreatic cancer. *Br J Cancer*. 2014;110(7):1698-704.
141. Xie Q. Synergetic anticancer effect of combined gemcitabine and photodynamic therapy on pancreatic cancer in vivo. *World Journal of Gastroenterology*. 2009;15(6):737.
142. Lucena SR, Salazar N, Gracia-Cazana T, Zamarron A, Gonzalez S, Juarranz A, et al. Combined Treatments with Photodynamic Therapy for Non-Melanoma Skin Cancer. *Int J Mol Sci*. 2015;16(10):25912-33.
143. Zhao B, He YY. Recent advances in the prevention and treatment of skin cancer using photodynamic therapy. *Expert review of anticancer therapy*. 2010;10(11):1797-809.
144. Vulcan TG, Zhu TC, Rodriguez CE, Hsi A, Fraker DL, Baas P, et al. Comparison between isotropic and nonisotropic dosimetry systems during intraperitoneal photodynamic therapy. *Lasers Surg Med*. 2000;26(3):292-301.
145. Nowis D, Makowski M, Stoklosa T, Legat M, Issat T, Golab J. Direct tumor damage mechanisms of photodynamic therapy. *Acta biochimica Polonica*. 2005;52(2):339-52.
146. van Geel IP, Oppelaar H, Oussoren YG, van der Valk MA, Stewart FA. Photosensitizing efficacy of MTHPC-PDT compared to photofrin-PDT in the RIF1 mouse tumour and normal skin. *Int J Cancer*. 1995;60(3):388-94.
147. Spikes JD. Porphyrins and related compounds as photodynamic sensitizers. *Annals of the New York Academy of Sciences*. 1975;244:496-508.
148. Yang X, Palasuberniam P, Kraus D, Chen B. Aminolevulinic Acid-Based Tumor Detection and Therapy: Molecular Mechanisms and Strategies for Enhancement. *Int J Mol Sci*. 2015;16(10):25865-80.
149. Baldea I, Ion RM, Olteanu DE, Nenu I, Tudor D, Filip AG. Photodynamic therapy of melanoma using new, synthetic porphyrins and phthalocyanines as photosensitisers - a comparative study. *Clujul Med*. 2015;88(2):175-80.

150. Frame FM, Savoie H, Bryden F, Giuntini F, Mann VM, Simms MS, et al. Mechanisms of growth inhibition of primary prostate epithelial cells following gamma irradiation or photodynamic therapy include senescence, necrosis, and autophagy, but not apoptosis. *Cancer Med*. 2016;5(1):61-73.
151. Tome JP, Neves MG, Tome AC, Cavaleiro JA, Soncin M, Magaraggia M, et al. Synthesis and antibacterial activity of new poly-S-lysine-porphyrin conjugates. *Journal of medicinal chemistry*. 2004;47(26):6649-52.
152. Bullous AJ, Alonso CM, Boyle RW. Photosensitiser-antibody conjugates for photodynamic therapy. *Photochem Photobiol Sci*. 2011;10(5):721-50.
153. Sutton JM, Clarke OJ, Fernandez N, Boyle RW. Porphyrin, chlorin, and bacteriochlorin isothiocyanates: useful reagents for the synthesis of photoactive bioconjugates. *Bioconjugate chemistry*. 2002;13(2):249-63.
154. Staneloudi C, Smith KA, Hudson R, Malatesti N, Savoie H, Boyle RW, et al. Development and characterization of novel photosensitizer : scFv conjugates for use in photodynamic therapy of cancer. *Immunology*. 2007;120(4):512-7.
155. Schmidt-Erfurth U, Diddens H, Birngruber R, Hasan T. Photodynamic targeting of human retinoblastoma cells using covalent low-density lipoprotein conjugates. *Br J Cancer*. 1997;75(1):54-61.
156. Vega DL, Lodge P, Vivero-Escoto JL. Redox-Responsive Porphyrin-Based Polysilsesquioxane Nanoparticles for Photodynamic Therapy of Cancer Cells. *Int J Mol Sci*. 2016;17(1).
157. Ribatti D. The chick embryo chorioallantoic membrane as a model for tumor biology. *Experimental cell research*. 2014;328(2):314-24.
158. Vargas A, Zeisser-Labouebe M, Lange N, Gurny R, Delie F. The chick embryo and its chorioallantoic membrane (CAM) for the in vivo evaluation of drug delivery systems. *Advanced drug delivery reviews*. 2007;59(11):1162-76.
159. Packard MJ. Evaluation of a protocol for studying the chick chorioallantoic membrane in vitro. *Comparative biochemistry and physiology Part A, Molecular & integrative physiology*. 1999;124(2):215-9.
160. Janse EM, Jeurissen SH. Ontogeny and function of two non-lymphoid cell populations in the chicken embryo. *Immunobiology*. 1991;182(5):472-81.
161. Janković BD, Isaković K, Lukić ML, Vujanović NL, Petrović S, Marković BM. Immunological capacity of the chicken embryo. I. Relationship between the maturation of lymphoid tissues and the occurrence of cell-mediated immunity in the developing chicken embryo. *Immunology*. 1975;29(3):497-508.
162. Murphy JB, Rous P. THE BEHAVIOR OF CHICKEN SARCOMA IMPLANTED IN THE DEVELOPING EMBRYO. *The Journal of Experimental Medicine*. 1912;15(2):119-32.
163. Murphy JB. TRANSPLANTABILITY OF TISSUES TO THE EMBRYO OF FOREIGN SPECIES: ITS BEARING ON QUESTIONS OF TISSUE SPECIFICITY AND TUMOR IMMUNITY. *The Journal of Experimental Medicine*. 1913;17(4):482-93.
164. Dagg CP, Karnofsky DA, Roddy J. Growth of transplantable human tumors in the chick embryo and hatched chick. *Cancer research*. 1956;16(7):589-94.
165. Burt HM, Jackson JK, Bains SK, Liggins RT, Oktaba AM, Arsenault AL, et al. Controlled delivery of taxol from microspheres composed of a blend of ethylene-vinyl acetate copolymer and poly (d,l-lactic acid). *Cancer Lett*. 1995;88(1):73-9.
166. Nowak-Sliwinska P, Clavel CM, Paunescu E, te Winkel MT, Griffioen AW, Dyson PJ. Antiangiogenic and Anticancer Properties of Bifunctional Ruthenium(II)-p-Cymene Complexes: Influence of Pendant Perfluorous Chains. *Molecular pharmaceutics*. 2015;12(8):3089-96.

167. Jaworski S, Sawosz E, Kutwin M, Wierzbicki M, Hinzmann M, Grodzik M, et al. In vitro and in vivo effects of graphene oxide and reduced graphene oxide on glioblastoma. *International journal of nanomedicine*. 2015;10:1585-96.
168. Kue CS. Chick embryo chorioallantoic membrane (CAM): an alternative predictive model. 2015;64(2):129-38.
169. Balke M, Neumann A, Kersting C, Agelopoulos K, Gebert C, Gosheger G, et al. Morphologic characterization of osteosarcoma growth on the chick chorioallantoic membrane. *BMC Research Notes*. 2010;3(1):1-8.
170. Schneiderhan W, Scheler M, Holzmann KH, Marx M, Gschwend JE, Bucholz M, et al. CD147 silencing inhibits lactate transport and reduces malignant potential of pancreatic cancer cells in in vivo and in vitro models. *Gut*. 2009;58(10):1391-8.
171. Gottfried V, Davidi R, Averguj C, Kimel S. In vivo damage to chorioallantoic membrane blood vessels by porphycene-induced photodynamic therapy. *Journal of photochemistry and photobiology B, Biology*. 1995;30(2-3):115-21.
172. Toledano H, Edrei R, Kimel S. Photodynamic damage by liposome-bound porphycenes: comparison between in vitro and in vivo models. *Journal of photochemistry and photobiology B, Biology*. 1998;42(1):20-7.
173. Hammer-Wilson MJ, Akian L, Espinoza J, Kimel S, Berns MW. Photodynamic parameters in the chick chorioallantoic membrane (CAM) bioassay for topically applied photosensitizers. *Journal of photochemistry and photobiology B, Biology*. 1999;53(1-3):44-52.
174. Reed MW, Wieman TJ, Schuschke DA, Tseng MT, Miller FN. A comparison of the effects of photodynamic therapy on normal and tumor blood vessels in the rat microcirculation. *Radiation research*. 1989;119(3):542-52.
175. Hammer-Wilson MJ, Cao D, Kimel S, Berns MW. Photodynamic parameters in the chick chorioallantoic membrane (CAM) bioassay for photosensitizers administered intraperitoneally (IP) into the chick embryo. *Photochem Photobiol Sci*. 2002;1(9):721-8.
176. Hornung R, Hammer-Wilson MJ, Kimel S, Liaw LH, Tadir Y, Berns MW. Systemic application of photosensitizers in the chick chorioallantoic membrane (CAM) model: photodynamic response of CAM vessels and 5-aminolevulinic acid uptake kinetics by transplantable tumors. *Journal of photochemistry and photobiology B, Biology*. 1999;49(1):41-9.
177. Vargas A, Pegaz B, Debefve E, Konan-Kouakou Y, Lange N, Ballini JP, et al. Improved photodynamic activity of porphyrin loaded into nanoparticles: an in vivo evaluation using chick embryos. *International journal of pharmaceutics*. 2004;286(1-2):131-45.
178. Sokolove PM, Westphal PA, Kester MB, Wierwille R, Sikora-VanMeter K. Duramycin effects on the structure and function of heart mitochondria. I. Structural alterations and changes in membrane permeability. *Biochimica et biophysica acta*. 1989;983(1):15-22.
179. Racker E, Riegler C, Abdel-Ghany M. Stimulation of glycolysis by placental polypeptides and inhibition by duramycin. *Cancer research*. 1984;44(4):1364-7.
180. Choung SY, Kobayashi T, Inoue J, Takemoto K, Ishitsuka H, Inoue K. Hemolytic activity of a cyclic peptide Ro09-0198 isolated from Streptoverticillium. *Biochimica et biophysica acta*. 1988;940(2):171-9.
181. Tan MH, Shimano T, Chu TM. Differential localization of human pancreas cancer-associated antigen and carcinoembryonic antigen in homologous pancreatic tumoral xenograft. *Journal of the National Cancer Institute*. 1981;67(3):563-9.
182. Fogh J, Wright WC, Loveless JD. Absence of HeLa cell contamination in 169 cell lines derived from human tumors. *Journal of the National Cancer Institute*. 1977;58(2):209-14.
183. Quinn LA, Moore GE, Morgan RT, Woods LK. Cell lines from human colon carcinoma with unusual cell products, double minutes, and homogeneously staining regions. *Cancer research*. 1979;39(12):4914-24.

184. Brattain MG, Fine WD, Khaled FM, Thompson J, Brattain DE. Heterogeneity of malignant cells from a human colonic carcinoma. *Cancer research*. 1981;41(5):1751-6.
185. Jackson N, Lowe J, Ball J, Bromidge E, Ling NR, Larkins S, et al. Two new IgA1-kappa plasma cell leukaemia cell lines (JJN-1 & JJN-2) which proliferate in response to B cell stimulatory factor 2. *Clinical and experimental immunology*. 1989;75(1):93-9.
186. Drewinko B, Romsdahl MM, Yang LY, Ahearn MJ, Trujillo JM. Establishment of a human carcinoembryonic antigen-producing colon adenocarcinoma cell line. *Cancer research*. 1976;36(2 Pt 1):467-75.
187. Soule HD, Vazguez J, Long A, Albert S, Brennan M. A human cell line from a pleural effusion derived from a breast carcinoma. *Journal of the National Cancer Institute*. 1973;51(5):1409-16.
188. Cailleau R, Young R, Olive M, Reeves WJ, Jr. Breast tumor cell lines from pleural effusions. *Journal of the National Cancer Institute*. 1974;53(3):661-74.
189. Yunis AA, Arimura GK, Russin DJ. Human pancreatic carcinoma (MIA PaCa-2) in continuous culture: sensitivity to asparaginase. *Int J Cancer*. 1977;19(1):128-35.
190. Goldman-Leikin RE, Salwen HR, Herst CV, Variakojis D, Bian ML, Le Beau MM, et al. Characterization of a novel myeloma cell line, MM.1. *The Journal of laboratory and clinical medicine*. 1989;113(3):335-45.
191. Nilsson K, Bennich H, Johansson SGO, Pontén J. Established immunoglobulin producing myeloma (IgE) and Lymphoblastoid (IgG) cell lines from an IgE myeloma patient. *Clinical and experimental immunology*. 1970;7(4):477-89.
192. Behrens BC, Hamilton TC, Masuda H, Grotzinger KR, Whang-Peng J, Louie KG, et al. Characterization of a cis-diamminedichloroplatinum(II)-resistant human ovarian cancer cell line and its use in evaluation of platinum analogues. *Cancer research*. 1987;47(2):414-8.
193. Collins SJ, Gallo RC, Gallagher RE. Continuous growth and differentiation of human myeloid leukaemic cells in suspension culture. *Nature*. 1977;270(5635):347-9.
194. Weiss A, Wiskocil RL, Stobo JD. The role of T3 surface molecules in the activation of human T cells: a two-stimulus requirement for IL 2 production reflects events occurring at a pre-translational level. *Journal of immunology (Baltimore, Md : 1950)*. 1984;133(1):123-8.
195. Keydar I, Chen L, Karby S, Weiss FR, Delarea J, Radu M, et al. Establishment and characterization of a cell line of human breast carcinoma origin. *European Journal of Cancer (1965)*. 1979;15(5):659-70.
196. Sundstrom C, Nilsson K. Establishment and characterization of a human histiocytic lymphoma cell line (U-937). *Int J Cancer*. 1976;17(5):565-77.
197. Koopman G, Reutelingsperger CP, Kuijten GA, Keehnen RM, Pals ST, van Oers MH. Annexin V for flow cytometric detection of phosphatidylserine expression on B cells undergoing apoptosis. *Blood*. 1994;84(5):1415-20.
198. Falls LA, Furie B, Furie BC. Role of Phosphatidylethanolamine in Assembly and Function of the Factor IXa−Factor VIIIa Complex on Membrane Surfaces†. *Biochemistry*. 2000;39(43):13216-22.
199. Smeets EF, Comfurius P, Bevers EM, Zwaal RF. Contribution of different phospholipid classes to the prothrombin converting capacity of sonicated lipid vesicles. *Thrombosis research*. 1996;81(4):419-26.
200. Zwaal RFA, Schroit AJ. Pathophysiologic Implications of Membrane Phospholipid Asymmetry in Blood Cells. *Blood*. 1997;89(4):1121-32.
201. Marki F, Hanni E, Fredenhagen A, van Oostrum J. Mode of action of the lanthionine-containing peptide antibiotics duramycin, duramycin B and C, and cinnamycin as indirect inhibitors of phospholipase A2. *Biochemical pharmacology*. 1991;42(10):2027-35.
202. Hou S, Johnson SE, Zhao M. A One-Step Staining Probe for Phosphatidylethanolamine. *Chembiochem : a European journal of chemical biology*. 2015.

203. Dive C, Gregory CD, Phipps DJ, Evans DL, Milner AE, Wyllie AH. Analysis and discrimination of necrosis and apoptosis (programmed cell death) by multiparameter flow cytometry. *Biochimica et Biophysica Acta (BBA) - Molecular Cell Research*. 1992;1133(3):275-85.
204. Haynes MK, Strouse JJ, Waller A, Leitao A, Curpan RF, Bologa C, et al. Detection of intracellular granularity induction in prostate cancer cell lines by small molecules using the HyperCyt high-throughput flow cytometry system. *Journal of biomolecular screening*. 2009;14(6):596-609.
205. Healy E, Dempsey M, Lally C, Ryan MP. Apoptosis and necrosis: mechanisms of cell death induced by cyclosporine A in a renal proximal tubular cell line. *Kidney international*. 1998;54(6):1955-66.
206. Wlodkowic D, Telford W, Skommer J, Darzynkiewicz Z. Apoptosis and beyond: cytometry in studies of programmed cell death. *Methods in cell biology*. 2011;103:55-98.
207. Zbytek B, Pikula M, Slominski RM, Mysliwski A, Wei E, Wortsman J, et al. Corticotropin-releasing hormone triggers differentiation in HaCaT keratinocytes. *The British journal of dermatology*. 2005;152(3):474-80.
208. Barranco WT, Eckhert CD. Cellular changes in boric acid-treated DU-145 prostate cancer cells. *Br J Cancer*. 2006;94(6):884-90.
209. Stock K, Estrada MF, Vidic S, Gjerde K, Rudisch A, Santo VE, et al. Capturing tumor complexity in vitro: Comparative analysis of 2D and 3D tumor models for drug discovery. *Scientific Reports*. 2016;6:28951.
210. Herrmann R, Fayad W, Schwarz S, Berndtsson M, Linder S. Screening for compounds that induce apoptosis of cancer cells grown as multicellular spheroids. *Journal of biomolecular screening*. 2008;13(1):1-8.
211. Jones AC, Stratford IJ, Wilson PA, Peckham MJ. In vitro cytotoxic drug sensitivity testing of human tumour xenografts grown as multicellular tumour spheroids. *British Journal of Cancer*. 1982;46(6):870-9.
212. Weiswald L-B, Bellet D, Dangles-Marie V. Spherical Cancer Models in Tumor Biology(). *Neoplasia (New York, NY)*. 2015;17(1):1-15.
213. Lessan K, Aguiar DJ, Oegema T, Siebenson L, Skubitz AP. CD44 and beta1 integrin mediate ovarian carcinoma cell adhesion to peritoneal mesothelial cells. *Am J Pathol*. 1999;154(5):1525-37.
214. Casey RC, Burleson KM, Skubitz KM, Pambuccian SE, Oegema TR, Jr., Ruff LE, et al. Beta 1-integrins regulate the formation and adhesion of ovarian carcinoma multicellular spheroids. *Am J Pathol*. 2001;159(6):2071-80.
215. Yeon SE, No da Y, Lee SH, Nam SW, Oh IH, Lee J, et al. Application of concave microwells to pancreatic tumor spheroids enabling anticancer drug evaluation in a clinically relevant drug resistance model. *PLoS One*. 2013;8(9):e73345.
216. Ho WJ, Pham EA, Kim JW, Ng CW, Kim JH, Kamei DT, et al. Incorporation of multicellular spheroids into 3-D polymeric scaffolds provides an improved tumor model for screening anticancer drugs. *Cancer science*. 2010;101(12):2637-43.
217. Myungjin Lee J, Mhawech-Fauceglia P, Lee N, Cristina Parsanian L, Gail Lin Y, Andrew Gayther S, et al. A three-dimensional microenvironment alters protein expression and chemosensitivity of epithelial ovarian cancer cells in vitro. *Laboratory investigation; a journal of technical methods and pathology*. 2013;93(5):528-42.
218. Schaller G, Meyer-Hermann M. Continuum versus discrete model: a comparison for multicellular tumour spheroids. *Philosophical Transactions of the Royal Society A: Mathematical, Physical and Engineering Sciences*. 2006;364(1843):1443.
219. Sherratt JA, Chaplain MA. A new mathematical model for avascular tumour growth. *Journal of mathematical biology*. 2001;43(4):291-312.

220. Herman AB, Savage VM, West GB. A Quantitative Theory of Solid Tumor Growth, Metabolic Rate and Vascularization. *PLoS ONE*. 2011;6(9):e22973.
221. L'Esperance S, Bachvarova M, Tetu B, Mes-Masson AM, Bachvarov D. Global gene expression analysis of early response to chemotherapy treatment in ovarian cancer spheroids. *BMC genomics*. 2008;9:99.
222. Gong X, Lin C, Cheng J, Su J, Zhao H, Liu T, et al. Generation of Multicellular Tumor Spheroids with Microwell-Based Agarose Scaffolds for Drug Testing. *PLoS One*. 2015;10(6):e0130348.
223. Galateanu B, Hudita A, Negrei C, Ion RM, Costache M, Stan M, et al. Impact of multicellular tumor spheroids as an in vivolike tumor model on anticancer drug response. *International journal of oncology*. 2016;48(6):2295-302.
224. Sutherland RM, McCredie JA, Inch WR. Growth of multicell spheroids in tissue culture as a model of nodular carcinomas. *Journal of the National Cancer Institute*. 1971;46(1):113-20.
225. Yuhas JM, Tarleton AE, Harman JG. In vitro analysis of the response of multicellular tumor spheroids exposed to chemotherapeutic agents in vitro or in vivo. *Cancer research*. 1978;38(11 Pt 1):3595-8.
226. Liao Q, Hu Y, Zhao YP, Zhou T, Zhang Q. Assessment of pancreatic carcinoma cell chemosensitivity using a three-dimensional culture system. *Chinese medical journal*. 2010;123(14):1871-7.
227. Algarni A, Greenman J, Madden LA. PO-48 - Assessment of the procoagulant potential state of tumour-MP in cancer patients. *Thrombosis research*. 2016;140 Suppl 1:S194.
228. Ronen SM, Stier A, Degani H. NMR studies of the lipid metabolism of T47D human breast cancer spheroids. *FEBS letters*. 1990;266(1-2):147-9.
229. Lu M, Gao R, Xiao L, Wang Z. Construction of three-dimensional in vitro culture model of ovarian carcinoma and the study of its multicellular drug resistance. *Journal of Huazhong University of Science and Technology Medical sciences = Hua zhong ke ji da xue xue bao Yi xue Ying De wen ban = Huazhong keji daxue xuebao Yixue Yingdewen ban*. 2006;26(6):741-3.
230. Tang Y, Liu J, Chen Y. Agarose multi-wells for tumour spheroid formation and anti-cancer drug test. *Microelectronic Engineering*. 2016;158:41-5.
231. Sciume G, Shelton S, Gray W, Miller C, Hussain F, Ferrari M, et al. A multiphase model for three-dimensional tumor growth. *New journal of physics*. 2013;15:015005.
232. Alzahrani EO, Asiri A, El-Dessoky MM, Kuang Y. Quiescence as an explanation of Gompertzian tumor growth revisited. *Mathematical biosciences*. 2014;254:76-82.
233. Zanoni M, Piccinini F, Arienti C, Zamagni A, Santi S, Polico R, et al. 3D tumor spheroid models for in vitro therapeutic screening: a systematic approach to enhance the biological relevance of data obtained. *Scientific Reports*. 2016;6:19103.
234. Erlichman C, Vidgen D, Wu A. Cytotoxicity of cisplatin and cisdiammine-1,1-cyclobutane dicarboxylate in MGH-U1 cells grown as monolayers, spheroids, and xenografts. *Journal of the National Cancer Institute*. 1985;75(3):499-505.
235. Bhuyan BK, Folz SJ, DeZwaan J, Northcott SE, Alberts DS, Garcia D, et al. Cytotoxicity of tetraplatin and cisplatin for human and rodent cell lines cultured as monolayers and multicellular spheroids. *Cancer communications*. 1991;3(2):53-9.
236. Carduner L, Picot CR, Leroy-Dudal J, Blay L, Kellouche S, Carreiras F. Cell cycle arrest or survival signaling through alphav integrins, activation of PKC and ERK1/2 lead to anoikis resistance of ovarian cancer spheroids. *Experimental cell research*. 2014;320(2):329-42.
237. Boylan KLM, Misemer B, DeRycke MS, Andersen JD, Harrington KM, Kalloger SE, et al. Claudin 4 Is Differentially Expressed between Ovarian Cancer Subtypes and Plays a Role in Spheroid Formation. *International Journal of Molecular Sciences*. 2011;12(2):1334-58.

238. Zhuang L, Peng JB, Tou L, Takanaga H, Adam RM, Hediger MA, et al. Calcium-selective ion channel, CaT1, is apically localized in gastrointestinal tract epithelia and is aberrantly expressed in human malignancies. *Laboratory investigation; a journal of technical methods and pathology*. 2002;82(12):1755-64.
239. Arvizo RR, Moyano DF, Saha S, Thompson MA, Bhattacharya R, Rotello VM, et al. Probing Novel Roles of the Mitochondrial Uniporter in Ovarian Cancer Cells Using Nanoparticles. *The Journal of biological chemistry*. 2013;288(24):17610-8.
240. Zong WX, Thompson CB. Necrotic death as a cell fate. *Genes & development*. 2006;20(1):1-15.
241. Verma A, Bhatt AN, Farooque A, Khanna S, Singh S, Dwarakanath BS. Calcium ionophore A23187 reveals calcium related cellular stress as "I-Bodies": an old actor in a new role. *Cell calcium*. 2011;50(6):510-22.
242. Long J, Zhang ZB, Liu Z, Xu YH, Ge CL. Loss of heterozygosity at the calcium regulation gene locus on chromosome 10q in human pancreatic cancer. *Asian Pacific journal of cancer prevention : APJCP*. 2015;16(6):2489-93.
243. Thompson K, Dockery P, Horobin RW. Predicting and avoiding subcellular compartmentalization artifacts arising from acetoxymethyl ester calcium imaging probes. The case of fluo-3 AM and a general account of the phenomenon including a problem avoidance chart. *Biotechnic & histochemistry : official publication of the Biological Stain Commission*. 2012;87(7):468-83.
244. Paredes RM, Etzler JC, Watts LT, Lechleiter JD. Chemical Calcium Indicators. *Methods (San Diego, Calif)*. 2008;46(3):143-51.
245. Bootman MD, Rietdorf K, Collins T, Walker S, Sanderson M. Ca2+-sensitive fluorescent dyes and intracellular Ca2+ imaging. *Cold Spring Harbor protocols*. 2013;2013(2):83-99.
246. Cheng H, Lederer WJ. Calcium sparks. *Physiological reviews*. 2008;88(4):1491-545.
247. Corcuff JB, Guerineau NC, Mariot P, Lussier BT, Mollard P. Multiple cytosolic calcium signals and membrane electrical events evoked in single arginine vasopressin-stimulated corticotrophs. *The Journal of biological chemistry*. 1993;268(30):22313-21.
248. Palta S, Saroa R, Palta A. Overview of the coagulation system. *Indian Journal of Anaesthesia*. 2014;58(5):515-23.
249. Chen B, Pogue BW, Hoopes PJ, Hasan T. Combining vascular and cellular targeting regimens enhances the efficacy of photodynamic therapy. *Int J Radiat Oncol Biol Phys*. 2005;61(4):1216-26.
250. Vrouenraets MB, Visser GW, Stewart FA, Stigter M, Oppelaar H, Postmus PE, et al. Development of meta-tetrahydroxyphenylchlorin-monoclonal antibody conjugates for photoimmunotherapy. *Cancer research*. 1999;59(7):1505-13.
251. Del Governatore M, Hamblin MR, Piccinini EE, Ugolini G, Hasan T. Targeted photodestruction of human colon cancer cells using charged 17.1A chlorin e6 immunoconjugates. *Br J Cancer*. 2000;82(1):56-64.
252. Polo L, Segalla A, Bertoloni G, Jori G, Schaffner K, Reddi E. Polylysine-porphycene conjugates as efficient photosensitizers for the inactivation of microbial pathogens. *Journal of photochemistry and photobiology B, Biology*. 2000;59(1-3):152-8.
253. Hermanson GT. Chapter 5 - Homobifunctional Crosslinkers. Bioconjugate Techniques (Third edition). Boston: Academic Press; 2013. p. 275-98.
254. Jung B, Theato P. Chemical Strategies for the Synthesis of Protein–Polymer Conjugates. In: Schlaad H, editor. Bio-synthetic Polymer Conjugates. Berlin, Heidelberg: Springer Berlin Heidelberg; 2013. p. 37-70.
255. Golab J, Nowis D, Skrzycki M, Czeczot H, Baranczyk-Kuzma A, Wilczynski GM, et al. Antitumor effects of photodynamic therapy are potentiated by 2-methoxyestradiol. A superoxide dismutase inhibitor. *The Journal of biological chemistry*. 2003;278(1):407-14.

256. Wang Y, Dong L, Cui H, Shen DH, Wang Y, Chang XH, et al. Up-regulation of mitochondrial antioxidation signals in ovarian cancer cells with aggressive biologic behavior. *J Zhejiang Univ Sci B*. 2011;12(5):346-56.
257. Broekgaarden M, Weijer R, van Gulik TM, Hamblin MR, Heger M. Tumor cell survival pathways activated by photodynamic therapy: a molecular basis for pharmacological inhibition strategies. *Cancer metastasis reviews*. 2015;34(4):643-90.
258. Yi YW, Oh S. Comparative analysis of NRF2-responsive gene expression in AcPC-1 pancreatic cancer cell line. *Genes Genomics*. 2015;37:97-109.
259. Bao LJ, Jaramillo MC, Zhang ZB, Zheng YX, Yao M, Zhang DD, et al. Nrf2 induces cisplatin resistance through activation of autophagy in ovarian carcinoma. *International journal of clinical and experimental pathology*. 2014;7(4):1502-13.
260. Cho JM, Manandhar S, Lee HR, Park HM, Kwak MK. Role of the Nrf2-antioxidant system in cytotoxicity mediated by anticancer cisplatin: implication to cancer cell resistance. *Cancer Lett*. 2008;260(1-2):96-108.
261. Hong YB, Kang HJ, Kwon SY, Kim HJ, Kwon KY, Cho CH, et al. Nuclear factor (erythroid-derived 2)-like 2 regulates drug resistance in pancreatic cancer cells. *Pancreas*. 2010;39(4):463-72.
262. Wang Y, Ma J, Shen H, Wang C, Sun Y, Howell SB, et al. Reactive oxygen species promote ovarian cancer progression via the HIF-1alpha/LOX/E-cadherin pathway. *Oncol Rep*. 2014;32(5):2150-8.
263. Sibenaller ZA, Welsh JL, Du C, Witmer JR, Schrock HE, Du J, et al. Extracellular superoxide dismutase suppresses hypoxia-inducible factor-1alpha in pancreatic cancer. *Free Radic Biol Med*. 2014;69:357-66.
264. Selvendiran K, Bratasz A, Kuppusamy ML, Tazi MF, Rivera BK, Kuppusamy P. Hypoxia induces chemoresistance in ovarian cancer cells by activation of signal transducer and activator of transcription 3. *Int J Cancer*. 2009;125(9):2198-204.
265. Saunders JA, Rogers LC, Klomsiri C, Poole LB, Daniel LW. Reactive oxygen species mediate lysophosphatidic acid induced signaling in ovarian cancer cells. *Free Radic Biol Med*. 2010;49(12):2058-67.
266. Nonaka M, Ikeda H, Inokuchi T. Inhibitory effect of heat shock protein 70 on apoptosis induced by photodynamic therapy in vitro. *Photochem Photobiol*. 2004;79(1):94-8.
267. Walsh N, Larkin A, Swan N, Conlon K, Dowling P, McDermott R, et al. RNAi knockdown of Hop (Hsp70/Hsp90 organising protein) decreases invasion via MMP-2 down regulation. *Cancer Lett*. 2011;306(2):180-9.
268. Kessel D, Poretz RD. Sites of photodamage induced by photodynamic therapy with a chlorin e6 triacetoxymethyl ester (CAME). *Photochem Photobiol*. 2000;71(1):94-6.
269. Kaufman N, Kinney TD, Mason EJ, Prieto LC. Maintenance of Human Neoplasm on the Chick Chorioallantoic Membrane. *The American Journal of Pathology*. 1956;32(2):271-85.
270. Chang HL, Pieretti-Vanmarcke R, Nicolaou F, Li X, Wei X, MacLaughlin DT, et al. Mullerian inhibiting substance inhibits invasion and migration of epithelial cancer cell lines. *Gynecologic oncology*. 2011;120(1):128-34.
271. Saw CL, Olivo M, Chin WW, Soo KC, Heng PW. Transport of hypericin across chick chorioallantoic membrane and photodynamic therapy vasculature assessment. *Biological & pharmaceutical bulletin*. 2005;28(6):1054-60.
272. Chin WW, Lau WK, Bhuvaneswari R, Heng PW, Olivo M. Chlorin e6-polyvinylpyrrolidone as a fluorescent marker for fluorescence diagnosis of human bladder cancer implanted on the chick chorioallantoic membrane model. *Cancer Lett*. 2007;245(1-2):127-33.

273. Saw CL, Olivo M, Chin WW, Soo KC, Heng PW. Superiority of N-methyl pyrrolidone over albumin with hypericin for fluorescence diagnosis of human bladder cancer cells implanted in the chick chorioallantoic membrane model. *Journal of photochemistry and photobiology B, Biology*. 2007;86(3):207-18.
274. Malik E, Meyhöfer-Malik A, Berg C, Böhm W, Kunzi-Rapp K, Diedrich K, et al. Fluorescence diagnosis of endometriosis on the chorioallantoic membrane using 5-aminolaevulinic acid. *Human Reproduction*. 2000;15(3):584-8.
275. Kalita N, Pathak N, Ahmed M, Saikia GK. Various causes related to dead-in-shell embryos of crossbred (PB-2 x Indigenous) chicken egg. *Veterinary World*. 2013;6(10):774-7.
276. Romanoff AL. Critical Periods and Causes of Death in Avian Embryonic Development. *The Auk*. 1949;66(3):264-70.
277. Nowak-Sliwinska P, Weiss A, van Beijnum JR, Wong TJ, Kilarski WW, Szewczyk G, et al. Photoactivation of lysosomally sequestered sunitinib after angiostatic treatment causes vascular occlusion and enhances tumor growth inhibition. *Cell death & disease*. 2015;6:e1641.
278. Ryter SW, Kim HP, Hoetzel A, Park JW, Nakahira K, Wang X, et al. Mechanisms of cell death in oxidative stress. *Antioxidants & redox signaling*. 2007;9(1):49-89.

Appendix A

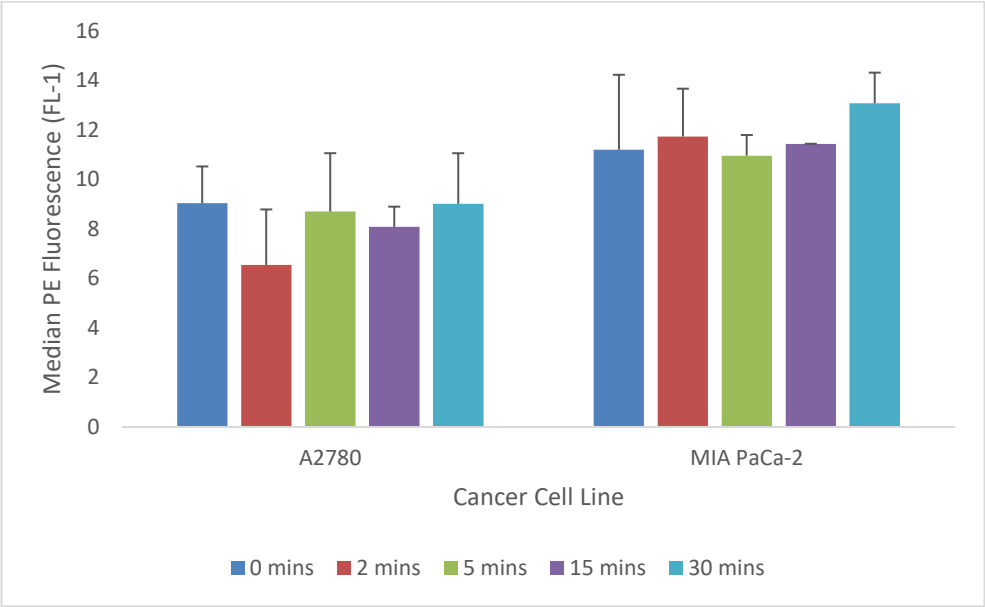

Figure A.1: Detection of phosphatidylethanolamine with duramycin (50 µM) on cancer cell lines.

There was no difference in the level of PE detected on the cancer cell lines A2780 and MIA PaCa-2 using duramycin (50 µM) at intervals over a 30 minute time period. Error bars represent SD of 2 replicates.

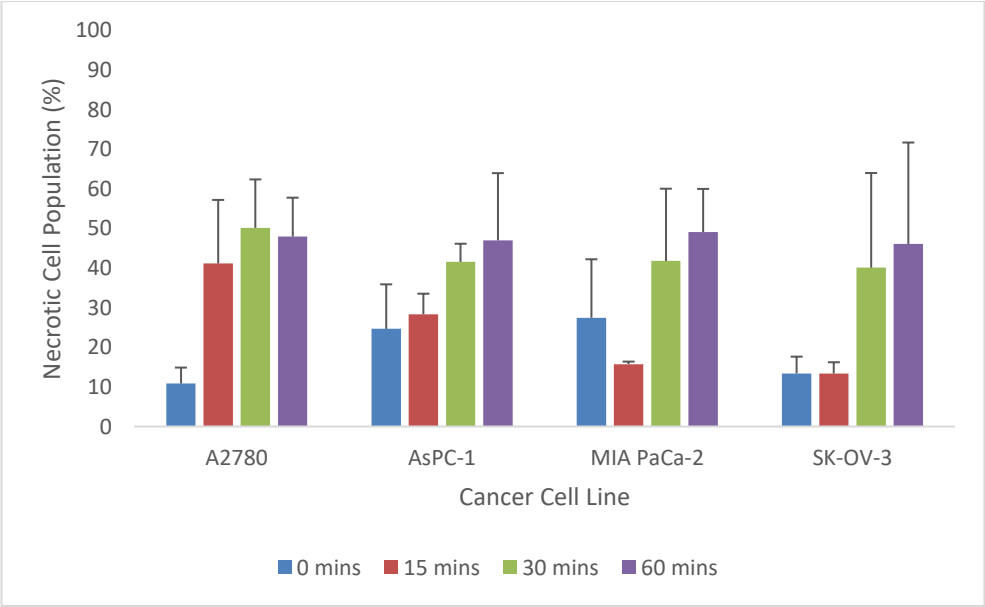

Figure A.2: Duramycin-induced necrotic cell death in cancer cell lines.

Duramycin (50 µM) treatment resulted in an increased amount of cells in the necrotic cell population over a 60 minute treatment period in the cancer cell lines A2780, AsPC-1 and SK-OV-3. Error bars represent SD of 2 replicates.

Appendix B

a)

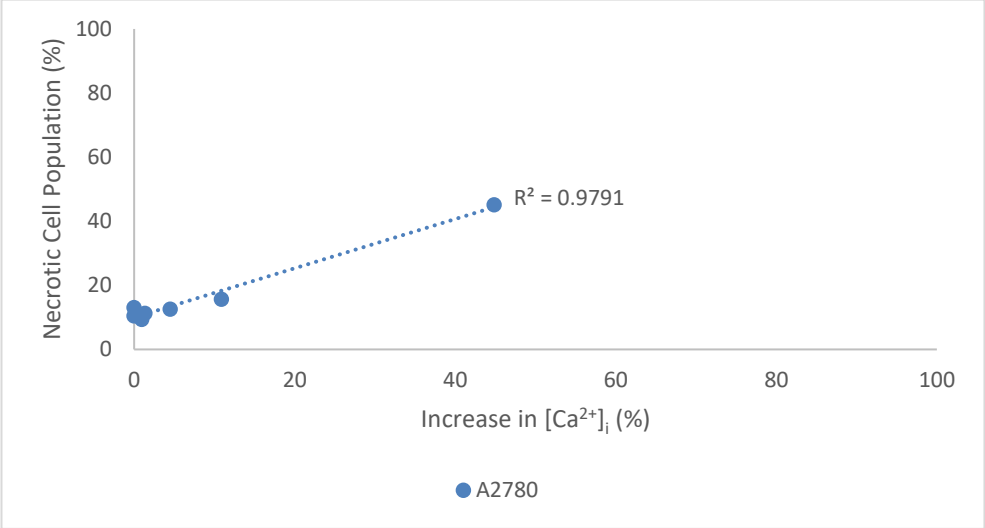

b)

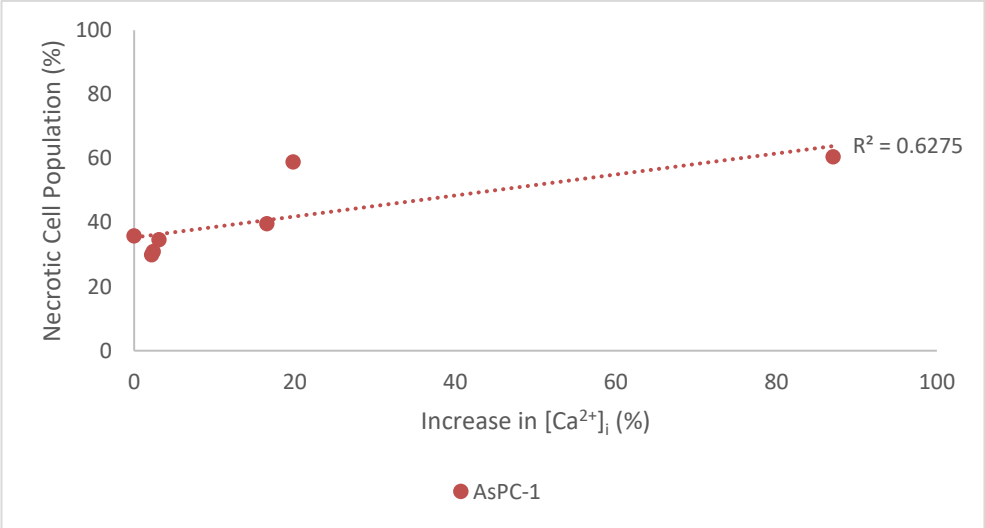

c)

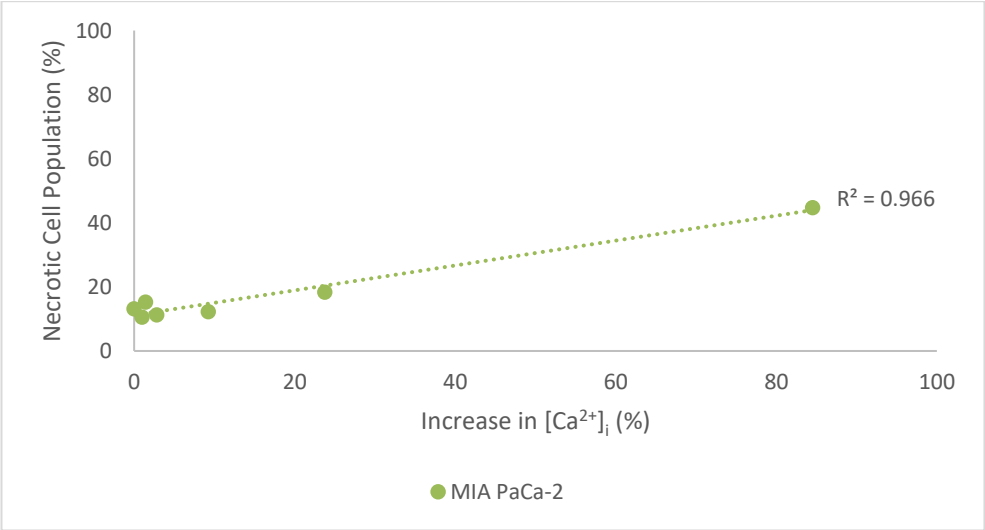

d)

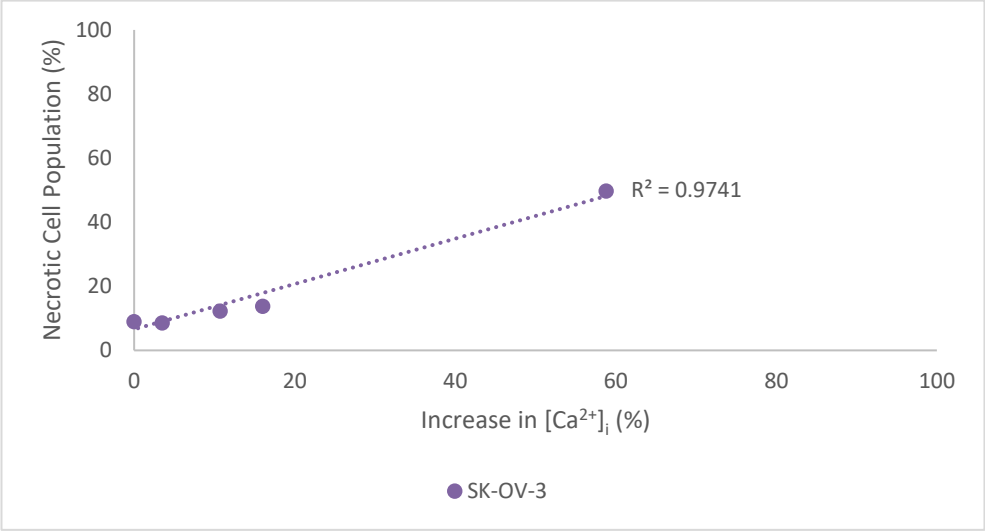

Figure B.1: Scatter plots of the relationship between duramycin-induced necrotic cell death and intracellular calcium ion concentration in cancer cell lines.

A strong positive correlation between the level of necrosis and amount of increase in $[Ca^{2+}]_i$ in cancer cell lines occurred when treated with duramycin (0-50 µM) for a) A2780, C) MIA PaCa-2 and d) SK-OV-3. A moderately strong correlation occurred in the cancer cell line b) AsPC-1.

Appendix C

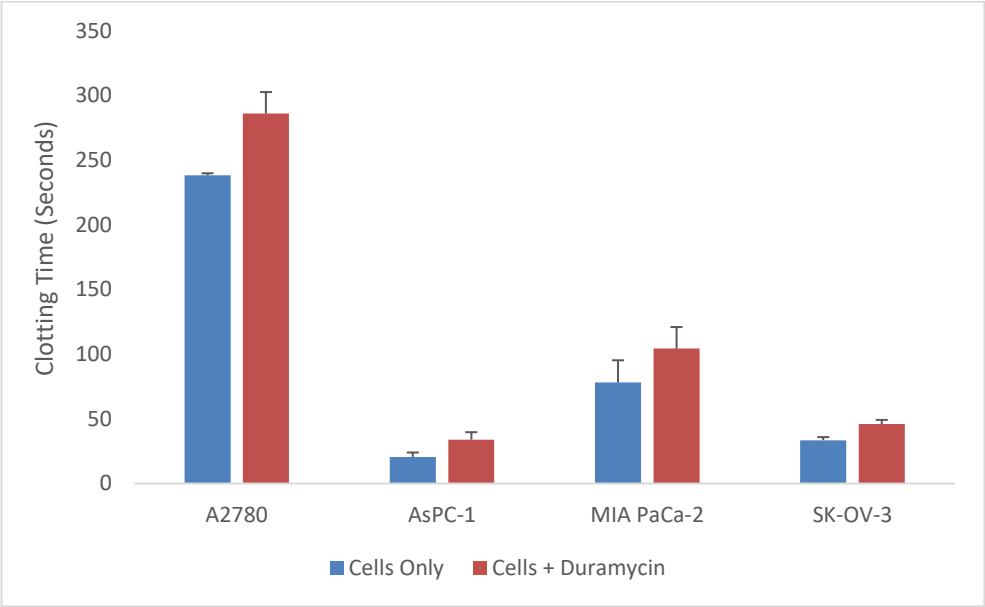

Figure C.1: Effect of duramycin on the pro-thrombin clotting time of cancer cells.

Duramycin (50 µM) treatment increased the pro-thrombin clotting time of the cancer cell lines A2780, AsPC-1, MIA PaCa-2 and SK-OV-3 compared to untreated control cells.